Synthetic and Mechanistic Studies into the Kinetic Resolution of α-olefins using C_1- and C_2- Symmetric Zirconocene Polymerization Catalysts

Thesis by
Jeffery A. Byers

In Partial Fulfillment of the
Requirements for the Degree of
Doctor of Philosophy

California Institute of Technology
Pasadena, California

2007
(Defended May 24, 2007)

ACKNOWLEDGEMENT

Trying to acknowledge everyone who helped me in this crazy journey would be as difficult as climbing multiple 14,000 foot peaks in a day or eating 16 hamburgers in an hour. Nevertheless, my time at Caltech would not be nearly as enjoyable without those who have joined me on the journey. First, my sisters Jennie and Vickie and my parents have been nothing but understanding and supportive of me ever since I made that long drive across the United States. Graduate school is such a foreign lifestyle that is difficult to understand for those not engulfed in it, but my family has tried hard to relate to me as best they could.

To my fellow comrades in the Bercaw group, you have been like a second family to me. I will truly miss all of the good times that I have had with you and hope that we will cross paths in the future. I am eternally grateful to Dr. Cliff Baar for being so patient with me as a young inexperienced first year student. Although I enjoyed spirited conversations about science and otherwise interesting topics with all of the postdocs that I encountered here, I particularly would like to thank Nilay, Travis, Parisa, and Patrick (though technically not a Bercaw postdoc) for always letting me vent or pass an idea by them. I would also like to dedicate this paragraph of my thesis to Tom Driver version 1.0 and subsequent versions. Tom taught me a lot about being a responsible scientist and how to behave appropriately in every possible situation. Thanks Tom!

As for my fellow graduate school brethren, I do not really know where to begin. I would like to thank the older members of the group: Susan, Sara, Lily, and Jonathan, for being good mentors to me and welcoming me so readily into the Bercaw group. I do not think I can remember my time at Caltech without recalling my longtime labmate and good friend, Endy. I always enjoyed our spirited conversations not only for their content, but also for the reactions that they would produce from others watching. Although she

had large shoes to fill, my new labmate Suzanne has been equally enjoyable to work with. One of my biggest regrets upon leaving Caltech will be not seeing you flourish in good old Noyes 201. As for the rest of the younger students: Ian, Ted, Alex, Paul Oblad, and Val I would like to thank you for keeping my enthusiasm up, especially during my last year. I wish you all the best.

Of course it would be a downright crime if I failed to mention my fellow classmates, Dave and Theo. Thankfully, I never adopted the strange habits that the two of you fell into, but hopefully I have earned as much respect and admiration as I have garnered for you two boys. Other than Dave and Theo, Steve has been around the longest with me. I would like to thank Steve for being a good friend and baseball companion for the past few years. Although your cynicism has not rubbed off on me (much), I appreciate the perspective you have towards science and wish you the best. For some reason the word cynical made me think about Paul Elowe whom I would like to thank for taking time to discuss everything from solvent effects to wine tasting to the curious things that Travis sings. Bolin and George, thanks for all of the insightful discussions.

Outside of the Bercaw group I have had help from many people both professionally and socially. Jay Labinger has been a patient and critical observer of my research. I very much appreciate all the input that he has had throughout my career, and hope that I will continue to learn from your expertise in the future. I would like to thank Julia Kornfield and Lucia Fernandez-Ballester for the use of their DSC instrumentation and for useful discussions about polymer chemistry. I would also like to thank Steven Cohen and Jerome Streeky at BP Chemicals (now Ineos) for molecular weight measurements. I am indebted to Mike Day and Larry Henling for the help and explanation of X-ray crystallography. I also had the privilege to work with Vera Mainz and have benefited greatly from her NMR expertise. I could not have functioned in the lab without our very talented glass blower, Rick Gerhart who bailed me out on numerous

occasions with his expertise and professionalism. Special thanks to the members of the Stoltz, Grubbs, Peters, and MacMillan groups for the generous use of their chemicals and equipment. Without these people much of my work could not have been completed.

There were many people in my past life from Washington U. that I am indebted to for all of the support that they have given me. Dan, Craig, and Sam, thanks for providing a geographical and emotional outlet for me when things became tough in Pasadena. Chris Clark, your mentorship and guidance through this process is invaluable, and I will always value our friendship. I would also like to thank my research mentors at Washington University, Karen Wooley and Ray Arvidson, thanks for instilling in me the cautious enthusiasm necessary to pursue a career in science.

I have been fortunate enough to meet some incredible people outside of my lab at Caltech. I owe many thanks to all of you for all of the good memories. In particular, I would like to thank Andy Hejl for being such a good friend and for not rubbing it in when he beat me at every competitive indoor sport. To my teammates on FBOD, it was a challenge to play with you all, but the rewards made it well worth it. I don't think my last years at Caltech would have been nearly as enjoyable without my lovely girlfriend, Crystal. Your enthusiasm is contagious and I love every minute of it!

Finally, I would like to thank John Bercaw for allowing me to join his group and work under his tutelage. John has been an excellent mentor and a good role model for me, and for that I will always be grateful.

“This research is profoundly unsatisfying”

-Jay Labinger, 2002-

ABSTRACT

Mechanistic and synthetic investigations into the kinetic resolution of racemic α-olefins by polymerization catalysis using C_1- and C_2-symmetric zirconocenes are reported. The importance of chain end control as a stereocontrol element was probed with ethylene and propylene copolymerizations catalyzed by the C_1-symmetric catalyst, {1,2-$(SiMe_2)_2$(η^5-3,5-$C_5H_1(CHMe_2)_2$)(η^5-4-C_5H_2((*S*)-$CHMeCMe_3$)]}$ZrCl_2$/MAO. Selectivity factors and pentad analysis of racemic α-olefin and propylene polymerizations catalyzed by a similar C_1-symmetric catalyst, {1,2-$(SiMe_2)_2$(η^5-3,5-$C_5H_1(CHMe_2)_2$)(η^5-4-C_5H_2((*S*)-$CHEtCMe_3$)]}$ZrCl_2$/MAO, indicate that site epimerization does not limit selectivity during kinetic resolution.

To avoid some of the issues involved with the C_1-symmetric catalysts, a route to enantiopure C_2-symmetric zirconocenes was pursued. With the aid of the chiral auxiliary, (*R*)-N^2,$N^{2'}$-di-*p*-tolyl-1,1'-binaphtyl-2,2'-diamine, enantiospecefic synthesis of (*S*,*S*)-{C_2H_4-1,2-$(1\text{-indene})_2$}$ZrCl_2$ was accomplished and its use for kinetic resolution was investigated. Although synthetically useful selectivities were not observed, it was determined that the C_2-symmetric catalyst does not racemize during polymerization, which substantiates a more thorough investigation of catalysts based on {C_2H_4-1,2-$(1\text{-indene})_2$}$ZrCl_2$.

TABLE OF CONTENTS

LIST OF FIGURES

CHAPTER ONE

CHAPTER TWO

CHAPTER THREE

APPENDIX B

APPENDIX C

APPENDIX H

APPENDIX I

LIST OF SCHEMES

INTRODUCTION

CHAPTER ONE

CHAPTER TWO

CHAPTER THREE

APPENDIX A

LIST OF TABLES

INTRODUCTION

CHAPTER ONE

CHAPTER TWO

CHAPTER THREE

APPENDIX B

APPENDIX E

APPENDIX F

APPENDIX H

APPENDIX I

LIST OF MULTIMEDIA FILES

GENERAL

SWIVELFRIT.MOV Demonstration of the swivel frit technique.

CHAPTER THREE

STRUCTURE01.AVI Movie of the crystal structure of (*rac*)-**18**.

STRUCTURE02.AVI Movie of the calculated minimum energy diastereomer for (*R*,*R*,*R*)-**7**.

STRUCTURE03.AVI Movie of the crystal structure of {(*S*,*S*)-THEBI}Ti{(*S*)-BINOL}.

INTRODUCTION

The polymerization of α-olefins catalyzed by a heterogeneous mixture of group IV metal(s) and Lewis acid cocatalyst(s) (Ziegler-Natta catalysts) is one of the most prolific reactions in the chemical industry. Using this process, useful engineering polymers such as polypropylene and polyethylene are being produced on the multi ton scale producing 10^{10} pounds of polymer, annually.[1] A continuing effort in the organometallic community has been the development of well-defined single-site catalysts that can be used as homogeneous analogs of the heterogeneous Ziegler-Natta polymerization catalysts. Many mechanistic features of Ziegler-Natta polymerization have emerged as a result of these studies, and several properties unique to the homogeneous systems have been identified.

For example, facial selectivity for olefin migratory insertion has been linked to the catalyst geometry by an intimate relay mechanism between the ligands on the catalyst, the polymer chain, and the incoming olefin.[2] The critical feature for this mechanism is an α-agostic interaction between the polymeryl chain and the 14-electron metal species that develops in the transition state for olefin migratory insertion (Scheme 0.1).[3] Since 1,2-migratory insertion results in a polymeryl chain with two α-hydrogens, the agostic interaction can occur in one of two ways. The ligand(s) on the metal fragment often dictate which of the two agostic interactions is preferred by encouraging the polymeryl group to reside in a conformation that avoids steric interactions with the ligand. These interactions are relevant to the facial selectivity of olefin insertion because the geometry of the incoming olefin is primarily controlled by the conformation of the polymeryl group with the substituent of the α-olefin tending to reside *anti* to the polymeryl chain (Scheme 0.1). The consequence of this relay mechanism is that C_2-symmetric catalysts, such as (*rac*)-{$C_2H_4(\eta^5$-1-indenyl$)_2$}$ZrCl_2$ (**1**), encourage olefin insertions from the same enantioface to give isotactic polymers, and some C_s-symmetric

symmetric catalysts, such as{1,2-$(SiMe_2)_2$(η^5-3,5-$C_5H_1(CHMe_2)_2$)(η^5-C_5H_5)}$ZrCl_2$ (**2**), encourage olefin insertions from alternating enantiofaces to give syndiotactic polymer. The production of syndiotactic polypropylene was particularly exciting because this microstructure could not be obtained with heterogeneous Ziegler-Natta catalysts. Unfortunately, syndiotactic polypropylene has not been used extensively as an engineering polymer due to poor processibility. Nevertheless, the production of new polymer materials previously inaccessible to Ziegler-Natta catalysts has spurred an intense research effort in homogeneous polymerization catalysis that have recently included α-olefin/ethylene random copolymerizations,[4] living polymerizations,[5] and stereoblock copolymerizations.[6]

Scheme 0.1 The interplay between catalyst, polymer chain, and olefin, and its effect on polypropylene polymer microstructure.

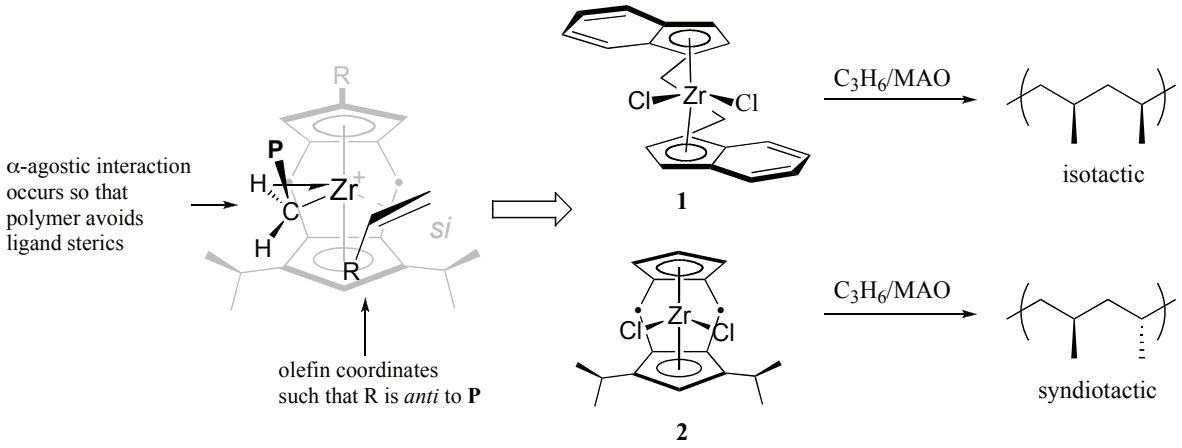

Recent efforts in our group have been devoted to enantioselective polymerizations, specifically kinetic resolution by selective polymerization of one antipode of a racemic mixture of an α-olefin (Scheme 0.2).[7] The success of kinetic resolution of such α-olefins would be valuable given that synthesis of enantiopure α-olefins is difficult especially in the absence of any polar directing groups.[8] For example, asymmetric dihydroxylation of dissymmetric internal olefins can only be achieved with

modest selectivity[9] although in some cases good selectivity is observed.[10] A notable exception to this limitation is the recent development of asymmetric alkylation of allylic phosphates, which proceed in impressive regio- and enantioselectivities.[11] Kinetic resolution by polymerization has the advantage that separation of the unreacted olefin product would only require a simple filtration. Additionally, kinetic resolution by polymerization would yield enantiopure polyolefins that could have unique physical, mechanical, and optical properties.

Scheme 0.2 Kinetic resolution of racemic α-olefins by polymerization catalysis

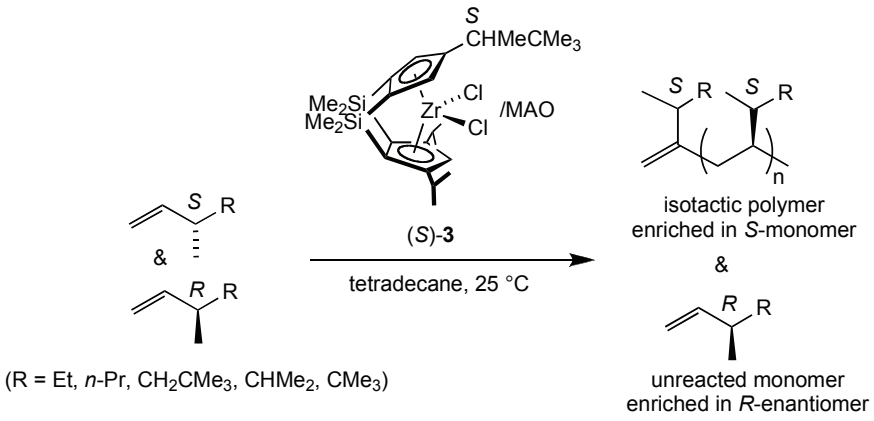

The foundation for this work was the development of an enantiopure version of the highly active C_1-symmetric catalyst, {1,2-$(SiMe_2)_2$(η^5-3,5-$C_5H_1(CHMe_2)_2$)(η^5-4-$C_5H_2(CHMeCMe_3)$]}$ZrCl_2$ (**3**) pioneered by Dr. Chris Levy. CBS reduction of the requisite ketone facilitated the synthesis of enantiopure (*S*)-**3,** and with the aide of Dr. Cliff Baar and a talented graduate student, Dr. Endy Min, a survey of the kinetic resolution of some simple racemic α-olefins was accomplished (Table 0.1).[7] Although selectivity factors ($s = k_{rel} = k_{fast}/k_{slow}$) determined for these reactions were low for most olefins studied, the selectivity factor for 3,4-dimethyl-1-pentene ($s = k_S/k_R = 16$) was within the range of synthetically useful kinetic resolutions (e.g., an *e.e.* of 75% is obtained for a reaction carried out to 50% conversion with $s = 16$).

Table 0.1 Selectivity and activity for the kinetic resolution of racemic α-olefins catalyzed by (*S*)-**3**/MAO.

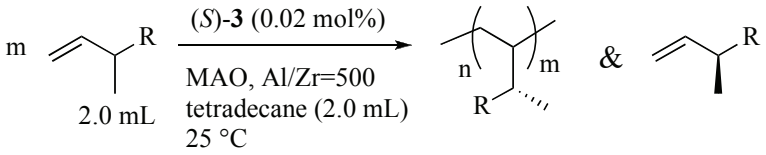

comonomer	TOF	s (k_S/k_R)
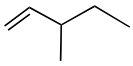	60 (12)	2.6 (0.2)
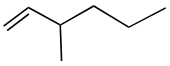	551 (50)	1.8 (0.2)
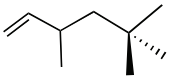	33 (10)	2.1 (0.1)
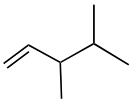	40 (11)	16.8 (0.8)
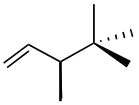	18 (2)	7.6 (0.8)

TOF = $mmol_{chiral\ olefin}/(mmol_{catalyst}*hr)$.

The preference for the catalyst to select for the *S* antipode was rationalized by an enantiomorphic site control mechanism (Scheme 0.3). A feature of C_1-symmetric catalysts such as (*S*)-**3**, is that the polymeryl group tends to reside away from the methyl group on the top cyclopentadienyl (as pictured) by a site epimerization mechanism that encourages olefin insertions to occur from the same side of the zirconocene wedge (see Chapter 2). To avoid unfavorable steric interactions, we rationalized that olefin coordination occurs with the hydrogen on the stereogenic carbon directed toward the zirconocene. In this conformation, *R* antipode coordination would display an unfavorable interaction between the large group of the chiral olefin (e.g. ethyl for 3-methyl-1-pentene) and the isopropyl groups on the bottom cyclopentadienyl group of (*S*)-**3** (as pictured).

Scheme 0.3 Transition states used to rationalize preferential *S* antipode uptake in the kinetic resolutions.

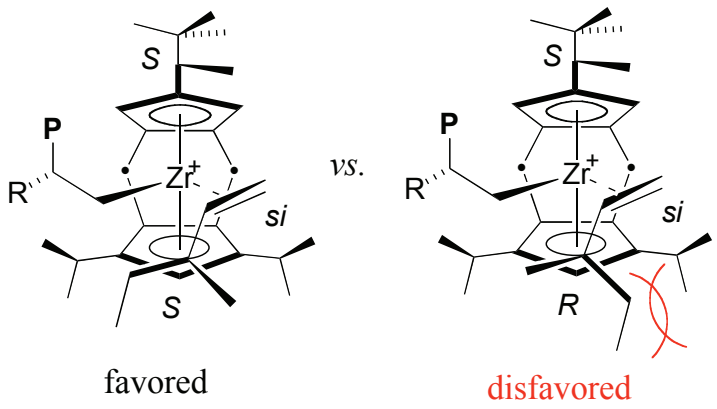

In a valiant synthetic effort, Dr. Endy Min and Dr. Cliff Baar undertook the modification of the bottom cyclopentadienyl (Cp) group of (*S*)-**3**. Unfortunately, these efforts met limited success. Replacement of the isopropyl groups of (*S*)-**3** was possible with other substituents such as 3-pentyl and cyclohexyl, but only modest differences in selectivity were observed.[12] The analogs prepared, however, were arguably sterically similar to the isopropyl groups of (*S*)-**3** because they were connected to the bottom Cp by tertiary carbons. Unfortunately, synthesis of the *tert*-butyl or trimethyl silyl analogs of (*S*)-**3** could not be completed due to either steric congestion or silyl-group migrations. Efforts were made to make the bottom Cp asymmetric, but this synthesis produced diastereomeric zirconocenes that were difficult to isolate and displayed poor activities and selectivities for kinetic resolution of racemic α-olefins.

At the time of my arrival, there were several synthetic and mechanistic questions that deserved attention. First, the model used to explain enantioselection in these catalysts involves direct interaction between the metal center and the chiral monomer. In addition to the chirality at the metal center, however, there exists chirality in the polymer chain end that may affect enantioselection during the reaction, the so-called chain end control. At the time it was unclear if chain end control is an important stereocontrol element, and if it is important whether it works cooperatively or uncooperatively with

enantiomorphic site control. A second point worth consideration for the C_1-symmetric system was whether or not inefficient site epimerization limits the selectivity of the kinetic resolutions. Since the polymerization sites of (*S*)-**3** are pseudo-enantiotopic, one might expect the slow reacting monomer to preferentially react for olefin insertions when the polymeryl group resides on the same side of the methyl group in (*S*)-**3**. Finally, since the synthesis of (*S*)-**3** and its analogs were both long and resulted in modest changes in selectivity, new enantiopure catalysts directed towards the kinetic resolution of racemic α-olefins were desired. The subsequent chapters describe attempts to address each of these questions in the order discussed above.

References and Notes

1. Odian, G. *Principles of Polymerization* Wiley-Interscience: New York, **1991**.

2. (a) Bercaw, J. E. *Bull. Inst. Chem. Academia Sinica*, **1999**, 46, 1; (b) Coates, G. W. *Chem. Rev.*, **2000**, 100, 1223.

3. Grubbs, R. H.; Coates, G. W. *Accts. Chem. Res.*, **1996**, *29*, 85.

4. Irwin, L. J.; Reibenspies, J. H.; Miller, S. A. *J. Am. Chem. Soc.*, **2004**, *126*, 16716.

5. (a) Mehrkhodavandi, P.; Schrock, R. R.; Pryor, L. L. *Organometallics*, **2003**, *22*, 4269; (b) Zhang, Y.; Reeder, E. K.; Keaton, R. J.; Sita, L. R. *Organometallics*, **2004**, *23*, 3512.

6. Harney, M. B.; Zhang, Y.; Sita, L. R. *Angew. Chem., Int. Ed.*, **2006**, *45*, 2400.

7. Baar, C. R.; Levy, C. J.; Min, E. Y.-J.; Henling, L. M.; Day, M. W.; Bercaw, J. E. *J. Am. Chem. Soc.*, **2004**, *126*, 8216.

8. Useful methods for the kinetic resolution of functionalized olefins have been accomplished for: allylic alcohols: (a) Gao, Y.; Hanson, R. M.; Klunder, J. M.; Ko, S. Y.; Masamune, H.; Sharpless, K. B. *J. Am. Chem. Soc.*, **1987**, *109*, 5765; (b) Martin,

V. S.; Woodard, S. S.; Katsuki, T.; Yamada, Y.; Ikeda, M.; Sharpless, K. B. *J. Am. Chem. Soc.*, **1981**, *103*, 6237; (c) Kitamura, M.; Kasahara, I.; Manbe, K.; Noyori, R.; Takaya, H. *J. Org. Chem.,* **1988**, *53*, 708; allylic ethers (d) Adams, J. A.; Ford, J. G.; Stamatos, P. J.; Hoveyda, A. H. *J. Org. Chem.*, **1999**, *64*, 9690; (e) Morken, J. P.; Didiuk, M. T.; Visser, M. S.; Hoveyda, A. H. *J. Am. Chem. Soc.*, **1994**, *116*, 3123; allylic acetates (f) Pamies, O.; Baeckvall, J.-E. *Chem. Rev.*, **2003**, *8*, 3247; and dienes (g) La, D. S.; Alexander, J. B.; Cefalo, D. R.; Graf, D. D.; Hoveyda, A. H.; Schrock, R. R. *J. Am. Chem. Soc.*, **1998**, *120*, 9720.

9. (a) VanNieuwenhze, M. S.; Sharpless, K. B. *J. Am. Chem. Soc.*, **1993**, *115*, 7864;

(b) Hamon, D. P. G.; Tuck, K. L.; Christie, H. S. *Tetrahedron*, **2001**, *57*, 9499;

(c) Christie, H. S.; Hamon, D. P. G.; Tuck, K. L. *Chem. Commun.*, **1999**, 1989.

10. Gardiner, J. M.; Norret, M.; Sadler, I. H. *Chem. Commun.*, **1996**, 2709.

11. Van Veldhuizen, J. J.; Campbell, J. E.; Giudici, R. E.; Hoveyda, A. H. *J. Am. Chem. Soc.*, **2005**, 127, 6877.

12. Min, E. Y.-J., Ph D thesis, California Institute of Technology, **2005**.

CHAPTER ONE

ENANTIOMORPHIC SITE VS. CHAIN END CONTROL IN THE KINETIC RESOLUTION OF RACEMIC α-OLEFINS USING C_1-SYMMETRIC ZIRCONOCENE POLYMERIZATION CATALYSTS

1.1 Abstract

Copolymerization of racemic α-olefins with ethylene and several prochiral α-olefins were carried out in the presence of enantiopure C_1-symmetric *ansa*-metallocene, {1,2-$(SiMe_2)_2$(η^5-3,5-$C_5H_1(CHMe_2)_2$)(η^5-4-C_5H_2((*S*)-$CHMeCMe_3$)]}$ZrCl_2$, (*S*)-**2**, to probe the affect of the polymer chain end on enantioselection for the *R* or *S* α-olefins during the kinetic resolution by polymerization catalysis. Copolymerizations with ethylene revealed that the polymer chain end is an important factor in the enantioselection of the reaction, and that for homopolymerization, chain end control generally works cooperatively with enantiomorphic site control. Results from propylene copolymerizations suggested that chain end control arising from a methyl group at the β-carbon along the main chain can drastically affect selectivity, but its importance as a stereo-directing element depends on the identity of the racemic olefin. Chain end control was also probed by the polymerization of enantioenriched chiral α-olefins in the presence of achiral catalysts, {1,2-$(SiMe_2)_2$(η^5-3,5-$C_5H_1(CHMe_2)_2$)(η^5-C_5H_5)}$ZrCl_2$ (**1**) and {Me_2C(η^5-$C_{13}H_8$)(η^5-C_5H_4)}$ZrCl_2$ (**3**). Selectivity for the olefins studied indicated that chain end control is a small but measurable factor.

1.2 Introduction

Simple chiral olefins in their enantiopure forms (e.g., (*R*)-3-methyl-1-pentene) would potentially be highly versatile substrates for asymmetric synthesis and as precursors to polymeric materials with previously inaccessible optical or physical properties. Thus, efficient routes to such enantiopure alkenes are highly desirable. Most of the methods used to synthesize enantiopure olefins are only suitable for functionalized substrates such as allylic alcohols,[1] allylic ethers,[2] and dienes,[3] which can participate in substrate directed catalysis, primarily through chelation to the catalytically active metal center. There are few examples where simple chiral alkenes can be enantioselectively synthesized or isolated by kinetic resolution of a racemic mixture.[4]

Ziegler-Natta and metallocene catalysts can be highly active and often exhibit very high levels of enantiofacial selectivity in the polymerization of prochiral olefins, producing polymers with well-defined microstructures.[5] Thus, enantiopure Ziegler-Natta or metallocene catalysts might be used as kinetic resolving agents to preferentially polymerize one enantiomer of a chiral alkene, leaving the less reactive enantiomer unreacted and recoverable by simple filtration. Moreover, the optically active polymer, by virtue of enantiopure substituents off the main chain, may likewise be isolated and could display interesting physical, mechanical, and optical properties.

That enantiopure sites in heterogeneous systems can preferentially polymerize a single antipode of a racemic olefin was first demonstrated by Pino in 1955, and later demonstrated by other research groups.[6,7] Because they are more well defined, single-site metallocene catalysts are better candidates for carrying out such resolutions.[8] For example, Ciardelli and coworkers have used enantiopure, C_2-symmetric (*S*,*S*)-{1,2-ethylene-*bis*(tetrahydroindenyl)}ZrX_2/methyl aluminoxane (MAO) to effect the partial resolution of 4-substituted chiral olefins such as 4-methyl-1-hexene (*s* =

k_{faster}/k_{slower} = 1.4).[9] For this system, low catalyst activities prevented the polymerization of α-olefins bearing chiral groups in the 3 position such as 3-methyl-1-pentene. 3-Methyl-1-pentene can be polymerized with other metallocene catalysts, but thus far only with C_s and certain types of unresolved *rac*-C_2-symmetric catalysts, precluding any possible kinetic resolution.[10,11]

We have reported that doubly-bridged *ansa* zirconocene catalyst {1,2-$(SiMe_2)_2$(η^5-3,5-$C_5H_1(CHMe_2)_2$)(η^5-C_5H_5)}$ZrCl_2$ (**1**) activated with MAO polymerize propylene with very high syndiospecificities and with extremely high activities.[12] Modification of this C_s-symmetric catalyst system with a racemic 3,3-dimethyl-2-butyl ("methylneopentyl") substituent has also been accomplished to give the C_1-symmetric zirconocene, {1,2-$(SiMe_2)_2$(η^5-3,5-$C_5H_1(CHMe_2)_2$)(η^5-4-$C_5H_2(CHMeCMe_3)$]}$ZrCl_2$ (**2**).[13]

Kinetic resolution of racemic chiral α-olefins by polymerization was realized using the enantiopure zirconocene precatalyst *(S)*-**2**, and selectivities, $s = k_{faster}/k_{slower} = k_S/k_R$, of 2 to 16 were obtained for several chiral 3-methyl-1-olefins (Scheme 1.1). Isotactic poly(3-methyl-1-pentene) is obtained, and based on the very high melting temperatures (T_m), the other poly(chiral monomers) are also likely isotactic.[14]

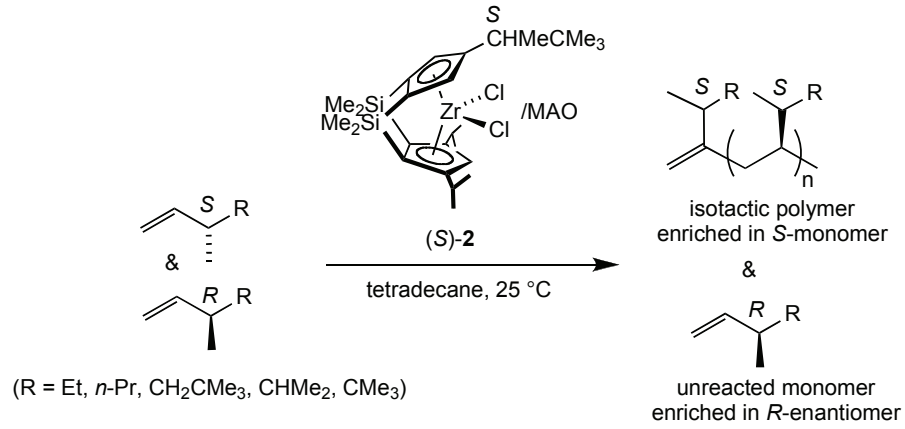

Scheme 1.1 Kinetic resolution of racemic α-olefins using (*S*)-**2**.

Although we attributed the stereoselection for the *S* antipode primarily to enantiomorphic site control, we speculated that the predominantly isotactic polymer is formed by enchainment of monomer at one of the two sites, with site epimerization following each insertion (Scheme 1.2).

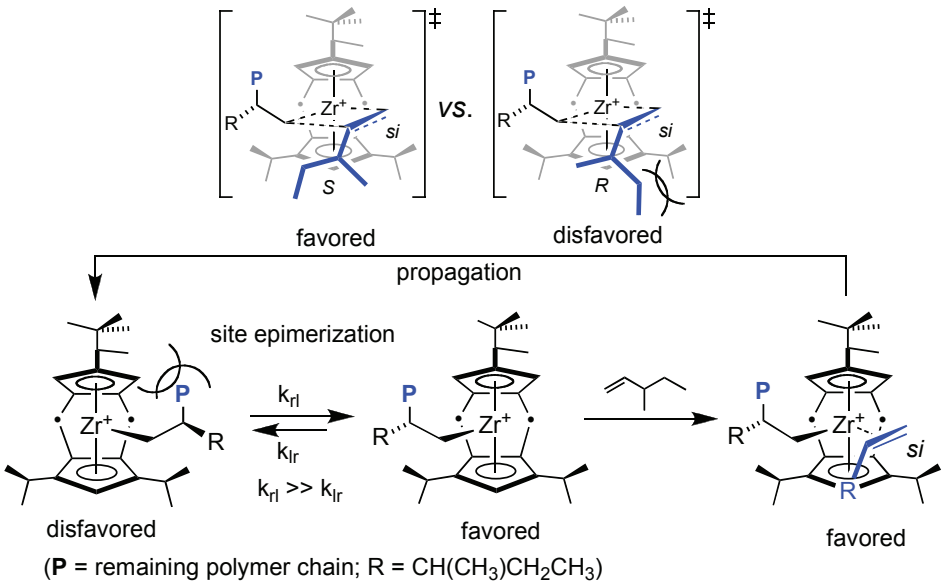

Scheme 1.2 Site epimerization in polymerization catalyzed by (*S*)-**2**.

Although this rationalization appears to reconcile the performance of these catalysts to first order, additional factors that affect stereoselection needed to be addressed. Unlike many catalysts used for kinetic resolutions, polymerization catalysts retain chirality in the polymeryl group attached to the catalyst. Thus, the next enchainment possesses not only the metal asymmetry, but also that from the last inserted monomer (and others farther from the catalytic site). Chiral induction in these reactions can therefore be derived from: (a) the catalyst asymmetry (following enantiomorphic site control statistics[15]), (b) the polymer asymmetry (chain end control following Bernoullian statistics[16]), or, most likely, (c) a combination of the two. Indications that chain end control could dominate enantiomorphic site control under some conditions, especially with 3-substituted monomers, have been reported.[7,10,17] Whereas the catalyst

[{$Me_2C(\eta^5$-$C_{13}H_8)(\eta^5$-$C_5H_4)$}$ZrCl_2$]/MAO (**3**) generates *syndio*tactic polypropylene, Zambelli *et al.* found that it catalyzes the polymerization of 3-methyl-1-pentene to yield "co-*iso*tactic" polymer (Scheme 1.3).[10]

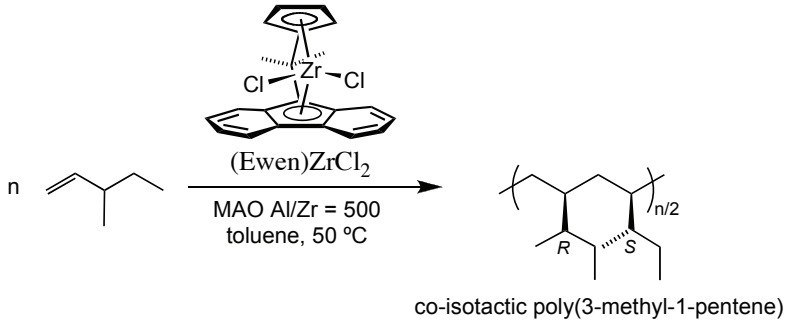

Scheme 1.3 Synthesis of co-isotactic poly(3-methyl-1-pentene) using **3**.

To probe the contribution that chain end control may exert in our kinetic resolutions, we have undertaken copolymerizations of racemic chiral olefins with achiral ethylene or propylene comonomers using (*S*)-**2** as the catalyst. Copolymerization effectively removes chain end control by "running out" the γ-stereocenter with achiral enchainments prior to another enchainment of chiral monomer (Scheme 1.4). Ethylene copolymerization (R' = H) thus isolates enantiomorphic site control as the only source of asymmetric induction. Similar copolymerizations with prochiral olefins such as propylene (R' = CH_3) could reveal the influence on stereocontrol of chirality in the polymer backbone (β-stereocenter) as opposed to the polymer side chain (γ-stereocenter).

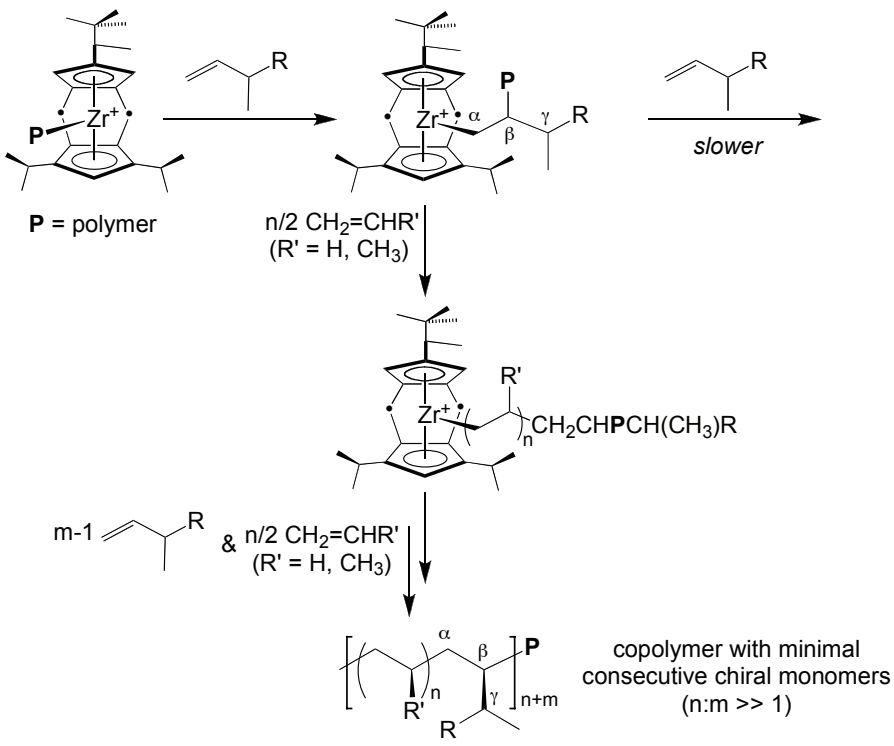

Scheme 1.4 Copolymerization experiments for probing chain end control.

1.3 Results and Discussion

The term "chain end control" is traditionally used to describe generic interactions between the polymer chain end and the incoming olefin that result in stereoregular olefin insertions.[18] In the context of prochiral olefin polymerization (e.g. α-olefin), chain end control refers to the enantiofacial differentiation exerted by the chiral carbon that results from the previously enchained monomer (at the β position in Scheme 1.4). Homopolymers of a chiral 3-methyl-1-ene have two stereocenters per repeat unit, making chain end control multidimensional, likely with a rather complex interplay of side chain (γ) and main chain (β) chirality influencing the choice of chiral monomer enantioface and stereochemistry at the 3-carbon. This complexity is important to recognize at the outset

when attempting to interpret experiments designed to probe chain end control in chiral olefin polymerization.

Ethylene copolymerizations. Results for ethylene copolymerizations along with the corresponding results for homopolymerizations of several chiral olefins, using (*S*)-**2** as precatalyst and MAO as cocatalyst are shown in Table 1.1. To ensure that the polymers contain a minimal number of consecutive chiral repeat units, the copolymerizations were carried out under a constant feed of ethylene. Relative to the previously reported homopolymerizations,[14] aluminum-to-zirconium ratios were reduced from 1000 to 500, and in some cases (entries 5 and 7) the chiral olefin concentration was reduced by addition of tetradecane or toluene. These experimental modifications were necessary to moderate the increased viscosity of the polymer solutions during copolymerization. For several olefins (entries 2 and 6) homopolymerizations were carried out using these experimental modifications, and the selectivities resulting from these control experiments were within experimental error the same (entries 1 and 5, respectively). It is interesting to note that diluting the chiral monomer with toluene increased the activity of the catalyst without affecting the selectivity of the reaction. This increase was found to be general and is attributed to improved solubility of the MAO/zirconocenium cation complex. Thus, the increase in activity is ascribed to an increase in the concentration of catalyst in solution.[19]

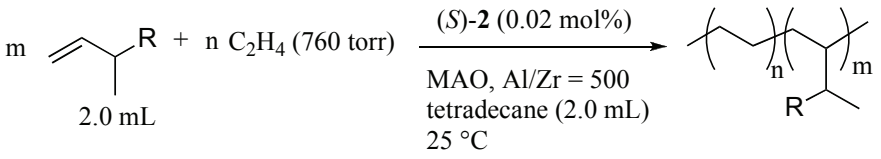

		Homopolymerization		Copolymerization			
entry	**comonomer**	**conv. rate[a]**	***s* = k_S/k_R**	**conv. rate[a]**	***s* = k_S/k_R**	**n:m**	**T_m (°C)[b]**
1	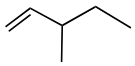	60 (12)	2.6 (0.2)	410 (160)	3.4 (0.1)	6:1	br[c]
2		449[d]	2.6				
3	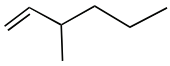	551 (50)	1.8 (0.2)	312 (76)	1.4 (0.1)	7:1	107
4	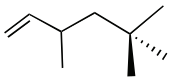	33 (10)	2.1 (0.1)	190 (6)	1.2 (0.1)	11:1	122
5	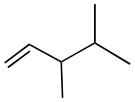	40 (11)	16.8 (0.8)	172 (33)[e]	13 (2)	20:1	119
6		223[f]	15.5				
7	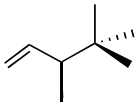	18 (2)[g]	7.6 (0.8)	143 (8)[g]	5.1 (0.9)	7:1	121[h]

[a] conv. rate = $mmol_{chiral\ olefin}/(mmol_{catalyst}*hr)$; [b] T_m for polyethylene = 136 °C. [c] br = broad thermal transition; [d] 1.5 mL toluene, 0.5 mL tetradecane; [e] 4.0 mL tetradeacane; [f] 4.0 mL toluene and 0.5 mL tetradecane; [g] 4.0 mL toluene, 0.5 mL tetradecane, and 300 torr C_2H_4; [h] multiple T_m observed

Table 1.1 Selectivity factors and thermal data in racemic α-olefin/ethylene copolymerizations catalyzed by (*S*)-**2** with corresponding homopolymerization data for comparison.

Because copolymerization yields different selectivity as compared to homopolymerization in every case, albeit in varying degrees, both chain end control and enantiomorphic site control must be significant stereocontrol elements in all of the homopolymerizations studied. Two possible scenarios may be envisioned for homopolymerization of the chiral monomer under such conditions: (1) the stereocontrol elements may work cooperatively, selecting for the same enantiomer, or (2) they may operate uncooperatively, selecting for opposite enantiomers. If chain end control

cooperates with enantiomorphic site control during homopolymerization, then the *s* value appears enhanced for homopolymerization relative to the copolymerization, because the added selectivity arising from the polymer chain end control is essentially absent in the copolymerization experiment. This first scenario appears to be the case for the majority of olefins investigated. However, selectivity for homopolymerization of 3-methyl-1-pentene is less than for copolymerization, suggesting that for this chiral olefin, enantiomorphic site and chain end control work uncooperatively and select for opposite antipodes.

Ethylene copolymer characterization. Our interpretation of the above results assumes that copolymerization effectively eliminates any significant contribution to *s* from chain end control, i.e., that ethylene is incorporated much more frequently than the chiral monomer such that the likelihood of consecutive chiral monomer repeat units is small. Enhanced chiral olefin conversion rates generally observed for copolymerization relative to homopolymerization suggest that this is indeed the case.[20] Migratory insertion of a sterically hindered 3-methyl-substituted α-olefin into the bulkier metal alkyl ({Zr-[$CH_2CH(CHMeR)]_m$…} (R > Me)) for homopolymerization is expected to be slow compared to copolymerization,[21] which involves primarily bulky olefin insertion into less-hindered {Zr-$[CH_2CH_2]_n$-$[CH_2CH(CHMeR)]$-$[CH_2CH_2]_m$…} (R > Me) units.

Additional evidence for a polymer microstructure with few consecutive chiral repeat units is in the thermal behavior of these polymers. Melting temperatures of ethylene/α-olefin random copolymers have been shown to decrease linearly as the concentration of α-olefin is increased in the copolymer. The α-olefin units disrupt the polyethylene crystal lattice by shortening the average methylene sequence length. Consistent with a largely random incorporation of chiral monomer units into the polyethylene, melting temperatures for ethylene/chiral monomer copolymers (Table 1.1) decrease roughly linearly with increasing chiral monomer concentration as shown in

Figure 1.1.[22] It is puzzling, however, that polymer melting points decrease more slowly with increasing comonomer content as compared to simple α-olefin/ethylene copolymers, especially considering that the identity of the α-olefin was reported to have little effect on the melting point of simple α-olefin/ethylene copolymers at a given comonomer concentration.[23,24] While we have no explanation for higher T_m values for the chiral monomer/ethylene copolymers, the linear dependence (Figure 1.1) of T_m with comonomer incorporation is, nonetheless, most consistent with random incorporation.

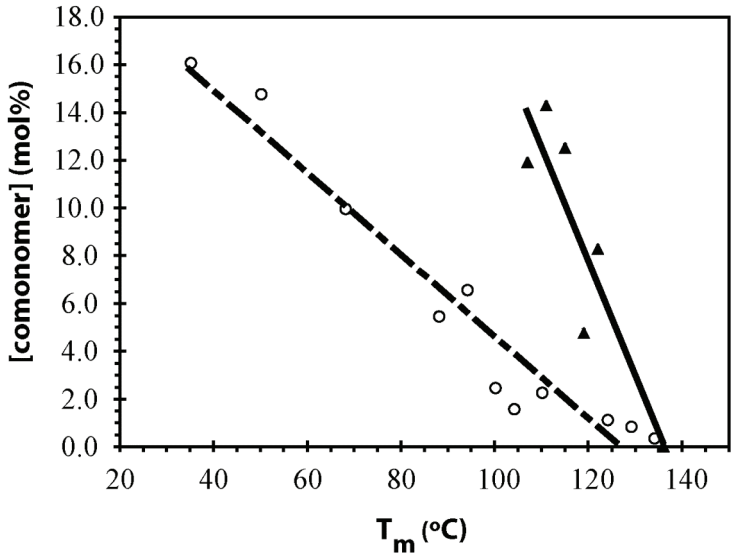

Figure 1.1 Plot of chiral monomer content vs. melting temperature (T_m) in ethylene copolymers of racemic α-olefin/ethylene (▲) and α-olefin/ethylene (○) copolymers.[23] Data for poly(3,4,4-trimethyl-1-pentene-*co*-ethylene) omitted due to multiple melting points likely from MW effects (see experimental section). To illustrate linear trend, data not appearing in Table 1.1 are included.

To further support the blocky nature of these polymers, a sequential nucleation and annealing (SNA) experiment was performed for poly(3,4-dimethyl-1-pentene-*co*-ethylene) using differential scanning calorimetry (DSC). An SNA experiment involves

heating a polymer sample to a temperature above the melting point of the polymer followed by an annealing time. After cooling to room temperature, the polymer sample is again heated and annealed, but this time to a temperature slightly lower than the first cycle. The sequence is repeated incrementally decreasing the temperature until the annealing temperature reaches room temperature. A thermograph is then obtained over the entire annealing range to probe the effect that SNA has on the polymer. Previous investigations revealed that SNA experiments performed on polyethylene encourage aggregation of polyethylene into microcrystalline domains, the melting point of which could be related to the methylene sequence length.[24,25] This correlation was established by measuring the correlation between melting temperatures and methylene sequence length of linear hydrocarbon standards with defined molecular weights. These experiments, therefore, allow for the identification and semiquantification of methylene sequence lengths in the polymer. Thermographs for the poly(3,4-dimethyl-1-pentene-*co*-ethylene) synthesized above with and without SNA appear in Figure 1.2, and the correlation between melting point and methylene sequence length using the relationship previously established[24,25] appears in Figure 1.3. Both Figures 1.2 and 1.3 appear to be bimodal indicating at least two copolymers with different average methylene sequence lengths. Despite this complication, it is clear from Figure 1.3 that there is a negligible amount of short (<10) methylene sequence lengths suggesting that consecutive chiral repeat units in this polymer are unlikely.

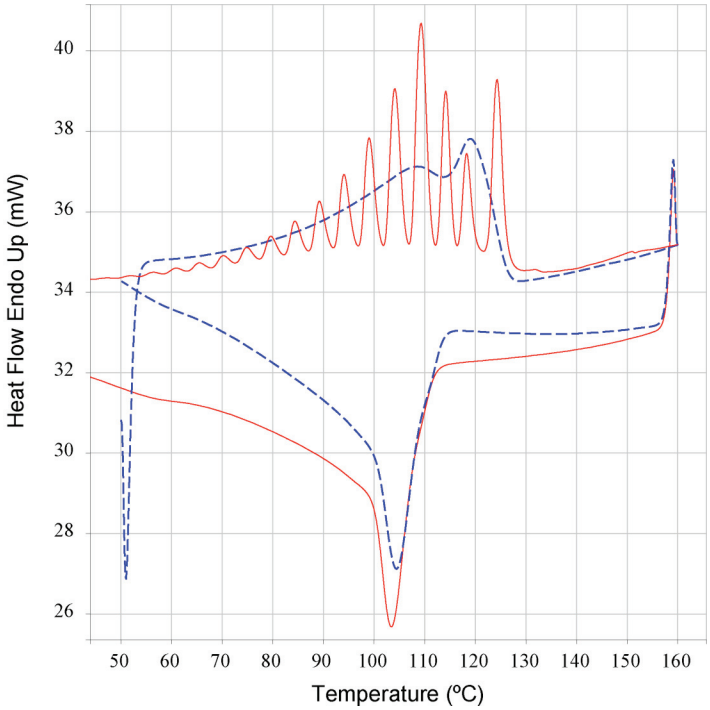

Figure 1.2 DSC thermographs for poly(3,4-dimethyl-1-pentene-*co*-ethylene) with (red, solid) and without (blue, dashed) sequential nucleation and annealing.

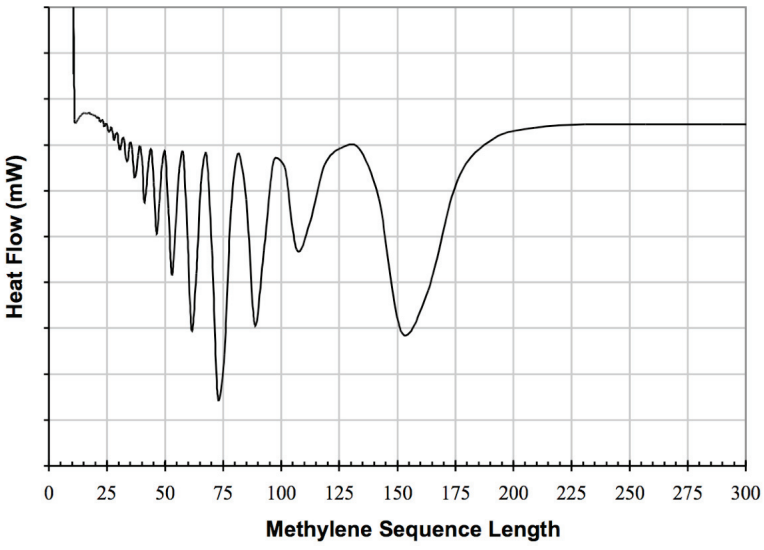

Figure 1.3 Methylene sequence length distribution from SNA analysis of poly(3,4-dimethyl-1-pentene-*co*-ethylene).

The random nature of these copolymers is further substantiated by their ^{13}C NMR spectra. The $^{13}C\{^1H\}$ NMR spectrum for poly(3,4-dimethyl-1-pentene-*co*-ethylene) is shown in Figure 1.4 and the corresponding calculations appear in Table 1.2.[26] Using parameters determined by Lindeman and Adams,[27] chemical shifts may be calculated for a polymer microstructure with and without consecutive 3,4-dimethyl-1-pentene repeat units (see Appendix B). The spectra of these copolymers are more complex, however, due to chirality in both the polymer main and side chain, making the polymer main chain methylene carbons (α, β, γ, etc.), and the side chain methyl carbons (1 and 2') diastereotopic. Unfortunately, Lindeman and Adams' parameters are not available to account for this asymmetry, but the authors note that for such cases calculated chemical shifts are often close to the geometric mean of the experimental chemical shifts, which we do in fact observe as well.

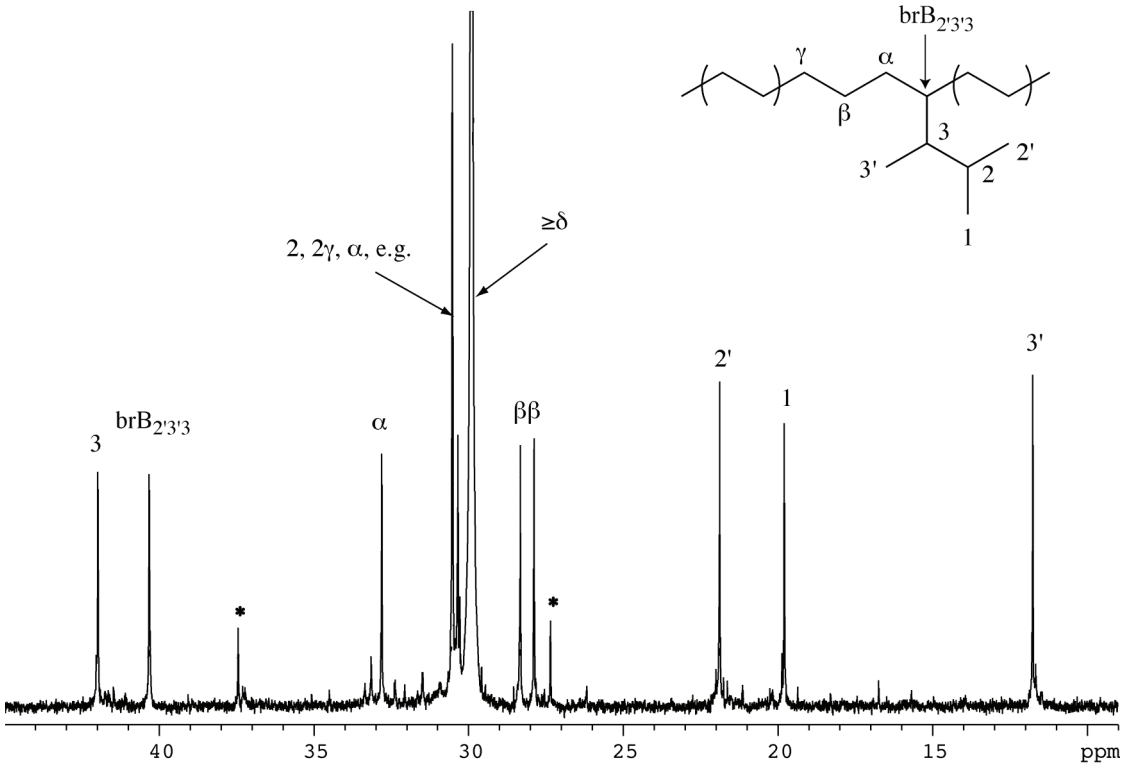

Figure 1.4 $^{13}C\{^1H\}$ NMR spectrum of poly(3,4-dimethyl-1-pentene-*co*-ethylene).

carbon	$B_{2'3'3}$[a]	1,3-$B_{2'3'3}$[b]	1,5-$B_{2'3'3}$[c]	poly(1,3-$B_{2'3'3}$)	observed	assignment	Λ[d]
3'	13.65	13.65	13.65	13.65	11.86	$3'B_{2'3'3}$	1.76
1, 2'	19.63	19.63	19.63	19.63	19.89, 21.98	$1B_{2'3'3}$, $2'B_{2'3'3}$	1.31
β'[e]	N/A	N/A	25.58	N/A	27.45		
β[f]	27.77	27.77	27.70	N/A	27.98, 28.43	$\beta B_{2'3'3}$	0.44
δ	30.00	30.00	30.00	30.00	30.00	$\delta B_{2'3'3}$	0.00
γ	30.21	30.21	30.21	N/A	30.63	$\gamma B_{2'3'3}$	0.08
2	30.71	30.71	30.71	30.71	30.63	$2B_{2'3'3}$	0.42
α	32.03	32.28	32.03	N/A	30.44, 32.91	$\alpha B_{2'3'3}$	0.36
α'	N/A	34.10	32.03	34.60	37.55		
br	39.77	37.95	39.77	36.13	40.43	$brB_{2'3'3}$	0.66
3	41.85	41.98	41.85	42.10	42.09	$3B_{2'3'3}$	0.24

[a] isolated branch; [b] consecutive branches; [c] branches separated by one ethylene unit; [d] Δ = |expt. – calc.| experimental diastereotopic carbons are averaged to get Λ; [e] α' and β' indicate carbons on the polymer chain between branching points; [f] α, β, γ, and δ indicate carbons on the polymer chain adjacent to the branching unit s

Table 1.2 Calculated and observed $^{13}C\{^1H\}$ NMR resonances for poly(3,4-dimethyl-1-pentene-*co*-ethylene).

Calculated ^{13}C NMR shifts for most carbons cannot distinguish between a microstructure with or without consecutive 3,4-dimethyl-1-pentene repeat units. However, the calculated shifts for the branching carbon ("$brB_{2'3'3}$") are sufficiently different to indicate a microstructure without consecutive chiral repeat units. Moreover, the observed spectrum can be completely assigned with fairly good agreement for calculated and experimental ^{13}C shifts (within 1.75 ppm accuracy) for all peaks, assuming a microstructure without consecutive 3,4-dimethyl-1-pentene repeat units, with only two substantial unassigned resonances (those marked with an asterisk in Figure 1.4). These could be attributed the α- and β-methylene carbons connecting a minor fraction of consecutive 3,4-dimethyl-1-pentene repeat units. For such an occurrence, however, multiple resonances would most likely occur due to the diastereotopic nature of such carbons. Alternatively, the resonances marked with an asterix in Figure 1.4 could also be associated with end groups.

$^{13}C\{^{1}H\}$ NMR spectra for the other copolymers presented in Table 1.1 were also measured (See Appendix B). With the exception of poly(3,4,4-trimethyl-1-pentene-*co*-ethylene) all of these spectra resemble that for poly(3,4-dimethyl-1-pentene-*co*-ethylene) and agree with calculations for a polymer microstructure with little evidence for consecutive chiral repeat units (see Appendix B). Because poly(3,4,4-trimethyl-1-pentene-*co*-ethylene) has very bulky side chains, termination occurs much more frequently, and the molecular weight accordingly is low (M_n = 2,688 g/mol). Consequently, the NMR spectrum is complicated by resonances from the polymer chain end, making it difficult to identify resonances associated with a polymer microstructure that contains isolated chiral repeat units. Nonetheless, the similarity of its chiral olefin content to the other higher molecular weight copolymers leads us to believe that it also has isolated chiral comonomer enchainments.

Copolymerization of ethylene with 1,2-bis-^{13}C-3,4-dimethyl-1-pentene. In a final attempt to prove that the ethylene copolymers synthesized above do not contain consecutive chiral repeat units, copolymerization of 1,2-bis-^{13}C-3,4-dimethyl-1-pentene (**4**) with ethylene was attempted (Scheme 1.5). The ^{13}C NMR for a copolymer with isolated **4** subunits would consist of two doublets from $^{1}J_{C1\text{-}C2}$ coupling, while additional $^{1}J_{C\text{-}C}$ coupling is expected for copolymer containing consecutive **4** subunits.

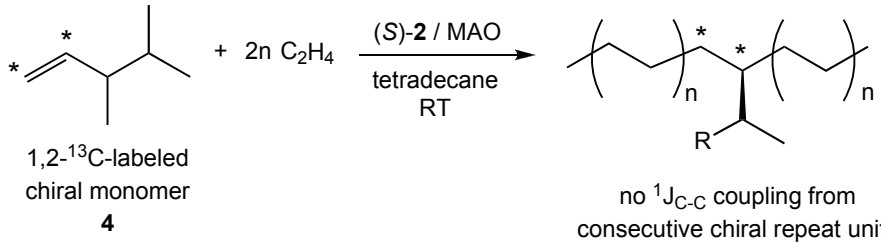

Scheme 1.5 Copolymerization of 1,2-^{13}C-3,4-dimethyl-1-pentene (**4**) with ethylene.

In order to accomplish this task, a short and efficient route to **4** was desired. A possible route became evident when Vitagliano and coworkers reported that the

dicationic platinum π-complex **5** served as a catalyst for the conversion of 2-methyl-2-butene and ethylene to 3,4-dimethyl-1-pentene.[28] Reproduction of these results was satisfactorily accomplished (see Appendix A), and we successfully synthesized doubly ^{13}C-labeled olefin **4** in modest yield using $^{13}C_2H_4$ (Scheme 1.6). Modest yields were likely due to the small-scale distillation required for the purification of **4** and not to any limitation from the catalysis (i.e., unselective reaction). Incorporation of the ^{13}C label at C_1 and C_2 in **4** was confirmed by ^{1}H and ^{13}C NMR spectroscopy as well as an appropriate isomer shift in the IR spectrum (See Experimental Section). The primary limitation being the cost of the $^{13}C_2H_4$, this route could be a general and efficient route to 1,2-^{13}C-labeled α-olefins, which to our knowledge have never been synthesized before.

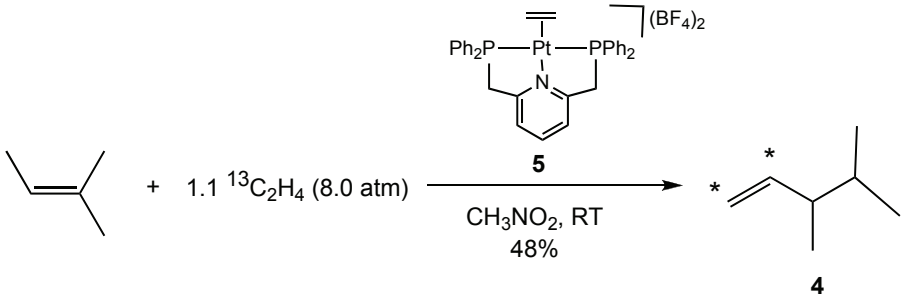

Scheme 1.6 Synthesis of **4** using **5**.

Because economics dictated that only small amounts of **4** could be synthesized, the ethylene copolymerization experiment had to be scaled down. This turned out to be quite problematic due to mass transfer issues. Polymerizations carried out at one quarter the scale in the same glassware used for polymerizations reported in Table 1.1 resulted in low chiral olefin conversion. With appropriately scaled glassware, chiral olefin incorporation was observed but selectivity factors were typically lower (i.e., $s = 9$ for 3,4-dimethyl-1-pentene copolymerization). Nevertheless, homopolymerization of **4** (s = 14.2) and ethylene copolymerization (s = 6.6) were carried out. Although the spectrum for poly(**4**) (Figure 1.5) was unexpectedly simple, the resonances observed were distinct

compared to those observed for poly-(3,4-dimethyl-1-pentene-*co*-ethylene) (Figure 1.4). To our disappointment, the spectrum for poly(**4**-*co*-ethylene) was very complicated (Figure 1.6). Resonances from isolated and consecutive **4** units are obvious as well as many resonances that are absent in Figures 1.4 or 1.5. We tentatively assigned these resonances to end groups or low molecular weight oligomers that resulted from mass transfer issues. This assignment is supported by molecular weight data, which indicate unusually low molecular weights (MW_n = 3,233 g/mol compared to 15,618 g/mol for unlabeled copolymer) and unusually broad polydispersities (PDI = 8.31 compared to 6.95 for unlabeled copolymer). Unfortunately, mass transfer issues could never be resolved for the small-scale reactions.

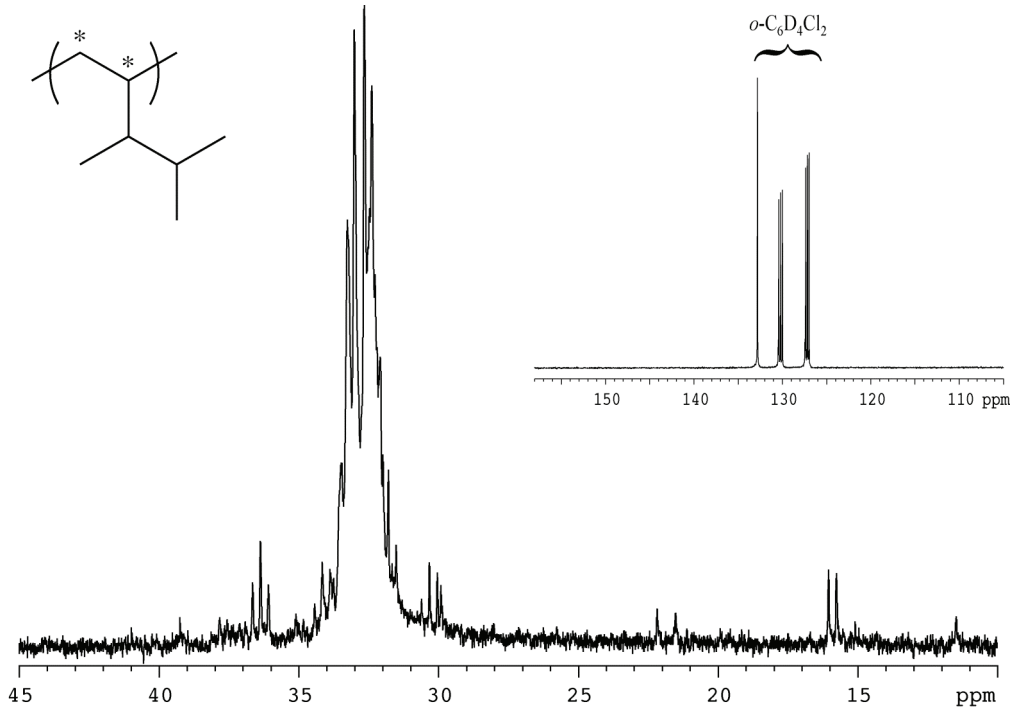

Figure 1.5 $^{13}C\{^{1}H\}$ NMR spectrum of poly(**4**).

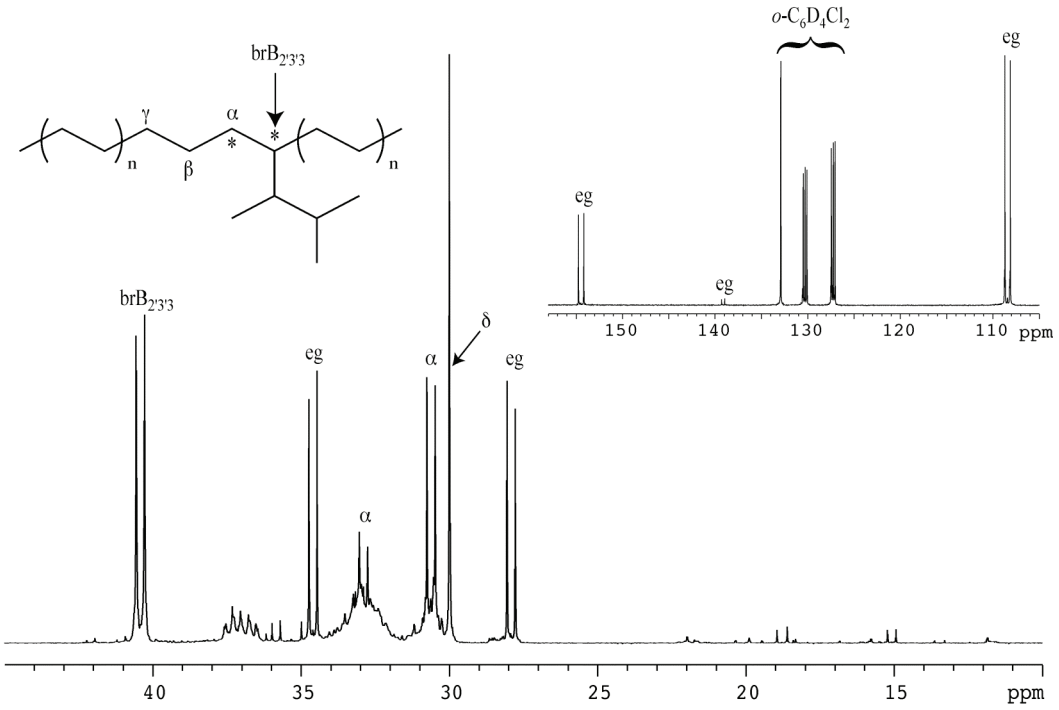

Figure 1.6 $^{13}C\{^{1}H\}$ NMR spectrum of poly(**4**-*co*-ethylene); eg = end group.

Propylene copolymerizations. Propylene copolymerizations with chiral α-olefins have also been carried out (Scheme 1.4, R' = CH_3) to probe how chain end control originating from methyl-substituted main chain (β) chirality affects enantioselectivity. Results for propylene copolymerizations are given in Table 1.3. Due to increased viscosity of the propylene copolymers in tetradecane, the propylene copolymerizations were carried out with added toluene. As noted above, toluene accelerates the homopolymerization of several olefins (*i. e.* entries 1 *vs*. 2 and 5 *vs*. 6 in Table 1.1). Thus, we are unable to strictly compare chiral conversion rates for propylene copolymerizations to those for the corresponding homopolymerizations. Nevertheless, it can be seen from entries 1, 4, and 5 (Table 1.3), with comparisons to data from Table 1.1, that propylene copolymerization rates with added toluene are slightly faster for the propylene copolymerization relative to the homopolymerization. Presumably this trend

holds true for the other monomers, implying that the chiral monomers insert primarily into {Zr-[$CH_2CHMe]_n$-[$CH_2CH(CHMeR)$]-[$CH_2CHMe]_m$} (R > Me) repeat units.[21]

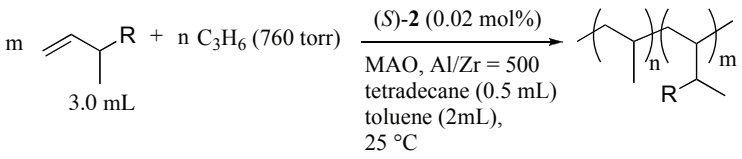

			copolymerization			
entry	**olefin**	**s = k_S/k_R[a]**	**conv. rate[b]**	**s = k_S/k_R**	**n:m**	**T_m (°C)[c]**
1	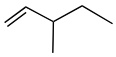	2.6 (0.2)	854 (58)	1.9 (0.1)	10:1	88
2	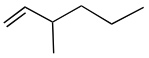	1.8 (0.2)	780 (90)	2.0 (0.2)	8:1	br[d]
3	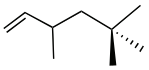	2.1 (0.1)	526 (56)	1.6 (0.2)	14:1	92
4	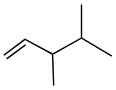	16.8 (0.8)	266 (37)	3.9 (0.3)	16:1	92
5	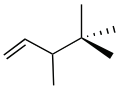	7.6 (0.8)	137 (1)[e]	1.0 (0.1)	21:1	99

[a] homopolymerization (Table 1.1); [b] conv. rate = $mmol_{chiral\ olefin}/(mmol_{catalyst}*hr)$; [c] T_m polypropylene = 109 °C; [d] br = broad melting transition; [e] 2.0 mL olefin, 4.0 mL toluene and 400 torr C_3H_6

Table 1.3 Selectivity factors and thermal data in racemic α-olefin/propylene copolymerizations catalyzed by (*S*)-**2**/MAO.

Selectivity factors in propylene copolymerizations were generally lower compared to homopolymerizations. This is particularly pronounced for propylene copolymerizations involving 3,4-dimethyl-1-pentene and 3,4,4-trimethyl-1-pentene (entries 4 and 5) with the latter monomer showing no selectivity during copolymerization. Furthermore, selectivity factors in propylene copolymerizations differ from the corresponding ethylene copolymerizations. These data suggest that polymer main chain chirality can be an important source of stereoinduction during homopolymerization, the magnitude of which is dependent on the identity of the olefin.

Propylene copolymer characterization. In order to establish a copolymer with randomly inserted chiral repeat units, studies analogous to those carried out for ethylene copolymers were undertaken for the propylene copolymers.

$^{13}C\{^{1}H\}$ NMR spectra were obtained for all the polymers in Table 1.3 (see Appendix C). Unlike ethylene copolymers, modeling of the ^{13}C NMR spectra for isolated comonomer incorporation in the propylene copolymers was difficult due to pentad sequences and overlapping peaks. However, the pentad sequences from propylene segments in the methyl region of the spectra are unobstructed by resonances from chiral olefin comonomer, and are informative for probing how chiral comonomer incorporation affects the propylene enantiofacial selectivity (Table 1.4).

entry	comonomer	[*mmmm*]	[*mmmr*]	[*rmmr*]	[*mmrr*]	[*xmrx*]	[*rmrm*]	[*rrrr*]	[*rrrm*]	[*mrrm*]	E[a]	B[b]
1	---	60.6	14.0	0.0	10.8	5.3	0.9	0.0	3.0	5.5	1.00	8.77
2	3-methyl-1-pentene	63.3	12.5	4.2	10.3	4.9	0.0	0.0	1.0	3.9	0.64	6.68
3	3-methyl-1-pentene	64.1	12.6	2.3	10.8	3.6	0.7	0.7	0.9	4.4	0.80	8.46
4	3,5,5-trimethyl-1-hexene	60.7	14.0	2.2	11.0	5.2	0.0	1.0	1.1	4.7	0.84	8.02
5	3,4-dimethyl-1-pentene	53.5	15.4	0.0	13.8	7.3	1.9	0.0	2.0	6.1	0.70	4.18
6	3,4,4-trimethyl-1-pentene	50.2	17.5	0.0	12.0	8.0	1.9	1.3	2.3	6.7	0.94	5.79

[a] enantiomorphic site control triad test, E = 2[*rr*]/[*mr*]. [b] Bernoulian chain end control triad test B = 4[*mm*][*rr*]/[*mr*].

Table 1.4 Pentad sequences and triad tests for racemic α-olefin/propylene copolymerizations.

When propylene alone is polymerized under the same conditions, the enantiomorphic model triad test[15,29] indicates enantiomorphic site control is operative for this catalyst system (E = 1.01). Interestingly, incorporation of chiral monomers perturbs the polypropylene pentad distribution away from enantiomorphic site control (E < 1).[30] Moreover, chain end control is not the dominant stereocontrol element that dictates the

polypropylene tacticity for the copolymerizations, because the Bernoullian triad test (B) established by Bovey[16] to identify polymers operating under chain end control shows that B is much greater than unity. Thus, whereas the copolymerizations appear to operate closer to enantiomorphic site control for enchainments of propylene units, the situation is more complex, and, once again, an interplay of chain end and enantiomorphic site control mechanisms appear to be at work for the poly(chiral monomer-*co*-propylene) as well as for the poly(chiral monomer) homopolymers.

Similar to the ethylene copolymers, the copolymers from Table 1.3 have depressed melting temperatures relative to polypropylene synthesized under the same reaction conditions. Unlike the polyethylene copolymers, however, melting points for these copolymers do not decrease linearly with increasing comonomer content. Coutinho et. al. have reported that, unlike polyethylene copolymers, melting temperatures for isotactic propylene-copolymers depend on the nature of the comonomer. This tendency arises from differing sizes of the side chains that allow for more or less facile molecular motions and consequently different melting temperatures.[31]

Whereas this observation may explain our findings, we believe that the side chains in these copolymers create similar sized defects. An alternative explanation for the observed thermal behavior is that incorporation of a chiral comonomer changes the concentration of stereoerrors in the copolymer, which also has an effect on the melting temperature by shortening the isotactic sequence length. De Rosa, Resconi, and coworkers recently reported that there is a linear dependence between melting point and [*rr*] stereo-errors for metallocene-prepared isotactic polypropylenes with predominately *rr* stereoerrors.[32] Similar to polyethylene copolymers, randomly inserted *rr* stereoerrors shorten the average isotactic sequence ($<L_{iso}>$) in the polymer, creating smaller crystalline domains and consequently lower melting temperatures. Considering the findings of De Rosa and Resconi, it is reasonable to assume that

incorporation of chiral monomer and [rr] stereoerrors, both of which shorten the average isotactic sequence, will decrease the melting temperature of the polymer. Therefore, the melting temperatures for the copolymers in Table 1.3 should be dependent on both [*rr*] and [chiral monomer], and if these are randomly inserted, their individual effects could be additive, giving rise to a linear dependence of T_m with [*rr*] + [chiral monomer].

Shown in Table 1.5 and plotted in Figure 1.7 are melting temperatures *vs.* [*rr*] + [chiral monomer] for the polymers from Table 1.3, together with the isotactic polymers studied by De Rosa and Resconi. As we hypothesized, there is indeed a roughly linear relationship between T_m and the sum of [*rr*] and [chiral monomer]. While the correlation agrees reasonably well with De Rosa and Resconi's results, in general the copolymers have higher melting points than the polypropylene samples at a given [*rr*] + [chiral monomer]. This discrepancy could be due to a significant number of chiral monomer repeat units existing as polymer chain ends. Because chain ends do not shorten the methylene sequence length, the melting points do not reflect their presence. The data point that best illustrates this explanation is the anomalous data point, poly(3,4,4-trimethyl-1-pentene-*co*-propylene). Because this monomer is very bulky, chain termination occurs more rapidly after comonomer insertion, leading to lower molecular weights and longer methylene sequence lengths at a given chiral monomer concentration. Nevertheless, the linear trend suggests chiral monomer insertions are random, and considering the small [chiral olefin] in the polymer, is indirect evidence that there are few consecutive chiral repeat units in the copolymer.

Entry	[*rr*]	[chiral olefin]	[*rr*]+ [chiral olefin]	T_m (°C)	$<L_{iso}>$
1	8.5	0.0	8.5	109	10.8
2	4.8	8.9	13.7	88	6.3
3	6.0	5.2	11.2	101	7.9
4	6.8	6.5	13.3	92	6.5
5	8.0	5.8	13.8	92	6.2
6	10.3	4.5	14.8	99	5.7

$<L_{iso}>$ = (100-[*rr*]-[chiral olefin])/([*rr*]+[chiral olefin])

Table 1.5 Dependence of average isotactic sequence ($<L_{iso}>$) on temperature. Entries are the same as in Table 1.4.

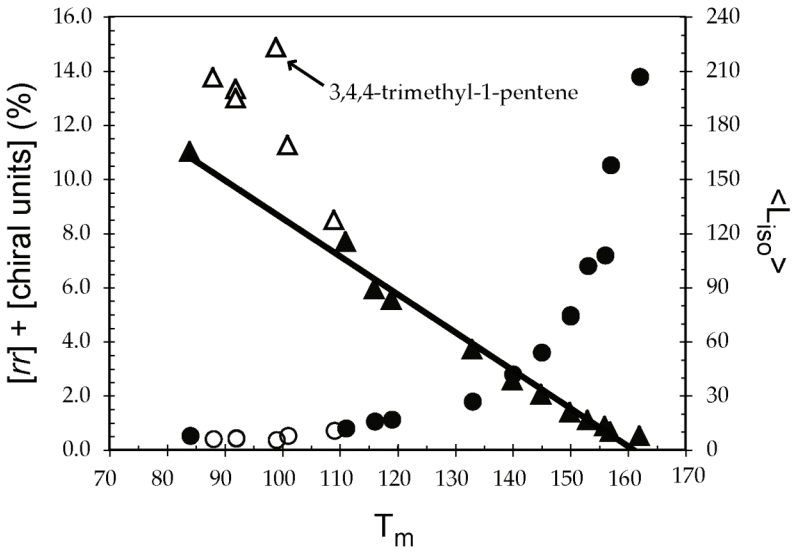

Figure 1.7 Melting temperature (T_m) vs. [*rr*] + [comonomer] (▲) and $<L_{iso}>$ (●) in propylene and chiral monomer/propylene copolymers, respectively. Open symbols indicate data points from this study while shaded symbols indicate data from the literature.

Other α-olefin copolymerizations. Since results in Table 1.3 suggest that polymer main chain chirality (β chirality) could be an important stereodetermining factor, a brief examination of bulkier α-olefin copolymerizations was undertaken to probe steric effects. Since comonomers larger than butene are liquids at room temperature, polymerizations were carried out using a large excess of achiral comonomer to insure a low probability of consecutive chiral repeat units in the copolymer. In initial experiments, 1-pentene was copolymerized with 3-methyl-1-pentene in a 10:1 ratio using (*S*)-**2** as the catalyst. Because the absolute concentration of 1-pentene was high in the reaction, however, complete polymerization of 1-pentene occurred with minimal 3-methyl-1-pentene incorporation.

To better understand the relative reactivity of the two monomers, the reactivity ratios (r_{3M1P}, r_{1P}) were determined by monitoring conversion for both monomers during polymerizations at various monomer ratios according to the method of Fineman and Ross (Appendix D).[33] Since reactivity ratios are defined by the relative rates of self-propagation to cross-propagation (i.e., $r_x = k_{xx}/k_{xy}$ where k_{xx} and k_{xy} indicate insertion rate constants for monomer x inserting after itself or monomer y, respectively) they indicate the likelihood of consecutive repeat units with $r > 0$ indicating a propensity for homopolymerization and a $r < 0$ indicating a propensity to insert comonomer. In this case, the reactivity ratios were determined to be $r_{3M1P} = 0.07$ and $r_{1P} = 23$, which suggests a large kinetic preference for consecutive 1-pentene polymerization with occasional 3-methyl-1-pentene insertions. Due to this large kinetic difference, 1-pentene/3-methyl-1-pentene copolymerizations were carried out with an *excess* of 3-methyl-1-pentene in hopes that olefin concentration would compensate for the large kinetic discrepancy. Unfortunately, the initial concentrations of 1-pentene required were too low to observe any amount of 3-methyl-1-pentene conversion before complete 1-pentene conversion precluding any accurate measure of selectivity. A constant feed of 1-pentene at low

concentrations would be required to ensure efficient incorporation of 3-methyl-1-pentene. Unfortunately, a constant feed of 1-pentene is not achievable with the current experimental setup. A similar problem was encountered when 4-methyl-1-pentene/3,4-dimethyl-1-pentene copolymerizations were attempted.

To compensate for the significant difference in rates, 3-methyl-1-butene/3-methyl-1-pentene copolymerizations were attempted. Reactivity ratios for this olefin combination indicate that the two monomers have a slight kinetic preference for homopolymerization ($r_{3M1P} = 2$, $r_{3M1B} = 2$). Without other evidence, these reactivity ratios suggest that there is a good possibility for consecutive chiral olefin incorporation. Considering that establishing the polymer microstructure would be difficult by either ^{13}C NMR or by melting temperatures, copolymerization attempts using this olefin were also abandoned.

Polymerization of enantioenriched olefins with achiral catalysts. Until now all of the experiments designed to probe chain end control have tried to isolate enantiomorphic site control. Alternatively, chain end control can be isolated from enantiomorphic site control if enantioenriched olefin is polymerized with an achiral catalyst (Scheme 1.7). Enantioinduction in these experiments can only come from the chiral polymer chain, so any change in *e.e.* can be attributed to chain end control.

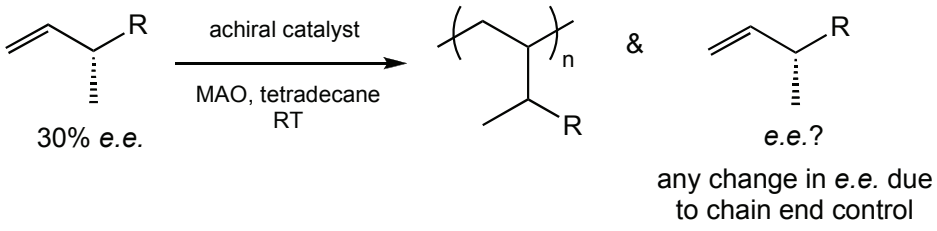

Scheme 1.7 Enantioenriched olefin polymerization experiments to probe chain end control.

Requisite for these experiments is access to enantioenriched olefins. Enantiopure (*S*)-3-methyl-1-pentene has previously been synthesized in our group using a classical route,[34] but other enantiopure olefins have yet to be synthesized. Attempts were made to synthesize enantiopure (*R*)-3,4-dimethyl-1-pentene using the Myers' pseudoephedrine chiral auxialliary[35] as outlined in Scheme 1.8. Amidation of isovaleryl chloride followed by alkylation proceeded smoothly and with high selectivity to give amide **6**, but removal of the chiral auxiliary with $LiAlH(OEt)_3$ was problematic due to the instability of aldehyde **7**. An alternate route to (*R*)-3,4-dimethyl-1-pentene, which avoids 7, involves platinum catalyzed conversion of 2-methyl-2-butene to (*rac*)-3,4-dimethyl-1-pentene (*vide supra*) followed by kinetic resolution of the racemic olefin by polymerization with (*S*)-**2** (Scheme 1.9). Synthesis of enantiopure 3,4-dimethyl-1-pentene on the multi-gram scale was easily accomplished with this route yielding 3,4-dimethyl-1-pentene (>95% *e.e*). This synthesis marks the first preparative scale reaction accomplished for the kinetic resolution by polymerization technique.

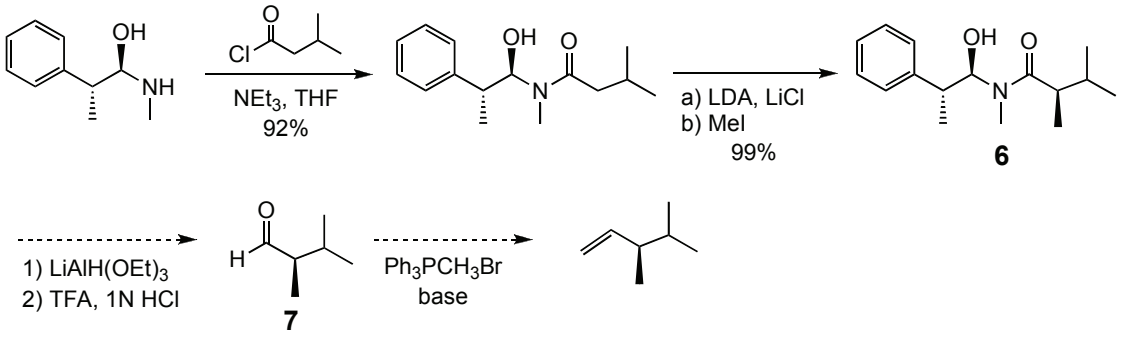

Scheme 1.8 Attempted synthesis of (*R*)-3,4-dimethyl-1-pentene using a chiral auxiliary.

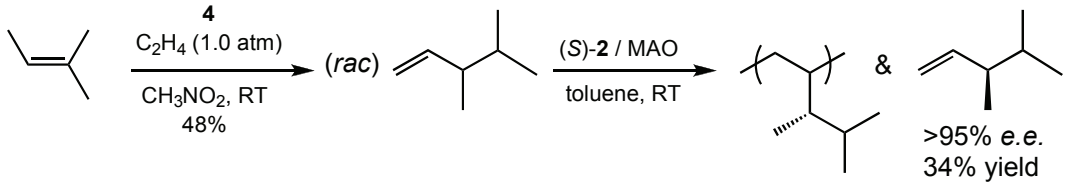

Scheme 1.9 Synthesis of (*R*)-3,4-dimethyl-1-pentene using kinetic resolution.

After an initial screen of some common achiral catalysts, it was determined that **1** and **3** were active for racemic α-olefin polymerizations. The results of 3-methyl-1-pentene (30% *e.e.* *S*-enriched) and 3,4-dimethyl-1-pentene (33% *e.e.* *R*-enriched) polymerizations with these catalysts appear in Table 1.6. In every case studied, erosion of *e.e.* in the starting material was observed, suggesting a slight preference for the monomer antipode present in excess. This result was somewhat surprising considering Zambelli's finding that **3** polymerizes 3-methyl-1-pentene to give co-*iso*-tactic polymer (*vide supra*). When starting from enantioenriched olefin, enhancement in *e.e.* would be expected for such a microstructure because *R* and *S* monomer antipodes are equally incorporated in the polymer. We currently do not have an explanation for this discrepancy.

Given the initial and final *e.e.*'s of the monomer ($e.e._0$ and $e.e._t$, respectively) and the conversion of the reaction (C), selectivity factors can be determined using equation (1.1).[36]

$$s = \frac{k_{fast}}{k_{slow}} = \frac{\ln\left(\frac{(1+e.e._t)*(1-C)}{(1+e.e._0)}\right)}{\ln\left(\frac{(1-e.e._t)*(1-C)}{(1-e.e._0)}\right)} \qquad (1.1)$$

As shown in Table 1.6, selectivity factors are low for both 3-methyl-1pentene and 3,4-dimethyl-1-pentene indicating that chain end control does not impart a significant amount of stereoinduction during the polymerization. Qualitatively, these results are consistent with the copolymerization experiments that appear above because in those studies similar *s*-factors were found for ethylene copolymerizations and homopolymerizations. It is interesting to note that despite their similar steric structure, **1** and **3** display different *s*-factors for enantioenriched 3-methyl-1-pentene (entries 2 and 4). This observation suggests that chain end control is partly dependent on catalyst structure even for *achiral*

catalysts, which illustrates how intimately connected the catalyst and polymer chain end are during kinetic resolution.

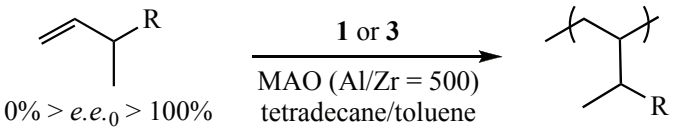

0% > *e.e.*$_0$ > 100%

olefin	entry	catalyst	T(ºC)	TOF[a]	*e.e.*$_0$ (%)	*e.e.*$_t$ (%)	*s* (k_{fast}/k_{slow})	k_{fast}
	1	**1**	25	28	0	2	1.0	N/A
	2	**1**	25	35(9)	32	25	1.3 (0.1)	S
	3	**3**	30	5	0	0	1.0	N/A
	4	**3**	30	6	33	12	2.0	S
	5[b]	**1**	25	8	0	2	1.0	N/A
	6[b]	**1**	25	53(5)	30	14	1.7 (0.1)	R

[a] turnover frequency = $mmol_{ol}/(mmol_{cat}*h)$. [b]observed dimer in the GC.

Table 1.6 Selectivity factors in enantioenriched olefin polymerizations catalyzed by achiral catalysts **1**/MAO and **3**/MAO.

1.4 Conclusions

Copolymerizations of chiral monomers with ethylene and propylene highlight the importance of chain end control for the kinetic resolution of chiral α-olefins by homopolymerization. The experimentally determined selectivity factors (*s*) for homopolymerization and for the two copolymerizations are summarized in Table 1.7. The various stereocontrol elements (enantiomorphic site ("Zr*"), polypropylene main chain chirality (β_{C3}), and enchained chiral monomer's main chain (β_{cm}) and side chain (γ) chirality) that determine *s* operate in a coupled fashion, each reinforcing or opposing the others (Scheme 1.10). Thus, the situation is complex, and effects of the individual stereocontrol elements are not simply additive, nor are they multiplicative. Copolymerization of chiral monomers with ethylene provides the simplest stereocontrol process: enantiomorphic site control in the absence of the other control elements. The

substituted 1-pentenes (entries 1, 4 and 5, Table 1.7) appear to give better *s* values than do the substituted 1-hexenes (entries 2 and 3). The subtle influence of an additional methylene on the ability of the catalyst site to choose between antipodes of monomer is striking, particularly for 3-methyl-1-pentene (*s* = 3.4 (0.1)) *vs*. 3-methyl-1-hexene (*s* = 1.4 (0.1)), where the latter might be expected to display the larger, not smaller *s* value, due to a greater size difference (3-*n*-propyl *vs*. 3-methyl as compared to 3-ethyl *vs*. 3-methyl). Hence, there is no clear correlation of high *s* with steric effects for this (admittedly limited) set of chiral 3-methyl-1-alkenes.

		Copolymerization		**Homopolymerizaion**
		C_2H_4	C_3H_6	
entry	**olefin**	$s = k_S/k_R$	$s = k_S/k_R$	$s = k_S/k_R$
1	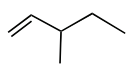	3.4 (0.1)	1.9 (0.1)	2.6 (0.2)
2	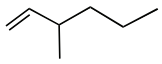	1.4 (0.1)	2.0 (0.2)	1.8 (0.2)
3	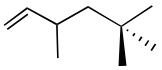	1.2 (0.1)	1.6 (0.2)	2.1 (0.1)
4	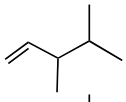	13 (2)	3.9 (0.3)	16.8 (0.8)
5	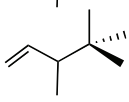	5.1 (0.9)	1.0 (0.1)	7.6 (0.8)

Table 1.7 Summary of selectivity factors in copolymerization experiments.

The copolymerizations of chiral monomers with propylene present new surprises. Under the influence of Zr*, and β_{C3} and/or $\beta_{C3'}$, the 1-hexenes once again behave differently from the 1-pentenes: the former displaying slight increase in *s*, as compared with the corresponding values of *s* for ethylene copolymerizations, and the latter decreases in *s*, ranging from modest (entry 1) to sizeable (entries 4 and 5). While one might expect the largest chain end effects for the bulkiest α-olefin, the magnitude of the effect on *s* of a β methyl group on the polymeryl chain was quite unexpected. Compared

to polymerizations operative under exclusive enantiomorphic site control, the stereoselection is greatly reduced for 3,4-dimethyl-1-pentene (*s* decreasing from 13 to 3.9, entry 4) and is essentially completely offset for 3,4,4-trimethyl-1-pentene (*s* decreases from 5.1 to 1.0, entry 5).

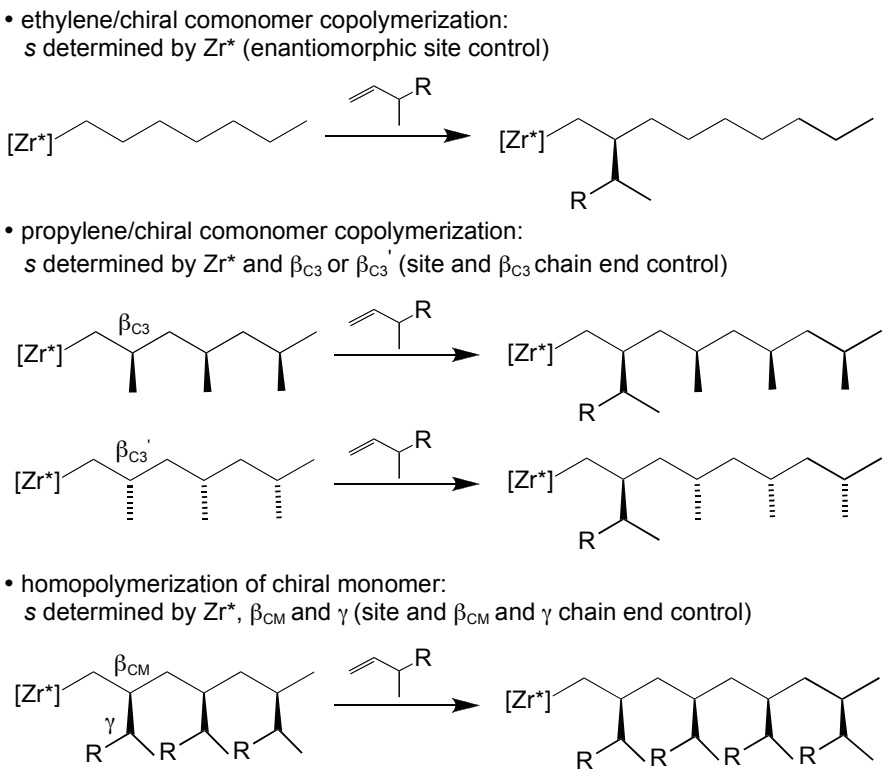

Scheme 1.10 Illustration of different stereocontrol elements during kinetic resolution by polymerization.

Finally, the most complex set of control elements operates during homopolymerization of chiral monomers. The combination of Zr*, β_{CM} and γ control elements, again unexpectedly, more closely resembles the enantiomorphic site control alone (ethylene copolymerizations) than it does Zr* and β_{C3} and/or β_{C3}'(propylene copolymerizations). Hence, the *s* values for homopolymerizations of all five 3-methyl-1-alkenes are fairly close to those obtained under enantiomorphic site control alone. Perhaps most unexpected is that the combination of β_{CM} and γ with Zr* more than

restores the stereoselection lost by combining β_{C3} and/or β_{C3}' with Zr* for 3,4-dimethyl-1-pentene and 3,4,4-trimethyl-1-pentene (entries 5 and 6). The effects on the 1-hexenes, on the other hand, are quite modest (entries 2 and 3). As noted earlier, the combination of β_{CM} and γ with Zr* leads to a slight reduction in *s* for 3-methyl-1-pentene, when compared with the *s* obtained when Zr* operates alone for this chiral monomer.

Whereas these data illustrate the complexity of the interplay of the various stereocontrol elements operating in these kinetic resolutions of chiral 3-methyl-1-alkenes using catalyst system (*S*)-**2**/MAO, we can draw the following conclusions: (1) Enantiomorphic site control (Zr*) chooses for the same antipode with roughly the same stereoselection (*s*) in ethylene/chiral monomer copolymerizations as does the combination of Zr*, β_{CM}, and γ chain end control, implicating enantiomorphic site control as an important stereocontrol element.

(2) With the exception of 3-methyl-1-pentene, enantiomorphic site control and the β_{CM} and γ chain end control elements select for the same antipode of chiral monomer in the homopolymerizations, and hence the *s* values are larger for homopolymerizations than for ethylene/chiral monomer copolymerizations.

(3) For copolymerizations with propylene, where Zr* and chain end control arising from a β-methyl group combine, surprisingly large offsetting effects on *s* are found for the alkenes having the sterically most demanding 3-substituents. The addition of β_{CM} and γ to Zr* more than restores the stereoselection lost by the combination of β_{C3} and/or β_{C3}' with Zr* for these two olefins.

(4) Whereas successful kinetic resolution (*s* > 10) is observed with 3,4-dimethyl-1-pentene, there are no clear correlations between the structure of the chiral olefin and the value of *s*, so that the guiding principles for design of a practical and general C_1-symmetric catalyst for kinetic resolutions by polymerization of chiral

monomers are not yet apparent. A successful and *general* strategy for kinetic resolution of chiral α-olefins will likely require a much larger enantiomorphic site control than that exhibited by (*S*)-**2**.

1.5 Experimental Section

General methods. All air- and/or moisture sensitive compounds were manipulated using standard high-vacuum line, swivel frit assembly (see swivelfrit.mov for a demo), Schlenk and cannula techniques or in a glove box under nitrogen atmosphere as described previously.[37] Argon, ethylene, and propylene were purified by passage through columns of MnO on vermiculite and activated 4 Å molecular sieves. All solvents and reagents were stored under vacuum over sodium benzophenenone ketyl, titanocene, lithium aluminum hydride, or calcium hydride prior to use. Unless otherwise stated α-olefins were purchased from Chemsampco. 2-methyl-2-butene, 2,3-dimethyl-2-butene, isovalaryl chloride, lithium aluminum hydride, and pseudoephedrine were purchased from Aldrich and were used without further purification. 1,2-^{13}C-ethylene was purchased from Cambridge Isotopes and was used without further purification. Methylaluminoxane (MAO) was purchased from Albemarle, and all volatiles were removed *in vacou* at 150 ºC overnight. It was found to be essential that all Me_3Al was removed from the MAO (See Chapter 2). Polymerization catalysts **1**,[12] (*S*)-**2**,[14] and **3**[38] were synthesized as described previously. Platinum complex **5** was synthesized by a modified literature procedure (See Appendix A).[28] Enantiopure 3-methyl-1-pentene was synthesized as described previously.[34]

NMR spectra of small molecules were obtained on a Varian Mercury spectrometer operating at 300 MHz for ^{1}H and 75 MHz for ^{13}C{^{1}H}. ^{13}C{^{1}H} NMR spectra of polymers were obtained at 100–120 ºC on a Varian Inova spectrometer operating at 125 MHz using an acquisition time of 3 s, a relaxation delay of 6 s, a sweep

width of 3000 Hz, and a 90º pulse angle. Spectra and line listings for all the polymers appear in Appendices B and C along with calculations for possible polymer microstructures for polyethylene copolymers.

Differential Scanning Calorimetry (DSC) thermographs were obtained on a Perkin Elmer DSC-7 using the Pyris software package for data analysis. The melting temperature and enthalpy were calibrated by standard substance indium. The polymers (7-8 mg) were heated to 130 ºC at 40 ºC/min. and held there for 5 minutes to erase thermal history. To induce crystallization, the polymer sample was cooled to 25 ºC at 20 ºC/min and heated to 160 ºC at the same rate. Finally, the samples were cooled to RT at 10 ºC/min and heated to 160 ºC at the same rate. Crystallization and melting temperatures were obtained from the thermographs during this last cycle. Sequential nucleation and annealing (SNA) experiments were performed following the temperature program outlined in Figure 1.8 and analyzed by heating sample from 0 ºC to 160 ºC at 10 ºC/min followed by cooling at the same rate. Data obtained from the heating curve was correlated to methylene sequence length in the same fashion as reported previously.[24]

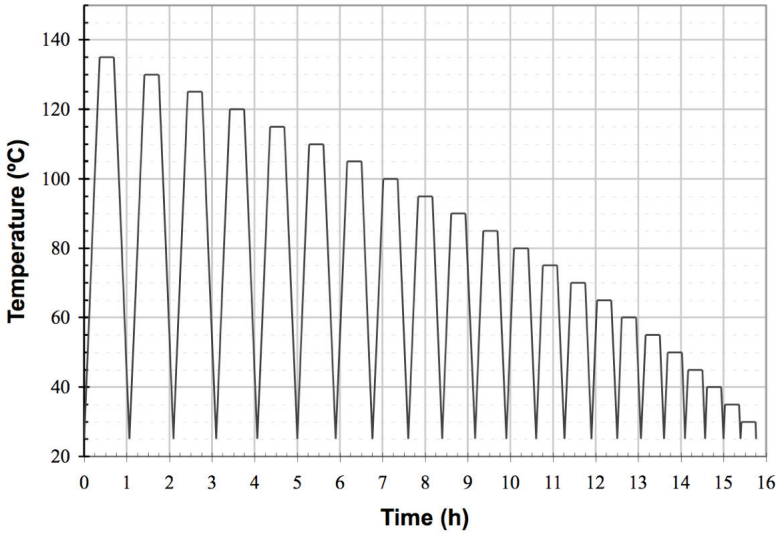

Figure 1.8 Diagram of sequential nucleation and annealing (SNA) temperature program.

Gas chromatographs (GC) were obtained on an Agilent 6890 gas chromatograph using a 30 m by 0.25 mm polysiloxane "HP-5" column from Agilent technologies for chiral monomer conversions and 30 m by 0.25 mm γ-cyclodextrin trifluoroacetyl "Chiraldex TA" column from Advanced Separations Technology for enantioassays. A summary of the GC methods for each monomer as well as observed retention times appear in Appendix E.

BP provided molecular weight analysis of the polymers by GPC using a Waters 2000 instrument. Measurements were carried out at 139 ºC in 1,2,4-trichlorobenzene running at 1 mL/min. Molecular weights and distributions were determined using a refractive index detector relative to polypropylene standards.

A summary of the molecular weight data as well as $^{13}C\{^{1}H\}$ NMR spectra and DSC thermographs appear in Appendices B and C for ethylene and propylene copolymers, respectively.

Synthesis of 1,2-bis-^{13}C-3,4-dimethyl-1-pentene, 4. A thick-walled 100 mL Schlenk tube equipped with a stir bar was charged with **5** (80 mg, 0.092 mmol) and evacuated. Nitromethane (0.75 mL) and 2-methyl-2-butene (3.0 mL, 2.0 g, 28 mmol) were added to the tube by vacuum transfer at –78 ºC. 1,2-^{13}C-ethylene (750 mL, 31 mmol) was condensed onto the biphasic reaction mixture at –180 ºC. The vessel was sealed and slowly brought to RT where it stirred for 1 day. A small amount of Pt^0 was observable after this reaction time. The volatile liquids were isolated by vacuum transfer, and the hydrocarbon phase was purified by spinning band fractional distillation to give a colorless liquid. NMR spectra of the nonvolatile liquid displayed dimerization products with no ^{13}C enriched resonances. The distillate was passed through a small plug of activated alumina to remove any traces of nitromethane. The alumina was washed with tetradecane (2 mL), and the small amount of product that remained on the alumina was

isolated by vacuum transfer from the tetradecane solution and combined with the rest of the colorless product (1.306 g, 46%). ^{1}H NMR (300 MHz, $CDCl_3$, 25ºC): δ = 0.84 (d, ^{3}J = 2.4 Hz, 3H, $CH(CH_3)_2$), 0.87 (d, ^{3}J = 2.4 Hz, 3H, $CH(CH_3)_2$), 0.96 (dd, ^{3}J = 6.9, 5.0 Hz, 3H, CH_3), 1.53 (m, 1H, $CH(CH_3)_2$), 1.96 (m, 1H, $CH(CH_3)$), 4.92 (dm, ^{1}J = 169 Hz, 1H, *cis*-$^{13}CH_2{}^{13}CH$), 4.98 (dm, ^{1}J = 140. Hz, 1H, *trans*-$^{13}CH_2{}^{13}CH$), 5.73 (dm, ^{1}J = 149 Hz, 1H, $^{13}CH_2{}^{13}CH$). $^{13}C\{^{1}H\}$ NMR (75 MHz, $CDCl_3$, 25 ºC): δ = 17.04 (CH_3), 19.9 ($CH(CH_3)_2$), 32.9 ($CH(CH_3)_2$), 44.3 (d, ^{1}J = 42 Hz, $CHCH_3$), 113.4 (d, ^{1}J = 69 Hz, $^{13}CH_2{}^{13}CH$), 143.4 (d, ^{1}J = 69 Hz, $^{13}CH_2{}^{13}CH$). IR($CDCl_3$): ν(cm^{-1}): 3077 (s, ^{13}C-H), 2960 (bs), 2874 (s), 1638 (s, $^{13}C=^{13}C$), 1456 (bs), 1418 (s), 1368 (s), 1260 (bs).

Synthesis of *N*-((1R,2R)-1-hydroxy-1-phenylpropan-2-yl)-*N*,3-dimethyl-butanamide. On the Schlenk line, pseudoephedrine (39.6168g, 239.8 mmol) was combined with triethyl amine (40.0 mL, 29.1 g, 288 mmol) and THF (850 mL) in a 2 L 2-neck flask. In a 500 mL 2-neck flask isovaleryl chloride (32.4 mL, 31.8 g, 264 mmol) was combined with THF (150 mL). At 0 ºC, the isovaleryl chloride solution was cannulated onto the amide solution. A white precipitate formed immediately. The reaction was stirred for 30 minutes then water (250 mL) was added to the reaction, the addition of which caused the precipitate to disappear. Ethyl acetate (500 mL) and brine (500 mL) were added to the reaction. The organic layer was washed three times with brine (500 mL). The organic layer was isolated and dried over sodium sulfate. The solvent was removed and the crude product was recrystallized from hexanes at -20 ºC. The white product was filtered, washed three times with cold hexanes (20 mL) and dried *in vacou* overnight. Yield = 54.745 g (92%). The ^{1}H NMR spectrum was consistent with the spectrum previously reported for the desired product.[35]

Synthesis of (*R*)-*N*-((1*R*,2*R*)-1-hydroxyl-1-phenylpropan-2-yl)-*N*,2,3-trimethylbutanamide (6). Under argon, lithium chloride (55.006 g, 1.30 mol) and di-

*iso*propyl amine (69 mL, 49.3g, 0.488 mol) were combined with THF (800 mL) in a 2 L 2-neck flask equipped with a 250 mL addition funnel. *N*-((1R,2R)-1-hydroxy-1-phenylpropan-2-yl)-*N*,3-dimethyl-butanamide (53.102g, 0.213 mol) and THF (500 mL) were combined in a 500 mL 2-neck flask. At -78 ºC, *n*-butyl lithium (280 mL of 1.6 M in hexanes, 0.45 mol) was added dropwise to the 2 L flask. After the addition, the mixture was brought to 0 ºC for 5 minutes and returned to -78 ºC (LDA solution). The solution containing *N*-((1R,2R)-1-hydroxy-1-phenylpropan-2-yl)-*N*,3-dimethyl-butanamide was cannulated onto the LDA solution and stirred at -78 ºC for 45 minutes followed by an additional 45 minutes at 0 ºC. At 0 ºC, methyl iodide (53 mL, 121g, 0.85 mol) was added dropwise to the reaction. The mixture was stirred for 1 h at which time aqueous ammonium chloride (500 mL) and diethyl ether (200 mL) were added. The aqueous layer was washed three times with diethyl ether (500 mL). The organics were combined, dried over sodium sulfate, and concentrated down. The yellow oil was purified by silica gel column chromatography (1:1 hexanes:acetone) to give a pale yellow oil. Yield = 55.426 g (99%). The ^{1}H NMR spectrum was consistent with the spectrum previously reported for **7**.[35] GC analysis indicated an 88% *d.e.*

Synthesis of (*rac*)-3,4-dimethyl-1-pentene. Platinum complex **5** (0.9212g, 1.06 mmol) was charged in a 250 mL flask. 2-methyl-2-butene (100 mL, 66 g, 940 mmol) and nitromethane (11 mL) were vacuum transferred onto the **5**. The reaction was backfilled with ethylene (1 atm) and was allowed to stir for 2 d. The volatiles were vacuum transferred into a 200 mL flask to give a biphasic mixture. The less dense layer was isolated and distilled by Vigarau column fractional distillation to give a colorless liquid that was 95% pure as determined by GC and ^{1}H NMR spectroscopy, the major byproduct being nitromethane. *Note: Polymerizations attempted with this purity of monomer were completely inhibited by the small amount of nitromethane.* The product was filtered over freshly dried alumina to remove all traces of nitromethane. Yield = 50.65g (55%). The

^{1}H NMR spectrum is consistent with an authentic sample of 3,4-dimethyl-1-pentene. ^{1}H NMR (300 MHz, CDCl3, 25 ºC): δ = 0.84 (d, ^{3}J = 2.4 Hz, 3H, CH(C*H*$_3$)$_2$), 0.87 (d, ^{3}J = 2.4 Hz, 3H, CH(C*H*$_3$)$_2$), 0.96 (d, ^{3}J = 7.2 Hz, 3H, CH(C*H*$_3$)), 1.53 (m, 1H, C*H*(CH$_3$)$_2$), 1.96 (m, 1H, C*H*(CH$_3$)), 4.92 (m, 1H, *cis*-C*H*$_2$CH), 4.96 (m, 1H, *trans*-C*H*$_2$CH), 5.73 (m, 1H, CH$_2$C*H*).

Synthesis of (*R*)-3,4-dimethyl-1-pentene. In the glove box, MAO (1.4312g, 24.7 mmol) and tetradecane (2.3713g) were placed in a 100 mL flask equipped with a stir bar and a 180º Kontes valve. (*S*)-**2** (0.02 g, 0.04 mmol) was added to a 10 mL Strauss flask. On the high vacuum line, (*rac*)-3,4-dimethyl-1-pentene (12.0 mL, 8.38 g, 85.3 mmol) and toluene (12.0 mL) were vacuum transferred onto the MAO/tetradecane mixture and toluene (3.0 mL) was vacuum transferred onto the (*S*)-**2**. After being allowed to stir for 1 h, an aliquot was taken for GC analysis for a t = 0 data point. Under positive argon pressure, the catalyst solution was rapidly introduced to the reaction mixture by syringe. The mixture immediately turned pale yellow. The reaction was monitored by periodic GC analysis of small aliquots using tetradecane as the internal standard. After 7 h the reaction was 66% complete. The reaction was stopped by vacuum transferring the volatiles and quenching the MAO by slow addition of acidic methanol (10% v/v HCl(aq)). The yield was determined from GC calibration curves of 3,4-dimethyl-1-pentene in toluene. An enantioassay was performed on the volatiles in the fashion described below and analyzed by chiral GC. Yield = 34%, *e.e.* = 96%.

Synthesis of (*rac*)-3,4,4-trimethyl-1-pentene. This olefin was prepared in an analogous fashion to 3,4-dimethyl-1-pentene except 2,3-dimethyl-2-butene (45 mL, 32g, 380 mmol), **4** (0.561 g, 0.643 mmol), and nitromethane (5 mL) were used and the reaction was stirred at room temperature under ethylene (760 torr) for 4 d. Unlike 3,4-dimethyl-1-pentene synthesis, complete conversion of the starting material was not observed by GC. Distillation of the volatiles was possible without any residual

nitromethane to give a colorless liquid 98% pure by ^{1}H NMR with the only observable impurity being 2,3-dimethyl-2-butene. Yield = 29.4 g (69%). The ^{1}H NMR was consistent with the spectrum of an authentic sample of 3,4,4-trimethyl-1-pentene. ^{1}H NMR (300 MHz, CDCl3, 25 ºC): δ = 0.85 (s, 9H, C(C*H*$_3$)$_3$), 0.94 (d, ^{3}J = 6.9 Hz, 3H, CH(C*H*$_3$)), 1.90 (m, 1H, C*H*(CH$_3$)), 4.92 (m, 1H, *cis*-C*H*$_2$CH), 4.96 (m, 1H, *trans*-C*H*$_2$CH), 5.77 (m, 1H, CH$_2$C*H*).

Generic copolymerization procedure. In the glove box, MAO (0.15 g, 2.6 mmol) and the tetradecane internal standard (2.0 g), were placed in a 10 mL Schlenk flask equipped with a stir bar and a side-arm which could be isolated from the flask by a stopcock. On the high vacuum line, racemic α-olefin (2.0 mL) was vacuum transferred onto the MAO/tetradecane and stirred for 30 minutes under ethylene or propylene (760 torr). In some cases different amounts of reagents were used, and toluene was sometimes added by vacuum transfer (See Tables 1.1 and 1.2). An aliquot was removed and analyzed by GC for a t = 0 data point. Under positive ethylene/propylene pressure, (*S*)-**2** was added to the reaction via the side arm as a toluene solution (0.5 mL, 5 μmol). For reactions run at ethylene or propylene pressures less than 760 torr, the reaction vessel was sealed and the manifold evacuated. The Schlenk flask was then introduced to the appropriate pressure and regulated with a Fisher/Porter valve. The reaction was stopped by removing an aliquot for GC analysis then rapidly frozen in a dry ice/acetone bath. The volatiles were collected by vacuum transfer, and an enantioassay was performed as described previously[27] and outlined below. Selectivity factors and monomer conversion rates were determined as an average of three separate polymerizations per chiral monomer/achiral monomer combination and appear in Tables 1.1 and 1.3.

Generic copolymerization procedure for liquid comonomers. In the glove box, MAO (0.2 g, 15 mmol) and tetradecane (2.0 g) were loaded in a 10 mL Schlenk flask equipped with a stir bar and a sidearm, which could be isolated from the flask by a

stopcock. On the high vacuum line, the racemic α-olefin (2 mL) and the appropriate amount of achiral olefin were vacuum transferred onto the reaction flask. The mixture was stirred for 30 minutes. An aliquot was removed and analyzed by GC for a t = 0 data point. (*S*)-**2** was introduced by syringe as a toluene solution (0.5 mL, 3 μmol). Olefin conversion could be monitored by periodic GC analysis of aliquots. Reactivity ratios were determined from conversion of the two olefins at t = 5 minutes. The reactions were stopped after conversion of the racemic olefin reached 25%–80%. Vacuum transfer and enantioassay were performed as described for the gaseous copolymerization reactions.

Determination of enantiomeric excess from recovered monomer. Some of the volatiles recovered from the polymerization (0.150 g) were combined with $RuCl_3(H_2O)_3$ (0.025 g, 0.096 mmol) and $NaIO_4$ (1g, 4.68 mmol) in a 20 mL scintillation vial equipped with a small stir bar. Carbon tetrachloride (5 mL), acetonitrile (5 mL), and water (6 mL) were added to the vial. The vial was sealed with a Teflon-lined cap and stirred for one day. The mixture was centrifuged for 5 minutes and the organic layer was separated and washed twice with aqueous sodium thiosulfate (6 mL). The organics were isolated and concentrated down until approximately 0.1 mL remained containing the organic acid (Note: this is particularly important for 3-methyl-1-pentene enantioassays because acetonitrile and methyl 2-methylbutanoate overlap in the gas chromatograph). Methyl esters of the organic acids were obtained with the addition of 10% BF_3/MeOH solution (4 mL) and heating the sealed vial to 50 ºC for 10 minutes. After cooling to room temperature, water (8 mL) was added to the mixture. Hexanes (2 mL) was added to the vial to extract the methyl ester. The organic layer was isolated and dried over magnesium sulfate before being analyzed by chiral GC (see Appendix E).

Polymer purification. A solution of HCl/methanol (10% v/v) was added to the reaction to quench the MAO. The polymer slurry was collected and the volatiles removed. The remaining residue was dissolved in toluene or chlorobenezene (50 mL)

and precipitated into MeOH (1.8 L). The precipitate was isolated and washed three times with MeOH (20 mL). The polymer was dried *in vacou* at room temperature overnight.

Comonomer content was estimated in two ways: from integrating the ^{13}C NMR spectra (see Appendices B and C) and from polymer weight measurements based on GC conversion and the polymer mass. The comonomer content obtained from NMR analysis was ≤5 mol% different from polymer weight measurements. Due to overlapping peaks and pentad sequences involving comonomer, comonomer content for polypropylene copolymers could not be estimated from the polymers' NMR spectra.

Nomenclature for copolymers. The ^{13}C resonances for ethylene copolymers are named according to the nomenclature proposed by Usami and Takayama.[39] The nomenclature consists of two parameters: (1) a number or Greek letter identifying a specific carbon on or near the polymer branch (#B_s), and (2) a descriptor of the type of polymer branch(es) of x length which is (are) closest to the specified carbon (#B_x). Numeric prefixes are used to identify carbons on the polymer branch with C_1 being the last carbon of the branch. Greek letters are used as prefixes to describe carbons on the main polymer chain with α describing the carbon closest to the branch. Branching carbons are identified with the prefix *br*. For example, $1B_3$ and βB_3 describe the last carbon of a three-carbon branch and the second carbon from the branching carbon of the three-carbon branch in the polymer main chain, respectively (see Figure 1.9).

For carbons that are between two branches, an additional descriptor is added to describe the relative relationship between the two branches. The carbons between the two branches are indicated with primed Greek letters. For example, the carbons adjacent to the branching carbon in between two 4-carbon branches separated by an ethylene unit would be described as $1,4\alpha'B_4$ (See Figure 1.9).

Because it is necessary to describe branches on branches to identify all the carbons in the polymer microstructures encountered in this study, an addition to the nomenclature was introduced. Primed numbers indicate one-carbon branches on the carbon of the longest branch from the main chain. For example, the methyl group in the 3 position of 3-methyl-1-pentene when incorporated in a polymer chain would be described as $3'B_{3'3}$ (two carbons from the monomer are in the polymer main chain and, therefore, do not appear in the nomenclature to describe the branch). See Figure 1.9.

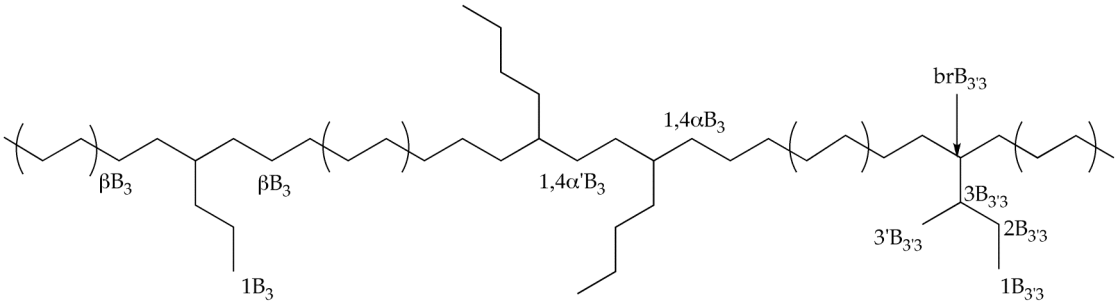

Figure 1.9 Illustration of nomenclature for copolymers.

Polyethylene. Yield = 0.789 g. T_m = 136 ºC, ΔH_m = 112.5 J/g, T_c = 114 ºC, ΔH_c = -111.9 J/g. M_n = 185,043, M_w = 552,720, M_w/M_n = 2.99. $^{13}C\{^1H\}$ NMR (125 MHz, *o*-dichlorobenzene-d_4, 120 ºC): δ = 30.00 (CH_2).

Poly(3-methyl-1-pentene-*co*-ethylene). GC analysis of recovered monomer gave: *e.e.* = 41.9% (C = 50.5%), $s = k_S/k_R = 3.53$. Polymer yield = 2.089 g (14.7 mol% 3-methyl-1-pentene by mass, 10.4% by NMR). T_m = broad thermal transition. M_n = 10,639, M_w = 46,168, M_w/M_n = 4.34. $^{13}C\{^1H\}$ NMR (125 MHz, *o*-dichlorobenzene-d_4, 120 ºC): δ = 12.41 ($1B_{3'3}$), 12.86 ($1,3\text{-}1B_{3'3}$), 15.66 ($3'B_{3'3}$), 27.23 ($2B_{3'3}$), 28.34 ($\beta B_{3'3}$), 28.54 ($\beta B_{3'3}$), 30.00 ($\geq\delta B_{3'3}$), 30.47 ($\gamma B_{3'3}$), 30.54 ($\gamma B_{3'3}$), 30.96 ($\alpha B_{3'3}$), 32.25 ($\alpha B_{3'3}$), 32.76 ($1,3\text{-}\alpha B_{3'3}$), 37.56 ($1,3\text{-}brB_{3'3}$ and $1,3\text{-}3B_{3'3}$), 37.63 ($3B_{3'3}$), 42.88 ($brB_{3'3}$).

Poly(3-methyl-1-hexene-*co*-ethylene). GC analysis of recovered monomer gave: *e.e.* = 14.7% (C = 54.2%), $s = k_S/k_R = 1.46$. Polymer yield = 2.148 g (12.0 mol% 3-

methyl-1-hexene by mass, 10.4% by NMR). T_m = 107 ºC, ΔH_m = 0.5 J/g, T_c = 93 ºC, ΔH_c = -6.3 J/g. M_n = 15,584, M_w = 79,133, M_w/M_n = 4.34. $^{13}C\{^1H\}$ NMR (125 MHz, *o*-dichlorobenzene-d_4, 100 ºC): δ = 14.74 ($1B_{4'4}$), 16.01 ($4'B_{4'4}$), 21.16 ($2B_{4'4}$), 28.34 ($\beta B_{4'4}$), 28.51 ($\beta B_{4'4}$), 30.00 ($\geq\delta B_{4'4}$), 30.46 ($\gamma B_{4'4}$), 30.51($\gamma B_{4'4}$), 30.78 ($\alpha B_{4'4}$), 32.07 ($\alpha B_{4'4}$), 35.01 ($4B_{4'4}$), 36.90 ($3B_{4'4}$), 42.96 ($brB_{4'4}$).

Poly(3,5,5-trimethyl-1-hexene-*co*-ethylene). GC analysis of recovered monomer gave: *e.e.* = 10.8% (C = 49.3%), $s = k_S/k_R$ = 1.38. Polymer yield = 2.478 g (8.2 mol% 3,5,5-trimethyl-1-hexene by mass, 4.6 % by NMR). T_m = 122 ºC, ΔH_m = 11.3 J/g , T_c = 99, 106 ºC, ΔH_c = -15.9 J/b. M_n = 20,007, M_w = 99,771, M_w/M_n = 4.99. $^{13}C\{^1H\}$ NMR(125 MHz, *o*-dichlorobenzene-d_4, 100 ºC): δ = 14.09 ($1B_n$), 18.59 ($4'B_{2'2'4'4}$), 22.86 ($2B_n$), 28.64 ($\beta B_{2'2'4'4}$), 28.75 ($\beta B_{2'2'4'4}$), 29.51 ($4B_n$), 30.00 ($\geq\delta B_{2'2'4'4}$), 30.32 ($1B_{2'2'4'4}$, $2'B_{2'2'4'4}$, $2'B_{2'2'4'4}$), 30.46 ($\gamma B_{2'2'4'4}$), 30.50 ($\gamma B_{2'2'4'4}$), 31.06 ($4B_{2'2'4'4}$), 31.20 ($2B_{2'2'4'4}$), 31.37 ($\alpha B_{2'2'4'4}$), 32.15 ($3B_n$), 32.19 ($\alpha B_{2'2'4'4}$), 43.5 (brB_n), 45.53 ($brB_{2'2'4'4}$), 49.33 ($3B_{2'2'4'4}$).

Poly(3,4-dimethyl-1-pentene-*co*-ethylene). GC analysis of recovered monomer gave: *e.e.* = 37.2% (C = 30.7%), $s = k_S/k_R$ = 16.5. Polymer yield = 3.268 g (4.8 mol% 3,4-dimethyl-1-pentene by mass, 3.7 mol% by NMR). T_m = 119 ºC, ΔH_m = 46.0 J/g, T_c = 100 ºC, ΔH_c = -52.1 J/g. M_n = 15,618, M_w = 108,479, M_w/M_n = 6.95. $^{13}C\{^1H\}$ NMR (125 MHz, *o*-dichlorobenzene-d_4, 120 ºC): δ = 11.86 ($3'B_{3'4'3}$), 19.89 ($1B_{3'4'3}$), 21.98 ($2'B_{3'4'3}$), 27.45 (end group), 27.98 ($\beta B_{3'4'3}$), 28.43 ($\beta B_{3'4'3}$), 30.00 ($\geq\delta B_{3'4'3}$), 30.39 (end group), 30.44 ($\alpha B_{3'4'3}$), 30.63 ($\gamma B_{3'4'3}$, $2B_{3'4'3}$), 32.91 ($\alpha B_{3'4'3}$), 37.55 (end group), 40.43 ($brB_{3'4'3}$), 42.09 ($3B_{3'4'3}$).

Poly(3,4,4-trimethyl-1-pentene-*co*-ethylene). GC analysis of recovered monomer gave: *e.e.* = 44.2% (C = 43.0%), $s = k_S/k_R$ = 5.9. Polymer yield = 1.791 g (12.4 mol% 3,4,4-trimethyl-1-pentene by mass). T_m = 105, 119, 122 ºC, ΔH_m = 79.5 J/g, T_c =

96, 108 ºC, ΔH_c = -78.9 J/g. M_n = 2,688, M_w = 16,008, M_w/M_n = 5.954. $^{13}C\{^1H\}$ NMR (125 MHz, *o*-dichlorobenzene, 100 ºC): δ 9.35, 9.40, 9.65, 14.53, 16.18, 27.52, 28.29, 28.61, 28.77, 28.84, 28.92, 29.05, 29.22, 29.67, 29.89, 29.93, 30.00, 30.32, 30.40, 30.53, 30.57, 31.45, 31.84, 32.18, 33.12, 33.63, 33.98, 34.07, 34.10, 34.53, 35.25, 35.30, 35.58, 36.09, 38.15, 38.51, 43.50, 44.38, 44.61, 45.61, 45.25, 50.06, 110.00, 154.00.

Synthesis of poly(1,2-bis-^{13}C-3,4-dimethyl-1-pentene-*co*-ethylene). Polymerization was carried out as outlined above but with smaller amounts of 1,2-bis-13C-3,4-dimethyl-1-pentene (0.60 mL, 0.42 g, 4.2 mmol), tetradecane (0.564 g) and catalyst solution (0.3 mL, 3 μmol). GC analysis of recovered monomer gave: *e.e.* = 94.1 % (C = 72.3 %), $s = k_S/k_R$ = 6.6. Polymer yield = 0.4902 g (22.9 mol% 3,4-dimethyl-1-pentene by mass). T_m = 121 ºC, ΔH = 35.2 J/g, T_c = 110 ºC, ΔH = 35.0 J/g. M_n = 3,233, M_w = 26,888, M_w/M_n = 8.31. $\{^1H\}^{13}C$ NMR (125 MHz, *o*-dichlorobenzene, 100 ºC): δ = 154.60 (d, ^1J = 36 Hz, ^{13}C), 139.00, 138.66, 108.10 (d, ^1J = 36 Hz, ^{13}C), 40.12 (d, ^1J = 35 Hz, ^{13}C), 36.7 (m, br, ^{13}C), 35.68, 35.40, 34.69, 34.30 (d, ^1J = 35 Hz, ^{13}C), 32.74 (d, ^1J = 35 Hz, ^{13}C), 32.6 (v. br), 30.31 (d, ^1J = 36 Hz), 29.70 ($\geq\delta B_{3',4',3}$), 27.62 (d, ^1J = 34 Hz, ^{13}C), 21.68, 19.58, 18.65, 18.30, 15.48, 14.92, 14.64, 11.54.

Synthesis of poly(1,2-bis-^{13}C-3,4-dimethyl-1-pentene). Polymerization was carried out in the same fashion as (*R*)-3,4-dimethyl-1-pentene polymerizations except small amounts of 1,2-bis-^{13}C-3,4-dimethyl-1-pentene (0.50 mL, 0.35 g, 3.48 mmol), tetradecane (1.01 g), and catalyst solution (0.2 mL, 3 μmol) were used. GC analysis of the recovered monomer gave: *e.e.* = 27.7 % (C = 25.0 %), $s = k_S/k_R$ = 14.2. Polymer yield = 0.08 g. $^{13}C\{^1H\}$ NMR (125 MHz, *o*-dichlorobenzene, 100 ºC): δ = 36.52 (d, ^1J = 36 Hz, ^{13}C), 36.24 (d, ^1J = 36 Hz), 33.13 (br. d, ^1J = 32 Hz), 32.52 (br. d, ^1J = 32 Hz), 32.5 (br. m), 30.32, 30.03, 29.93, 22.18, 21.51, 16.04, 15.74, 11.48.

Polypropylene. Yield = 2.873 g. T_m = 108 ºC, ΔH_m = 20.2 J/g, T_c = 72, 80 ºC, ΔH_c = -26.7 J/g. M_n = 2,878, M_w = 5,219, M_w/M_n = 1.81.

Poly(3-methyl-1-pentene-*co*-propylene). GC analysis of recovered monomer gave: *e.e.* = 10.0% (C = 27.6%), $s = k_S/k_R$ = 1.88. Polymer yield = 3.731 g (8.9 mol% 3-methyl-1-pentene by mass). T_m = 101 ºC, ΔH_m = 27.3 J/g, T_c = 53, 70 ºC, ΔH_c = -35.0 J/g. M_n = 3,155, M_w = 5,291, M_w/M_n = 1.68.

Poly(3-methyl-1-hexene-*co*-propylene). GC analysis of recovered monomer gave: *e.e.* = 24.3% (C = 54.4%), $s = k_S/k_R$ = 1.87. Polymer yield = 4.647 g (10.8 mol% 3-methyl-1-hexene by mass). T_m = broad, T_c = 31.6 ºC, ΔH_c = -9.7 J/g. M_n = 2,812, M_w = 4,873, M_w/M_n = 1.73.

Poly(3,5,5-trimethyl-1-hexene-*co*-propylene). GC analysis of recovered monomer gave: *e.e.* = 13.0% (C = 43.2%), $s = k_S/k_R$ = 1.58. Polymer yield = 5.383 g (6.5 mol% 3,5,5-trimethyl-1-hexene by mass). T_m = 92, ΔH_m = 11.7 J/g, T_c = 45, 56 ºC, ΔH_c = -21.9J/g. M_n = 2,673, M_w = 4,891, M_w/M_n = 1.83.

Poly(3,4-dimethyl-1-pentene-*co*-propylene). GC analysis of recovered monomer gave: *e.e.* = 22.8% (C = 32.5%), $s = k_S/k_R$ = 3.47. Polymer yield = 4.171 g (5.8 mol% 3,4-dimethyl-1-pentene by mass). T_m = 92 ºC, ΔH_m = 19.1 J/g, T_c = 48, 68 ºC, ΔH_c = -22.8 J/g. M_n = 2,455, M_w = 4,121, M_w/M_n = 1.68.

Poly(3,4,4-trimethyl-1-pentene-*co*-propylene). GC analysis of recovered monomer gave: *e.e.* = 1.8 % (C = 42.8 %), $s = k_S/k_R$ = 1.07. Polymer yield = 5.986 g (4.5 mol% 3,4,4-trimethyl-1-pentene by mass). T_m = 99 ºC, ΔH_m = 10.7 J/g, T_c = 60, 66 ºC, ΔH_c = -18.8 J/g. M_n = 1,912, M_w = 3,484, M_w/M_n = 1.82.

1.6 References and Notes

1. (a) Martin, V. S.; Woodard, S. S.; Katsuki, T.; Yamada, Y.; Ikeda, M.; Sharpless, K. B. *J. Am. Chem. Soc.*, **1981**, *103*, 6237; (b) Gao, Y.; Hanson, R. M.; Klunder, J. M.; Ko, S. Y.; Masamune, H.; Sharpless, K. B. *J. Am. Chem. Soc.*, **1987**, *109*, 5765; (c) Kitamura, M.; Kasahara, I.; Manbe, K.; Noyori, R.; Takaya, H. *J. Org. Chem.*, **1988**, *53*, 708.

2. (a) Morken, J. P.; Didiuk, M. T.; Visser, M. S.; Hoveyda, A. H. *J. Am. Chem. Soc.*, **1994**, *116*, 3123; (b) Adams, J. A.; Ford, J. G.; Stamatos, P. J.; Hoveyda, A. H. *J. Org. Chem.*, **1999**, *64*, 9690.

3. La, D. S.; Alexander, J. B.; Cefalo, D. R.; Graf, D. D.; Hoveyda, A. H.; Schrock, R. R. *J. Am. Chem. Soc.*, **1998**, *120*, 9720.

4. (a) VanNieuwenhze, M. S.; Sharpless, K. B. *J. Am. Chem. Soc.*, **1993**, *115*, 7864;
(b) Hamon, D. P. G.; Tuck, K. L.; Christie, H. S. *Tetrahedron*, **2001**, *57*, 9499;
(c) Christie, H. S.; Hamon, D. P. G.; Tuck, K. L. *Chem. Comm.*, **1999**, 1989;
(d) Gardiner, J. M.; Norret, M.; Sadler, I. H. *Chem. Comm.*., **1996**, 2709.

5. (a) Brintzinger, H. H.; Fischer, D.; Mulhaupt, R.; Rieger, B.; Waymouth, R. M. *Ang. Chem., Int. Ed.*, **1995**, *34*, 1143; (b) Britovsek, G. J. P.; Gibson, V. C.; Wass, D. F. *Ang. Chem., Int. Ed.*, **1999**, *38*, 428; (c) Coates, G. W. *Chem. Rev.*, **2000**, *100*, 1223;
(d) Resconi, L.; Cavallo, L.; Fait, A.; Piemontesi, F. *Chem. Rev.*, **2000**, *100*, 1253;
(e) Eds. Jacobs, M., In *Chem. Eng. News*, Vol. 79, p. 42.

6. (a) Pino, P.; Lorenzi, G. P.; Ciardelli, F. *J. Am. Chem. Soc.*, **1963**, *85*, 3888;
(b) Carlini, C.; Altomare, A.; Menconi, F.; Ciardelli, F. *Macromolecules*, **1987**, *20*, 464; (c) Vizzini, J.; Ciardelli, F.; Chien, J. C. W. *Macromolecules*, **1992**, *25*, 108;
(d) Zambelli, A.; Proto, A.; Pasquale, L. *Ziegler Catalysis* (Eds. G. Fink); Springer-Verlage: Heidelber, **1995**, 218.

7. Zambelli, A.; Ammendola, P. *Macromolecules*, **1983**, *16,* 341.

8. Chien, J. C. W.; Vizzini, J.; Kaminsky, W. *Macromol. Rap. Commun.*, **1992**, *13*, 479.

9. Ciardelli, F.; Carlini, C.; Altomare, A. *Ziegler Catalysis* (Eds. G. Fink, R. Mulhaupt and H. H. Brintzinger); Springer-Verlag: Heidelberg, **1995**, 455.

10. Oliva, L.; Longo, P.; Zambelli, A. *Macromolecules*, **1996**, *29*, 6383.

11. Sacchi, C.; Barsties, E.; Tritto, I.; Locatelli, P.; Brintzinger, H. H.; Stehling, U. *Macromolecules*, **1997**, *30*, 1267.

12. Herzog, T. A.; Zubris, D. L.; Bercaw, J. E. *J. Am. Chem. Soc.*, **1996**, *118*, 11988.

13. Veghini, D.; Henling, L. M.; Burkhard, T. J.; Bercaw, J. E. *J. Am. Chem. Soc.*, **1999**, *121*, 564.

14. Baar, C. R.; Levy, C. J.; Min, E. Y.-J.; Henling, L. M.; Day, M. W.; Bercaw, J. E. *J. Am. Chem. Soc.*, **2004**, *126*, 8216.

15. (a) Doi, Y.; Asakuru, T. *Makromol. Chem.*, **1975**, *176*, 507; (b) Sheldon, R. A.; Rueno, T.; Tsunstsungu, T.; Kurukawa, J. *J. Poly. Sci.*, **1965**, *3*, 23.

16. Bovey, F. A.; Tiers, G. V. D. *J. Polym. Sci.*, **1960**, *44*, 173.

17. Grisi, F.; Longo, P.; Zambelli, A.; Ewen, J. A. *J. Mol. Cat. A*, **1999**, *140*, 225.

18. (a) Ewen, J. A. *J. Am. Chem. Soc.*, **1984**, *106*, 6355; (b) Mitani, M.; Furuyama, R.; Mohri, J.; Saito, J.; Ishii, S.; Terao, H.; Nakano, T.; Tanaka, H.; Fujita, T. *J. Am. Chem. Soc.*, **2003**, *125*, 4293; (c) De Rosa, C.; Circelli, T.; Auriemma, F.; Mathers, R. T.; Coates, G. W. *Macromolecules*, **2004**, *37*, 9037; (d) Erker, G.; Nolte, R.; Aul, R.; Wilker, S.; Kruger, C.; Noe, R. *J. Am. Chem. Soc.*, **1991**, *113*, 7594.

19. Molecular weight distributions for these polymers were broad (6 > PDI > 3). Although multiple polymerization sites cannot be definitively ruled out, broad

molecular weight distributions are believed to be due to mass transport issues. This conclusion was reached considering the narrow molecular weight distributions found for polypropylene copolymers (see Experimental Section) and a significant portion (85 wt%) of the ethylene copolymers containing the desired microstructure established by solvent fractionation.

20. The homopolymerization *vs.* copolymerization comparisons from Table 1.1 under the same polymerization conditions are: for 3-methyl-1-pentene: entry 1; for 3-methyl-1-hexene: entry 3; for 3,5,5-trimethyl-1-hexene: entry 4. Entries 5 and 7 were for runs under somewhat different polymerization conditions.

21. Casey, C. P.; Tunge, J. A.; Lee, T.; Fagan, M. A. *J. Am. Chem. Soc.*, **2003**, *125*, 2641.

22. DSC for isotactic poly(3-methyl-1-pentene) displayed no melting point at all and decomposition at 250 ºC as evidence by DSC/TGA. Therefore, the lack of a high temperature melting point in these copolymers does not necessitate an absence of consecutive chiral repeat units in the copolymer.

23. (a) Xu, X.; Xu, J.; Feng, L.; Chen, W. *J. App. Poly. Sci.*, **2000**, *77*, 1709; (b) Villar, M. A.; Failla, M. D.; Quijada, R.; Mauler, R. S.; Valles, M.; Galland, G. B.; Quinzani, L. M. *Polymer*, **2001**, *42*, 9269.

24. Zhang, M.; Lynch, D. T.; Wanke, S. E. *Polymer*, **2001**, *42*, 3067.

25. Mang, M.; Wanke, S. E. *Poly. Eng. Sci.*, **2003**, 43, *12*, 1878.

26. $^{13}C\{^{1}H\}$ NMR spectrum for polyethylene synthesized under the same reaction conditions showed no evidence for incorporation of long chain branches.

27. Lindeman, L. P.; Adams, J. Q. *Anal. Chem.*, **1971**, *43*, 1245.

28. Hahn, C.; Cucciolito, M. E.; Vitagliano, A. *J. Am. Chem. Soc.*, **2002**, *124*, 9038.

29. Doi, Y.; Suzuki, T.; Keii, T. *Makromol. Chem. Rapid Commun.*, **1981**, *2*, 293.

30. A more thorough statistical analysis was carried out for the origin of the enantiofacial selectivity, but results from this analysis do not provide any more profound insight than the simple triad tests discussed.

31. Lovisi, H.; Tavares, M. I. B.; Silva, N. M.; Menezes, S. M. C.; Santa Maria, L. C.; Coutinho, F. M. B. *Polymer*, **2001**, *42*, 9791.

32. De Rosa, C.; Auriemma, F.; Capua, A. D.; Resconi, L.; Guidotti, S.; Camurati, I.; Nifani, I. E.; Laishevtsev, I. P. *J. Am. Chem. Soc.*, **2004**, *126*, 17040.

33. Fineman, M.; Ross, S. D. *J. Poly. Sci.*, **1950**, *5*, 259.

34. Min, E. Y.-J., Ph D Thesis, California Institute of Technology, **2005.**

35. Myers, A. G.; Bryant, H. Y.; Chen, H.; McKinstry, L.; Kopecky, D. J.; Gleason, J. L. *J. Am. Chem. Soc.*, **1997**, *119*, 6496.

36. (a) Chen, C.-S.; Fujimoto, Y.; Girdaukas, G.; Sih, C. J. *J. Am. Chem. Soc.*, **1982**, *104*, 7294; (b) Wang, Y.-F.; Chen, C.-S.; Girdaukas, G.; Sih, C. J. *J. Am. Chem. Soc.*, **1984**, *106*, 3695; (c) Ismagilov, R. F. *J. Org. Chem.*, **1998**, *63*, 3772.

37. Burger, B. J.; Bercaw, J. E. *New Developments in the Synthesis, Manipulation and Characterization of Organometallic Compounds* (Eds. A. Wayda and M. Y. Darensbourg); American Chemical Society: Washington DC, **1987**.

38. Ewen, J. A.; Jones, R. L.; Razavi, A. *J. Am. Chem. Soc.*, **1988**, *110*, 6255.

39. Usami, T.; Takayama, S. *Macromolecules*, **1984**, *17*, 1756.

CHAPTER TWO

SITE EPIMERIZATION IN THE KINETIC RESOLUTION OF RACEMIC α-OLEFINS USING C_1-SYMMETRIC ZIRCONOCENE POLYMERIZATION CATALYSTS

2.1 Abstract

The use of a new C_1-symmetric olefin polymerization precatalyst, (1,2-$SiMe_2$)$_2${η^5-C_5H_2-4-((*S*)-$CHEtCMe_3$)}{η^5-C_5H-3,5-$(CHMe_2)_2$}$ZrCl_2$, (*S*)-**2**, for the kinetic resolution of 3-methyl substituted racemic α-olefins was investigated. Selectivity factors for most olefins were greater for the ethylneopentyl derivative (*S*)-**2** as compared to its previously reported methylneopentyl analog, (1,2-$SiMe_2$)$_2${η^5-C_5H_2-4-((*S*)-$CHMeCCMe_3$)}{η^5-C_5H-3,5-$(CHMe_2)_2$}$ZrCl_2$, (*S*)-**1**. Pentad analysis of polypropylene polymerized with (*S*)-**2** at various propylene concentrations indicated that (*S*)-**2** undergoes more rapid site epimerization at intermediate propylene concentrations compared to (*S*)-**1**. At low propylene concentrations, however, the two catalysts behaved similarly. Polymerization of 3,5,5-trimethyl-1-hexene at different olefin concentrations and temperatures illustrated that selectivity differences between the two catalysts are likely not a consequence of inefficient site epimerization. The effect of added trimethylaluminum on polymerizations catalyzed by (*S*)-**1** and its relationship to site epimerization during such reactions was also investigated.

2.2 Introduction

Polymerization catalysts are among the most active and stereoselective catalysts in homogeneous catalysis.[1] Due to their potential commercial value, much effort has been devoted to understanding how catalyst structure affects polymer microstructure. In particular there often is a correlation between catalyst symmetry and poly-α-olefin tacticity with C_2-symmetric catalysts yielding isotactic polymer and C_s-symmetric catalysts giving syndiotactic polymer. As a consequence of these studies, a detailed mechanistic picture is emerging for these catalysts.[2]

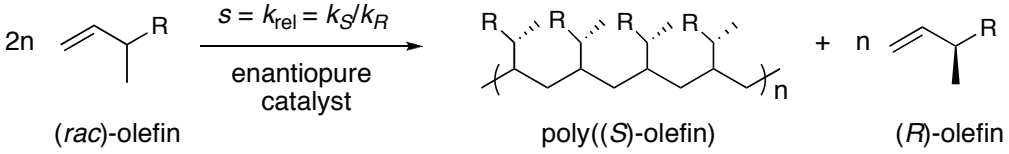

Scheme 2.1 Kinetic resolution of racemic α-olefins by polymerization.

As discussed extensively in the introduction and in Chapter 1, the remarkable stereoselectivities displayed by polymerization catalysts inspired our to group to explore the kinetic resolution of racemic α-olefins by polymerization using enantiopure catalysts (Scheme 2.1).[3,4] Due to their high degree of activity, the doubly linked C_1-symmetric catalyst precurser

(1,2-$SiMe_2$)$_2${η^5-C_5H_2-4-((*S*)-CHMeCCMe$_3$)}{η^5-C_5H-3,5-(CH(CH$_3$)$_2$}$ZrCl_2$ ((*S*)-**1**) and related compounds were initially investigated for the kinetic resolution of 3-substituted-1-olefins (e.g., 3-methyl-1-pentene or 3,4-dimethyl-1-pentene) to afford isotactic polymer at all concentrations examined.[3]

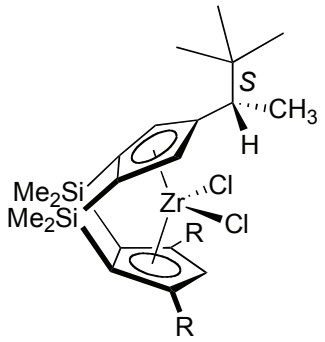

R = *i*-Pr ((*S*)-**1**), 3-pentyl, cyclohexyl

On the other hand, these catalysts polymerize propylene to give isotactic polypropylene at low propylene concentrations and syndiotactic polypropylene at high propylene concentrations.[5] A switch from syndiotactic polypropylene produced at high [propylene] to isotactic polypropylene produced at low [propylene] has been explained by a polymerization mechanism whereby unimolecular site epimerization competes with bimolecular chain propagation (Scheme 2.2). It was argued that the bulky methyl neopentyl group of these catalysts pushes the polymer chain away from the methyl group. At low concentrations of propylene, unimolecular site epimerization precedes enchainment of another monomer, and chain propagation occurs mainly by propylene coordination to the same side of the zirconocene wedge using the same enantioface of the olefin, thus yielding isotactic polymer. At high monomer concentrations, bimolecular chain propagation is relatively favored over site epimerization, allowing for propylene enchainments from both sides of the zirconocene wedge with alternating enantiofacial preferences producing syndiotactic polymer. For 3-methyl substituted α-olefins, chain propagation is believed to be much slower than site epimerization even at high olefin concentrations, leading to isotactic polymer as shown for the blue pathway of Scheme 2.2.

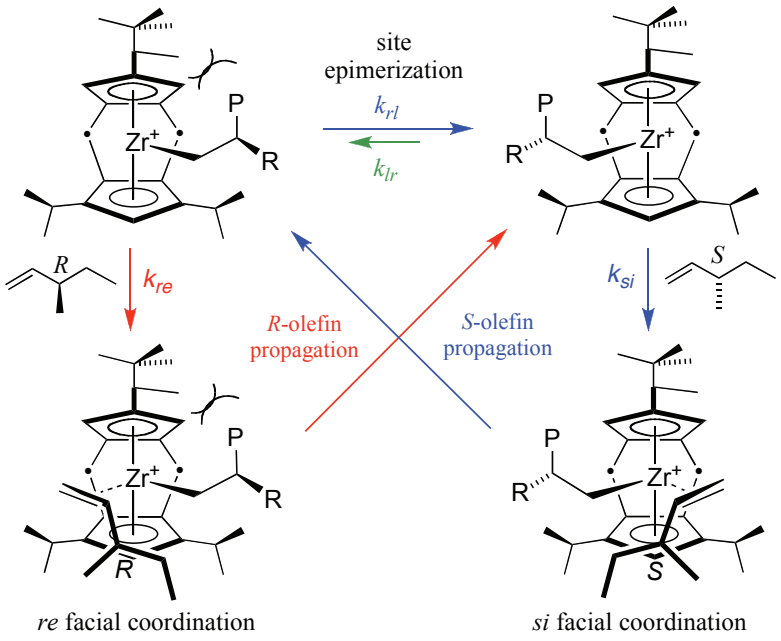

(P = remaining polymer chain; R = $CH(CH_3)CH_2CH_3$)

- blue pathway much faster than red pathway with k_{rl} relatively large: isotactic polymer: (*S*) olefin propagation
- alternating (red, then blue, then red, *etc.*) pathway with k_{rl} relatively small: syndiotactic polymer; (*R*) and (*S*) olefin propagation

Scheme 2.2 Site epimerization in α-olefins polymerizations catalyzed by C_1-symmetric zirconocenes.

The most convincing evidence for the production of isotactic polymer during kinetic resolution of racemic olefins, however, is a $^{13}C\{^1H\}$ NMR spectrum of poly(3-methyl-1-pentene) which was compared to authentic samples of isotactic poly(3-methyl-1-pentene).[6] Unlike NMR spectra for polypropylene, poly(3-methyl-1-pentene) spectra are much less diagnostic due to poor polymer solubility and broad overlapping peaks. Consequently, stereoerrors, arising for example by occasional operation of the red pathway of Scheme 2.2, are harder to detect than for polypropylene. The analyses of microstructures of the other polymers obtained in these kinetic resolutions are similarly difficult to establish.

We therefore considered that low selectivity factors observed during kinetic resolutions are at least in part a consequence of inefficient site epimerization (*i.e.* occasional insertion from the red pathway in Scheme 2.2). Occasional olefin uptake when the polymeryl chain lies on the sterically more hindered side of the zirconocene wedge would likely result in olefin insertions with opposite enantiofacial and diastereoselectivities compared to enchainments occurring when the polymeryl chain resides on the sterically less-hindered side. That is to say that for these misinsertions, the normally disfavored antipode of the monomer (*R* for (*S*)-**1**) is preferentially incorporated over the favored antipode (*S* for (*S*)-**1**). The consequence of this behavior is a selectivity factor that is artificially low with the magnitude of retardation depending on the frequency of inefficient site epimerization.

To examine the possibility that incomplete site epimerization operates with catalyst system (*S*)-**1**, Endy Min in our group carried out the synthesis of the ethylneopentyl analog (*S*)-**2** and reported initial experiments towards kinetic resolution of racemic α-olefins.[7] Should inefficient site epimerization limit the efficacy of (*S*)-**1**, we anticipated the more bulky ethyl group in (*S*)-**2** would encourage site epimerization resulting in higher selectivity factors during kinetic resolution. Indeed, these initial experiments revealed higher selectivity factors when (*S*)-**2** was used as the catalyst for all monomers studied.

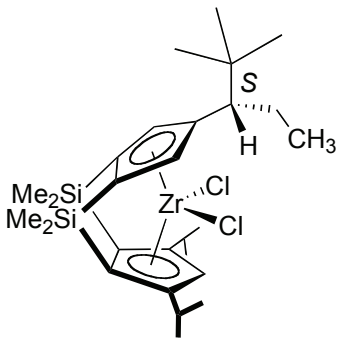

(*S*)-**2**

To further probe the possibility that inefficient site epimerization limits selectivity, reported herein is a more extensive examination of the scope of the kinetic resolutions catalyzed by (*S*)-**2**. Additionally, propylene and racemic α-olefin polymerizations carried out at various monomer concentrations and temperatures were accomplished. For catalysts where unimolecular site epimerization competes with bimolecular chain propagation these changes in experimental conditions should affect selectivity factors in a predictable way.

2.3 Results and Discussion

Polymerization of racemic α-olefins with (*S*)-2. Although the synthesis of (*S*)-**2** was described previously,[7] the limitations of the synthetic route and comparison with the reported synthesis of (*S*)-**1**[3] deserves some comment. Whereas synthesis of the upper cyclopentadiene for (*S*)-**1** (as pictured) was achieved by CBS reduction of pinacolone followed by S_N2 displacement of the corresponding mesylate with cyclopentadienyl (Cp) anion, analogous procedures were problematic for (*S*)-**2** (Scheme 2.3). Instead of the 10 mol% *in situ* prepared CBS catalyst which was used for pinacolone reduction, a stoichiometric amount of solid preformed CBS catalyst was required to reduce **3** to the corresponding alcohol, (*R*)-**4**, in high optical purities.[8] Lower temperatures (-78 ºC *vs.* -20 ºC) as well as longer addition times were required to achieve high enantiomeric excess. Treating the mesylate of (*R*)-**4** with Cp anion was also more challenging for the synthesis of (*S*)-**5** compared to the analogous reaction during the synthesis of (*S*)-**1**. Although the product of the reaction was obtained with complete inversion of stereochemistry, yields of (*S*)-**5** were low. In fact, the major product of this reaction was elimination of the mesylate rather than S_N2 displacement. Nevertheless, synthesis of (*S*)-**5** could be accomplished, albeit in low yields, and elaboration to (*S*)-**2** was carried out in complete analogy and in similar yields to (*S*)-**1**.

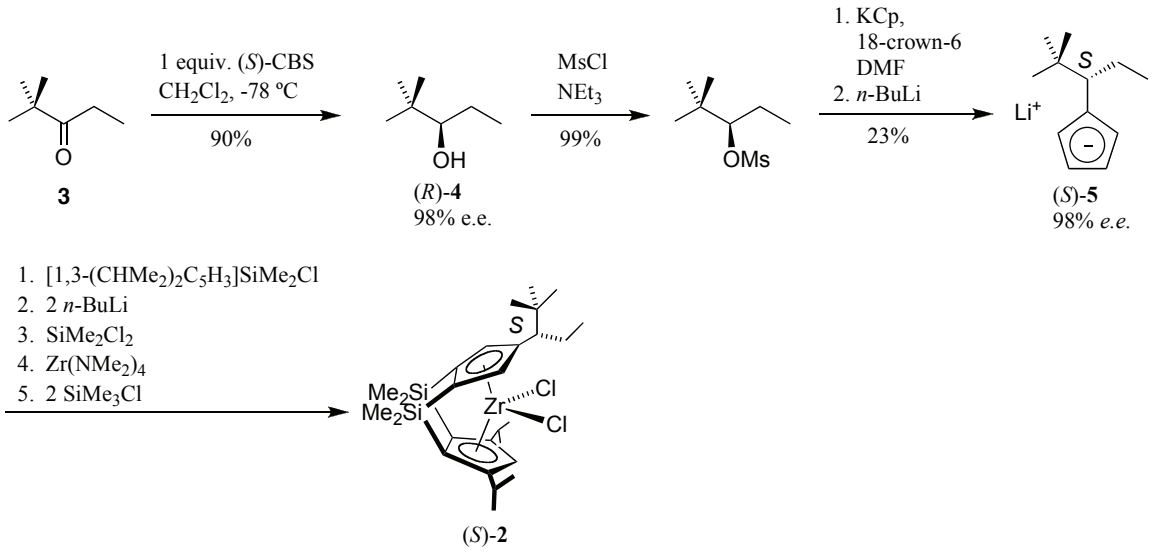

Scheme 2.3 Synthesis of (*S*)-**2**.

Structurally, (*S*)-**2** displays similar features to (*S*)-**1** as indicated by an X-ray crystal structure, which was obtained for (*S*)-**2** and appears in Figure 2.1. The ethyl group occupies the right side of the zirconocene wedge (as pictured) in a similar fashion to the methyl group of (*S*)-**1**. The distance between the two isopropyl groups on the bottom cyclopentadienyl ring are 5.123 Å for (*S*)-**2** compared to 5.163 Å for (*S*)-**1**. The angle between the two cyclopentadienyl rings is 73.1º and 72.2 for (*S*)-**2** and (*S*)-**1**, respectively. The only major difference between the two structures is that the torsional angle between the methyl (methylene) group on the top Cp, the Cp centroid, and zirconium, which is 39.1º for (*S*)-**1** is more obtuse for (*S*)-**2** (46.7º). Other relevant bond distances and angles appear in Appendix F.

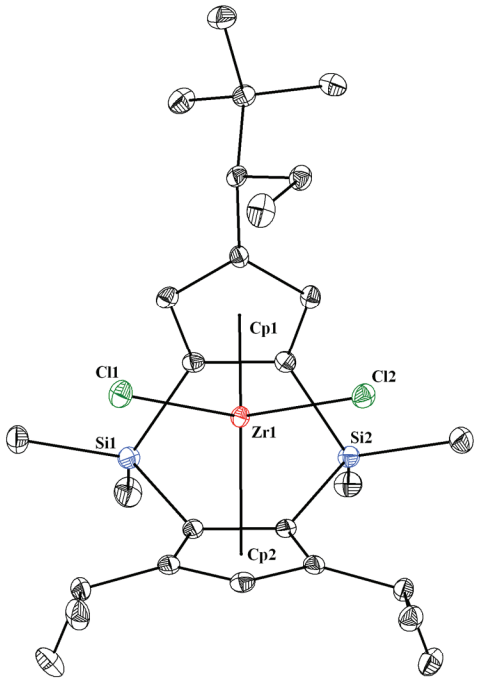

Figure 2.1 Molecular structure for (*S*)-**2**.

The results for polymerization of the racemic α-olefins using (*S*)-**2** as the precatalyst appear in Table 2.1 along with analogous reactions using (*S*)-**1** as the precatalyst for comparison. In general, (*S*)-**2** was the more active catalyst. This is in accord with the larger bite angle for (*S*)-**2** compared to (*S*)-**1**. In most cases, the selectivity factors for (*S*)-**2** were larger than for (*S*)-**1** particularly for 3,5,5-trimethyl-1-hexene. The one exception is the polymerization of 3,4,4-trimethyl-1-pentene where (*S*)-**1** is more selective than (*S*)-**2** during kinetic resolution. We cannot explain this anomaly, but it could be due to lower molecular weights for polymers obtained when (*S*)-**2** rather than (*S*)-**1** was used as the catalyst. Inherent to lower molecular weight polymer are more olefin insertions into zirconium hydrides, a process that has been shown to have poor enantiofacial selectivity. This hypothesis is supported by the observation of dimers in the gas chromatograph used to follow the polymerization reaction. Additionally, the polymer that was recovered from these reactions accounted for only 60%–70% of the

converted olefin. The remainder of the mass was presumably lost during the purification of the polymer as methanol soluble oligomers. Although the substrates represented in Table 2.1 are limited and the difference in selectivities is substrate dependent, these data are consistent with there being more efficient site epimerization during polymerization when (*S*)-**2** is employed as the catalyst rather than (*S*)-**1** (*vide supra*). To further probe this possibility, propylene polymerizations as well as polymerization of racemic α-olefins under different reaction conditions were carried out.

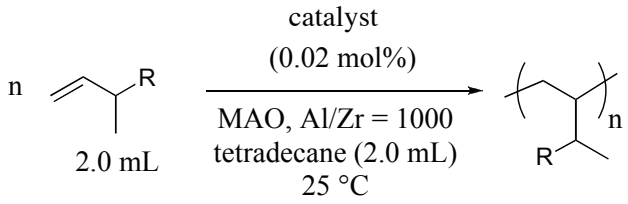

	(*S*)-1		(*S*)-2	
olefin	**TOF (h^{-1})**	***s* = k_S/k_R**	**TOF (h^{-1})**	***s* = k_S/k_R**
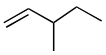	47	2.4	280	3.2
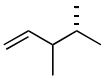	34	15.9	75	20.5
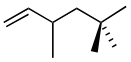	37	2.1	988	8.5
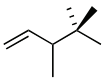	18[a]	7.6	16[a]	3.2

[a] 3 mg catalyst and toluene (2.0 mL) was used instead of tetradecane.

Table 2.1 Selectivity and activity for racemic α-olefin polymerizations catalyzed by (*S*)-**1**/MAO and (*S*)-**2**/MAO.

Propylene polymerizations catalyzed by (*S*)-2. As noted above, we have previously reported that precatalyst (*S*)-**1** produces moderately syndiotactic polypropylene in neat propylene and moderately isotactic polypropylene at low propylene concentrations due to competition between site epimerzation and chain propagation.[5] If

(*S*)-**2** undergoes faster site epimerization than (*S*)-**1**, then polymers produced from (*S*)-**2** should be more isotactic (lower [*r*]) than polymers produced from (*S*)-**1** at all concentrations of propylene. Propylene polymerizations were therefore carried out at various propylene concentrations, and the tacticity of these polymers was determined by ^{13}C NMR spectroscopy. Results from these experiments along with similar experiments carried out with (*S*)-**1** appear in Table 2.2.

As was the case with (*S*)-**1**, isotacticity decreased with increasing propylene concentration when (*S*)-**2** was used as the catalyst (*i.e.* [*mmmm*] = 62.3% and 12.9% for [C_3H_6] of 0.8 M and 8.1 M, respectively). Figure 2.2 is a plot of [*r*] *versus* [C_3H_6], which was made to help compare the two catalysts. To better illustrate the trends, the methyl region of the NMR spectra for polypropylene obtained at three concentrations appears in Figure 2.3. Both catalysts display saturation behavior at low and high propylene concentrations. At low propylene concentration ([C_3H_6] = 0.8 M), isotactic polypropylene is produced with virtually identical microstructures for the two catalysts (Table 2.2, entries 1 and 2 and Figure 2.3), whereas at high propylene concentration the two catalysts yield syndiotactic polypropylene with similar but not identical microstructures (entries 7 and 8). At intermediate propylene concentrations, however, differences between the two catalysts are evident (entries 3-6, Figure 2.3). Although [*r*] increases with propylene concentration to similar saturation points for both catalysts, the increase is more rapid for (*S*)-**1** than **(***S*)-**2** (Figure 2.2).

Table 2.2 Propylene polymerizations at various [C_3H_6]. Polymerizations carried out in 20 mL toluene and under constant pressure of propylene at 20 °C.

entry	catalyst	[C_3H_6] (M)	activity ($g_{poly}/(g_{cat}*h)$	[mmmm]	[mmmr]	[rmmr]	[mmrr]	[mrmm] +[rrmr]	[mrmr]	[rrrr]	[mrrr]	[mrrm]	[r]
1	(*S*)-**1**	0.8	2.5×10^3	62.9	14.0	0.9	12.7	3.8	0.0	0.0	1.5	4.4	14.1
2	(*S*)-**2**	0.8	1.2×10^3	62.3	14.5	0.8	11.8	5.0	0.0	0.0	1.1	4.5	14.0
3	(*S*)-**1**	3.4	5.3×10^3	17.7	15.0	3.3	19.9	9.1	0.0	14.6	12.0	8.3	49.4
4	(*S*)-**2**	3.4	6.1×10^3	30.7	16.7	2.7	19.2	7.1	0.0	6.8	8.1	8.7	36.8
5	(*S*)-**1**	4.6	1.0×10^4	9.9	11.6	3.7	18.9	10.3	0.0	23.9	16.2	5.7	60.4
6	(*S*)-**2**	4.6	7.2×10^3	21.8	15.7	3.2	20.0	8.4	0.0	11.6	11.1	8.1	45.0
7	(*S*)-**1**	8.1	6.8×10^3	8.8	10.1	3.4	16.6	9.5	0.0	29.9	15.9	5.9	64.7
8	(*S*)-**2**	8.1	2.0×10^4	12.9	13.0	3.5	18.9	10.1	0.0	19.5	15.2	7.0	56.2
9[a]	(*S*)-**1**	12.1	1.5×10^3	4.0	5.4	3.8	12.6	6.8	0.0	49.6	14.4	3.5	77.2
10[a]	(*S*)-**2**	12.1	2.9×10^5	2.8	6.4	3.2	11.6	10.0	0.0	44.4	16.4	5.2	76.8

[a] neat propylene, 0 °C

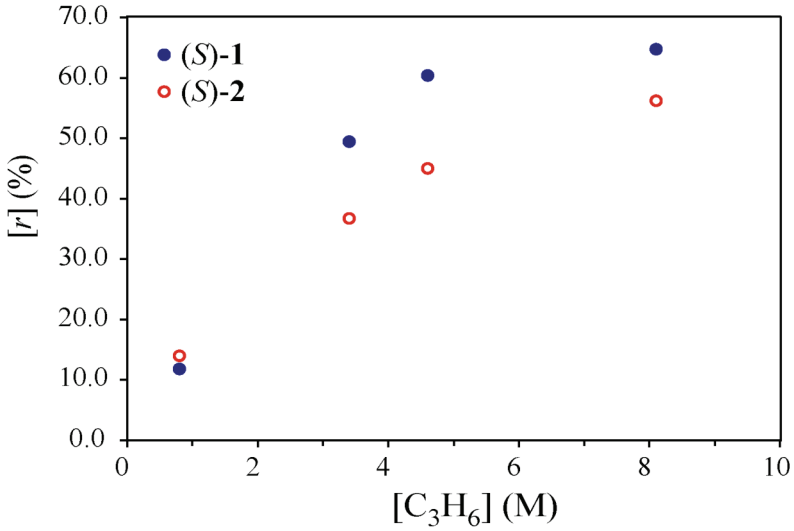

Figure 2.2 Plot of [*r*] *versus* [C_3H_6] for propylene polymerizations catalyzed by (*S*)-**1** and (*S*)-**2**.

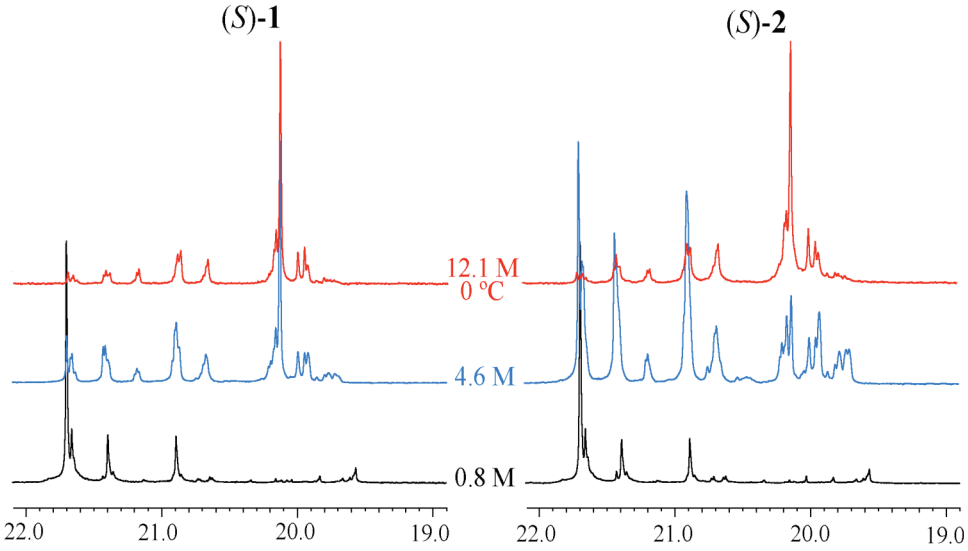

Figure 2.3 Methyl region of $^{13}C\{^1H\}$ NMR for polypropylene polymerized at different [C_3H_6] catalyzed by (*S*)-**1** and (*S*)-**2**.

These data can be rationalized as follows. At low propylene concentration, site epimerization occurs after practically every olefin insertion for both catalysts. The microstructure observed for these polymers, therefore, is primarily controlled by the enantiofacial selectivity of the olefin insertion when the polymer chain lies on the

sterically less hindered side of the zirconocene wedge. Furthermore, the enatiofacial selectivities for this polymerization site are similar for the two catalysts because similar microstructures are obtained at this limit. At intermediate propylene concentrations site epimerization competes with olefin insertion for both catalysts. As expected, the ethyl group of (*S*)-**2** encourages site epimerization more than (*S*)-**1** because [*r*], which is proportional to the number of consecutive olefin insertions without site epimerization, increases more gradually with propylene concentration for (*S*)-**2**. At high propylene concentration, chain propagation begins to dominate for both catalysts. The differences between the two catalysts is not as evident because under these conditions site epimerization is not as important. Polymer microstructure is again controlled by the enantiofacial selectivity of the inserted monomer, but this time facial selectivity from both sides of the zirconocene wedge affect polymer microstructure. In accord with this explanation, polymerizations carried out in liquid propylene at 0 ºC with both catalysts displayed almost identical polymer microstructures (Table 2.2, entries 9 and 10).

To further support the above explanation, the pentad distributions for polymerization carried out in the data at liquid propylene were modeled with a unidirectional site epimerization model.[9] The model considers three mechanisms that can effect the polypropylene pentad distribution. These mechanisms are represented by three parameters: α, the enantiofacial selectivity of olefin insertions when the polymeryl group lies on the sterically less-hindered side of the zirconocene, β, the enantiofacial selectivity of olefin insertions when the polymeryl group lies on the sterically more-crowded side, and ε, the probability for site epimerization when the polymeryl group moves from the sterically more crowded to the sterically less-hindered side. The model does not take into account the possibility of insertions after a site epimerization from the sterically *less*-hindered to the sterically *more*-hindered side. Least squares fit of the neat polypropylene data show that α is 0.99 and 0.99, β is 0.16 and 0.13, and ε is 0.13 and 0.21, for (*S*)-**1** and

(*S*)-**2**, respectively (RMS = 0.871 and 0.904). These data are in full agreement with the above explanation. As anticipated, the major difference between the two catalysts is site epimerization with more efficient site epimerization occurring for (*S*)-**2** compared to (*S*)-**1** as indicated by a larger ε for (*S*)-**2.** The enantiofacial selectivity parameters (α and β) are also easily rationalized. These parameters not only describe the selectivity of the olefin polymerized, but they also indicate which face of the olefin is favored. Values for α or β that are 0 or 1 indicate perfectly selective insertions from opposite olefin enantiofaces, while a value of α or β close to 0.5 describe unselective insertions. For polymerizations catalyzed by (*S*)-**1** or (*S*)-**2**, enantiofacial selectivities when the polymer chain lies on the sterically less-hindered side (described by α) are very high and approximately the same. As expected, β is less than 0.5 and is approximately the same for the two catalysts. The enantiofacial selectivity values suggest that highly syndiotactic polymer (insertions into alternating enantiofaces) would be produced in the absence of site epimerization. The two catalysts display similar values for α and β, which indicates that substitution of the methyl group in (*S*)-**1** for an ethyl group in (*S*)-**2** does not significantly affect the facial selectivity for olefin insertions. It is interesting to note that for both catalysts β is not as close to 0 as α is to 1. A possible explanation is that the methyl/ethyl group on the top Cp competes with the isopropyl group on the bottom Cp to direct the polymer chain down rather than up (as pictured in Scheme 2.2). Propylene coordination occurs so that the methyl group avoids the polymer chain thereby undergoing insertions from the "wrong" enantioface for the polymer chain directed down.

Using α and β from the neat propylene data, the rest of the data in Table 2.2 can be modeled by changing ε. Modeling all of the data in Table 2.2 by varying all three parameters yields better least squares fits (See Appendix G), but it is unclear why α and β would change much with propylene concentration. Neat propylene data was used for obtaining the values for α and β because there is a good probability for insertion from

both polymerization sites under these conditions. Figure 2.4 is a plot of ε *versus* $[C_3H_6]$ for both catalysts. As can be seen from Figure 2.4, ε decreases with increasing propylene concentration for both catalysts indicating that site epimerization occurs more readily at low propylene concentration. Figure 2.4 also shows that at intermediate and high propylene concentrations, ε is larger for (*S*)-**2** compared to (*S*)-**1** with changes in ε being more significant for (*S*)-**2**. This suggests that the ethyl group of (*S*)-**2** is more effective at directing the polymeryl group towards the sterically less hindered side of the zirconocene wedge.

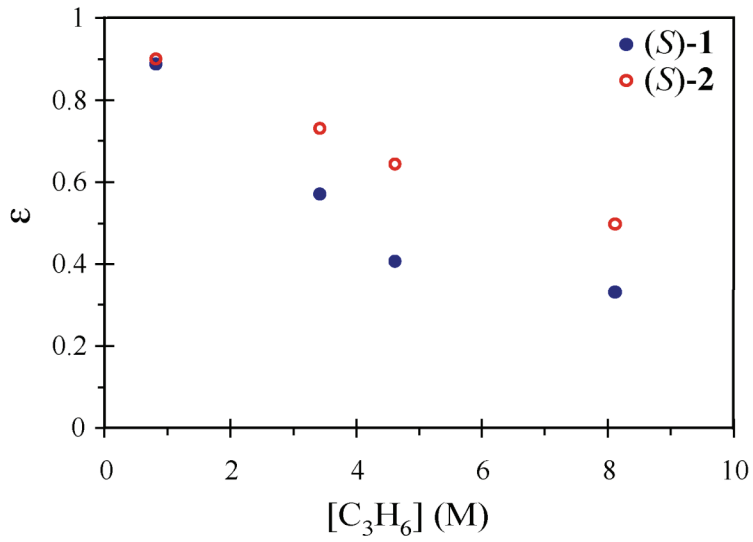

Figure 2.4. Propylene concentration dependence on the probability of site epimerization parameter (ε) used to model data in Table 2.2.

The rate constant for site epimerization (k_{epim}) relative to olefin insertion when the polymer chain resides on the sterically congested side of the zirconocenes ($k_{\beta\text{-ins}}$) can be obtained from the data in Figure 2.4. The probability of site epimerization can be expressed in terms of these rate constants using the simple relationshiop shown in equation (2.1):

$$\varepsilon = \frac{k_{epim}}{k_{epim} + k_{\beta-ins}[C_3H_6]} \qquad (2.1)$$

The inverse of equation 2.1 gives the relationship:

$$\frac{1}{\varepsilon} = 1 + \frac{k_{\beta-ins}}{k_{epim}}[C_3H_6] \qquad (2.2)$$

Therefore, a plot between 1/ε and $[C_3H_6]$ should give a line with a slope equal to $k_{\beta\text{-ins}}/k_{\text{epim}}$. A plot of 1/ε *versus* $[C_3H_6]$ was made for the data in Figure 2.4 and appear in Figure 2.5. The data for each catalyst fits reasonably well to equation (2.2) producing linear plots with y-intercepts equal to 1. The inverse of the slopes of these plots reveal that $k_{\text{epim}}/k_{\beta\text{-ins}}$ is 3.8 and 8.2 for polymerization catalyzed by (*S*)-**1** and (*S*)-**2**, respectively, indicating that both catalysts prefer to undergo site epimerization rather than olefin insertion. Consistent with our qualitative analysis, catalyst (*S*)-**2** is approximately two times more likely to undergo site epimerization rather than olefin insertion compared to catalyst (*S*)-**1**. This difference is not substantial from an energy standpoint indicating that the catalysts behave similarly. At this point it is important to emphasize that the information from Figure 2.5 does not indicate the absolute value for the site epimerization rate constants nor does it provide any information about absolute and relative olefin insertion rates when the polymer chain resides on the sterically *less*-hindered side of the zirconocene. Nevertheless, these data show that (*S*)-**2** encourages site epimerization marginally better than (*S*)-**1** for propylene polymerizations.

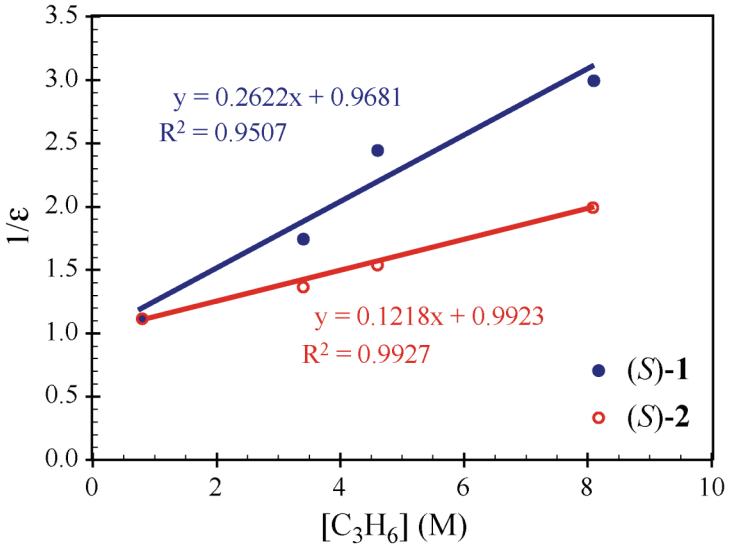

Figure 2.5 Plot of 1/ε *versus* $[C_3H_6]$ for propylene polymerizations catalyzed by (*S*)-**1** and (*S*)-**2**.

Polymerization of 3,5,5-trimethyl-1-hexene at different temperatures and olefin concentrations. Because chain propagation is believed to be much slower for 3-substituted olefins,[10] we hypothesized that the 3-methyl substituted racemic α-olefins used for kinetic resolution would behave much like propylene polymerization at low propylene concentrations. In other words, chain propagation would be too slow to compete with site epimerization. To help verify this we monitored the selectivity of 3,5,5-trimethyl-1-hexene polymerizations at different olefin concentrations and temperatures (Table 2.3).

If chain propagation, which is dependent on olefin concentration, is in competition with olefin independent site epimerization during racemic α-olefin polymerization, then selectivity factors should increase at lower olefin concentrations (*vide supra*). Qualitatively, we have noticed that selectivity factors are insensitive to conversion during racemic α-olefin polymerization. Olefin concentration decreases as the reaction proceeds, so selectivity factors should increase with conversion if site epimerization competes with chain propagation. This observation is not conclusive,

however, because olefin concentration does not vary much under typical reaction conditions.

entry	catalyst	[olefin] (M)	T (ºC)	TOF (h^{-1})	$s = k_S/k_R$
1	(*S*)-**1**[a]	2.4	0	40 (10)	3.9 (0.2)
2	(*S*)-**1**[a]	0.85	20	110 (30)	2.9 (0.2)
3	(*S*)-**1**	2.4	20	110 (30)	3.2 (0.2)
4	(*S*)-**1**	2.4	50	1400 (300)	2.6 (0.1)
5	(*S*)-**2**[a]	2.3	0	50 (40)	11.5 (0.5)
6	(*S*)-**2**[a]	0.86	20	100 (10)	5.8 (0.4)
7	(*S*)-**2**	2.3	20	90 (70)	8.4 (0.1)
8	(*S*)-**2**	2.3	50	420 (30)	4.9 (0.3)

[a] 3 μmol of catalyst used.

Table 2.3 Selectivity and activity for 3,5,5-trimethyl-1-hexene polymerizations carried out at various olefin concentrations and temperatures. Polymerizations were carried out in toluene with MAO (1000 equiv.) and 1 mmol catalyst. Numbers in parenthesis indicate average error.

We therefore undertook the polymerization of 3,5,5,-trimethyl-1-hexene at different initial olefin concentrations using (*S*)-**1** and (*S*)-**2** as precatalysts (Table 2.3, entries 2, 3, 6, and 7). Curiously, for polymerizations catalyszed by (*S*)-**1**, selectivity factors are greater when toluene is used as opposed to tetradecane (compare entry 3 in Table 2.3 with entry 2 in Table 2.1). Previously, we reported that selectivity factors were insensitive to the solvent used for the reaction,[11] but we did not polymerize 3,5,5-trimethyl-1-hexene in toluene in that study. At this time we have no explanation for this anomaly. Nevertheless, the results presented in Table 2.3 are inconsistent with polymerizations where site epimerization competes with chain propagation because selectivity factors remain the same (for (*S*)-**1**) or even decrease with decreasing olefin concentration (for (*S*)-**2**). The only explanation that we have for the latter trend is that polymers obtained at lower olefin concentrations should have lower molecular weights

and consequently lower selectivities (*vide supra*). However, this explanation is not very satisfying because oligomers were not observed in the gas chromatograph used for determining conversion, and a near quantitative mass balance was obtained from the polymer yields for all the polymerizations. It seems unlikely that there will be enough unselective initiation events to impact the selectivity factor much when primarily polymer is formed in the reaction.

To compliment the olefin concentration results, 3,5,5-trimethyl-1-hexene was polymerized at different temperatures using (*S*)-**1** and (*S*)-**2** as catalysts (Table 2.3). The results are displayed graphically in Figure 2.6 and clearly show that selectivity decreases with increasing temperature for both catalysts. Selectivity factors are expected to be particularly sensitive to temperature if second order chain propagation is in competition with first order site epimerization. Under these circumstances the second order process, typically characterized by a more negative entropy of activation, should be less important than the first order process at higher temperatures. Therefore, site epimerization should predominate at higher temperatures, and selectivity factors should increase with temperature. This expectation is the opposite to what is observed for the polymerization of 3,5,5-trimethyl-1-hexene suggesting once again that chain propagation is not in competition with site epimerization.

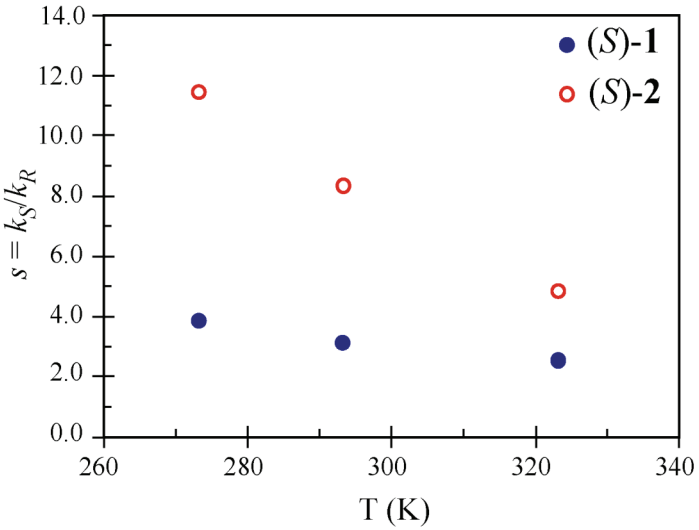

Figure 2.6. Temperature dependence of selectivity factors (*s*) during 3,5,5-trimethyl-1-hexene polymerizations catalyzed by (*S*)-**1** and (*S*)-**2**.

Effect of added trimethylaluminum on selectivity during 3,4-dimethyl-1-pentene polymerizations. During the course of these investigations an interesting observation was made. If the methylaluminoxane (MAO) used was not exhaustively dried, selectivity factors during kinetic resolutions would be erroneously low. It was surmised that MAO containing traces of trimethylaluminum caused increased amounts of chain transfer and consequently more insertions into metal hydrides, which are known to be unselective (*vide supra*). To test whether adventitious trimethylaluminum was affecting selectivity, 3,4-dimethyl-1-pentene polymerizations were carried out by adding known amounts of trimethylaluminum to exhaustively dried MAO (using (*S*)-**1** as the catalyst). The results from this brief investigation appear in Table 2.4.

As anticipated, the addition of 175 equivalents of trimethylaluminum (relative to zirconium) to the reaction significantly decreased the selectivity from 15.3 to 3.4 (Table 2.4). The addition of 328 equivalents of trimethylaluminum degraded the selectivity even further but the difference in selectivity between 175 and 328 equivalents of added trimethylaluminum was modest. In conjunction with the lower selectivities, 3,4-

dimethyl-1-pentene dimers were observable in the GC used to follow the reaction. The observation of dimers in the GC is consistent with the molecular weight explanation for the low selectivities observed in the presence of trimethylaluminum. However, this explanation does not explain why increasing the trimethylaluminum equivalents from 175 to 328 did not affect selectivity as significantly as going from no added trimethylaluminum to 175 equivalents.

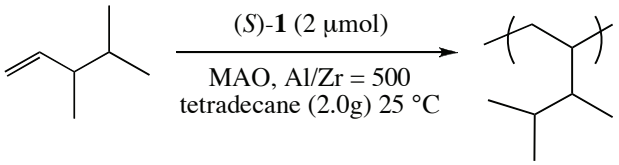

Al/Zr	Me_3Al (equiv.)	conv.(%)	TOF	e.e.(%)	s (k_S/k_R)
1100	0	39.7	40	52.7	15.3
764	175	48.2	21	38.3	3.4
1114	328	19.5	16	11.0	3.0

Table 2.4 Effect of added trimethylaluminum on selectivity during 3,4-dimethyl-1-pentene polymerizations catalyzed by (*S*)-**1**/MAO.

An alternative explanation for this behavior is that trimethylaluminum impedes site epimerization relative to olefin propagation thereby allowing for insertions to occur from both sides of the zirconocene wedge. As shown in Scheme 2.4, coordination of trimethylaluminum to the zirconocene polymerization should slow site epimerization because the polymer chain would have to displace the coordinated trimethylaluminum. This explanation is consistent with the saturation behavior observed for the selectivity factors because at some trimethylaluminum concentration all of the active catalytic sites would contain bound trimethylaluminum. It is also reasonable to think that trimethylaluminum would affect the site epimerization rates more than the *relative* insertion rates from the two catalytic sites.

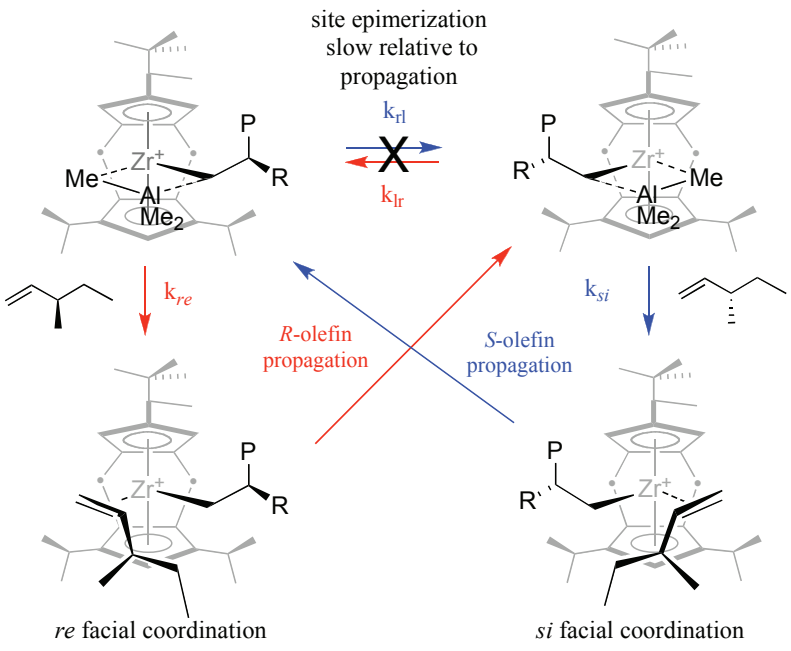

(P = remaining polymer chain; R = $CH(CH_3)CH_2CH_3$)

Scheme 2.4 Trimethylaluminum coordination and its effect on site epimerization.

To probe this possibility, the $^{13}C\{^1H\}$ NMR of poly(3,4-dimethyl-1-pentene) produced in the presence and absence of trimethylaluminum were obtained. To our surprise, the spectrum for each polymer was exceedingly simple each containing a single resonance for every carbon in the polymer. Equally surprising was that the spectra with and without added trimethylaluminum were identical despite the fact that the two samples displayed different solubility properties. Furthermore, the solubility properties complicated our understanding of the situation as the sample polymerized in the presence of added trimethylaluminum was *less* soluble than the sample polymerized *without* trimethylaluminum. The simple NMR spectra indicate that highly isotactic poly(3,4-dimethyl-1-pentene) was produced in the presence and absence of trimethylaluminum. This conclusion suggested that the selectivity degradation observed during kinetic resolution is likely due to the molecular weight phenomena. On the other hand, the solubility properties for the polymers do not support this explanation because it is commonly observed that polymer solubility increases with *decreasing* molecular weight,

which is opposite to what was observed as the polymer produced in the presence of trimethylaluminum (producing lower molecular weight polymer) is *less* soluble. Unfortunately, the results from this NMR study were inconclusive.

It stands to reason that if trimethylaluminum affects site epimerization rates, this should manifest itself in propylene polymerizations and could be modeled in a similar fashion as above. A propylene polymerization carried out in dilute propylene with added trimethylaluminum was therefored accomplished using (*S*)-**1** as the catalyst. The most striking thing about this polymerization is the three orders of magnitude decrease in turnover frequency (Table 2.5). The polymer produced was clearly isotactic and appeared similar to polypropylene produced without trimethylaluminum. However, a careful examination of the pentads revealed some differences. Notably, the [*mmmm*] was 54% compared to 63% for polymerizations carried out in the presence and absence of trimethylaluminum, respectively. The decrease in [*mmmm*] content is consistent with trimethylaluminum impeding site epimerization. However, using the unidirectional site epimerization model and α and β determined previously, ε for the polymerization carried out with added trimethylaluminum was approximately the same (0.86) compared to ε for the polymerization carried out without trimethylaluminum (0.89). It is important to note that α and β could be different in the presence of added trimethylaluminum. At this time we do not have the neat polypropylene data necessary to derive α and β accurately.

Me_3Al (equiv.)	activity ($g_{poly}/(g_{cat}*h)$	[*mmmm*]	[*mmmr*]	[*rmmr*]	[*mmrr*]	[*mrmm*]+ [*rrmr*]
0	2.5×10^3	62.9	14.0	0.9	12.7	3.8
125	7.5×10^1	53.6	16.6	1.2	11.7	6.5
Me_3Al (equiv.)	activity ($g_{poly}/(g_{cat}*h)$	[*mrmr*]	[*rrrr*]	[*mrrr*]	[*mrrm*]	[*r*]
0	2.5×10^3	0.0	0.0	1.5	4.4	14.1
125	7.5×10^1	0.0	1.5	3.0	6.0	19.6

Table 2.5 Pentad analysis for propylene produced in the presence and absence of added trimethylaluminum at $[C_3H_6]$ = 0.8 M. Polymerizations carried out in 20 mL toluene and under constant pressure of propylene at 20 ºC.

2.4 Conclusions

The synthesis of (*S*)-**2** and its use for the kinetic resolution of racemic α-olefins by polymerization revealed enhanced selectivity compared to (*S*)-**1** for most olefins studied. Several experiments were completed which demonstrated that although (*S*)-**2** undergoes more efficient site epimerization than (*S*)-**1** in propylene polymerizations, this mechanism does not account for the difference in selectivities obtained during kinetic resolution of racemic 3-substituted-1-olefins. Due to slow insertion rates, it seems 3-substituted-1-olefins behave similarly to propylene polymerizations at low olefin concentrations where polymer produced from (*S*)-**1** and (*S*)-**2** are indistinguishable. A possible explanation for the observed differences in selectivity is that chain end control is more or less important for (*S*)-**2** compared to (*S*)-**1**. This explanation is particularly attractive because the olefin that displays the biggest difference in selectivity between the two catalysts, 3,5,5-trimethyl-1-hexene, belonged to a class of olefins (the substituted hexene monomers) that displayed different chain end control behavior for polymerizations catalyzed by (*S*)-**1** (See Chapter 1). Indeed, initial ethylene/3,5,5-

trimethyl copolymerizations, which probe chain end control by removing the chiral chain with long runs of achiral comonomer, suggest that chain end control is more important for (*S*)-**2** compared to (*S*)-**1** because a copolymerization selectivity factor of 1.7 was observed compared to 8.0 for homopolymerization. For comparison the corresponding selectivity factors for homo- and ethylene copolymerizations catalyzed by (*S*)-**1** are 2.1 and 1.2, respectively.[11]

Finally, the challenges associated with the synthesis of (*S*)-**2** preclude any further modification of catalysts based on (*S*)-**1** for the kinetic resolution of racemic α-olefins. Unfortunately, replacing the ethyl group with something more sterically bulky like isopropyl would likely not be possible for several reasons. First, reduction of the ketone used to synthesize (*S*)-**2** required stoichiometric amounts of the chiral CBS borane to produce the alcohol product with high *e.e.*'s (Scheme 2.3). It is unlikely that a less sterically biased ketone could be reduced with high enantioselectivities with the CBS catalyst or any other chiral reducing agent. Even if enantioselective reduction were possible (or another route to the alcohol was devised), formation of the chiral Cp may be difficult because it involves S_N2 displacement of a tertiary mesylate or tosylate with cyclopentadiene anion. S_N2 displacement of the mesylated (*R*)-**3**, during the synthesis of (*S*)-**2** was plagued with a competing elimination reaction to give internal alkenes. Finally, substituting an ethyl group with an isopropyl group in **2** may allow rotation of the C-C bond between the cyclopentadiene and the stereogenic carbon. Steric difference between *tert*-butyl and isopropyl groups may not be enough to lock this C-C bond in one rotational conformation, and free rotation of this bond would effectively epimerize the chirality of the zirconocene by oscillating the sterically more hindered side of the zirconocene wedge (Scheme 2.5)

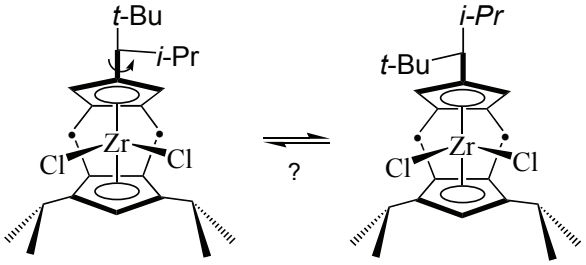

Scheme 2.5 Decreased rotational barrier for a hypothetical isopropyl-neopentyl catalyst.

For all of these reasons, other classes of enantiopure catalysts are currently being pursued for kinetic resolution of racemic α-olefins including C_2-symmetric zirconocenes (Chapter 3) and non-metallocene catalysts.

2.5 Experimental Section

General methods. All air and/or moisture sensitive materials were handled using high-vacuum line, swivel frit assembly (see swivelfrit.mov for a demo), glove box, Schlenk, and cannula techniques under a nitrogen or argon atmosphere.[12] Argon was purified by passage through MnO on vermiculite and activated 4 Å molecular sieves. Propylene (polymer purity, Matheson) was passed through an Oxisorb column (Matheson) before use. All glassware was oven dried before use.

Solvents were dried and degassed over sodium benzophenone ketyl, calcium hydride, or over titanocene.[13] Trimethylaluminum was purchased from Aldrich and used as received. Polymerization catalysts (*S*)-**1**[3] and (*S*)-**2**[7] were synthesized as previously reported. 3-methyl-1-pentene and 3,5,5,-trimethyl-1-hexene were purchased from Chemsampco. 3,4,4-trimethyl-1-pentene and 3,4-dimethyl-1-pentene were prepared as previously described. All olefins were dried and degassed over $LiAlH_4$ for 2 d, then vacuum transferred and stored in Schlenk flasks over CaH_2. In some cases, olefins stored over $LiAlH_4$ formed into an unusable gel. Methylaluminoxane (MAO) was purchased from Albemarle as 10% or 30% toluene solution. All volatiles were removed *in vacuo* to give a white powder. The white MAO solid was dried at 150 ºC for 12 h *in vacuo* high.

Tetradecane was dried over sodium and vacuum distilled into a Schlenk flask, which was stored in the glove box.

NMR spectra to characterize compounds were recorded on a Varian Mercury VX300 spectrometer (^{1}H, 300 MHz, ^{13}C{^{1}H}, 75 MHz). ^{13}C{^{1}H} NMR spectra of polymers were obtained at 100 120 ºC on a Varian Inova spectrometer operating at 125 MHz using an acquisition time of 3 s, a relaxation delay of 6 s, a sweep width of 3000 Hz, and a 90º pulse angle. At least 3000 transients were obtained. Conversions for polymerizations were determined by gas chromatography (Agilent 6890) using a 30 m x 0.25 mm polysiloxane "HP 5" column or a 10 m x 0.1 mm "DB-1" column from Agilent technologies. Enantiomeric excess was determined by gas chromatography (Agilent 6890) using a 30 m x 0.25 mm γ cyclodextrin trifluoroacetyl "Chiraldex TA" column from Advanced Separations Technology. Single crystal X-ray crystallography was carried out on a Bruker SMART 1000 difractometer. Atomic coordinates as well as bond distances and angles for (*S*)-**2** appear in Appendix F.

The three parameter unidirectional site epimerization model was developed previously[9] and fits to the theoretical model were performed by least squares analysis using Excel. A short description of the model as well as results from the model varying all three parameters and only ε using α and β from neat polypropylene polymerizations appear in Appendix G.

Generic polymerization procedure for racemic α-olefins. MAO (500-1000 equiv.) and tetradecane (1.5 mL) were added to a Schlenk flask (10 mL) with a side arm containing a glass stopcock. The appropriate olefin (1.5-2.0 mL) was vacuum transferred onto the reaction mixture. For reactions in toluene, toluene was also vacuum transferred onto the reaction (in these cases only a small amount of tetradecane was added to the reaction for an internal standard). The mixture was stirred under argon for a minimum of 30 minutes. An aliquot was removed via the side arm for a t = 0 reference point. A

catalyst stock solution (2 μM) was generally made in toluene or benzene by vacuum transferring the appropriate solvent (3.5 mL) onto the catalyst (5 mg). This solution was used within a few d of preparation. No difference in selectivity or turnover was noticed for older catalyst solutions. The catalyst solution (1-2 x 10^{-3} mmol) was added by syringe to the reaction vessel via the side arm. The reaction mixture generally turned pale yellow. The polymerization was followed by GC by taking occasional aliquots from the reaction (reactions generally take 13-24 h.). When the reaction was 30%-70% complete, it was stopped by vacuum transferring the remaining volatiles. The MAO was quenched with 10% HCl in methanol (10 mL). The polymer was further purified by precipitation into methanol (200 mL) and stirring overnight. The polymer was dried *in vacuo* at room temperature overnight. Enantioassay was performed as previously described[3] and as outlined in Chapter 1.

Polymerization of racemic α-olefins at T = 0 ºC. The procedure is the same as the generic polymerization procedure except that the reaction was equilibrated at 0 ºC with a circulating bath prior to the t = 0 GC aliquot, and toluene was used as the internal standard. Catalyst loadings were also higher for these polymerizations (3-4 x 10^{-3} mmol in 0.5 mL benzene).

Polymerization of racemic α-olefins at T = 50 ºC. The procedure is the same as the generic polymerization procedure except a Schlenk tube (50 mL) without a side arm was used. This change was made to avoid olefin loss at elevated temperatures. Unfortunately, this change also precludes following the reaction by multiple aliquot removal for fear that olefin evaporation would be significant. Additionally, the catalyst solution (1 x 10^{-3} mmol) was introduced to the reaction at ambient temperatures via the Teflon stopcock of the Schlenk tube, then rapidly brought to 50 ºC where it stirred for 2-4 h.

Polymerization of propylene in toluene solutions. MAO (250 mg, ~1000 equiv.) and toluene (20 mL) were added to a glass reactor (125 mL, Andrews Glass Co, max. pressure 200 psig) equipped with a septum port, a three way valve connected to a quick disconnect, a large stir bar, and a pressure gauge (0-300 psig*). CAUTION: this procedure should be preformed behind a blast shield*. The flask was connected to the propylene tank and purged with propylene at pressures slightly greater than 1 atm for 5 minutes. The flask was pressurized to the appropriate pressure of propylene[14] for 15 minutes prior to catalyst injection. A catalyst stock solution (2 μM) was made in the glove box by dissolving the catalyst (5 mg) in toluene (3.5 mL). This solution was used within a few d and was stored at -30 ºC in the glove box. No differences in activity or tacticity were noticed for polymerizations run with older catalyst solutions. An aliquot of the stock solution (0.5 mL, 1 x 10^{-3} mmol) was loaded in a 1 mL gas-tight syringe equipped with a long 18-gauge steel needle. The needle was stopped with a septum, and brought out of the glove box. The catalyst solution was injected via the septum port against the propylene pressure of the reaction. The reaction was run open to the propylene tank at the appropriate pressure with rapid stirring (700 rpm). The reaction was run for 10-30 minutes depending on the propylene pressures with lower propylene pressures requiring longer reaction times. The polymerization was stopped by slowly releasing the excess propylene pressure. The MAO was quenched by slow addition of 10% HCl/MeOH (20 mL). After stirring for 30 minutes, the polymer was further purified by precipitation into methanol (400 mL). This mixture was allowed to stir a few hours to dissolve all of the aluminoxane. The polymer was isolated by filtration and washed with fresh methanol (3 x 10 mL). The polymer was dried *in vacuo* at 110 ºC overnight. The polymer microstructure was determined by $^{13}C\{^{1}H\}$ NMR (1,1,2,2-tetrachloroethane-d_2, 110 ºC).

Polymerization of propylene in neat propylene (T = 0 ºC). The procedure was the same as for propylene polymerizations carried out in toluene solutions except only 3 mL of toluene was initially loaded into the reaction vessel. Propylene (~20 mL) was condensed into the reaction vessel at 0 ºC. The reaction was maintained at 0 ºC with an ice bath. The reaction was run for 10 minutes before quenching as outlined above.

2.6 References and Notes

1. (a) Brintzinger, H. H.; Fischer, D.; Mu'lhaupt, R.; Rieger, B.; Waymouth, R. M. *Ang. Chem., Int. Ed.*, **1995**, *34*, 1143; (b) Britovsek, G.; Gibson, J. P.; Wass, D. F. *Ang. Chem., Int. Ed.*, **1999**, *38*, 428; (c) Coates, G. W. *Chem. Rev.*, **2000**, *100*, 1223; (d) Resconi, L.; Cavallo, L.; Fait, A.; Piemontesi, F. *Chem. Rev.*, **2000**, *100*, 1253; (e) Wang, B. *Coord. Chem. Rev.*, **2006**, *250*, 242.
2. (a) Corrandini, P.; Guerra, G.; Vacatello, M.; Villani, V. *Gazz. Chim. Ital.*, **1988**, *118*, 173; (b) Corrandini, P.; Guerra, G.; Cavallo, L.; Moscardi, G.; Vacatello, M. *Ziegler Catalysis,* (Eds. G. Fink, R. Mu'lhaupt and H. H. Brintzinger); Springer-Verlag: Berlin, **1995**, 237; (c) Gilchrist, J. H.; Bercaw, J. E. *J. Am. Chem. Soc.*, **1996**, *118*, 12021; (d) Grubbs, R. H.; Coates, G. W. *Acc. Chem. Res.*, **1996**, *29*, 85.
3. Baar, C. R.; Levy, C. J.; Min, E. Y.-J.; Henling, L. M.; Day, M. W.; Bercaw, J. E. *J. Am. Chem. Soc.*, **2004**, *126*, 8216.
4. (a) Ciardelli, F.; Carlini, C.; Altomare, A. *Ziegler Catalysis* (Eds. G. Fink, R. Mulhaupt and H. H. Brintzinger); Springer-Verlag: Heidelberg, **1995**, 455; (b) Chien, J. C. W.; Vizzini, J. C.; Kaminsky, W. *Mak. Chem., Rap. Comm.*, **1992**, *13*, 479.
5. (a) Herzog, T. A.; Zubris, D. L.; Bercaw, J. E. *J. Am. Chem. Soc.*, **1996**, *118*, 11988; (b) Veghini, D.; Henling, L. M.; Burkhardt, T. J.; Bercaw, J. E. *J. Am. Chem. Soc.*, **1999**, *121*, 564.

6. (a) Zambelli, A.; Proto, A.; Pasquale, L. *Ziegler Catalysis* (Ed. G. Fink); Springer-Verlage: Heidelber, **1995**, 218; (b) Oliva, L.; Longo, P.; Zambelli, A. *Macromolecules*, **1996**, *29*, 6383; (c) Sacchi, C.; Barsties, E.; Tritto, I.; Locatelli, P.; Brintzinger, H. H.; Stehling, U. *Macromolecules*, **1997**, *30*, 1267.

7. Min, E. Y.-J., Ph D thesis, California Institute of Technology, **2005**.

8. Enzymatic kinetic resolution of (*R*)-**4** was also attempted, but the desired alcohol could not be recovered in high yields and optical purities.

9. Miller, S. A., Ph D thesis, California Institute of Technology, **2000.**

10. (a) Casey, C. P.; Tunge, J. A.; Lee, T.; Fagan, M. A. *J. Am. Chem. Soc.*, **2003**, *125*, 2641; (b) Klamo, S. B., Ph D thesis, California Institute of Technology, **2005.**

11. Byers, J. A.; Bercaw, J. E. *Proc. Nat. Acad. Sci.*, **2006**, *103*, 15289.

12. Burger, B. J.; Bercaw, J. E. *New Developments in the Synthesis, Manipulation and Characterization of Organometallic Compounds* (Eds. A. Wayda and M. Y. Darensbourg); American Chemical Society: Washington DC, **1987**.

13. Marvich, R. H.; Brintzinger, H. H. *J. Am. Chem. Soc.*, **1971**, *93*, 203.

14. Frank, H. P. *Oster. Chem. Zeit.*, **1967**, *11*, 360.

CHAPTER THREE

SYNTHESIS OF ENANTIOPURE C_2-SYMMETRIC ZIRCONOCENES FOR THE KINETIC RESOLUTION OF RACEMIC α-OLEFINS

3.1 Abstract

Enantiopure synthesis of C_2-symmetric zirconocenes and their use for kinetic resolution of racemic α-olefins by polymerization is reported. Although the classical resolution of racemic zirconocenes was unsuccessful with reagents such as 1,1'-bi-2-naphthol (BINOL) or (*R*)-O-acetyl-mandelic acid, enantioselective synthesis of the zirconocenes was possible using chelating chiral auxiliaries. When coordinated to zirconium, the bisphenoxide ligand (*R*)-3,3'-di-tert-butyl-5,5',6,6'-tetramethyl-1,1'-bi-2-phenol ((*R*)-BIPHEN) (**5**) could effectively direct the coordination of Li{Me_2Si(1-indene)$_2$} (Li{SBI}) to form one C_2-symmetric enantiomer, {(*R*,*R*)-SBI}Zr{(*R*)-BIPHEN}. Attempts to remove the BIPHEN chiral auxiliary were unsuccessful often resulting in zirconocene racemization. To circumvent this problem, the diamine ligand (*R*)-N^2,$N^{2'}$-di-*p*-tolyl-1,1'-binaphtyl-2,2'-diamine ((*R*)-tolBINAM, (*R*)-**5**) was synthesized. When coordinated to zirconium, (*R*)-tolBINAM effectively directed the coordination of Li{C_2H_4-1,2-(1-indene)$_2$} (Li_2{EBI}) to give one diastereomer, {(*S*,*S*)-EBI}Zr{(*R*)-tolBINAM} (*S*,*S*,*R*)-**18**, which underwent a ligand metathesis reaction with hydrochloric acid to give (*S*,*S*)-(EBI)$ZrCl_2$, (*S*,*S*)-**3**. Enantiopure zirconocenes could be synthesized for EBI ligands with substituents located on the indenyl six-membered rings but substituents installed on the five-membered ring were not tolerated. Racemic α-olefin polymerization with (*S*,*S*)-**3**, and (*S*,*S*,*R*)-**18** gave identical selectivity factors (*s*) but

lower activities for the latter. This suggests that the chiral auxiliary does not play a role in asymmetric induction but does inhibit initiation. Low selectivity factors ($s = k_S/k_R$ = 1.5-4.0) were observed for all olefins investigated, but a constant selectivity was observed for a range of conversions suggesting that the zirconocene does not racemize during polymerization.

3.2 Introduction

In the previous two chapters, mechanistic considerations were investigated that may limit kinetic resolution of racemic α-olefins by polymerization using C_1-symmetric zirconocene catalysts based on **1**.[1] Because modification of **1** was synthetically challenging and only modest changes in selectivity resulted,[2] investigation into other catalysts for kinetic resolution was and continues to be pursued in our laboratory.[3] When considering alternative catalysts, it is instructive to return to the original design principles. First, the catalyst must be very active for polypropylene polymerizations because polymerization rates are much slower for bulky 3-substituted olefins that are used for kinetic resolution.[4] Next, the catalyst should show high levels of isospecificity so that olefin insertions occur from the same enantioface for every insertion. Finally, an enantiopure catalyst that does not undergo racemization during polymerization must be synthesized.

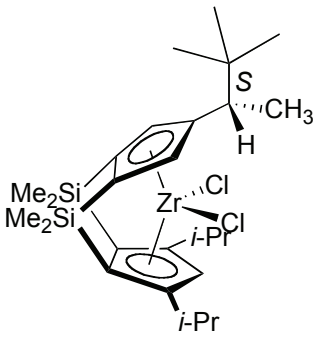

1

An attractive class of catalyst that meets most of these criteria are C_2-symmetric bis-indenyl *ansa*-zirconocenes such as (*rac*)-{$Me_2Si(\eta^5$-1-indenyl$)_2$}$ZrCl_2$ **2** ((*rac*)-(SBI)$ZrCl_2$)[5] and (*rac*)-{$C_2H_4(\eta^5$-1-indenyl$)_2$}$ZrCl_2$ **3** ((*rac*)-(EBI)$ZrCl_2$).[6] These catalysts are very active for propylene polymerizations (190 and 188 $kg_{poly}/mmol_{cat}$*h, respectively),[7,8] and since the two polymerization sites on the catalysts are identical, olefin insertions occur from the same enantioface leading to highly isotactic polypropylene ([*mmmm*] = 81.7 and 78.5, respectively).[7]

It seems that the major limitation for these catalysts is the ability to synthesize them in an enantiopure fashion. It is important to emphasize the complexity associated with this limitation. Zirconocenes such as **2** and **3** are typically synthesized either by salt metathesis between the deprotonated ligand precursor and zirconium tetrachloride or by an amine elimination route from reaction of the protonated ligand with zirconium tetrakis dimethylamide followed by chlorination with reagents such as trimethylsilyl chloride. During the course of either metallation reaction, three stereoisomers can form two C_2-symmetric isomers (*R*,*R* and *S*,*S* or the *rac* isomers) and one C_s-symmetric isomer (*S*,*R* = *R*,*S* or *meso* isomer) (Scheme 3.1). Statistically, the *meso* and *rac* diastereomers should form in a 1:1 ratio, but thermodynamics can favor one or the other diastereomer depending on the ligand identity and reaction conditions. Since the *meso* diastereomer has been shown to yield atactic polypropylene[9] and its separation from the isospecific *rac* isomers can be difficult, much effort has been devoted towards the synthesis of C_2-symmetric catalysts devoid of the *meso* diastereomer.[10-16] In addition to this complication, there is evidence that interconversion between the stereoisomers can occur either with the assistance of salts such as lithium chloride or by a radical mechanism (Scheme 3.1).[16-18] All of these factors make any attempt to synthesize enantiopure C_2-symmetric zirconocene complicated.

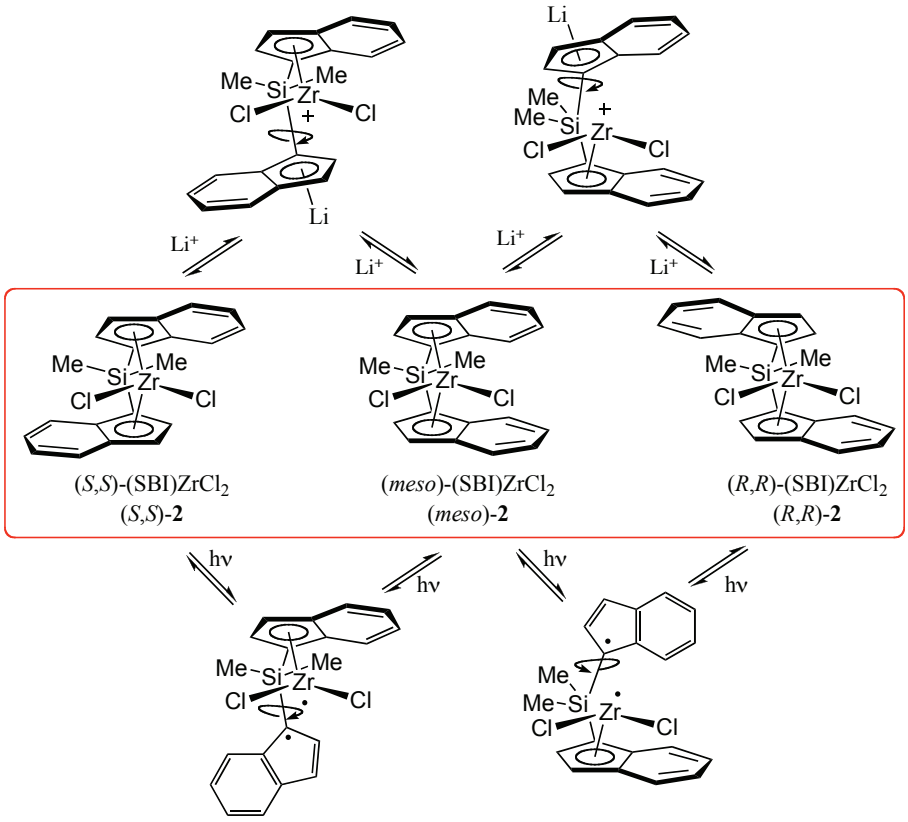

Scheme 3.1 Stereoisomers and known racemization mechanisms for **2**.[16-18]

At the onset of our investigation, only a few enantiopure C_2-symmetric Group III/IV metallocenes had been synthesized,[16,19-23] the most notable of which was Brintzinger's catalyst, {C_2H_4-1,2-(η^5-4,5,6,7,-tetrahydro-1-indenyl)}$ZrCl_2$ **4** ((EBITHI)$ZrCl_2$).[20,21,23] Brintzinger showed that enantiopure (*S*,*S*)-**4** could be obtained by resolving a racemic mixture of the zirconocene upon reaction with (*S*)-1,1'-bi-2-naphthol ((*S*)-BINOL) or (*R*)-O-acetylmandelic acid followed by treatment with hydrochloric acid.[23] Buchwald improved on the BINOL procedure and provided access to both chiral antipodes of **4** by treating the reaction mixture with an equivalent of 4-aminobenzoic acid, which coordinates the unreacted antipode and causes it to precipitate out of solution. Isolation of the enantiomer in the precipitate can be achieved by treatment with 1,1'-biphen-2,2'diol (Scheme 3.2).[20]

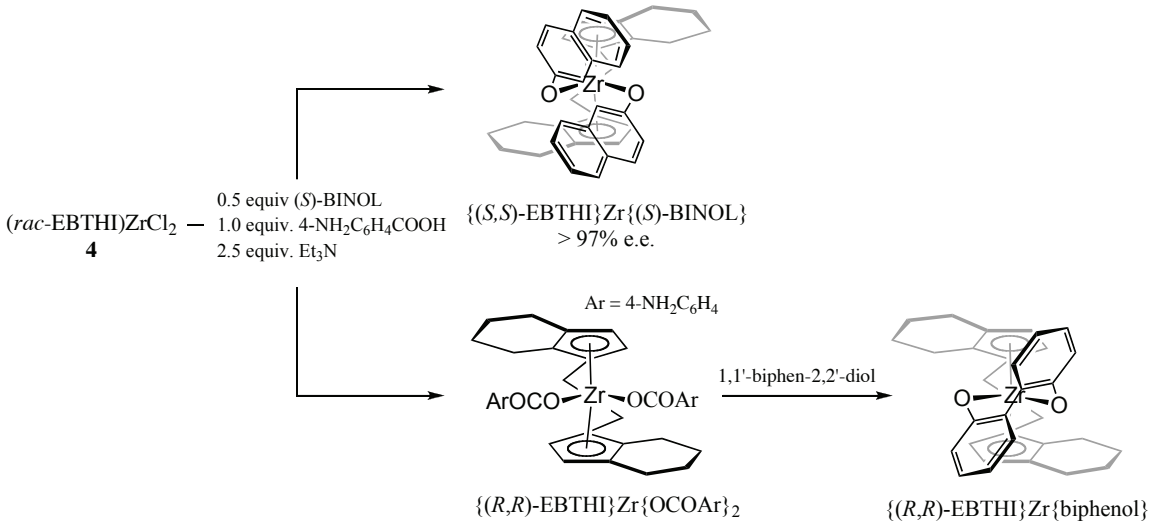

Scheme 3.2 Resolution of (*rac*)-**4** with BINOL.[20]

Enantiopure **4** has been shown to be an effective catalyst for the asymmetric hydrogenation of olefins,[24] ketimines,[23] and enamines.[25] Ciardelli *et. al.* found that {(*S*,*S*)-EBTHI}Zr{(*R*)-O-acetylmandelic acid}$_2$ could be used as a polymerization catalyst for the kinetic resolution of 4-methyl-1-hexene, but the selectivity factor was low ($s = k_S/k_R = 1.4$) (Scheme 3.3).[26] Furthermore, the authors found that the catalyst was inactive for the polymerization of 3-substituted racemic α-olefins such as 3-methyl-1-pentene.

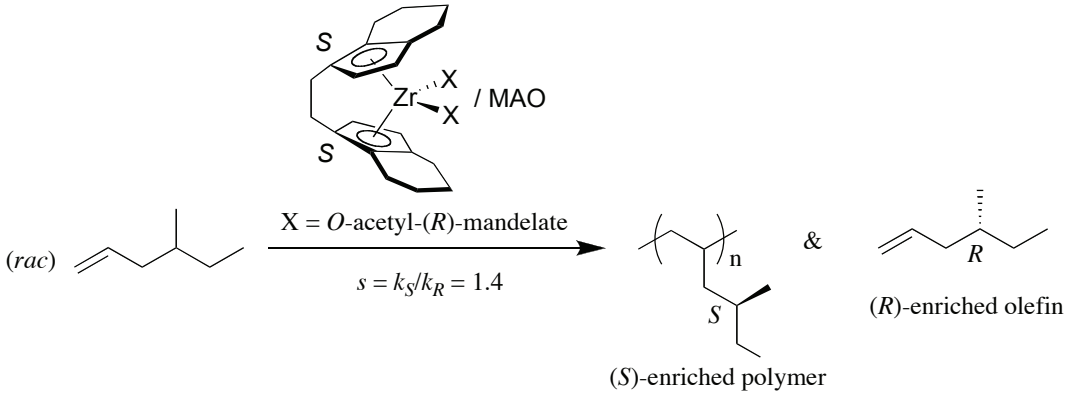

Scheme 3.3 Kinetic resolution of 4-methyl-1-hexene with {(*R*,*R*)-THEBI}Zr{(*R*)-*O*-acetylmandelate}$_2$.

Since the indenyl-based catalysts **2** and **3** were known to polymerize 3-methyl-1-pentene,[27,28] and rapid modification of these catalysts seemed possible due to well-established indene chemistry,[7,8,11,29-31] enantiopure versions of **2** and/or **3** were initially targeted as catalysts for kinetic resolution. There were two main problems that needed to be overcome: (1) a route to enantiopure zirconocenes **2** and/or **3** needed to be devised and (2) it must be shown that racemization of the zirconocene both as the precatalyst and in the activated form does not occur. We now report both a classical resolution approach as well as a chiral auxiliary approach to meet the first requirement, while selectivity factors observed during the course of the kinetic resolution reaction have provided some insight into the question of catalyst racemization.

3.3 Results and Discussion

Attempted resolution of racemic C_2-symmetric zirconocenes. Since resolution of **4** was possible using BINOL or *O*-acetyl mandelic acid, we initially tried to resolve **2** using the methods outlined by Brintzinger[23] and Buchwald.[20] Treatment of **2** with BINOL in the presence of triethylamine in aromatic solvents led to protonation of the dimethylsilyl-*bis*-indenyl ligand and decomposition of the complex. In a second experiment, **2** was treated with the lithium salt of BINOL in the hope that lithium chloride precipitation would drive the product towards one diastereomer.[16] Unfortunately, this reaction was plagued by the insolubility of the deprotonated BINOL and decomposition of the zirconium complex at higher temperatures. When the experiments were repeated in coordinating solvents or with chelators such tetramethylethylenediamine (TMEDA), rapid decomposition occurred. Similar problems were encountered when (*R*)-O-acetylmandelic acid was employed as the resolving reagent. Reaction of (*R*)-O-acetylmandelic acid with **2** in the presence of triethylamine led to the formation of what was believed to be the diastereomeric pair as indicated by

NMR spectroscopy. However, the indenyl ligand was still protonated at a rate comparable to ligand substitution.

Stereospecific synthesis of enantiopure C_2-symmetric zirconocenes using a bisphenolate chiral auxiliary. An alternative route to enantiopure C_2-symmetric zirconocenes is by stereospecific synthesis using a chiral auxiliary followed by removal of the chiral auxiliary to give the zirconocene dichloride or dialkyl precatalysts. Damrau and Brintzinger[15] have used this strategy to synthesize several diastereomerically pure C_2-symmetric zirconocenes including **2** using achiral bisphenolate ligands.[15]

Initially, BINOL was considered as a chiral replacement for the biphenol ligands in order to achieve an enantiospecific reaction, but previous attempts to synthesize related (BINOL)$TiCl_2$ by Heppert and coworkers led to multi-nuclear complexes.[32] Presumably this tendency could be avoided by using a chelating bisphenol with substitution on the carbon adjacent to the alcohol functionality. A convenient compound that meets this requirement was the commercially available 3,3'-di-tert-butyl-5,5',6,6'-tetramethyl-1,1'-bi-2-phenol (BIPHEN). With the racemic bisphenol, a short synthesis of diastereomeric pure C_2-symmetric zirconocenes was accomplished (Scheme 3.4). Treatment of the sodium salt of (*rac*)-BIPHEN (**5**) with $ZrCl_4(THF)_2$ gave (*rac*)-(BIPHEN)$ZrCl_2(THF)_2$, **6**, in 60% yield. When **6** was treated with $Li_2(SBI)\bullet Et_2O$ only one diastereomer of (SBI)Zr(BIPHEN), **7**, was observable by ^1H NMR spectroscopy (Figure 3.1)! Furthermore, racemization of the compound is slow as the ^1H NMR spectrum remained unchanged after several days in solution at room temperature with no precautions taken to shield the reaction from light.

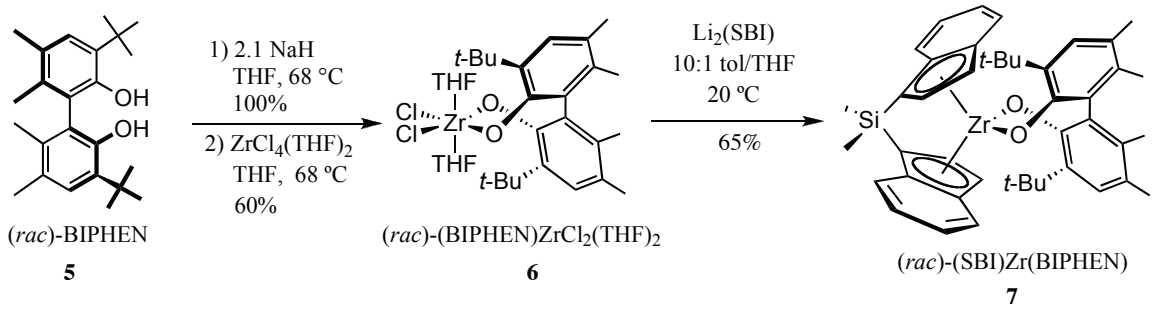

Scheme 3.4 Diastereospecific synthesis of **7** using BIPHEN chiral auxiliary. Note: enantiomer shown for **7** is {(*S*,*S*)-SBI}Zr{(*S*)-BIPHEN}.

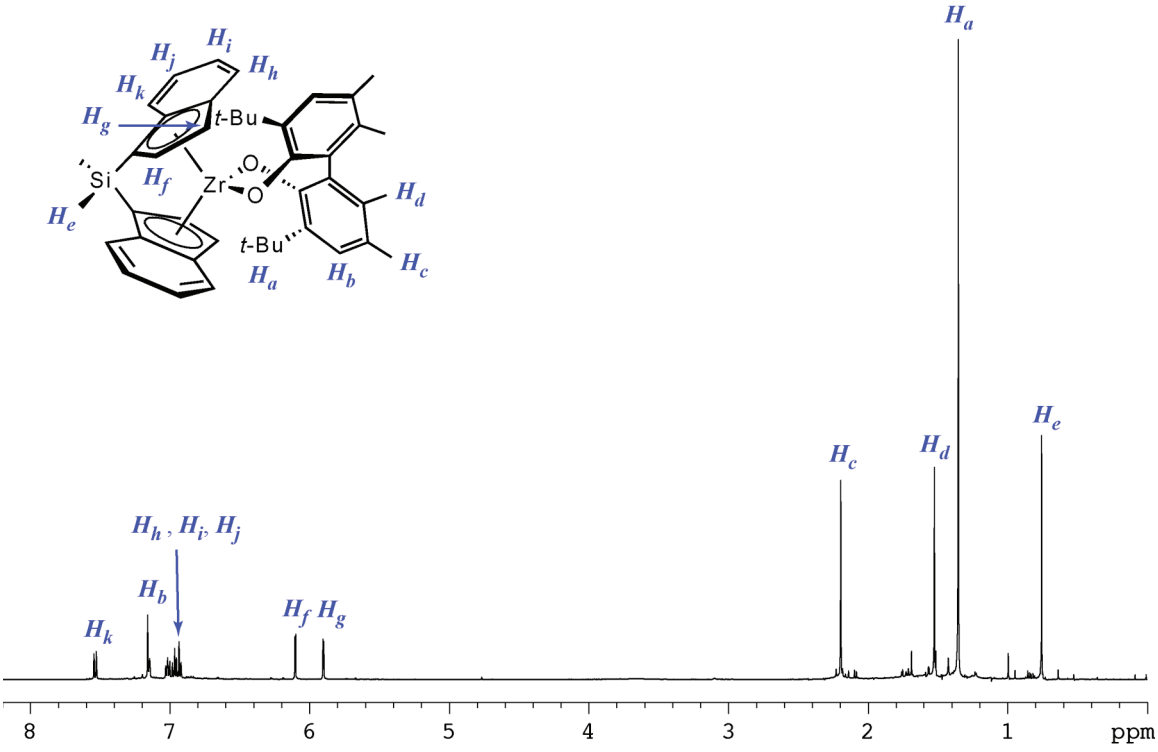

Figure 3.1 ^{1}H NMR of (*rac*)-**7** in C_6D_6.

Since the ^{1}H NMR spectrum of **7** was so simple, it was deduced that the compound was C_2-symmetric. The diastereomer with the indenyl ligand in a *meso* conformation would result in many inequivalent proton resonances that would otherwise be equivalent for a C_2-symmetric diastereomer. Particularly diagnostic was the single dimethylsilyl resonance that appears upfield (0.7 ppm). For (*meso*)-**2**, these protons appear as two singlets whereas (*rac*)-**2** displays only one resonance.[5]

The generality of the synthetic route was investigated on an NMR scale by reacting **6** with several different deprotonated ligands (Scheme 3.5). The method appears to tolerate different *ansa* backbones as demonstrated by the reaction with the ethylene-linked Li_2(EBI), which produced only one C_2-symmetric diastereomer **8**. Additionally, the method is promising for the synthesis of enantiopure cyclopentadiene-based zirconocenes because one major C_2-symmetric diastereomer **9** was observed in the NMR spectrum when 1-$Me_2Si(3\text{-}C_5H_3(CMe_3))_2$ was reacted with **6**.

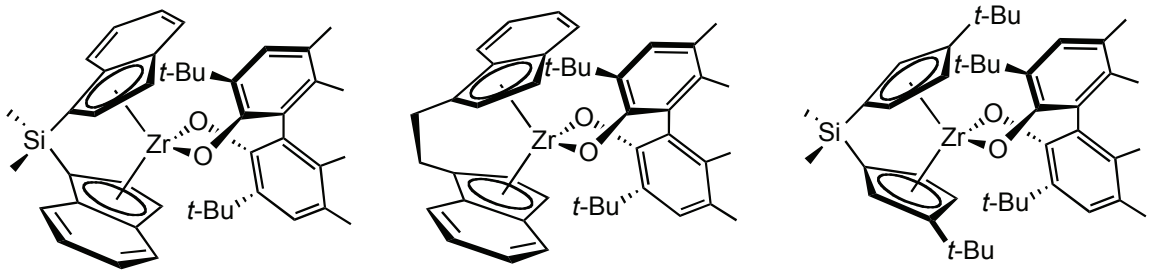

{(*S*,*S*)-SBI}Zr{(S)-BIPHEN} **7**

{(*S*,*S*)-EBI}Zr{(S)-BIPHEN} **8**

{(*S*,*S*)-Dp}Zr{(S)-BIPHEN} **9**

Scheme 3.5 Proposed structures for **7-9** (enantiomers omitted for clarity).

Crystallization of **7** was attempted in order to determine which C_2-symmetric diastereomer was formed by X-ray crystallography (i.e., *R*,*R*,*R* or *S*,*S*,*R* and their respective enantiomeric pair for SBI,SBI,BIPHEN, respectively). Several solvents and mixtures of solvents were tried as well as slow evaporation techniques, but all of these attempts were unsuccessful due to the tendency for **7** to precipitate out of solution as an amorphous solid.

To model the steric interactions involved, PM3 calculations were carried out on the three diastereomers. Figure 3.2 shows the optimized structures from these calculations with their relative free energies using the *meso* isomer as a reference. Although these calculations were carried out at a low level of theory, it was reassuring that the lowest energy diastereomer was a C_2-symmetric diastereomer. Analysis of these structures indicated that the major steric interaction that favors the (*R*,*R*,*R*) diastereomer

is between the *tert*-butyl groups on BIPHEN and the six-membered ring of SBI. This interaction occurs once in the (*meso*,*R*) and twice in the (*S*,*S*,*R*) diastereomers, but not at all in the (*R*,*R*,*R*) diastereomers in which both *tert*-butyl groups occupy space adjacent to the five-membered ring of SBI.

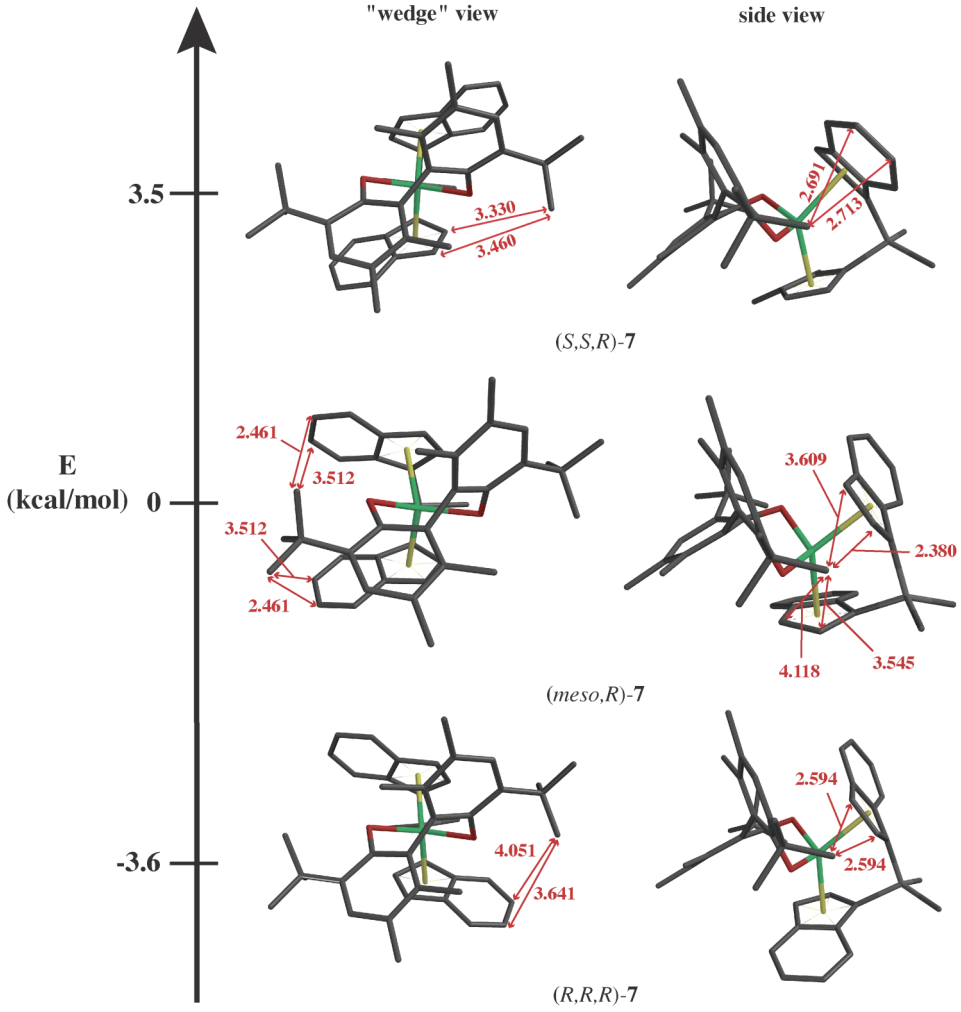

Figure 3.2 PM3 calculations for the three possible diastereomers of **7**. Note: ligand enantiomer shown is (*R*)-BIPHEN.

To corroborate the calculations, a steady-state 1-D nOe difference experiment was carried out on **7**. We anticipated from the calculations that the (*S*,*S*,*R*) diastereomer would display a strong nOe between the *tert*-butyl group and the resonances from the SBI six-membered ring whereas the *tert*-butyl groups for the (*R*,*R*,*R*) diastereomer would have a stronger nOe with resonances from the five-membered ring. When the *tert*-butyl group was irradiated (Figure 3.3), a strong nOe was observed for the doublets at 5.88 and 6.08 ppm as well as for the singlet at 7.13 ppm. A somewhat weaker nOe was observed for resonances at 6.90 and 7.51 ppm. With the aide of other nOe spectra and by analogy to other SBI zirconocenes, the spectrum for **7** could be completely assigned as shown in Figure 3.1. The doublets at 5.88 and 6.08 ppm are distinctive for SBI zirconocenes and are undoubtedly the indenyl hydrogens on the five-membered rings of SBI.[5] The singlet at 7.13 ppm is assigned to the Ar-*H* proton on BIPHEN. The multiplet centered at 6.90 ppm is a combination of three chemically distinct protons (6H in all due to C_2-symmetry) assigned to the indenyl hydrogens on the six-membered rings of SBI. The doublet at 7.51 ppm can be assigned to H_j (Figure 3.1). This assignment was made primarily from the observance of a strong nOe between this resonance and the singlet assigned to the Me_2Si group (0.72 ppm). Qualitatively, the observation of a strong nOe between the *tert*-butyl group of BIPHEN and the five-membered rings of SBI supports an assignment for the (*R*,*R*,*R*) diastereomer for **7** in full agreement with the lowest energy diastereomer found by computation.

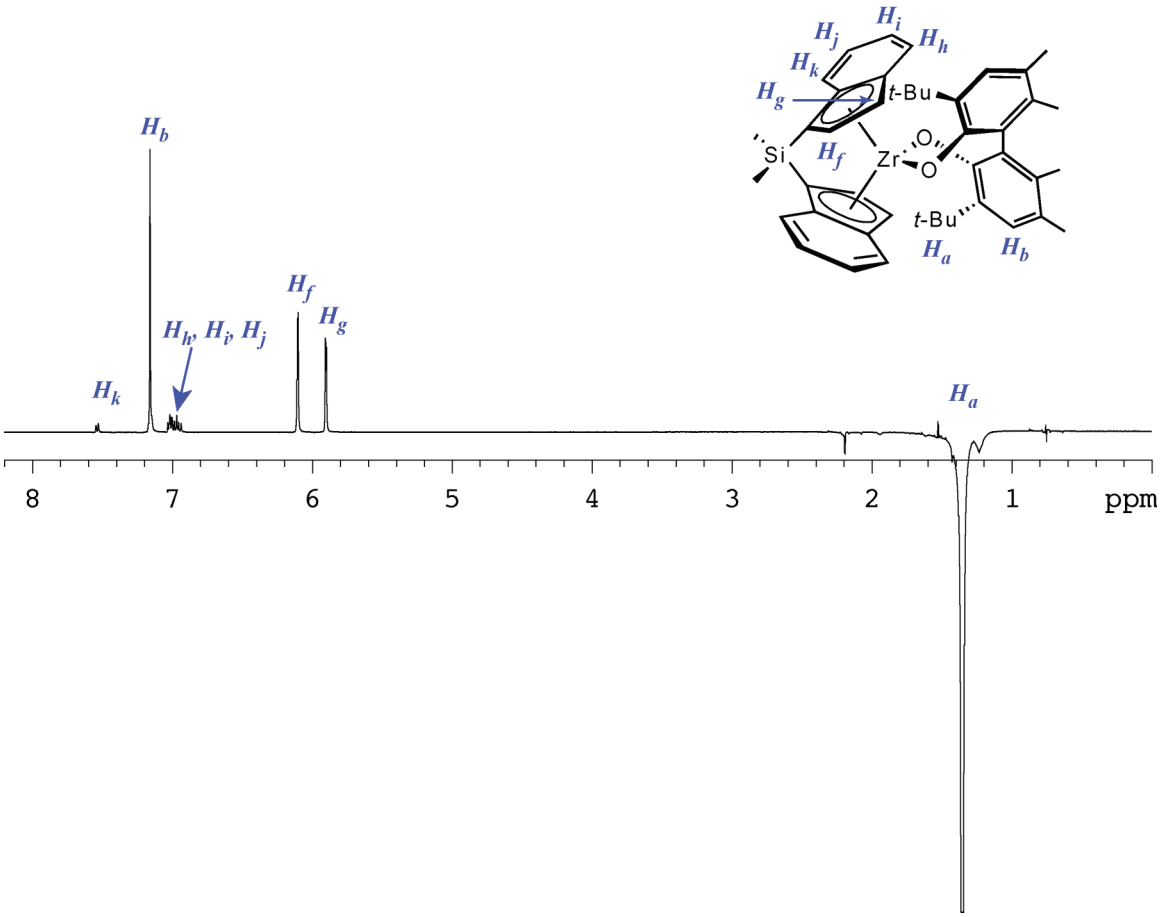

Figure 3.3 1-D nOe difference spectrum of **7** when *tert*-butyl group of BIPHEN was irradiated.

A more quantitative assignment can be achieved by using the *tert*-butyl–Ar-*H* nOe as an internal reference. The calculations suggest that this distance is likely to be insensitive to the diastereomer formed. Therefore, the magnitude of the observed *tert*-butyl–Ar-*H* nOe can be correlated to the value for the corresponding distance from the calculations and an estimate for the distance between the *tert*-butyl group and the five- and six-membered ring protons of the SBI ligand can be made using the well-known $1/r^6$ relationship between the nOe intensity and distance (r).[33] These estimates along with the expected distances for both C_2-symmetric diastereomers from the calculations are presented in Table 3.1. From these data and considering that the (*R*,*R*,*R*) diastereomer is

the diastereomer calculated to be lowest in energy, **7** can be assigned as the (*R*,*R*,*R*) diastereomer with reasonable confidence. Although nOe studies were not carried for **8** and **9**, the major diastereomer for these compounds is presumably (*R*,*R*,*R*) by analogy to **7**.

					distances from PM3 (Å)	
hydrogen	**chemical shift**	**nOe integral**	**normalized nOe[a]**	**calculated distance (Å)**	***(R,R,R)*-7**	**(*S*,*S*,*R*)-7**
H_b	7.13	3.27	1.64	2.27	2.27	2.25
H_g	5.88	1.73	0.86	2.52	2.68	3.46
H_f	6.08	1.98	0.99	2.46	2.59	3.33
H_h	6.91	0.09	0.05	4.09	4.15	3.81
H_i & H_j	7.02	0.99	0.25	3.11[b]	3.85[b]	2.70[b]
H_k	7.51	0.20	0.10	3.62	3.81	3.85

[a] normalized by the number of protons contributing to the signal. [b] average of the two distances.

Table 3.1 Estimated *tert*-butyl–H_n distances from the nOe difference spectrum of **7** and comparison with corresponding distances for the (*S*,*S*,*R*) and (*R*,*R*,*R*) diastereomers from PM3 calculations.

The final step to reach enantiopure precatalysts from **7** is removal of the chiral auxiliary. Unfortunately, this step proved to be problematic. Many different reagents were used in attempts to convert **7** to the corresponding dihalide or dialkyl zirconocene (Scheme 3.6). Attempts to halogenate **7** with trimethylsilyl chloride lead to no reaction whereas treatment with hydrochloric acid lead only to protonated SBI ligand. Aluminum trichloride seemed to react with **7**, but no new Me_2Si resonances were observed in the ^1H NMR spectrum perhaps indicating aluminum coordination to oxygen. Aluminum tribromide successfully converted **7** into (*rac*)-(SBI)$ZrBr_2$ but its formation was apparently accompanied by racemization as an equal amount of (*meso*)-(SBI)$ZrBr_2$ was observed in the ^1H NMR spectrum. When a ligand exchange reaction with zirconium tetrachloride was attempted, the solution turned pale green and the NMR broadened indicating either a paramagnetic or multinuclear species.

Alkylations were initially avoided because Grignards and lithium reagents typically used for alkylations are known to racemize C_2-symmetric zirconocenes.[17] Since halogenation reactions were unsuccessful, however, alkylations were attempted. Unfortunately, reactions with methyl lithium or dimethyl Grignard were messy and irreproducible. Alkylations with trimethyl aluminum suffered a similar fate to aluminum trichloride reactions. Finally, alkylating reagents such as lithium tetramethyl aluminate, typically used for late transition metals, were unreactive towards **7**. The oxophilicity of zirconium and/or the steric hindrance provided by the *tert*-butyl groups of BIPHEN are likely reasons for the complications associated with its removal from **7**.

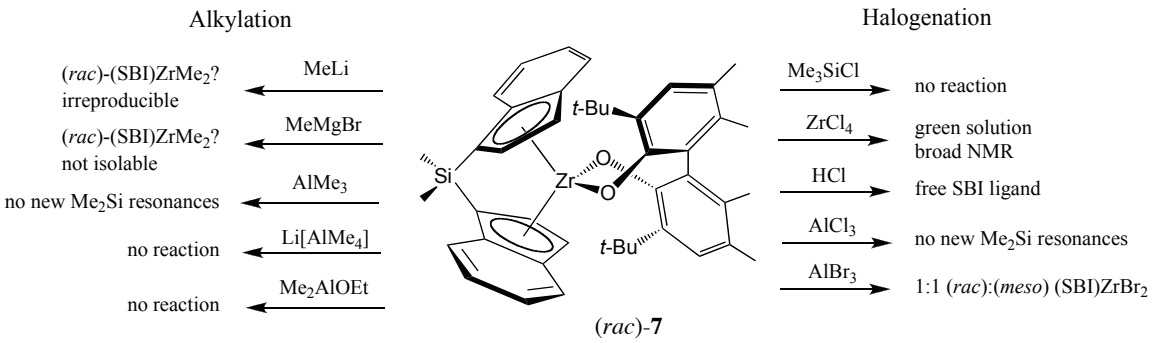

Scheme 3.6 Attempts to remove BIPHEN from (*rac*)-**7** by alkylation or halogenation.

Polymerization of racemic α-olefins using the enantiopure zirconocene catalyst, (*R*,*R*,*R*)-7. Although enantiopure zirconocene dichloride or dialkyl precatalysts were inaccessible with the bisphenoxide route, there are reported examples where bisalkoxide zirconocenes are activated *in situ* with MAO without any detrimental effects to catalyst activity.[15] In these cases MAO is believed to first alkylate the bisalkoxide then activate the dialkyl species towards polymerization by methide abstraction. Figure 3.4 is a plot of conversion versus time for the polymerization of 3-methyl-pentene catalyzed by (*rac*)-**7**/MAO and (*rac*)-**2**/MAO. It is clear from this plot that (*rac*)-**7**/MAO is less active than (*rac*)-**2**/MAO presumably because MAO activates only a small portion of (*rac*)-**7**

towards polymerization. Turnover frequencies after 30 hours of polymerization indicate that (*rac*)-**2**/MAO is approximately six times faster than (*rac*)-**7**/MAO.

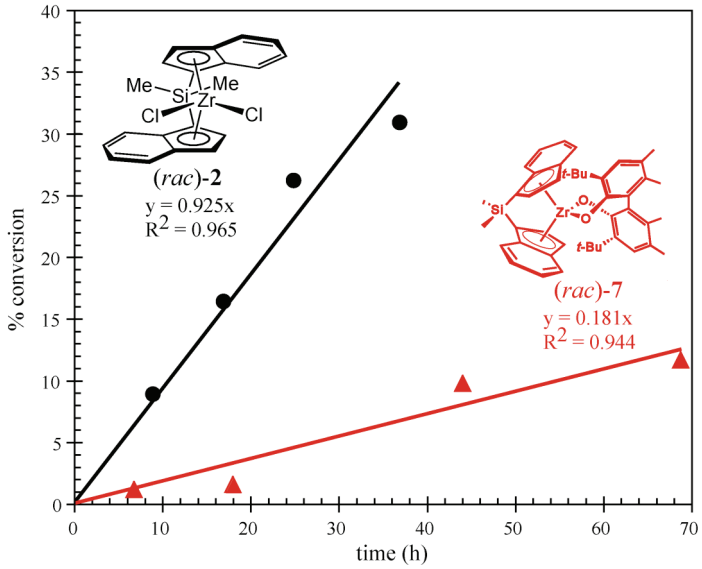

Figure 3.4 Plot of conversion *versus* time for 3-methyl-1-pentene polymerizations catalyzed by (rac)-**2** or (*rac*)-**7**.

Although 3-methyl-1-pentene polymerization was slow, enantiopure (*R*,*R*,*R*)-**7** was synthesized in complete analogy to Scheme 3.4 (using (*R*)-BIPHEN), and kinetic resolution of racemic α-olefin by polymerization was attempted. To compensate for the loss in activity, these experiments were carried out at 45 ºC. The selectivity factors and turnover frequencies for these experiments appear in Table 3.2 and indicate that this system is not useful for the kinetic resolution of any of the racemic α-olefins tested. It is possible that low selectivity factors were observed because high reaction temperatures were required. However, these data are also consistent with rapid racemization of the C_2-symmetric catalyst after or during MAO activation and/or offsetting effects from the chiral counter ion which results from *in situ* activation of (*R*,*R*,*R*)-**7**. Because of this ambiguity, an alternative strategy for the synthesis of C_2-symmetric zirconocenes was devised.

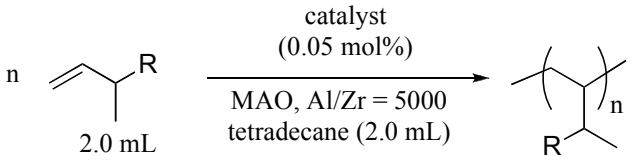

entry	catalyst	T (°C)	monomer	TOF[a]	$s = k_R/k_S$
1	**2**	25	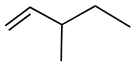	85	---
2	**7**	25		13	---
3	(*R*,*R*,*R*)-**7**	45		75	1.10
4	(*R*,*R*,*R*)-**7**	45	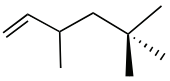	58	1.07
5	(*R*,*R*,*R*)-**7**	45	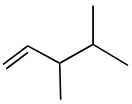	52	1.00

[a] TOF = $mmol_{olefin}/(mmol_{cat}*h)$

Table 3.2 Selectivity factors in racemic α-olefin polymerizations catalyzed by (*R*,*R*,*R*)-**7**/MAO.

Stereospecific synthesis of enantiopure C_2-symmetric zirconocenes using a diamine chiral auxiliary. Since zirconium amide bonds are generally weaker than zirconium alkoxide bonds,[34] replacement of the BIPHEN ligand with a diamine ligand should make the chiral auxiliary more labile. Indeed, Jordan and coworkers have shown that the achiral diamine ligand $PhNH(CH_2)_3NHPh$ can be used to direct the coordination of EBI to form a C_2-symmetric zirconocene, which, when reacted with hydrochloric acid, gives **3** without any *meso* isomer.[12] The tendency for the coordinated ligand to adopt a C_2-symmetric conformation provided the steric bias required to favor the *rac* diastereomer. This observation coupled with the success we had with the bisphenoxide ligands prompted the synthesis of a chiral diamine ligand based on 1,1'-binaphtyl-2,2'-diamine (BINAM). It is important to note that during the course of this work Jordan published similar findings for the enantiopure diamine ligand

(*R*,*R*)-PhNHCH(Me)CH_2CH(Me)NHPh.[22] However, no catalysis was reported using the enantiopure zirconocene and only one example was synthesized ((*S*,*S*)-**3**). Additionally, synthesis of Jordan's ligand is lengthy and the starting material is costly.

In order to mimic the coordination geometry of Jordan's achiral ligand *N*,*N'*-di-substitution of the BINAM ligand was necessary. Alkylation of (*rac*)-BINAM was possible by condensation with benzaldehyde followed by lithium aluminum hydride reduction to give (*rac*)-*N,N*-dibenzyl BINAM (benzBINAM, Scheme 3.7). Deprotonation of (*rac*)-benzBINAM followed by reaction with zirconium tetrachloride was straightforward to form (*rac*)-(benzBINAM)$ZrCl_2(THF)_2$ **10**, but reaction with Li_2(SBI) gave a 1:1 mixture of *rac* and *meso* diastereomers by ^{1}H NMR spectroscopy.

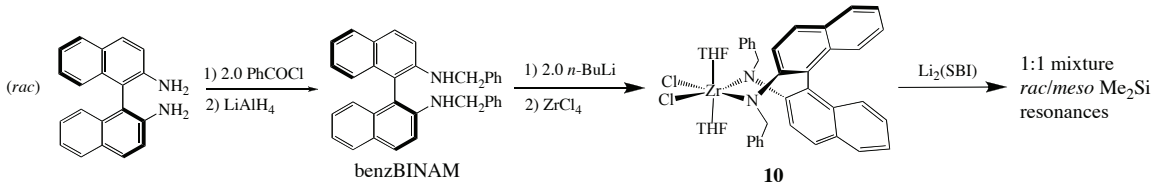

Scheme 3.7 Synthesis of benzBINAM and attempted metallation.

A curious feature of this NMR was that only one set of benzyl resonances (with identical chemical shifts to **10**) was observed despite the evidence from the dimethylsilyl resonances for at least two species in solution. At the time, it was rationalized that the NMR resonances were coincidental, and that benzBINAM poorly directed the coordination of SBI because of conformational flexibility originating from N–CH_2Ph bond rotation. This rationale prompted the synthesis of *N*,*N'*-di-arylated BINAM ligands. After more careful examination of the data and considering the observations made with the *N*,*N'*-di-arylated BINAM ligands (*vide infra*), it was later concluded that the species resulting from the deprotonation of (*rac*)-benzBINAM and $ZrCl_4(THF)_2$ was a 1:1 mixture of (*rac*)-$(benzBINAM)_2Zr$ and $ZrCl_4(THF)_2$. When Li_2(SBI) was reacted with this mixture, it reacted unselectively with $ZrCl_4(THF)_2$ to give a 1:1 mixture of *rac*:*meso*

diastereomers. During the course of this reaction (*rac*)-(benzBINAM)$_2$Zr was left unchanged thereby explaining the unexpected NMR spectrum. Since the *N*,*N*'-di-arylated ligands were successful for synthesizing enantiopure zirconocenes (*vide infra*), however, the *N*,*N'*-di-alkylated ligands were not pursued further.

Access to (*rac*)-N^2,$N^{2'}$-di-phenyl-1,1'-binaphthyl-2,2'-diamine ((*rac*)-phenBINAM, **11**) was accomplished with a palladium-catalyzed Buchwald/Hartwig coupling reaction between (*rac*)-BINAM and 2 equivalents of phenyl bromide (Scheme 3.8). Metallation of (*rac*)-phenBINAM was attempted three different ways (Scheme 3.8). First, deprotonation of the ligand with *n*-butyl lithium followed by treatment with $ZrCl_4(THF)_2$ gave a mixture of products by ^{1}H NMR spectroscopy. The major product of this mixture was determined to be (*rac*)-(phenBINAM)$_2$Zr by comparison to an independently synthesized sample of the bis-ligated species. Bis-ligation could not be prevented even with an excess of $ZrCl_4(THF)_2$. Isolation of a mono-ligated zirconium species was possible by reacting (*rac*)-phenBINAM with a slight excess of tetrabenzyl zirconium to give (*rac*)-(phenBINAM)Zr$(CH_2Ph)_2$ (**12**). Unfortunately, no reaction occurred when **12** was treated with SBI even after heating to 80 ºC in benzene.

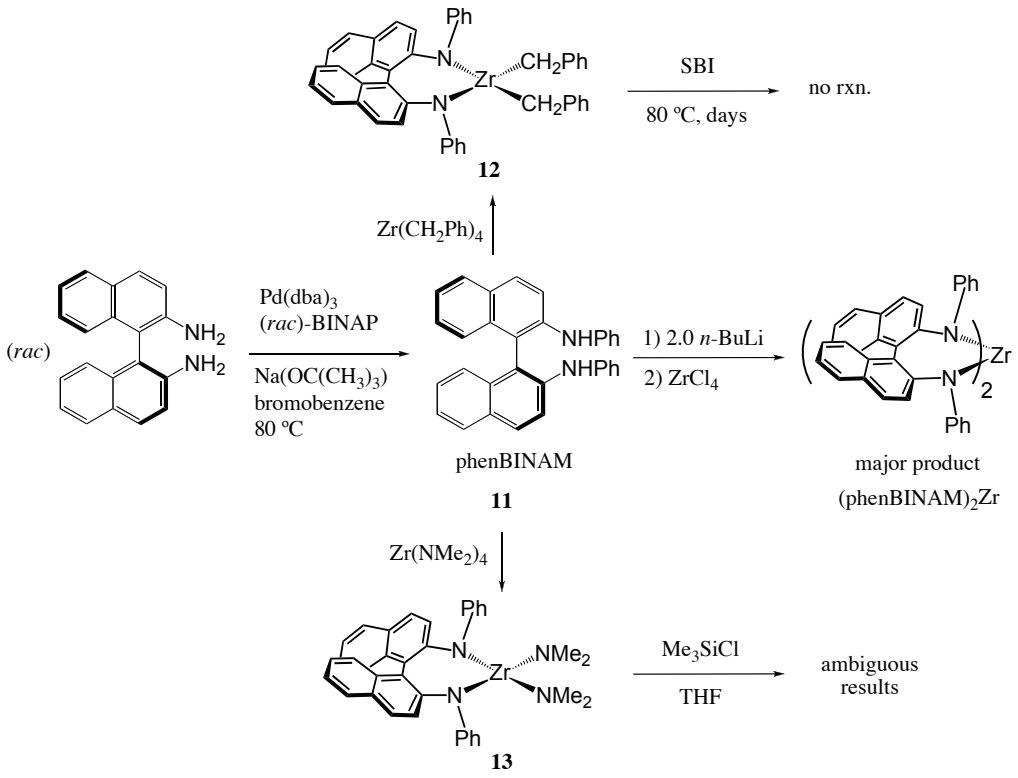

Scheme 3.8 Synthesis of (*rac*)-phenBINAM (**11**) and attempted metallation.

Finally, successful mono-ligation of (*rac*)-phenBINAM could be achieved by reacting the ligand with an excess of $Zr(NMe_2)_4$. This reaction was spontaneous to give (*rac*)-(phenBINAM)$Zr(NMe_2)_2$ (**13**) and did not require conditions that expel dimethyl amine suggesting a large thermodynamic preference for the formation of **13**. Furthermore, it was critical that an excess of $Zr(NMe_2)_4$ was used in order to prevent bis-ligation, which occurred when stoichiometric amounts of $Zr(NMe_2)_4$ were employed. An amine elimination route[13, 14] to the zirconocene was explored by treating **13** with the EBI ligand. However, no reaction occurred even after heating to 60 ºC for a few days. A more circuitous route to the desired zirconocene is converting **13** to the zirconium dichloride species (*rac*)-(phenBINAM)$ZrCl_2(THF)_2$ (**14**) followed by salt metathesis with deprotonated *ansa* ligand. Unfortunately, attempts to convert **13** to **14** using trimethylsilyl chloride gave ambiguous results, because without the aid of aliphatic

protons, identification of the number and identity of the product(s) by NMR spectroscopy was difficult.

To circumvent this problem, *p*-bromotoluene was used in the Buchwald/Hartwig coupling reaction to give (*rac*)-N^2,$N^{2'}$-di-*p*-tolyl-1,1'-binaphthyl-2,2'-diamine ((*rac*)-tolBINAM, **15**). Unlike phenBINAM, useful NMR handles are present for tolBINAM as both the tolyl methyl groups and the AB quartet of 1,4-substituted aryls are characteristic. Using (*rac*)-tolBINAM, a successful route to diastereomerically pure C_2-symmetric zirconocene was finally found (Scheme 3.9). Synthesis of (*rac*)-(tolBINAM)$ZrCl_2(THF)_2$ (**16**) was achieved via the amine elimination route. Unlike **14**, however, NMR-identification of **16** was possible when (*rac*)-(tolBINAM)$Zr(NMe_2)_2$ (**17**) was treated with trimethylsilyl chloride. Care must be taken during the chlorination reaction as trimethylsilyl chloride contaminated with hydrochloric acid led to free (*rac*)-tolBINAM. When **16** was exposed to Li_2(EBI) it was satisfying to observe only one C_2-symmetric diastereomer **18** in the ^{1}H NMR spectrum as evidence by the single methyl resonance and the relatively simple aryl resonances including an AB quartet from the tolyl group of tolBINAM (Figure 3.5).[35] Unlike the BIPHEN ligands, removal of the tolBINAM chiral auxiliary could be achieved by treating **18** with hydrochloric acid to give **3** without any evidence for the *meso* isomer. Interestingly, **3** could not be obtained by treating **18** with trimethylsilyl chloride possibly due to the steric congestion about **18**.

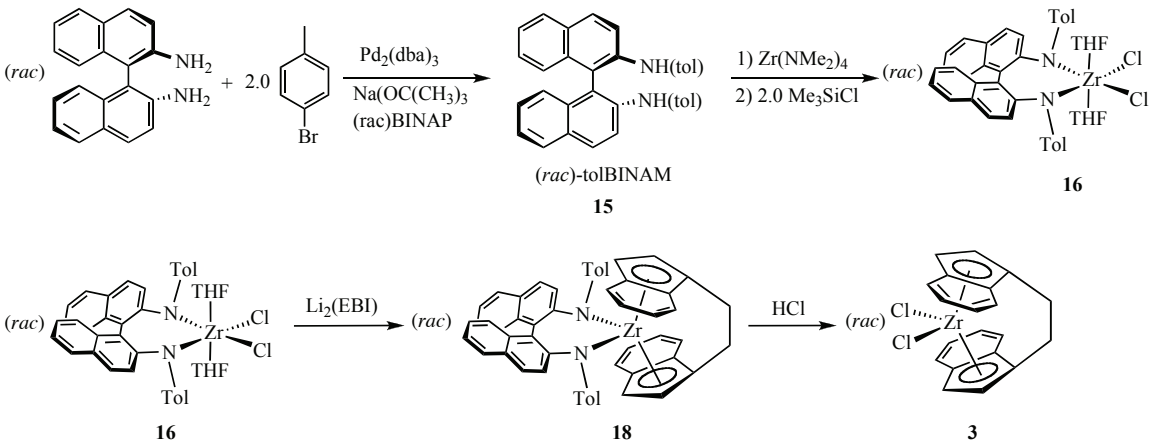

Scheme 3.9 Synthesis of (*S*,*S*,*R*)-**18** and removal of the chiral auxiliary with hydrochloric acid. Note: Enantioselective synthesis proceeded similarly using (*R*)-tolBINAM to give the enantiomer illustrated, {(*S*,*S*)-EBI}Zr{(*R*)-tolBINAM} (*vide infra*).

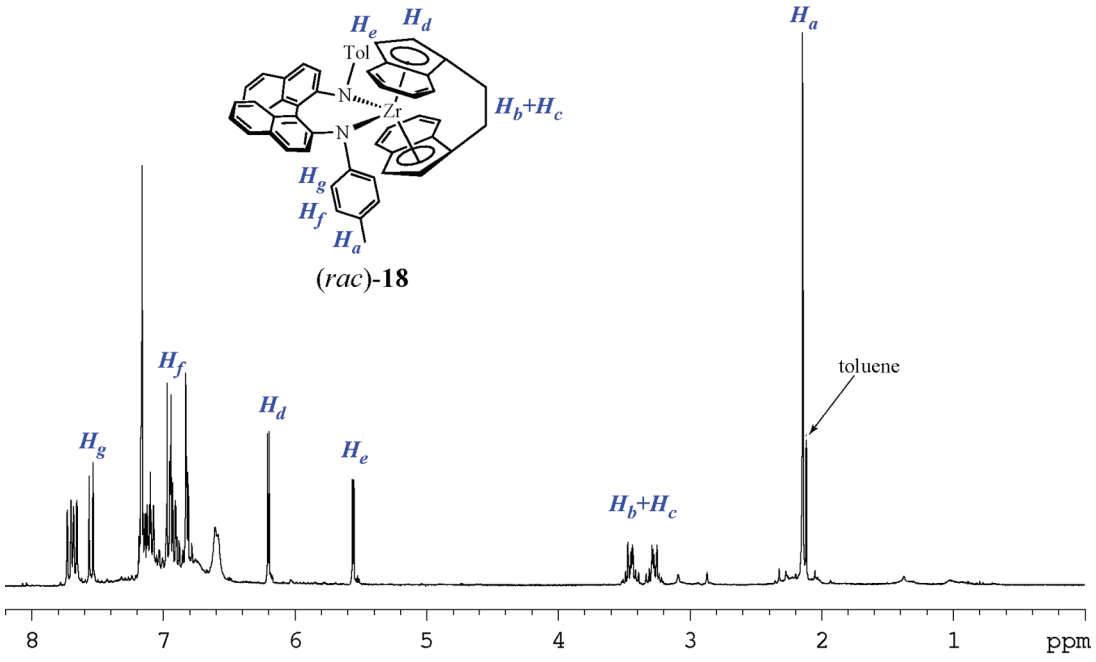

Figure 3.5 ^{1}H NMR of (*rac*)-**18** in C_6D_6.

Crystallization of **18** from toluene/petroleum ether solutions gave bright orange crystals suitable for single-crystal X-ray crystallography. Several views of the X-ray crystal structure of **18** appear in Figure 3.6. Consistent with the NMR solution data, the

solid-state crystal structure indicates a C_2-symmetric coordination mode for the EBI ligand. Furthermore, the six-membered rings of the EBI adopt the stereochemistry required to avoid the tolyl groups of the protruding tolBINAM ligand. This tendency is particularly evident for the wedge view of the zirconocene (Figure 3.6, view A). The stereochemical consequence of this interaction is that the *R* antipode of the tolBINAM ligand encourages EBI ligand binding with *S,S* to give the (*S,S*-EBI)Zr(*R*-tolBINAM) diastereomer or (*S,S,R*)-**18** (To better visualize the coordination environment of **18** see structure01.avi).

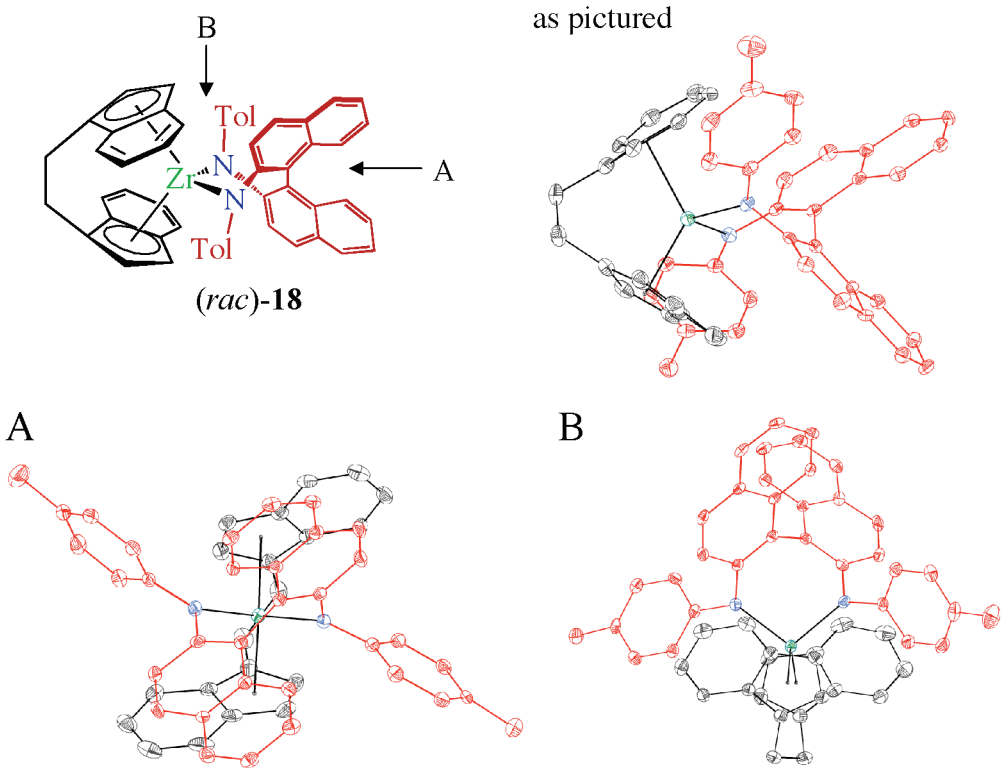

Figure 3.6 Molecular structure of (*rac*)-**18** from three different angles. tolBINAM and EBI ligands are depicted in red and black, respectively. Thermal ellipsoids are drawn to 50% probability (see Appendix I for complete list of bond distances and angles).

Enantioselective synthesis of (*S,S,R*)-**18** was performed by analogy to the racemic synthesis described in Scheme 3.9 using enantiopure (*R*)-tolBINAM. The synthesis

proceeded similarly giving high yields of (*S*,*S*,*R*)-**18**, but solubility of the enantiopure zirconium compounds were different compared with the racemic compounds (see experimental section). Solubility became particularly problematic when (*S*,*S*,*R*)-**18** was treated with hydrochloric acid to remove the chiral auxiliary. During the racemic synthesis, **3** could be separated from the diamonium chloride salt of (*rac*)-tolBINAM (**19**) by toluene solvent extraction. Surprisingly, (*R*)-**19** was found to be soluble in all aromatic and ethereal solvents tested. Fractional recrystallization of the reaction mixture was successful for the isolation of (*S*,*S*)-**3**, but several recrystallizations were necessary leading to low yields. Anion exchange with sodium tetraphenylborate and tetrabutylammonium hexafluorophosphate were attempted, but the solubility properties of the diammonium salt were not altered greatly. Several metallic reagents were added to the reaction mixture in hopes that chelation to (*R*)-**19** would occur, but all of these attempts were unsuccessful.

During the course of this latter investigation, however, some interesting unrelated reactivity was revealed. When a mixture of (*R*,*R*)-**3** and (*R*)-**19** was treated with $Zr(NMe_2)_4$, four new indenyl resonances were observed in the ^1H NMR spectrum rather than the expected resonances for (*R*)-(tolBINAM)$Zr(NMe_2)_2$. This observation suggested that $Zr(NMe_2)_4$ reacted with (*R,R*)-**3** rather than (*R*)-**19**. To verify this hypothesis, racemic **3** was reacted with $Zr(NMe_2)_4$. The reaction cleanly formed one product, the indenyl resonances of which were identical to those previously observed. Additionally, without resonances from tolBINAM to complicate the NMR spectrum, it became apparent that the new species contained a dimethylamide functional group. The presence of four different indenyl resonances was consistent with an asymmetric compound. Crystallization of the compound was possible and an X-ray crystal structure revealed that the compound synthesized was (*rac*)-(EBI)$Zr(NMe_2)Cl$. This finding was exciting because it could potentially be used as a general route to mixed zirconocene dialkyls by

the route proposed in Scheme 3.10. Zirconocene dialkyl compounds have been shown to be very useful for mechanistic studies.[36]

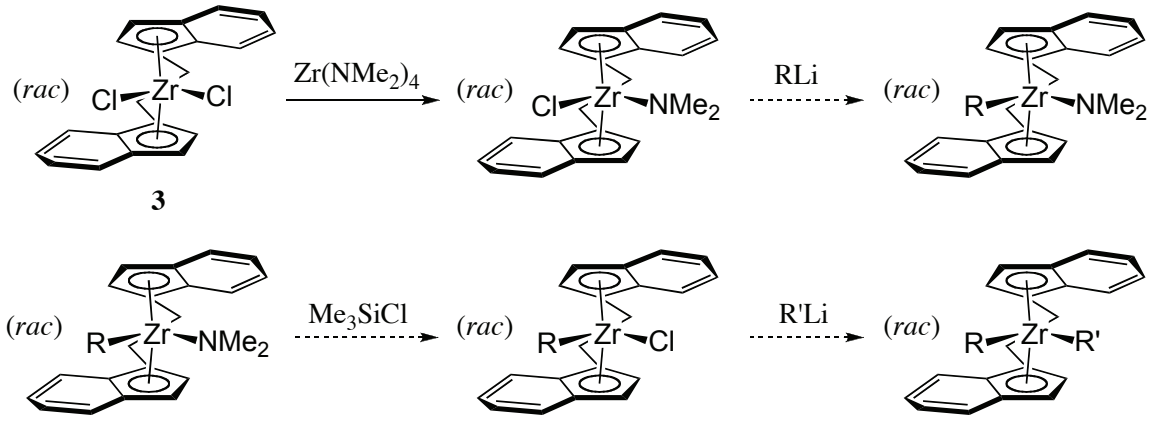

Scheme 3.10 Synthesis of (*rac*)-(EBI)Zr(NMe_2)$_2$Cl and proposed synthesis of mixed zirconocene dialkyl complexes.

The generality of using (*R*)-**16** for the stereospecific synthesis of C_2-symmetric zirconocenes other than **3** was not investigated extensively in favor of a brief investigation of how the synthetic method tolerated substituted EBI ligands (Scheme 3.11).[37] Synthesis of 1,2-bis(2-methyl-1-indenyl) ethane (**20**),[31] 1,2-bis(3-methy-1-indenyl)ethane (**21**),[30] and 1,2-bis(4,7-dimethyl-1-indenyl)ethane (**22**)[11] "EBI" ligands were carried out and NMR-scale reactions with (*R*)-**16** were performed. Disappointingly, unselective reactions occurred for the 2-methyl and 3-methyl substituted ligands, **20** or **21**.

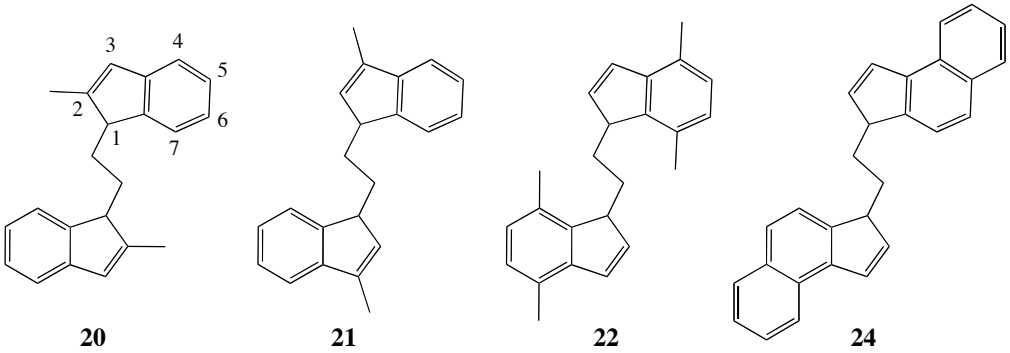

Scheme 3.11 Different "EBI" ligands.

Reaction with **22** initially gave a complex NMR spectrum but after stirring at room temperature the spectrum became increasingly simplified until after a day of stirring a single C_2-symmetric product was evident. The complex NMR spectrum was likely due to the formation of many intermediates including all the possible diastereomers for κ^1-coordination of **22** as well as the reversible formation of the high-energy diastereomers with κ^2-coordination. Although intermediates have not been identified, the NMR behavior is consistent with a reaction under thermodynamic control. This result was reproducible on a preparative scale to give enantiopure (*S*,*S*-4,4',7,7'-tetramethyl-EBI)Zr(*R*-tolBINAM) (*S*,*S*,*R*)-**23**, the relative stereochemistry of which was determined by X-ray crystallography (Figure 3.7). Considering that substituents installed on the six-membered ring was tolerated, investigation into a 4,5-benzanulated EBI ligand (**24**, Scheme 3.11) is being pursued. Although the results are preliminary, NMR evidence supports preferential formation of C_2-symmetric zirconocene in this case as well.

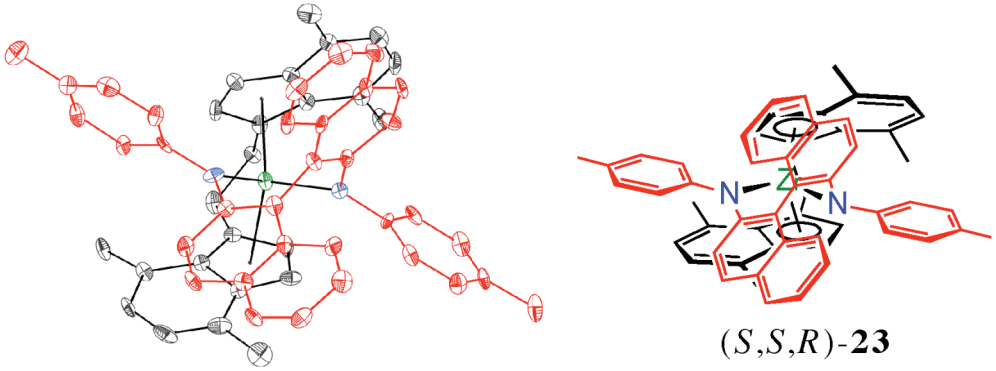

Figure 3.7 X-ray crystal structure for (*S*,*S*,*R*)-**23**. tolBINAM and **22** are depicted in red and black, respectively for clarity. Thermal ellipsoids are drawn to 50% probability.

Polymerization of racemic α-olefins using enantiopure C_2-symmetric zirconocene catalysts, (*S*,*S*)-3 and (*S*,*S*,*R*)-18. MAO activation of (*S*,*S*,*R*)-**18** for racemic α-olefin polymerization was accomplished in a similar fashion to (*R*,*R*,*R*)-**7**. Unlike (*R*,*R*,*R*)-**7**/MAO, however, room temperature polymerizations of 3-methyl-1-

pentene catalyzed by (*S*,*S*,*R*)-**18**/MAO proceeded at reasonable rates. The activity and selectivity factors for these polymerizations appear in Table 3.3.

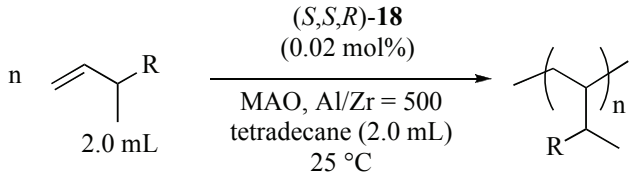

entry	monomer	TOF[a]	$s = k_S/k_R$
1	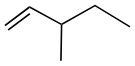	22 (3)	1.6 (0.1)
2[b]		86 (10)	1.8 (0.1)
4	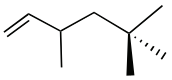	34 (8)	2.1 (0.1)
5	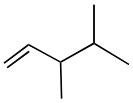	9 (1)	4.4 (0.4)
6	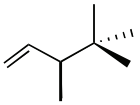	2.3[c] (0.4)	2 (1)

[a] TOF = $mmol_{chiral\ olefin}/(mmol_{catalyst}*hr)$;
[b] catalyst = (*S*,*S*)-**3**; [c] low conversion.

Table 3.3 Selectivity factors in polymerization of racemic α-olefins catalyzed by (*S*,*S*,*R*)-**18**/MAO and (*S*,*S*)-**3**/MAO.

In every case studied, the *S* antipode was preferentially polymerized, but selectivity factors were low with 3,4-dimethyl-1-pentene polymerizations being the highest ($s = k_S/k_R = 4.4$). Despite the low selectivities, these results were encouraging because modification of (*S*,*S*)-**18** is possible and doing so could increase selectivity. As previously mentioned, enantiopure 4,7-dimethyl substituted zirconocene (*S*,*S*,*R*)-**23** could be obtained using the tolBINAM chiral auxiliary. However, it was disappointing to find that both (*S*,*S*,*R*)-**23** and the corresponding zirconocene dichloride were inactive towards chiral α-olefin polymerizations. A possible solution to this problem is a 4,5-benzanulated EBI ligand (**24**). Similar ligands with this substitution pattern have been

synthesized and propylene polymerization catalyzed by the corresponding zirconocenes proceeded without compromising facial selectivity or activity.[8,27] Unfortunately, investigation into this catalyst is still in its preliminary stages.

In addition to using (*S*,*S*,*R*)-**18** as the precatalyst, preliminary data for 3-methyl-1-pentene polymerizations using (*S*,*S*)-**3** appear in Table 3.3. The selectivity factors for these polymerizations are, within experimental error, the same (entry 1 *vs*. entry 2) indicating that selectivity is not effected by the presence of the chiral auxiliary in (*S*,*S*,*R*)-**18** polymerizations. As anticipated, the activity for polymerizations catalyzed by (*S*,*S*)-**3** were greater compared to (*S*,*S*,*R*)-**18**. However, turnover frequencies were only four times faster for the zirconocene dichloride. As previously stated, turnover frequencies for **2** were six times faster than the corresponding bisphenoxide-containing zirconocene, **7**. This difference is again reflective of the lability of tolBINAM compared to BIPHEN.

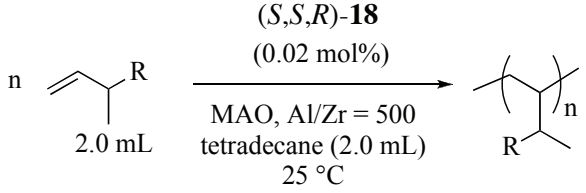

entry	olefin	time	conv. (%)	e.e. (%)	TOF[a]	$s = k_S/k_R$
1	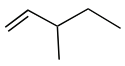	45 h	37.4	9.8	19	1.52
2		38 h	59.7	24.0	25	1.70
3	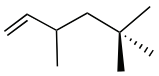	24 h	38.7	18.2	26	2.14
4		25 h	65.9	37.8	42	2.05
5[b]		107 h	30.4	11.4	10	1.90

[a]TOF = $mmol_{chiral\ olefin}/(mmol_{catalyst}*hr)$. [b] 0.003 mmol catalyst.

Table 3.4 Kinetic data from selected polymerizations that comprise Table 3.3.

Finally, it is important to note that polymerizations catalyzed by (*S*,*S*,*R*)-**18** do not display behavior consistent with catalyst racemization. To illustrate this point, Table 3.4 contains data from selected individual polymerizations that comprise Table 3.3. For a

catalyst that racemizes during the course of a reaction, selectivity factors should degrade at higher olefin conversions. Table 3.4 clearly shows that this is not the case for two different olefins indicating that the active species formed from (*S*,*S*,*R*)-**18**/MAO does not racemize during the polymerization.

3.4 Conclusions

Many of the potential obstacles associated with using C_2-symmetric zirconocene polymerization catalysts for the kinetic resolution of racemic α-olefins have been overcome. The steric interactions important for the successful synthesis of enantiopure C_2-symmetric zirconocenes were defined by using the BIPHEN and tolBINAM chiral auxiliaries. It is interesting to compare the results using these chiral auxiliaries. As previously discussed, the preferred C_2-symmetric conformation for the EBI ligand in (*R*,*R*,*R*)-**7** is opposite to what was observed for (*S*,*S*,*R*)-**18**. This indicates that tolBINAM directs the coordination of EBI differently than BIPHEN. The crystal structure of (*S*,*S*,*R*)-**18** (Figure 3.6) suggests that the major steric interaction preventing the formation of (*R*,*R*,*R*)-**18** is between the *N*-tolyl substitution of BINAM and the six-membered rings of EBI. Similarly, the PM3 calculations for **7** (Figure 3.2) suggest that the (*S* ,*S*,*R*)-**7** diastereomer is disfavored by steric interactions between the *tert*-butyl groups of BIPHEN and the six-membered rings of SBI. This discrepancy arises because the substituents translate the axial chirality from the binapthyl group in orthogonal directions. The tolyl substituent of tolBINAM runs roughly parallel to the long axis of the naphthyl moeity, effectively extending the same sense of axial chirality past the principle rotation axis. In order to avoid the tolyl groups, the EBI ligand is forced to adopt the conformation with an *opposite* sense of axial chirality. On the other hand, the *tert*-butyl groups of BIPHEN extend roughly perpendicular to the long axis of the biphenyl groups effectively relegating the *tert*-butyl groups to occupy the same steric space that the 3,3'-methyl groups occupy. In order to avoid the *tert*-butyl groups, the EBI ligand adopts the

conformation with the *same* sense of axial chirality (to better visualize this see structure01.avi and structure02.avi).

Before leaving this point, it is interesting to note that (*R*,*R*,*R*) diastereomer is the preferred diastereomer found for the resolution of **4** with BINOL.[20,38] The authors note that the major diastereomer is formed due to a steric interaction between the "backside" of BINOL (distal to the phenol functionality) and the six-membered ring of the EBTHI ligand. The data presented herein, however, indicate that the major steric interaction involves the "front side" of the chiral auxiliaries either as substituents proximal to the phenol functional group as in BIPHEN or as *N*-substitution as in tolBINAM. Particularly supportive of this analysis is the observation that tolBINAM, despite its similarity to BINOL, prefers to form the *opposite* C_2-symmetric diastereomer to what was observed for **4** (see structure03.avi).

In retrospect, it is possible to understand why (*R*)-BINOL was unable to resolve **2**. The hydrogenated six-membered ring in **4** affords a bulkier group for stereo-differentiation. The unsaturated indenes of **2** do not extend enough to interact with the "front side" of BINOL. Stereodifferentiation is not realized until the steric congestion is increased either by substitution adjacent to the phenol functionality as in **7** or by bringing the steric bulk closer to the metal as in **18**.

Despite generally observing low selectivities, MAO activation of enantiopure zirconocenes (*S*,*S*,*R*)-**18** and (*S*,*S*)-**3** for the polymerization of racemic α-olefins revealed two important points. First, the presence of residual chiral auxiliary does not affect the selectivity of the reaction since selectivity was the same when either (*S*,*S*,*R*)-**18** or (*S*,*S*)-**3** were used. Second, constant selectivity factors over a range of conversion indicate that the catalyst does not racemize during the polymerization.

This second point is particularly exciting because it indicates that C_2-symmetric zirconocenes based on **3** can be synthesized which may display higher selectivity. Initial

ligand screens show that the synthetic methodology tolerated substitution on the six-membered rings of EBI but is intolerant to substitution on the five-membered rings. Although disappointing, this observation is consistent with our steric model because substituents on the five-membered rings (*i.e.* ligands **20** and **21**) would be directed into the tolyl group of tolBINAM for the (*S*,*S*,*R*) diastereomer thereby raising the ground state energy of this diastereomer. On the other hand, substituents appended to the six-membered rings of EBI reside away from the tolyl groups for the (*S*,*S*,*R*) diastereomer. Unfortunately, the only enantiopure derivative of EBI that has been synthesized thus far, (*S*,*S*,*R*)-**23**, is inactive towards racemic olefin polymerization. Encouraging initial results have been obtained for the synthesis of an enantiopure 4,5-benzo substituted EBI zirconocene substantiating further investigation into its use for kinetic resolution. Additionally, application of the synthetic methodology towards the synthesis of enantiopure zirconocenes based on the sterically more open SBI zirconocenes may give a more active catalyst and may also be pursued.

3.5 Experimental Section

General methods. All air- and/or moisture-sensitive compounds were manipulated using standard high-vacuum line, swivel frit assembly (see swivelfrit.mov for a demo), Schlenk and cannula techniques or in a glove box under nitrogen atmosphere as described previously.[39] Argon was purified by passage through columns of MnO on vermiculite and activated 4 Å molecular sieves. All solvents and liquid reagents were stored under vacuum over sodium benzophenenone ketyl, titanocene, or calcium hydride prior to use. Unless otherwise stated α-olefins were purchased from Chemsampco. 3,4-dimethyl-1-pentene and 3,4,4-trimethyl-1-pentene were prepared as described in Chapter 1. Methylaluminoxane (MAO) was purchased from Abermarle, and all volatiles were removed *in vacuo* at 150 ºC overnight. It was found to be essential that all trimethyl aluminum was removed from the MAO (see Chapter 2). Racemic and enantiopure **5**,

$Pd(dba)_3$ and racemic 2,2'-bis(diphenylphosphino)-1,1'-binaphthyl (BINAP) were purchased from Strem and were used without further purification. Racemic and enantiopure 1,1'-binapthyl-2,2'-diamine (BINAM), racemic 1,1'-binapthyl-2,2'-diol (BINOL), sodium hydride, trimethyl aluminum and *n*-butyl lithium were purchased from Aldrich and were used without further purification. Sodium *tert*-butoxide was purchased from Aldrich and purified by sublimation before use. The *ansa* ligands: di(1-indenyl)dimethylsilane (SBI),[5] 1,2-di(1-indenyl)ethane (EBI),[6] bis(3-*tert*-butylcyclopentadienyl)dimethylsilane,[40] **20**,[31] **21**,[30] and **22**[41] were synthesized and deprotonated as described previously. The zirconium compounds: **2**,[41] **3**,[6] $ZrCl_4(THF)_2$,[42] $Zr(NMe_2)_4$,[13] and $Zr(CH_2Ph)_4$[43] were synthesized as described previously. The reagents $Me_2Al(OCH_2CH_3)$[44] and $Li[Me_4Al]$[45] were prepared as described previously. Unless otherwise noted, racemic and enantiopure syntheses proceeded similarly.

NMR spectra were obtained on a Varian Mercury spectrometer operating at 300 MHz for ^1H and 125 MHz for $^{13}C\{^1H\}$. All chemical shifts are reported in ppm relative to tetramethylsilane. 1-D nOe difference spectra were spectra were obtained on a Varian Inova spectrometer operating at 500 MHz.

Gas chromatographs (GC) were obtained on an Agilent 6890 gas chromatograph using a 30 m x 0.25 mm polysiloxane "HP-5" column from Agilent technologies for chiral monomer conversions and 30 m x 0.25 mm γ-cyclodextrin trifluoroacetyl "Chiraldex TA" column from Advanced Separations Technology for enantioassays. Summaries of the GC methods for each monomer as well as observed retention times appear in Appendix E.

Single crystal X-ray crystallography was carried out on a Bruker SMART 1000 difractometer. Atomic coordinates as well as bond distances and angles for (*rac*)-(EBI)$Zr(NMe_2)Cl$ and (*rac*)-**18** appear in Appendices H and I, respectively. Crystals from (*S*,*S*,*R*)-**22** were unsuitable for obtaining accurate bond distances and angles, but

connectivity could be established as indicated in Figure 3.7 and the space group in which the crystals formed was determined to be $P2_12_12_1$.

Optical rotations were measured on a JASCO P1010 polarimeter at ambient temperature. PM3 calculations were carried out using Mac SPARTAN v 1.0.4e. Ligands and zirconocene dichlorides were constructed and their minimum energy conformation was found using PM3. The two fragments were then connected and a molecular mechanics (MM3) minimum was found before calculating the minimum energy conformation using PM3.

Synthesis of sodium (*rac*)-3,3'-di-*tert*-butyl-5,5',6,6'-tetramethylbiphenyl-2,2'-bis(olate)•THF, Na_2{(*rac*)-BIPHEN}•THF. A slurry of sodium hydride (0.1891 g, 7.89 mmol) in THF (25 mL) was cannulated onto a solution of (*rac*)-BIPHEN (1.208 g, 3.41 mmol) in THF (25mL) precooled to –78 °C. With the system open to a bubbler, the solution was slowly brought to room temperature and then heated to reflux for 24 h. The solution turned blue within an hour followed by a second color change to yellow at approximately 12 h of heating. The solvent was removed to give 1.452 g (100%). ^{1}H NMR (300 Mhz, THF-d_8): δ = 1.35 (s, 18H, CCH_3), 1.61 (s, 6H, PhCH_3), 2.12 (s, 6H, PhCH_3), 6.75 (s, 2H, PhH). ^{13}C NMR (125 MHz, THF-d_8): δ = 17.1, 20.8, 30.6, 35.2, 116.5 (br), 123.5, 126.3, 132.8, 133.5, 134.0, 165.6 (br).

Synthesis of (*rac*)-(BIPHEN)$ZrCl_2(THF)_2$, 6. In a swivel frit assembly equipped with 100 mL round bottom flasks, THF (60 mL) was vacuum transferred onto a mixture of Na_2{(*rac*)-BIPHEN}•THF (0.960 g, 2.56 mmol) and $ZrCl_4(THF)_2$ (0.977 g, 2.56 mmol). The reaction mixture was brought to 50 ºC and stirred overnight at which time a white precipitate was evident. The precipitate was filtered and the solvent was removed *in vacuo*. In the glove box, diethyl ether (30 mL) was added to dissolve the resulting white foam. After a few minutes, a white crystalline precipitate began to form from the homogeneous solution. The solution was kept at –35 °C for 1 day. The white

precipitate was isolated by filtration and washed one time with cold diethyl ether to yield 0.7948 g (47.2%) a white solid. Concentration of the mother liquor and cooling yielded a second crop (0.2 g, 12 %) to give an overall yield of 59%. ^{1}H NMR (300 MHz, C_6D_6): δ = 1.17 (m, 8H, THF), 1.69 (s, 6H, PhC*H*$_3$), 1.74 (s, 18H, C(C*H*$_3$)$_3$), 2.18 (s, 6H, PhC*H*$_3$), 4.01 (m, 8H, THF), 7.28 (s, 2H, Ph*H*).

Synthesis of (*rac*)-(BIPHEN)Zr(SBI), 7. A 10:1 mixture of toluene and THF (11 mL) was added rapidly to a mixture of **5** (0.245 g, 0.377 mmol) and (SBI)Li_2•(Et_2O) (0.144 g, 0.321 mmol) at room temperature. The mixture immediately turned orange and a precipitate formed within an hour. After stirring for five hours the solvent was removed. Toluene (10 mL) was added to the residue and the precipitate (LiCl) was filtered off. The toluene was then removed *in vacuo* to give an orange powder, 0.133 g (64.8%). ^{1}H NMR (300 MHz, C_6D_6): δ = 0.72 (s, 6H, *H*$_e$), 1.32 (s, 18H, *H*$_a$), 1.50 (s, 6H, *H*$_d$), 2.17 (s, 6H, *H*$_c$), 5.88 (d, 2.8 Hz, 2H, *H*$_g$), 6.08 (d, 3.3 Hz, 2H, *H*$_f$), 6.89-7.01 (m, 6H, *H*$_h$, *H*$_i$, *H*$_j$), 7.13 (s, 2H, *H*$_b$), 7.51 (d, 8.2 Hz, 2H, *H*$_k$). ^{1}H NMR (300 MHz, THF-*d*$_8$): δ = 1.13 (s, 6H, *H*$_e$), 1.19 (s, 18H, *H*$_a$), 1.28 (s, 6H, *H*$_d$), 2.18 (s, 6H, *H*$_c$), 5.65 (d, 2.8 Hz, 2H, *H*$_f$), 6.08 (d, 2.8 Hz, 2H, *H*$_g$), 6.76 (d, 8.2 Hz, 2H, *H*$_h$), 6.99 (s, 2H, *H*$_b$), 7.08 (t, 7.1 Hz, 4H, *H*$_i$ and *H*$_j$), 7.67 (d, 8.8 Hz, 2H, *H*$_k$). ^{13}C{^{1}H} NMR (125 MHz, THF-*d*$_8$): δ = -1.2, 16.3, 20.4, 31.7, 35.6, 93.3, 110.3, 118.2. 124.3, 125.4, 126.6, 126.7, 127.3, 128.2, 128.4, 132.4, 134.7, 136.6. $C_{44}H_{50}O_2SiZr$ cal'd: 72.4 % C, 6.9 % H found: 71.4 % C, 6.9 % H. 1-D nOe (500 MHz, C_6D_6, irradiated: observed): *H*$_e$: *H*$_f$ (2.5%), *H*$_k$ (5.4%); *H*$_a$: *H*$_g$ (1.9%), *H*$_f$ (2.1%), *H*$_h$, *H*$_i$, and *H*$_j$ (1.4%), *H*$_b$ (3.4%), *H*$_k$ (0.3%); *H*$_d$: *H*$_c$ (3.4%); *H*$_c$: *H*$_d$ (4.0%), *H*$_b$ (3.1%); *H*$_g$: *H*$_a$ (2.9%), *H*$_f$ (6.6%), *H*$_h$ (6.1%); *H*$_f$: *H*$_e$ (4.5%), *H*$_a$ (4.8%), *H*$_g$ (9.3%), *H*$_k$ (4.1%).

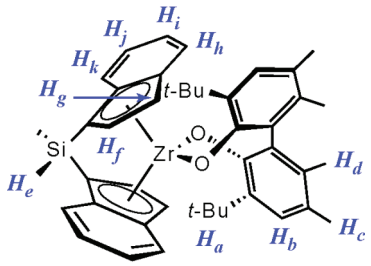

NMR-scale generation of (*rac*)-(BIPHEN)Zr(EBI), 8. At room temperature, Li_2(EBI)•2THF (21.0 mg, .050 mmol) was dissolved in a 10:1 mixture of THF-d_8/C_6D_6 (0.4 mL) and slowly added to a 10:1 THF-d_8/C_6D_6 solution (0.75 mL) of **6** (33.3 mg, 0.050 mmol). The reaction turned yellow. The ^{1}H NMR was consistent with the formation of only one C_2-symmetric product. ^{1}H NMR (300 MHz, 10:1 C_6D_6/THF-d_8): δ = 1.39 (s, 18H, C(CH_3)$_3$), 1.75 (s, 6H, CH_3), 2.20 (s, 6H, CH_3), 3.16 (m, 2H, CH_2), 3.35 (m, 2H, CH_2), 5.59 (d, ^{3}J = 2.8 Hz, 2H, Ind-*H*), 5.93 (d, ^{3}J = 2.8 Hz, 2H, Ind-*H*), 6.76 (d, ^{3}J = 3.3 Hz, 2H, Ar*H*), 6.94 (dd, ^{3}J = 9.0, 7.5 Hz, 2H, Ar*H*), 7.08 (dd, ^{3}J = 8.5, 7.8 Hz, 2H, Ar*H*), 7.18 (s, 2H, Ar*H*), 7.42 (d, ^{3}J = 8.3 Hz, 2H, indenyl Ar*H*).

NMR-scale generation of (*rac*)-(BIPHEN)Zr{1-Me_2Si(3-C_5H_3(CMe_3))$_2$}, 9. Li_2(1-Me_2Si(3-C_5H_3(CMe_3))$_2$) (32.8 mg, 0.105 mmol) and **6** (79.3 mg, 0.124 mmol) were dissolved in a 10:1 mixture of C_6D_6/THF-d_8 (1.0 mL). A precipitate began to form after a few hours. The ^{1}H NMR was consistent with the formation of one major C_2-symmetrc product. There does seem to be evidence for a minor product that may be the *meso* isomer. ^{1}H NMR (300 MHz, 10:1 C_6D_6): δ = 0.45 (s, 6H, Si(CH_3)$_2$), 0.98 (s, 18H, CpC(CH_3)$_3$), 1.51 (s, 18H, ArC(CH_3)$_3$), 2.15 (s, 6H, CH_3), 5.8 (m, 4H, Cp*H*), 5.94 (m, 2H, Cp*H*), 7.12 (s, 2H, Ar*H*).

Synthesis of N^2,$N^{2'}$-dibenzylidene-1,1'-binapthyl-2,2'-diamine. BINAM (3.027 g, 10.6 mmol) and N,N'-dimethylacetamide (150 mL) were combined in a 250 mL 2-neck flask. Benzoyl chloride (3.15g, 22.4 mmol) was dissolved in N,N'-dimethylacetamide (5 mL) and added to the BINAM solution dropwise. The solution was heated to 45 ºC for four hours. The product was precipitated by pouring the reaction

mixture into water (1400 mL). The product was isolated and redissolved into methylene chloride (250 mL). The golden solution was washed three times with water (100 mL) and once with brine (100 mL). The organic phase was dried with magnesium sulfate and the solvent was removed *in vacuo* to give an off white solid. Yield = 5.317 g (80%) The NMR data are consistent with literature.[46]

Synthesis of N^2,$N^{2'}$-dibenzylidene-1,1'-binapthyl-2,2'-diamine (benzBINAM). N^2,$N^{2'}$-dibenzylidene-1,1'-binapthyl-2,2'-diamine (3.003 g, 6.09 mmol) was dissolved in THF (75 mL). At 0 ºC, the solution was cannulated onto a THF (75 mL) slurry of lithium aluminum hydride (1.297 g, 34.18 mmol). The reaction was slowly brought to room temperature and stirred for 1 h. The solution was heated at reflux for 18 h. The reaction was quenched at 0 ºC by slow addition of water (4.5 mL) followed by 10% aqueous sodium hydroxide (4.5 mL) and another aliquot of water (13.5 mL). The slurry was stirred for 30 m and the precipitate was filtered. The bright yellow solution was dried with magnesium sulfate and the solvent was removed *in vacuo* to give a yellow oil. Purification of the product was accomplished by silica gel chromatography using a 5:1 mixture of hexanes:ethyl acetate as the eluent. The compound with R_f (5:1 hexanes:ethyl acetate) = 0.55 was isolated and the solvent was removed to give a yellow solid. Yield = 1.738 g (61%). ^{1}H NMR (300 MHz, DMSO-d_6): δ = 4.42 (d, ^{3}J = 4.1 Hz, 4H, C*H*$_2$), 4.85 (t, ^{3}J = 4.6 Hz, 2H, N*H*), 6.78 (m, 2H, Ar*H*), 7.19 (m, 16H, Ar*H*), 7.79 (m, 4H, Ar*H*) . ^{13}C{^{1}H} NMR (125 MHz, DMSO-d_6): δ 46.2, 111.0, 114.3, 121.2, 123.0, 126.1, 126.4, 126.6, 126.9, 128.0, 128.1.

Synthesis of Li_2(benzBINAM). In a 100 mL round bottom flask, benzBINAM (0.912 g, 1.96 mmol) was dissolved in toluene (50 mL). At -78 ºC, *n*-butyl lithium (3.0 mL of 1.6 M solution in hexanes, 4.8 mmol) was added to the solution. The solution immediately turned orange. The solution was slowly warmed to room temperature and left to stir overnight overnight. The solution turned dark yellowish green. The toluene

was removed *in vacuo* and replaced with petroleum ether (50 mL). The solid was filtered and washed three times with petroleum ether (40 mL). The solvent was removed *in vacuo* to give a yellow/green solid. Yield = 0.7908 g (100%). ^{1}H NMR (300 MHz, THF-d_8): δ = 4.37 (d, ^{3}J = 15.7 Hz, 2H, C*H*$_2$), 4.48 (d, ^{3}J = 15.4 Hz, 2H, C*H*$_2$), 6.61 (m, 4H, Ar*H*), 6.74 (m, 2H, Ar*H*), 6.93 (d, ^{3}J = 9.8 Hz, 2H, Ar*H*), 7.02 (m, 2H, Ar*H*), 7.12 (ps. t., ^{3}J = 8.2 Hz, 4H, Ar*H*), 7.33 (m, 8H, Ar*H*). ^{13}C NMR (125 MHz, THF-d_8): δ = 54.3, 114.3, 116.7, 117.0, 124.9, 125.3, 125.6, 126.0, 128.2, 128.6 (2C), 129.0, 137.6, 146.9, 158.7.

Reaction between Li_2(benzBINAM) and $ZrCl_4(THF)_2$, 10. At -78 ºC, diethyl ether (12 mL) and THF (12.5 mL) were vacuum transferred onto a 50 mL flask containing Li_2(benzBINAM) (0.2806 g, 0.787 mmol) and $ZrCl_4$ (0.1843 g, 0.791 mmol). The reaction was slowly brought to 0 ºC where it turned deep red and a precipitate formed. After stirring for 2 h, the reaction was brought to room temperature where it stirred an additional 6 h. The solvent was removed *in vacuo* and replaced with benzene (12 mL). The mixture was allowed to stir at room temperature for 30 m. The white precipitate was filtered and washed twice with benzene (5 mL). The solvent was removed *in vacuo*. In the glove box, the product was precipitated into petroleum ether (15 mL) from a toluene solution (10 mL). The product was filtered and washed three times with petroleum ether (10 mL) then dried *in vacuo* to give a yellow solid. Yield = 0.281 g (48.5%). ^{1}H NMR (300 MHz, C_6D_6): δ = 0.99 (br s, THF), 1.22 (br s, THF), 4.00 (d, ^{3}J = 15.9 Hz, C*H*$_2$), 4.2 (br s, THF), 4.27 (d, ^{3}J = 15.9 Hz, C*H*$_2$), 6.70 (d, ^{3}J = 8.6 Hz, Ar*H*), 6.81 (m, Ar*H*), 6.97 (m, Ar*H*), 7.49 (m, Ar*H*).

Synthesis of (*rac*)-*N*^{2},*N*$^{2'}$-diphenyl-1,1'-binapthyl-2,2'-diamine (phenBINAM) 11. In an inert atmosphere, (*rac*)-BINAM (0.821 g, 2.89 mmol), $Pd_2(dba)_3$ (0.26 g, 0.28 mmol), (*rac*)-BINAP (0.353 g, 0.570 mmol), sodium *tert*-butoxide (2.92 g, 34.0 mmol), and toluene (15 mL) were combined in a 25 mL Schlenk tube. At room temperature and

under rapid stirring, bromobenzene (12.2 g, 71.5 mmol) was injected onto the reaction mixture and stirred 10 minutes. The reaction was brought to 85 ºC for 2 h. Toluene (30 mL) and water (10 mL) were added to the reaction. The organic phase was extracted three times with water (30 mL) and dried over magnesium sulfate. The solution was concentrated to give a red oil, which was further purified by silica gel column chromatography using toluene as the eluent. Fractions from the high R_f compound were combined and the toluene was removed *in vacuo*. The resulting yellow oil was triturated twice with petroleum ether (100 mL) and the solvent was removed *in vacuo* overnight to give a yellow solid. Yield = 1.222 g (97%). ^{1}H NMR spectrum agrees with the literature spectrum.[47] ^{1}H NMR (300 Hz, $CDCl_3$, 20 ºC): δ = 4.34 (br s, 2H, N*H*), 6.93 (m, 6H, Ar*H*), 7.23 (m, 10H, Ar*H*), 7.67 (d, ^{3}J = 8.3 Hz, 2H, Ar*H*), 7.87 (m, 4H, Ar*H*). ^{13}C NMR (125 MHz, $CDCl_3$): δ = 116.5, 118.0, 120.1, 122.4, 123.7, 124.7, 127.3, 128.4, 129.4, 129.6, 134.2, 140.5, 142.7, 146.8.

Synthesis of (*rac*)-(phenBINAM)Zr($CH_2Ph)_2$, 12. $Zr(CH_2Ph)_4$ (0.306 g, 0.672 mmol) was dissolved in toluene (15 mL) and added to a toluene (15 mL) solution of **11** (0.286 g, 0.654 mmol) at room temperature. The reaction was stirred at room temperature overnight and then at 60 ºC for 2 h. The solvent was removed *in vacuo* and the reaction vessel was brought into the box. The solid was recrystallized from a 1:1 toluene/petroleum ether mixture at -35 ºC. Yellow crystals formed, which were isolated and washed with cold toluene (1 mL). The solvent was removed *in vacuo* overnight. Yield = 0.184 g (41 %). ^{1}H NMR (300 MHz, C_6D_6): δ = 1.93 (d, ^{3}J = 10.2 Hz, 2H, C*H*$_2$C$_6$H$_5$), 2.35 (d, ^{3}J = 10.2 Hz, 2H, C*H*$_2$C$_6$H$_5$), 6.66 (d, ^{3}J = 7.4 Hz, 4H, Ar*H*), 6.74 (m, 2H, Ar*H*), 6.86 (m, 6H, Ar*H*), 6.97 (m, 4H, Ar*H*), 7.18 (m, 8H, Ar*H*), 7.33 (d, ^{3}J = 8.4 Hz, 2H, Ar*H*), 7.60 (d, ^{3}J = 9.0 Hz, 4H, Ar*H*).

Synthesis of (*rac*)-(phenBINAM)Zr($NMe_2)_2$, 13. At -78 ºC, toluene (50 mL) was vacuum transferred onto a mixture of **11** (0.497 g, 1.13 mmol) and $Zr(NMe_2)_4$ (0.370

g, 1.38 mmol). The reaction was brought to room temperature where it stirred for 4 h. The solvent was removed and replaced with petroleum ether. A yellow precipitate formed after stirring for 1 h. The precipitate was filtered and washed with cold petroleum ether then dried *in vacuo* overnight. Yield = 0.6070 g (87 %). ^{1}H NMR (300 MHz, C_6D_6): δ = 2.62 (s, 12H, N(C*H*$_3$)$_2$), 6.79 (m, 2H, Ar*H*), 6.95 (m, 4H, Ar*H*), 7.15 (m, 8H, Ar*H*), 7.31 (m, 2H, Ar*H*), 7.49 (m, 4H, Ar*H*), 7.60 (m, 2H, Ar*H*).

Synthesis of (*R*)-*N*^{2},*N*$^{2'}$-di-*para*-tolyl-1,1'-binapthyl-2,2'-diamine (tolBINAM), (*R*)-15. In an inert atmosphere, (*R*)-BINAM (9.751 g, 34.3 mmol), $Pd_2(dba)_3$ (3.15 g, 3.43 mmol), (*rac*)-BINAP (4.26 g, 6.85 mmol), and toluene (120 mL) were combined in a 150 mL Schlenk tube. At room temperature and under rapid stirring, *p*-bromotoluene (8.8 mL, 12.23 g, 71.5 mmol) was injected onto the reaction mixture and stirred 10 minutes. Sodium *tert*-butoxide (35.59 g, 413.5 mmol) was added to the reaction portion wise over the course of 30 minutes. The reaction was stirred at room temperature for 15 minutes, then brought to 85 ºC for 24 h. The reaction was diluted with toluene (400 mL). and was washed three times with water (100 mL). The organics were isolated and the aqueous layer was washed twice with toluene (50 mL). The organic layer was dried over magnesium sulfate, and the solvent was removed to give a red oil. Purification of the product was achieved by silica gel column chromatography using toluene as the eluent. The high R_f (R_f (3:1 hexanes/acetone) = 0.74) product was isolated as a pale yellow solid and was determined to be the desired product. Yield = 21.612g (78.3%). $[\alpha]_D^{25}$(0.412, THF) = 89.7. ^{1}H NMR (300 MHz, $CDCl_3$): δ = 2.27 (s, 6H, C*H*$_3$), 5.54 (s, 2H, N*H*), 6.90 (d, ^{3}J = 8.3 Hz, 4H, tolyl-Ar*H*), 7.02 (d, ^{3}J = 8.3 Hz, 4H, tolyl-Ar*H*), 7.12-7.33 (m, 6H, naphthyl-Ar*H*), 7.61 (d, ^{3}J = 8.8 Hz, 2H, naphthyl-Ar*H*), 7.84 (ps.t, J = 8.1 Hz, naphthyl-Ar*H*) . ^{13}C{^{1}H} NMR (125 MHz, $CDCl_3$): δ = 20.7, 115.3, 117.3, 121.1, 123.1, 124.3, 126.9, 128.2, 129.1, 129.3, 129.7, 132.1, 134.0, 139.8, 141.1. The low R_f spot (R_f (hexanes/acetone) = 0.59) was isolated and determined to be the mono arylated product.

Yield = 0.410g (3.2%). ^{1}H NMR (300 MHz, $CDCl_3$): δ = 2.27 (s, 3H, C*H*$_3$), 3.72 (bs, 2H, N*H*$_2$), 5.50 (s, 1H, N*H*), 6.84-7.32 (m, 10H, Ar*H*), 7.62 (d, ^{3}J = 8.8 Hz, 2H, napthyl-ArH), 7.83 (ps. t, J = 8.1 Hz, 4H, naphthyl-Ar*H*).

Synthesis of (*R*)-(tolBINAM)Zr(NMe$_2$)$_2$, (*R*)-17. (*R*)-**15** (4.16 g, 8.95 mmol) and $Zr(NMe_2)_4$ (2.99 g, 11.1 mmol) were placed in a 250 mL round bottom flask equipped with stir bar and affixed to a large swivel frit assembly. Toluene (200 mL) was vacuum transferred onto the solids at -78 ºC. The reaction was slowly brought to room temperature were it was allowed to stir overnight open to a mercury bubbler. The solvent was removed from the bright yellow solution and replaced with hexamethyl disiloxane (100 mL) (petroleum ether was used for racemic synthesis, but (*R*)-**19** is soluble in petroleum ether). After stirring 30 min. at room temperature, a yellow precipitate formed. The precipitate was filtered and washed four times with hexamethyl disiloxane (20 mL) followed by once with cold pentane (10 mL) (pentane was not necessary for racemic synthesis). The solvent was removed and the solids were dried *in vacuo* to yield a yellow powder which was >95% pure with $Zr(NMe_2)_4$) being the minor impurity. Yield = 5.003 g (87.1%). The product was further purified by recrystallization from petroleum ether to give 4.018 g (70.0%) product free of $Zr(NMe_2)_4$. $[\alpha]_D^{27}$ (0.2, THF) = -772.6. ^{1}H NMR (300 MHz, C_6D_6): δ = 2.13 (s, 6H, C*H*$_3$), 2.67 (s, 12H, N(C*H*$_3$)$_2$), 6.90-7.04 (m, 8H, Ar*H*), 7.06-7.20 (m, 4H, Ar*H*), 7.33 p (d, ^{3}J = 7.4 Hz, 2H, napthyl-Ar*H*), 7.49 (d, ^{3}J = 7.2 Hz, 2H, napthyl-Ar*H*), 7.58 (dd, ^{3}J = 8.9 Hz, 4H, napthyl-Ar*H*) . ^{13}C{^{1}H} NMR (125 MHz, C_6D_6): δ = 21.12, 40.75, 121.16, 123.19, 124.32, 125.21, 126.78, 127.81, 128.61, 130.01, 130.90, 131.30, 132.28, 136.00, 143.85, 149.86. $C_{38}H_{38}N_4Zr$ cal'd: 71.10% C, 5.97% H, 8.73% N found: 70.80% C, 6.01% H, 8.36% N.

Synthesis of (*R*)-(tolBINAM)ZrCl$_2$(THF)$_2$, (*R*)-16. (*R*)-**17** (1.537 g, 2.39 mmol) was placed in a 250 mL round bottom flask equipped with a stir bar, and affixed to a large swivel frit assembly. THF (125 mL) was vacuum transferred onto the solid. At -78

ºC, trimethylsilyl chloride (0.51 g, 4.7 mmol) was vacuum transferred onto the reaction mixture. The reaction was slowly brought to room temperature and stirred overnight under argon. The THF was removed and replaced with petroleum ether (150 mL). The mixture was stirred for 1 h at which time a yellow precipitate formed. The precipitate was filtered and washed four times with cold petroleum ether (50 mL). The solvent was removed *in vacuo* to give a yellow solid. Yield = 1.687 g (95.6%). $[\alpha]_D^{27}$(0.2, THF) = 205.7. ^{1}H NMR (300 MHz, C_6D_6): δ = 1.29 (s, 8H, THF), 2.04 (s, 6H, C*H*$_3$), 3.80 (s, 4H, THF), 4.13 (s, 4H, THF), 7.46 (d, ^{3}J = 8.3 Hz, 4H, tolyl-Ar*H*), 6.91 (ps. t, J = 7.6 Hz, 2H, napthyl-Ar*H*), 7.00 (ps. t, J = 7.4 Hz, 2H, napthyl-Ar*H*), 7.09 (d, ^{3}J = 8.0 Hz, 4H, tolyl-Ar*H*), 7.48 (d, ^{3}J = 8.3 Hz, napthyl-Ar*H*), 7.63 (ps. t, J = 8.8 Hz, 2H, napthyl-Ar*H*), 7.82 (d, J = 8.5 Hz, 2H, napthyl-Ar*H*). ^{13}C NMR (125 MHz, C_6D_6): δ = 20.93, 26.00, 73.04, 119.73 (br), 121.70, 126.00, 126.68, 128.90, 129.68, 130.39, 131.64, 132.80, 134.59, 139.70 (br), 151.11. $C_{42}H_{42}Cl_2N_2O_2Zr$ cal'd: 65.78% C, 5.52% H, 3.65% N found: 62.85% C, 6.03% H, 3.85% N.

Synthesis of {(*S*,*S*)-EBI)}Zr{(*R*)-tolBINAM}, (*S*,*S*,*R*)-18. (*R*)-**16** (1.49 g, 2.02 mmol) and Li_2(EBI)•Et_2O (0.799 g, 2.03 mmol) were placed in a 250 mL round bottom flask. At -78 ºC THF (150 mL) was vacuum transferred onto the solids. The reaction was brought to –10 ºC and stirred under argon for 24h. The reaction turned deep red. The THF was removed and the oily residue was triturated twice with petroleum ether (20 mL). Toluene (75 mL) was added to the mixture and stirred for 20 minutes. A fine orange precipitate formed. The precipitate was filtered over celite and washed three times with toluene (10 mL). The mother liquor was concentrated in half, and petroleum ether (75 mL) was added. A yellow/orange precipitate formed which was filtered. The solvent was removed from the mother liquor and the orange product was triturated twice with petroleum ether then dried *in vacuo* overnight to give an orange solid. Yield = 1.0993g (67.2%). For the racemic synthesis, crystals suitable for X-ray crystallography

were obtained by slow petroleum ether diffusion in a toluene solution. ^{1}H NMR (300MHz, C_6D_6): δ = 2.14 (s, 6H, C*H*$_3$), 3.18-3.34 (m, 2H, C*H*$_2$), 3.36-3.52 (m, 2H, C*H*$_2$), 5.56 (d, ^{3}J = 3.03 Hz, 2H, indenyl C*H*), 6.20 (d, ^{3}J = 3.3 Hz, 2H, indenyl C*H*), 6.60 (br. s, 4H, Ar*H*), 6.70-7.02 (m, 12H, Ar*H*), 7.06-7.22 (m, 6H, Ar*H*), 7.55 (d, ^{3}J = 9.1 Hz, 2H, Ar*H*), 7.69 (dd, ^{3}J = 8.5 Hz, 4H, Ar*H*). ^{13}C NMR (125 MHz, C_6D_6): δ = 20.7, 29.1, 105.5, 117.0, 118.4, 121.7, 124.2, 124.5, 124.8, 126.0, 126.3, 126.7, 127.3, 127.7, 128.9, 129.1, 130.0, 130.5, 131.4, 134.6, 151.2, 156.4. $C_{54}H_{42}N_2Zr$ cal'd = 79.87 %C, 5.63 %H, 3.65 %N found = 80.06 %C, 5.23 % H, 3.46 % N.

Synthesis of (*rac*)-3. In a small swivel frit assembly, (*rac*)-**18** (0.190 g, 0.236 mmol) was dissolved in benzene (10 mL). At 0 ºC, ethereal hydrochloric acid (0.52 mmol) was syringed onto the reaction mixture. The mixture immediately turned dark orange then faded to pale yellow-orange. After stirring 1 h, the benzene was removed and fresh benzene was added to the reaction. A yellow precipitate formed, which was filtered and washed once with benzene (2 mL). The solvent was removed and the yellow product was obtained from the filtrant. Yield = 0.030 g (31 %). The ^{1}H NMR was consistent with the literature.[6] (*S*,*S*)-**3** was obtained in a similar manner starting with 0.478 g (0.590 mmol) of (*S*,*S*,*R*)-**18**. For the enantiopure synthesis three recrystallization of the filtrant from diethyl ether was necessary free the product from (*S*)-**19**. Yield = 0.025 mg (10.1 %).

Synthesis of (*rac*)-(EBI)Zr(NMe$_2$)Cl. Toluene (25 mL) was vacuum transferred onto a mixture of Zr(NMe$_2$)$_4$ (0.139 g, 0.519 mmol) and **3** (0.216 g, 0.516 mmol) at -78 ºC. The reaction was slowly brought to room temperature where it stirred overnight. The solution became bright orange. The solvent was removed *in vacuo* and petroleum ether (25 mL) was added to the flask. A precipitate formed after stirring at room temperature for 1 h. The precipitate was isolated and washed twice with petroleum ether (2 mL) then dried *in vacuo* for a few hours to give an orange solid 85% pure by NMR with the major

biproduct presumably being $Zr(NMe_2)_3Cl$ (br s 2.78 in ^1H NMR). Yield = 0.186 g (84%). Crystals suitable for X-ray crystallography were obtained by recrystallization from diethyl ether at -30 ºC. ^1H NMR (300 MHz, C_6D_6): δ = 2.52 (s, 6H, $N(CH_3)_2$), 3.10 (m, 3H, CH_2), 3.39 (m, 1H, CH_2), 5.61 (d, ^3J = 3.0 Hz, 1H, Ind-C*H*), 5.98 (d, ^3J = 3.1 Hz, 1H, Ind-C*H*), 6.33 (d, ^3J = 3.5 Hz, 1H, Ind-C*H*), 6.45 (d, ^3J = 3.0 Hz, 1H, Ind-C*H*), 6.65 (ps. t., 1H, Ar*H*), 6.98 (ps. t., 1H, Ar*H*), 7.16 (m, 1H, Ar*H*), 7.28 (m, 3H, Ar*H*), 7.47 (d, ^3J = 8.8 Hz, 1H, Ar*H*). $^{13}C\{^1H\}$ NMR (125 MHz, C_6D_6): δ = 29.7, 30.1, 48.0, 103.0, 106.0, 113.5, 116.3, 118.1, 119.5, 121.2, 121.6, 121.7, 123.7, 123.9, 124.2, 125.8, 126.3, 126.4, 130.1, 131.9.

Synthesis of {(*S*,*S*)-1,2-bis(4,7-dimethyl-1-indenyl)ethane}Zr{(*R*)-tolBINAM}, (*S*,*S*,*R*)-23. A THF (8 mL) solution of Li_2{**22**} (0.200 g, 0.552 mmol) was added dropwise to a frozen THF (12 mL) solution of (*R*)-**16** (0.405 g, 0.548 mmol). The solution was allowed to come to room temperature where it turned a dark reddish brown. After stirring 1 d, the solvent was removed *in vacuo* and replaced with benzene (20 mL). The solution was filtered over celite and the celite was washed twice with benzene (4 mL). The mother liquor was lyophilized to give a reddish brown solid 90% pure by NMR. Yield = 0.464 g (98%). Pure product was obtained by dissolving the solid in toluene (4 mL) and layered with petroleum ether (10 mL). After slow diffusion at -30 ºC, the precipitate was filtered and the solvent was removed from the mother liquor to give an orange solid. Yield = 0.40 g (87 %). Crystals suitable for X-ray crystallography were obtained by recrystallization from diethyl ether at -30 ºC. ^1H NMR (300 MHz, C_6D_6): δ = 0.99 (s, 6H, CH_3), 2.12 (s, 6H, tolyl-CH_3), 2.79 (s, 6H, CH_3), 3.19 (m, 2H, CH_2), 3.86 (m, 2H, CH_2), 6.03 (d, ^3J = 3.7 Hz, 2H, indenyl C*H*), 6.38 (m, 4H, Ar*H*), 6.57 (d, ^3J = 8.9 Hz, 4H, Ar*H*), 6.78 (m, 12H, Ar*H*), 7.12 (m, 4H, Ar*H*), 7.30 (d, ^3J = 8.7 Hz, 2H, Ar*H*), 7.53 (d, ^3J = 8.0 Hz, 2H, Ar*H*). $^{13}C\{^1H\}$ NMR (125 MHz, C_6D_6): δ = 18.6, 21.2, 22.9,

28.8, 100.6, 112.4, 114.7, 118.3, 121.7, 124.5, 126.3, 126.8, 127.1, 127.3, 127.5, 127.6, 129.4, 129.7, 130.4, 131.1, 131.2, 131.3, 131.7, 133.5, 135.0, 153.0, 159.0.

Generic procedure for the polymerization of racemic α-olefins. An 8 μM solution of catalyst in toluene was made in a Straus flask prior to polymerization. This stock solution was stored under argon at –30 °C and used as needed. Stock solutions older than a week were not used. Methyl aluminoxane (MAO) (250 mg, 3 mmol) was combined with tetradecane (3 mL) in a 10 mL Schlenk flask equipped with a side arm for reaction sampling. Racemic α-olefin (2 mL, ~15 mmol) was transferred onto the reaction mixture and stirred for at least 30 minutes. An aliquot was removed for GC analysis for a t = 0 point. Under an argon purge, the catalyst solution (0.5 mL, 4 μmmol) was syringed onto the reaction mixture. Aliquots from the reaction were abstracted and analyzed by GC to get conversion. In order to minimize error, reaction sampling was kept at a minimum. At the appropriate olefin conversion, the reaction was stopped by vacuum transferring the volatiles. The MAO was quenched with a 10% solution of aqueous hydrochloric acid in methanol. The polymer was collected as a toluene slurry, and where appropriate isolated by precipitation into methanol as described in Chapter Two. Enantiomeric excess was determined as previously described[1] and outlined in Chapter One.

3.6 References and Notes

1. Baar, C. R.; Levy, C. J.; Min, E. Y.-J.; Henling, L. M.; Day, M. W.; Bercaw, J. E. *J. Am. Chem. Soc.*, **2004**, *126*, 8216.

2. See Chapter Two for a more extensive explanation.

3. Agapie, T., Ph D thesis, California Institute of Technology, **2007.**

4. Klamo, S. B., Ph D thesis, California Institute of Technology, **2005**; (b) Casey, C. P.; Tunge, J. A.; Lee, T.; Fagan, M. A. *J. Am. Chem. Soc.*, **2003**, *125*, 2641.

5. Spaleck, W.; Antberg, M.; Boehm, L.; Rohrmann, J.; Lueker, H.: EP 399348, **1990**.

6. Wild, F. R. W. P.; Wasiucionek, M.; Gottfriend, H.; Brintzinger, H. H. *J. Organomet. Chem.*, **1985**, 288, *1*, 63.

7. Spaleck, W.; Kuber, F.; Winter, A.; Rohrmann, J.; Bachmann, B.; Antberg, M.; Dolle, V.; Paulus, E. F. *Organometallics*, **1994**, *13*, 954.

8. Stehling, U.; Diebold, J.; Kirsten, R.; Roll, W.; Brintzinger, H. H.; Jungling, S.; Mulhaupt, R.; Langhauser, F. *Organometallics*, **1994**, *13*, 964.

9. Cheng, H. N.; Ewen, J. A. *Makromolekulare Chem.*, **1989**, 190, *8*, 1931.

10. (a) Nifant'ev, I. E.; Ivchenko, P. V. *Organometallics*, **1997**, *16*, 713; (b) Kane, K. M.; Shapiro, P. J.; Vij, A.; Cubbon, R. *Organometallics*, **1997**, *16*, 4567; (c) Resconi, L.; Balboni, D.; Baruzzi, G.; Fiori, C.; Guidotti, S. *Organometallics*, **2000**, *19*, 420; (d) Konemann, M.; Erker, G.; Frohlich, R.; Kotila, S. *Organometallics*, **1997**, *16*, 2900; (e) Huttenhofer, M.; Prosenc, M.-H.; Rief, U.; Schaper, F.; Brintzinger, H. H. *Organometallics*, **1996**, *15*, 4816; (f) Diamond, G. M.; Jordan, R. F. *Organometallics*, **1996**, *15*, 4030; (g) Christopher, J. N.; Diamond, G. M.; Jordan, R. F. *Organometallics*, **1996**, 15, 4038; (h) LoCoco, M. D.; Jordan, R. F. *Organometallics*, **2003**, *22*, 5498.

11. Resconi, L.; Piemontesi, F.; Camurati, I.; Balboni, D. *Organometallics*, **1996**, *15*, 5046.

12. Zhang, X.; Zhu, Q.; Guzei, I. A.; Jordan, R. F. *J. Am. Chem. Soc.*, **2000**, *122*, 8093.

13. Diamond, G. M.; Rodewald, S.; Jordan, R. F. *Organometallics*, **1995**, *14*, 5.

14. Diamond, G. M.; Jordan, R. F.; Peterson, J. L. *Organometallics*, **1996**, *15*, 4045.

15. Damrau, H.-R., H.; Royo, E.; Obert, S.; Schaper, F.; Weeber, A.; Brintzinger, H. H. *Organometallics*, **2001**, *20*, 5258.

16. Schmidt, K.; Reinmuth, A.; Rief, U.; Diebold, J.; Brintzinger, H. H. *Organometallics*, **1997**, *16*, 1724.

17. Yoder, J. C.; Day, M. W.; Bercaw, J. E. *Organometallics*, **1998**, *17*, 4946.

18. (a) Vathauer, M.; Kaminsky, W. *Macromolecules*, **2000**, *33*, 1955; (b) Harrigan, R. W.; Hammond, G. S.; Gray, H. B. *J. Organomet. Chem.*, **1974**, *81*, 79; (c) Kaminsky, W.; Shauwienold, A. M.; Freidanck, F. *J. Mol. Cat., Part A: Chem.*, **1996**, *112*, 37; (d) Vitz, E.; Brubaker, C. H., Jr. *J. Organomet. Chem.*, **1974**, *82*, C16; (e) Vitz, E.; Wagner, P. J.; Brubaker, C. H., Jr. *J. Organomet. Chem.*, **1976**, *107*, 301.

19. (a) Burk, M.; Colletti, S. L.; Halterman, R. L. *Organometallics*, **1991**, *10*, 2998; (b) Ellis, W. W.; Hollis, T. K.; Odenkirk, W.; Whelan, J.; Ostrander, R.; Rheingold, A. L.; Bosnich, B. *Organometallics*, **1993**, *12*, 4391; (c) Mitchell, J. P.; Sharad, H.; Brookhart, S. K.; Hardcastle, K. I.; Henling, L. M.; Bercaw, J. E. *J. Am. Chem. Soc.*, **1996**, 118, *5*, 1045.

20. Chin, B.; Buchwald, S. L. *J. Org. Chem.*, **1997**, *62*, 2267.

21. (a) Grossman, R. B.; Davis, W. M.; Buchwald, S. L. *Organometallics*, **1991**, *10*, 1501; (b) Schafer, A.; Karl, E.; Huttner, G.; Brintzinger, H. H. *J. Organomet. Chem.*, **1987**, *328*, 87.

22. LoCoco, M. D.; Jordan, R. F. *J. Am. Chem. Soc.*, **2004**, *126*, 13918.

23. Schafer, A.; Karl, E.; Zsolnai, L.; Huttner, G.; Brintzinger, H. H. *J. Organomet. Chem.*, **1987**, *328*, 87.

24. Troutman, M. V.; Appella, D. H.; Buchwald, S. L. *J. Am. Chem. Soc.*, **1999**, *121*, 4916.

25. Lee, N. E.; Buchwald, S. L. *J. Am. Chem. Soc.*, **1994**, *116*, 5985.

26. Ciardelli, F.; Carlini, C.; Altomare, A. *Ziegler Catalysis* (Eds. G. Fink, R. Mulhaupt and H. H. Brintzinger); Springer-Verlag: Heidelberg, **1995**, 455.

27. Sacchi, C.; Barsties, E.; Tritto, I.; Locatelli, P.; Brintzinger, H. H.; Stehling, U. *Macromolecules*, **1997**, *30*, 1267.

28. Oliva, L.; Longo, P.; Zambelli, A. *Macromolecules*, **1996**, *29*, 6383.

29. (a) Izmer, V. V.; Lebedev, A. Y.; Mikhail, V. N.; Ryabov, A. N.; Asachenko, A. F.; Lygin, A. V.; Sorokin, D. A.; Voskoboynikov, A. Z. *Organometallics*, **2006**, *25*, 1217; (b) Lee, I. M.; Gauthier, W. J.; Ball, J. M.; Iyengar, B.; Collins, S. *Organometallics*, **1992**, *11*, 2115; (c) Leino, R.; Luttikhedde, H.; Wilen, C. E.; Sillanpaa, R.; Nasman, J. H. *Organometallics*, **1996**, *15*, 2450; (d) Leino, R.; Luttikhedde, H.; Lehtonene, A.; Ekholm, P.; Nasman, J. H. *J. Organomet. Chem.*, **1998**, *558*, 181; (e) Spaleck, W.; Antberg, M.; Dolle, V.; Klein, R.; Rohrmann, J.; Winter, A. *New J. Chem.*, **1990**, *14*, 499.

30. Resconi, L.; Piemontesi, F.; Camurati, I.; Rychlicki, H.; Colonnesi, M.; Balboni, D. *Polym. Mat. Sci. Eng.*, **1995**, 516.

31. Winter, A.; Martin, A.; Spaleck, W.; Jorgen, R.; Volker, D.: CA 2055218, **1990**.

32. (a) Boyle, T. J.; Eilerts, N. W.; Heppert, J. A.; Takusagawa, F. *Organometallics*, **1994**, 13, 2218; (b) Boyle, T. J.; Barnes, D. L.; Heppert, J. A.; Morales, L.; Takusagawa, F. *Organometallics*, **1992**, 11, 11112.

33. Drago, R. S. *Physical Methods for Chemists* Surfside Scientific: Gainsville, **1992**.

34. Ziegler, T.; Vincenzo, T.; Versluis, L.; Baerends, E. J.; Ravenek, W. *Polyhedron*, **1988**, *7*, 16.

35. SBI ligands were not initially investigated because previous experience suggested **2** would likely racemize during or after its synthesis.

36. See for example: Schofer, S. S., Ph D thesis, California Institute of Technology, **2004.**

37. Preliminary data suggest that selective reactions occur with Li_2(1-Me_2Si(3-$C_5H_3(CMe_3)$)$_2$) whereas a 1:1 mixture of *rac*/*meso* isomers were observed in the NMR for Li_2(SBI).

38. Wild, F. R. W. P.; Zsolnai, L.; Huttner, G.; Brintzinger, H. H. *J. Organomet. Chem.*, **1982**, *232*, 233.

39. Burger, B. J.; Bercaw, J. E. *New Devolopments in the Synthesis, Manipulation and Characterization of Organometallic Compounds* (Eds. A. Wayda and M. Y. Darensbourg); American Chemical Society: Washington DC, **1987**.

40. Wiesenfeldt, H.; Annette, R.; Elke, B.; Evertz, K.; Brintzinger, H. H. *J. Organomet. Chem.*, **1989**, 369, 3, 359.

41. Winkler, U. F.; Ao, M.-S. US 6252098 B1, **2001**.

42. Fackler, *Inorganic Synthesis* **1982**, 137.

43. Zucchini, U.; Albizzati, E.; Giannini, U. *J. Organomet. Chem.*, **1971**, *26*, 357.

44. Pasynkiewicz, S.; Pikul, S.; Poplawska, J. *J. Organomet. Chem.*, **1985**, *293*, 125.

45. Karsch, H. H.; Appelt, A.; Muller, G. *Organometallics*, **1985**, *4*, 1624.

46. Lustig, S. R.; Everlof, G. J.; Jaycox, G. D. *Macromolecules*, **2001**, *34*, 2364.

47. Vyskocil, S.; Jaracz, S.; Smrcina, M.; Sticha, M.; Hanus, V.; Polasek, M.; Kocovsky, P. *J. Org. Chem.*, **1998**, *63*, 7727.

APPENDIX A

REACTIVITY OF DICATIONIC π-COMPLEXES OF PLATINUM AND THEIR USE TO SYNTHESIZE CHIRAL α-OLEFINS

A.1 Introduction

As work progressed towards the development of a polymerization catalyst for the kinetic resolution of racemic α-olefins, it became evident that an efficient route to the substrates would be desirable. This need became more evident because many olefins including the most bulky olefins were never commercially available or are no longer available. In the past, bulky olefins such as 3,4,4-trimethyl-1-pentene were obtained in a multi-step classical synthesis involving Wittig chemistry.[1] A brief survey of the recent literature revealed a communication from Vitagliano and coworkers describing a platinum-catalyzed olefin dimerization between ethylene and 2-methyl-2-butene to form 3,4-dimethyl-1-pentene, an olefin we typically use in our studies (Scheme A.1).[2]

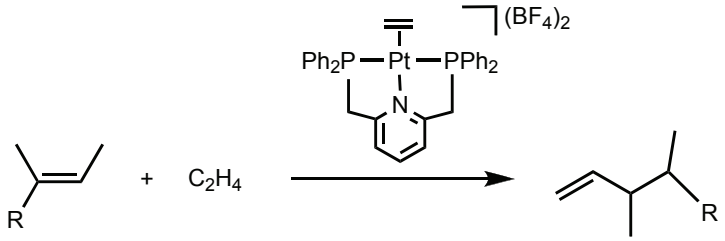

Scheme A.1 Platinum-catalyzed synthesis of 3,4-dimethyl-1-pentene.

Through a series of labeling experiments and ligand exchange reactions, Vitagliano proposed the mechanism proposed in Scheme A.2. The dicationic platinum complex **1** used for the catalyst activates coordinated ethylene to nucleophillic attack by

2-methyl-2-butene to form a platinum alkyl containing a stabilized tertiary carbocation (**2**). A series of consecutive hydride shifts occur which transform **2** to the 3,4-dimethyl-1-pentene platinum complex **3**. Finally, a rate determining olefin substitution with ethylene occurs to reveal 3,4-dimethyl-1-pentene and **1**.

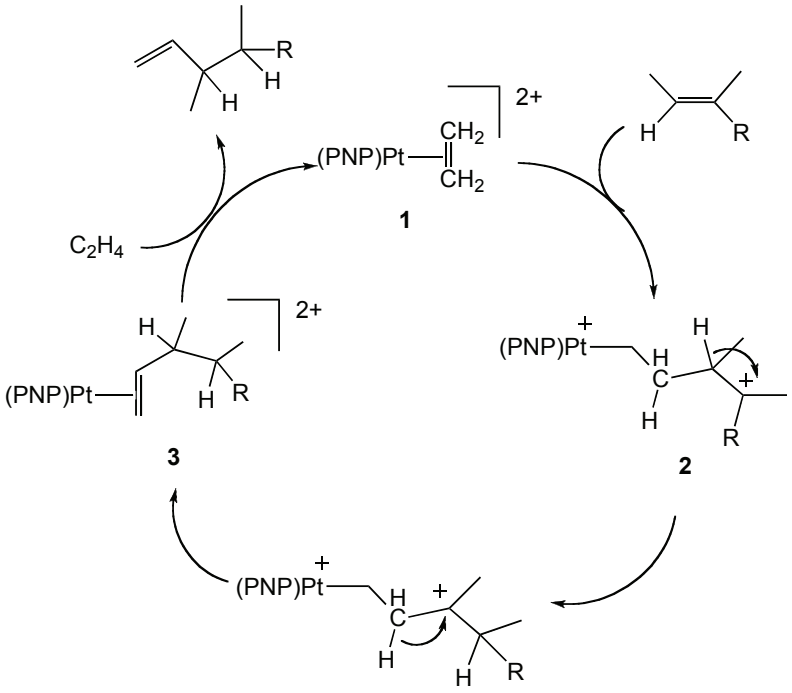

Scheme A.2 Mechanism for 3,4-dimethyl-1-pentene formation.

The authors comment that 3,4,4-trimethyl-1-pentene can be synthesized in a similar fashion from ethylene and 2,3-dimethyl-2-butene, but 3-methyl-1-pentene could not be produced catalytically from 2-butene presumably due to the required formation of a secondary carbocation for this internal olefin.

Subsequent to this report, Gagne and coworkers reported that **1** also facilitates cycloadditions of 1,6-dienes by a similar mechanism to form cyclohexenes by a similar mechanism.[3] In the same communication, Gagne reported catalysts similar to **1** also undergo cyclization of 1,6-dienes, but the catalytic loop is closed by a cyclopropanation reaction instead of a second hydride shift.

Since olefins we typically use for our kinetic resolutions were synthesized with **1** from inexpensive starting materials, we decided to investigate this catalyst for the synthesis of racemic olefins. We also briefly investigated the reactivity of **1** towards other non-classical nucleophiles and attempted to synthesize enantiopure platinum compounds for the enantioselective synthesis of chiral 3-substituted olefins.

A.2 Results and Discussion

Although **1** was obtained by the same route that Vitagliano reported, adapted procedures were necessary to get satisfactory yields (see experimental section). With **1** in hand, we were able to satisfactorily reproduce the catalysis reported by Vitagliano for the synthesis of 3,4-dimethyl-1-pentene in dichloromethane. Although GC yields were high for these reactions, isolated yields tended to be low because methylene chloride was difficult to remove from the reaction. A convenient solvent for reactions on a preparative scale is nitromethane. Catalyst decomposition is rapid in nitromethane leading to platinum complexes which dimerize the internal olefin,[2] but the solvent is immiscible with both the starting material and the product of reaction. The product can be separated by simple filtration followed by a single distillation to remover residual starting material and dimer. Olefin suitable for polymerization can be obtained by passing the distillate through a small plug of alumina to remove residual nitromethane. An additional advantage for using nitromethane is that the reaction occurs in the polar phase so low catalyst loadings can be used without sacrificing much activity.

With this procedure, a multi-gram (60 g) synthesis of of 3,4-dimethyl-1-pentene and 3,4,4-trimethyl-1-pentene could be accomplished using 0.1 mol% **1**. Attempts to synthesize 3-methyl-1-pentene from 2-butene failed, but small scale reactions between ethylidene cyclohexene and **1** under an atmosphere of ethylene gave 3-cyclohexyl-1-butene in modest GC yields. Unfortunately, a preparative scale of this reaction was not performed.

Since Gagne had success with dienes as nucleophiles for this reaction, investigation into nucleophillic addition of other non-classical nucleophiles to the coordinated olefin of **1** was investigated. In particular, we were interested in the reactivity of enamines or enol ethers towards **1** with the hopes that homoallylic alcohols or amines would be formed by a mechanism similar to Scheme A.2 (Scheme A.3). The rationale was that formation of eneamonium or oxonium ion would stabilize the positive charge in a similar fashion to the tertiary carbocation in **2**.

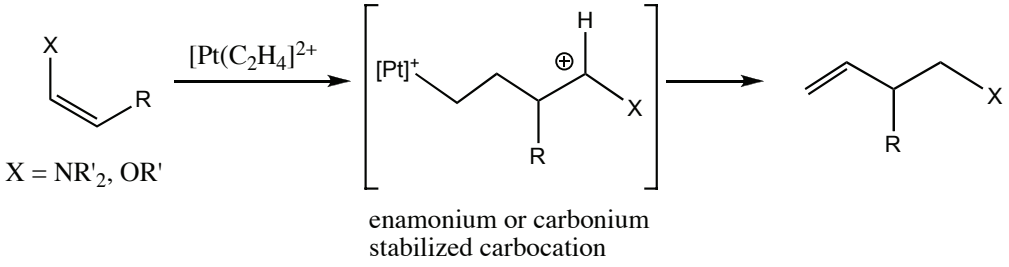

Scheme A.3 Potential products from eneamine or enol ethers.

Unfortunately, when **1** was treated with enol ethers such as 2,3-dihydrofuran or ethyl-1-propenyl ether, rapid oligomerization of the substrate occurred. These oligomerization products were the same products observed by treating the enol ethers with simple acids. It is likely that the platinum catalyst or HBF_4 produced from catalyst decompositions serves as a Lewis acid to dimerize the enol ethers.

Although no catalysis was observed in the presence of ethylene, an NMR-scale stoichiometric reaction between **1** and *N*-methyl indole was somewhat clean to form one product at 0 ºC within one hour (^{31}P = 33.97 ppm, $^{1}J_{Pt\text{-}P}$ = 2635 Hz, CD_2Cl_2). Although these results a very preliminary, the ^{1}H NMR displayed no evidence of free or coordinated ethylene suggesting that some reaction occurred between the indole and the bound olefin rather than olefin displacement. Upon warming to room temperature, resonances from the initially formed product disappear and are ultimately replaced by two new platinum products in the ^{31}P NMR (^{31}P = 33.2 and 32.1 ppm). Unfortunately,

liberation of the indole product(s) from the platinum was not possible by treatment with acetonitrile or acid, and the experiment was not repeated. Nevertheless, these results are encouraging and deserve future consideration.

Finally, we were intrigued by the possibility that enantiopure unfunctionalized olefins could be obtained directly from the platinum catalysis instead of via kinetic resolution by polymerization. From a fundamental standpoint, this was particularly interesting because it would require an unprecedented stereospecefic hydride transfer. The synthesis of the enantiopure platinum catalyst **4** based on a bisphosphine ligand (**5**) previously synthesized by Osbourne[4] and Zhang[5] was proposed for this purpose following Scheme A.4.

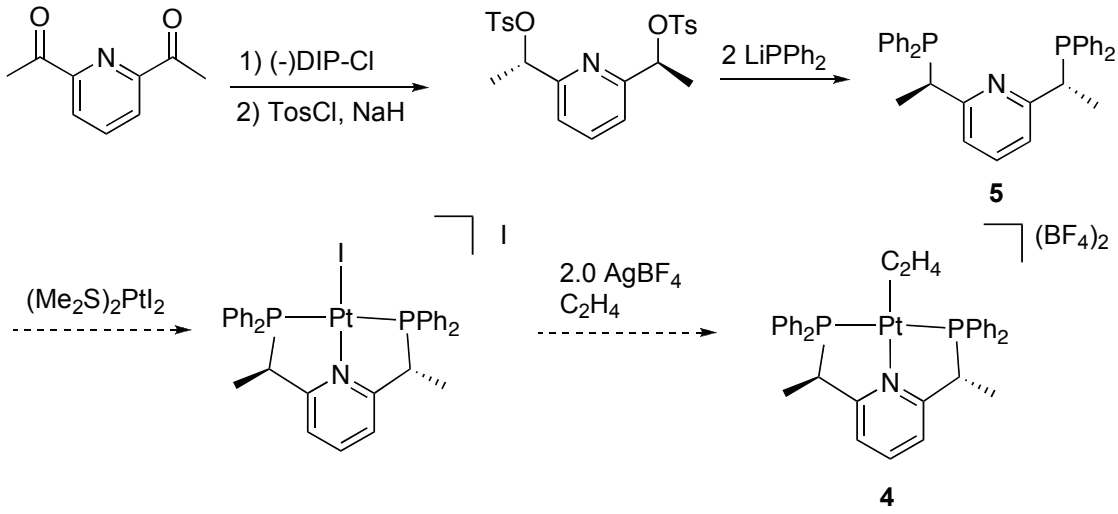

Scheme A.4 Proposed synthesis of **4**.

Due to time constraints the desired platinum complex was never synthesized, but Osbourne and Zhang's syntheses of the bisphosphine ligand was repeated. An important modification to their procedure, however, was that a stoichiometric quantity of the lithium diphenyl phosphide was required to avoid racemization. Before leaving this subject, some important control experiments were completed that indicate that the dicationic platinum compounds do not racemize enantiopure olefins. First, complex **1**

was treated with enantioenriched 3,4-dimethyl-1-pentene (see chapter 1) and subjected to reaction conditions. The optical purity of 3,4-dimethyl-1-pentene remained the same after days of exposure to **1** indicating that **1** by itself does not racemize the enantiopure olefin. Second, the olefin dimerization catalysis was performed for the synthesis of 3,4,4-trimethyl-1-pentene in the presence of enantioenriched 3,4-dimethyl-1-pentene using **1** as the catalyst. Again, enantioassay of the product olefin mixture indicated that racemization of the 3,4-dimethyl-1-pentene did not occur. Therefore, by-products that may be produced during catalysis also do not racemize enantiopure olefins.

A.3 Conclusions

Vitagliano's claim that olefin dimerization between an internal olefin and ethylene catalyzed by **1** was reproduced and optimized for large-scale production of 3,4-dimethyl-1-pentene and 3,4,4-trimethyl-1-pentene. Investigation into alternative non-classical nucleophiles was somewhat disappointing with acid catalysis often dominating. However, stoichiometric reactions between **1** and *N*-methyl indole suggest that reaction between the coordinated olefin and indole occur in this case. The compatibility of **1** with enantiopure olefins was established thereby making enantioselective versions of the olefin dimerization catalysis possible using catalysts such as **4**.

A.4 Experimental Section.

Synthesis of 2,6-bis(diphenylphosphino)methyl)pyridine (PNP). In a 500 mL round bottom flask, diphenyl phosphine (2.376 g, 13.44 mmol) was combined with THF (200 mL) and dioxane (20 mL). At 0 ºC, a THF (100 mL) slurry of sodium hydride (0.68 g, 28.3 mmol) was cannulated onto the diphenyl phosphine mixture. The reaction was slowly brought to room temperature then to 40 ºC open to a mercury bubbler. The reaction mixture turned yellow within an hour and after heating overnight, the reaction turned orange. The mixture was brought to 0 ºC where 2,6-bis(chloromethyl)pyridine (2.3676 g, 13.44 mmol) dissolved in THF (70 mL) was added via cannula transfer. The

color immediately disappeared. The reaction was brought to 60 ºC for 10 minutes then the solvent was removed *in vacou*. In the glovebox, THF (200 mL) was added to the mixture, and the mixture was filtered through celite. The solution was concentrated down until one half of the original volume of THF remained. Diethyl ether (100 mL) was layered on the THF mixture and the product was recrystallized at -35 ºC for a week. The white precipitate was isolated and washed three times with cold THF (6 mL) then dried *in vacou* for a few hours. Yield = 5.0541 g (79 %). ^{1}H, ^{31}P NMR spectra agree with literature.[6]

Synthesis of $(Me_2S)_2PtI_2$. Potassium tetrachloroplatinate (2.1080 g, 5.08 mmol) was added to degassed water (250 mL) in a 500 mL 2-neck flask. Potassium iodide (3.4396 g, 20.66 mmol) was added to the solution. The solution darkened in minutes. An ethanol (100 mL) solution of dimethyl sulfide (0.93 mL, 0.78 g, 13 mmol) was slowly cannulated onto the reaction mixture. An precipitate formed within minutes. The mixture was allowed to stir overnight. The orange precipitate was filtered to yield 2.78 g product (98%). The platinum complex can be used without further purification, but purification by recrystallization from ethanol was often done.

Synthesis of [(PNP)PtI]I. At room temperature, PNP (0.472 g, 0.992 mmol) was dissolved in CH_2Cl_2 (20 mL) and cannulated onto a CH_2Cl_2 (50 mL) solution of $(Me_2S)_2PtI_2$. The reaction was stirred at room temperature for 2 h. The reaction was concentrated to a volume of 15 mL and diethyl ether (65 mL) was added to the reaction dropwise. A yellow precipitate formed. After stirring 1 h, the yellow precipitate was filtered and washed three times with diethyl ether (5 mL). The solid was dried *in vacuo* overnight. Yield = 0.9102 g (99 %). ^{1}H, ^{31}P NMR consistent with the literature.[6]

Synthesis of 1. [(PNP)PtI]I (0.6507 g, 0.705 mmol) was dissolved in CH_2Cl_2 (30 mL). The mixture was purged with ethylene for 5 minutes and remained under an atmosphere of ethylene. At 0 ºC, a CH_2Cl_2 (10 mL) slurry of silver tetrafluoroborate

(0.281 g, 1.44 mmol) was cannulated onto the reaction mixture. A yellow-green precipitate formed within minutes. After 1 h, the precipitate was filtered and washed three times with CH_2Cl_2. Diethyl ether (125 mL) was added dropwise to the reaction to precipitate the product. The white precipitate was filtered and dried *in vacou* overnight. Yield = 0.4875 g (79 %). ^{1}H, ^{31}P NMR consistent with literature.[6]

A.5 References and Notes

1. Min, E. Y.-J., Ph D thesis, California Institute of Technology, **2005**.

2. Hahn, C.; Cucciolito, M. E.; Vitagliano, A. *J. Am. Chem. Soc.*, **2002**, *124*, 9038.

3. Kerber, W. D.; Koh, J. H.; Gagne, M. R. *Organic Lett.*, **2004**, 6, *7*, 3013.

4. Sablong, R.; Newton, C.; Dierkes, P.; Osborn, J. A. *Tett. Lett.*, **1996**, *37*, 4933.

5. Jiang, Q.; Van Plew, D.; Murtuza, S.; Zhang, X. *Tett. Lett.*, **1996**, *37*, 797.

6. Hahn, C.; Morvillo, P.; Herdtweck, E.; Vitagliano, A. *Organometallics*, **2002**, *21*, 1807.

APPENDIX B

CHARACTERIZATION DATA FOR ETHYLENE/CHIRAL α-OLEFIN COPOLYMERS

The following pages contain: gel permeation chromatographs (GPC), differential scanning calorimetry (DSC) thermographs, and proton decoupled carbon-13 nuclear magnetic resonance ($^{13}C\{^{1}H\}$ NMR), data for ethylene/chiral α-olefin copolymers described in Chapter One. Additionally, theoretical calculations for the $^{13}C\{^{1}H\}$ NMR spectra for polymer microstructures with and without consecutive chiral repeat units are included. For detailed experimental procedures see the experimental section of Chapter One.

Figure B.1 GPC traces and corresponding molecular weight data for ethylene/chiral α-olefin copolymers

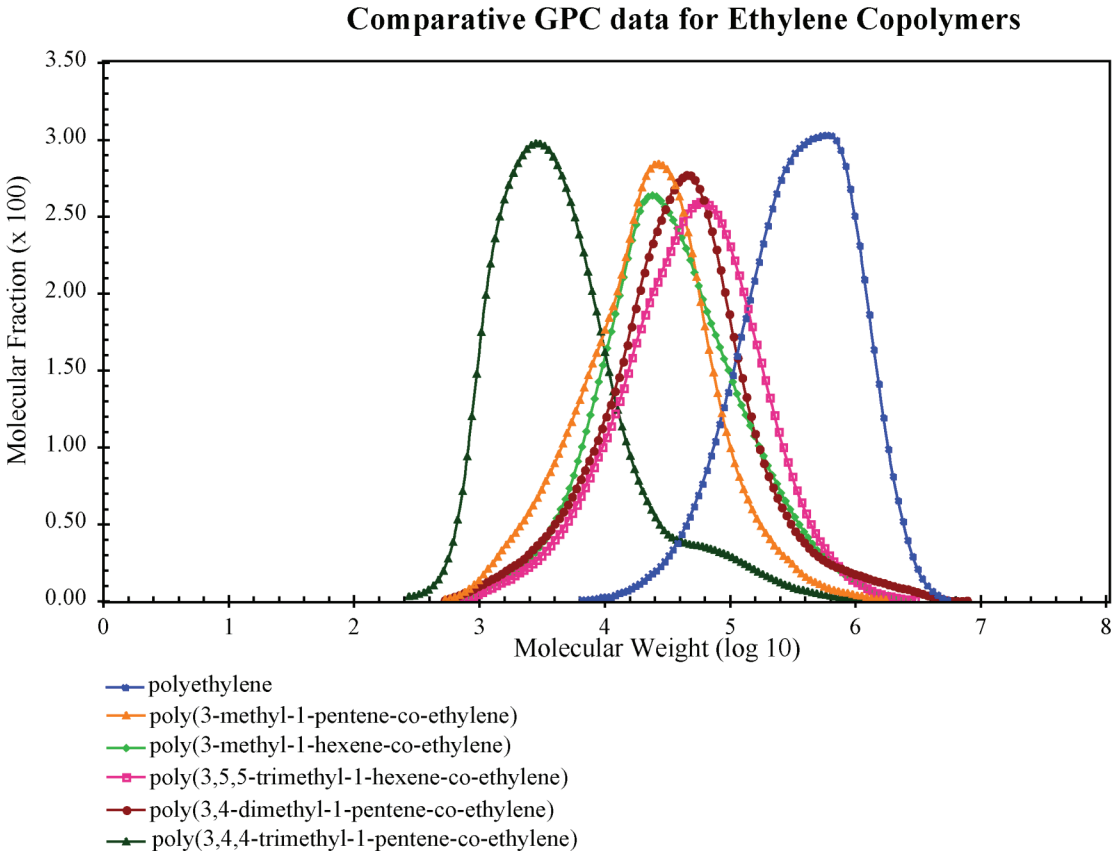

polymer	M_n	M_w	M_p	PDI = M_w/M_n
polyethylene	185,043	552,720	603,075	2.99
poly(3-methyl-1-pentene-*co*-ethylene	10,639	46,168	26,623	4.34
poly(3-methyl-1-hexene-*co*-ethylene)	15,584	79,133	24,044	5.08
poly(3,5,5-trimethyl-1-hexene-*co*-ethylene)	20,007	99,771	58,150	4.99
poly(3,4-dimethyl-1-pentene-*co*-ethylene)	15,618	108,479	45,264	6.95
poly(3,4,4-trimethyl-1-pentene-*co*-ethylene)	2,688	16,008	2,831	5.95

Figure B.2 $^{13}C\{^{1}H\}$ NMR (125 MHz, *o*-dichlorobenzene-d_4, 100 ºC) spectrum for polyethylene.

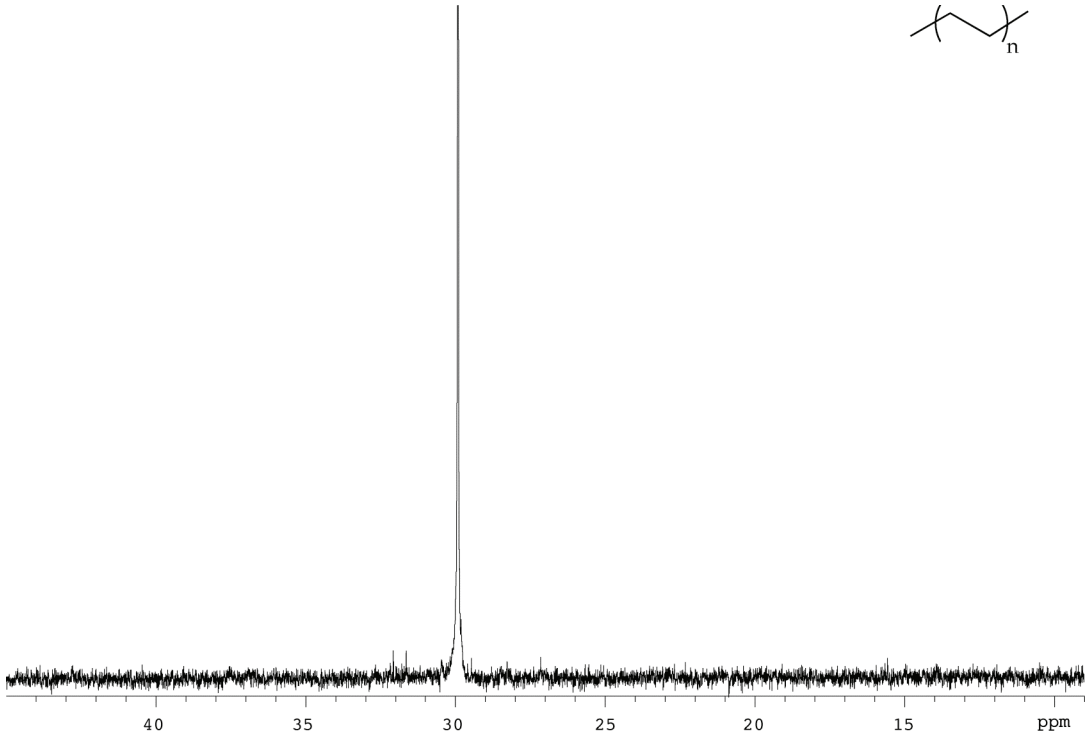

Figure B.3 DSC thermograph for polyethylene

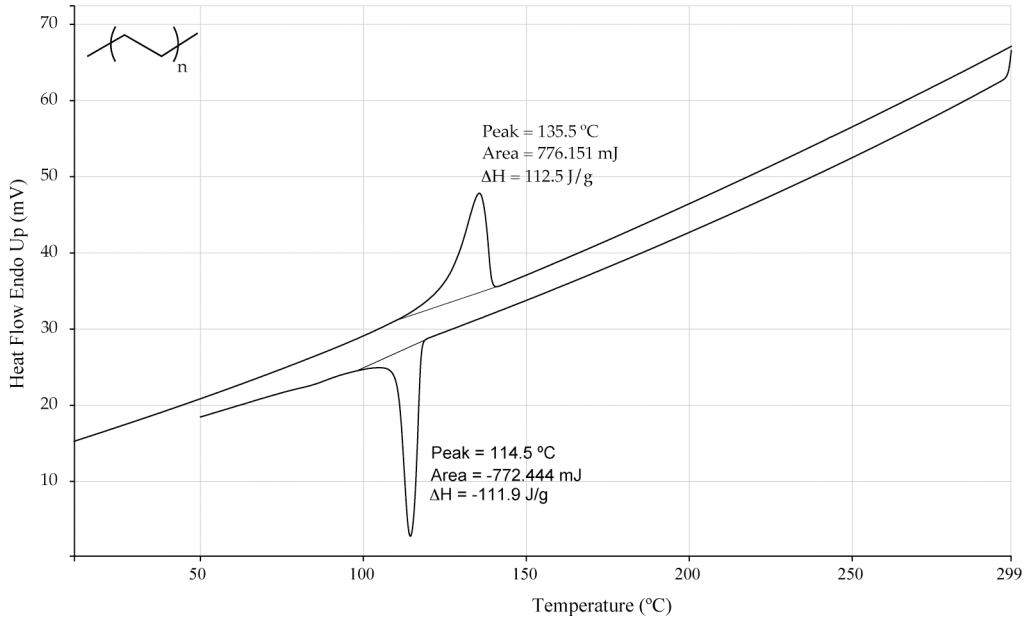

Figure B.4 $^{13}C\{^{1}H\}$ NMR (125 MHz, *o*-dichlorobenzene-d_4, 100 ºC) spectrum for poly(3-methyl-1-pentene-*co*-ethylene).

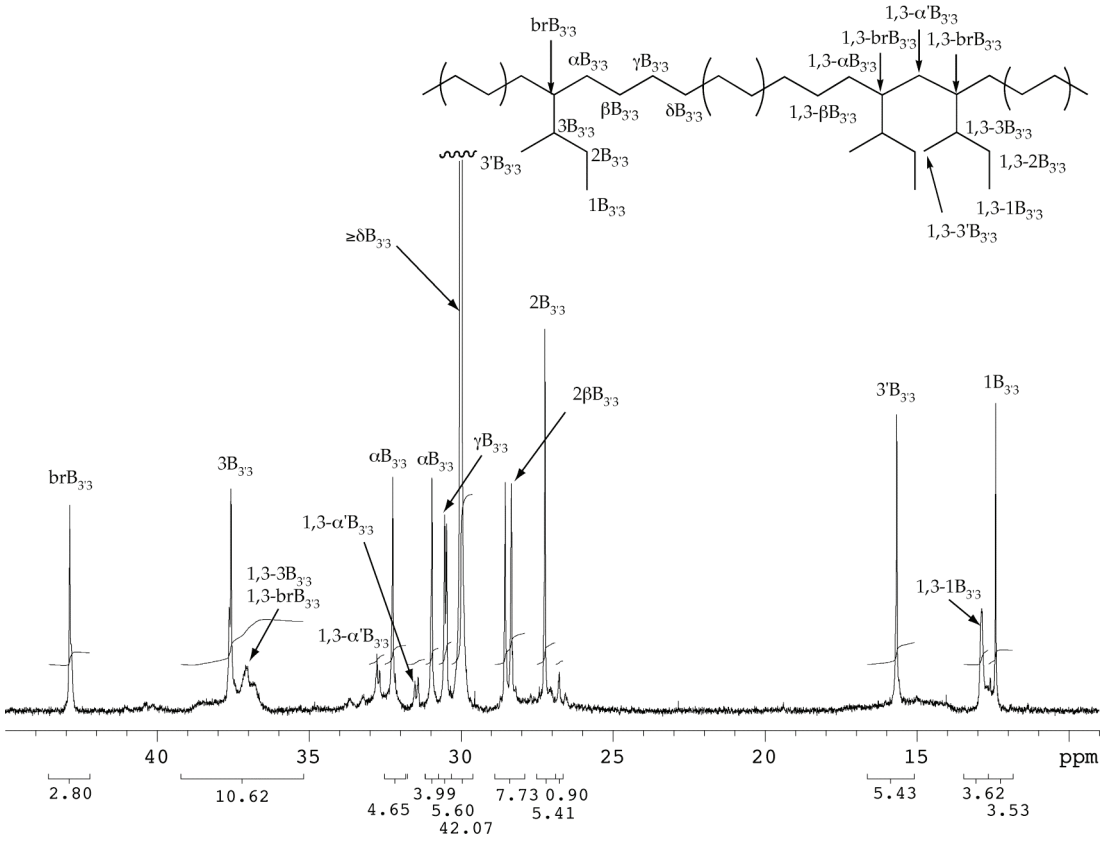

Figure B.5 DSC thermograph for poly(3-methyl-1-pentene-*co*-ethylene).

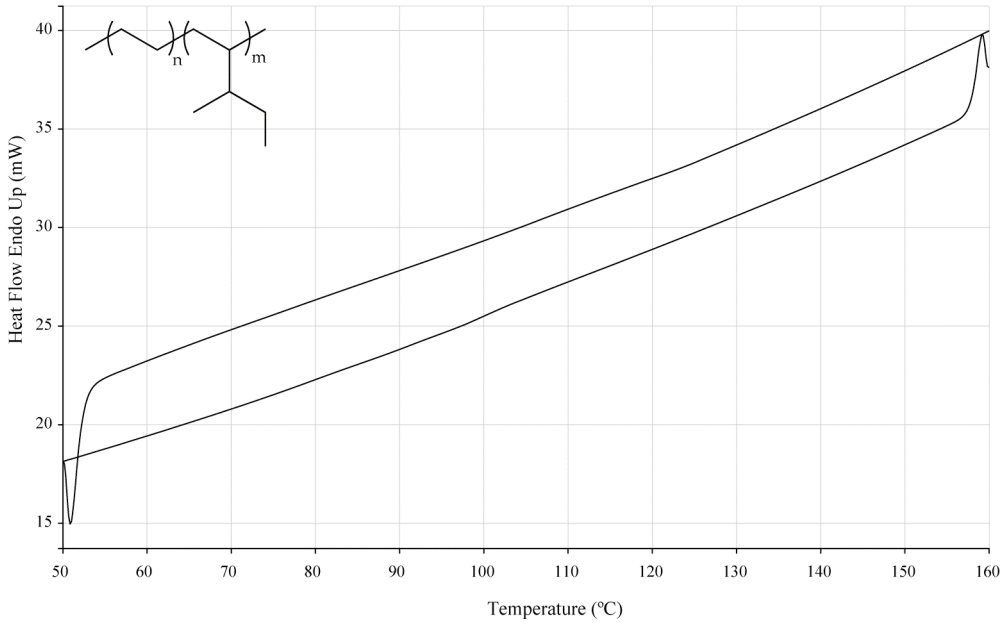

Figure B.6 $^{13}C\{^{1}H\}$ NMR (125 MHz, *o*-dichlorobenzene-d_4-d_2, 100 ºC) spectrum for poly(3-methyl-1-hexene-*co*-ethylene).

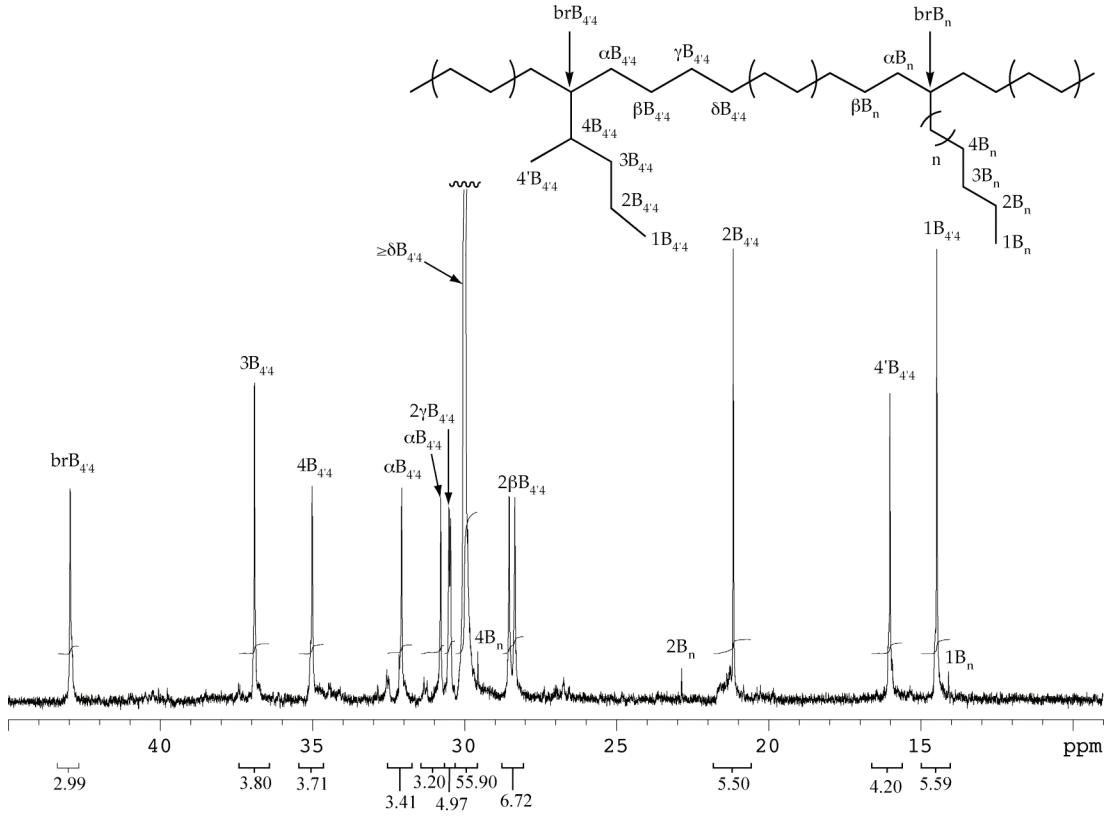

Figure B.7 DSC thermograph for poly(3-methyl-1-hexene-*co*-ethylene).

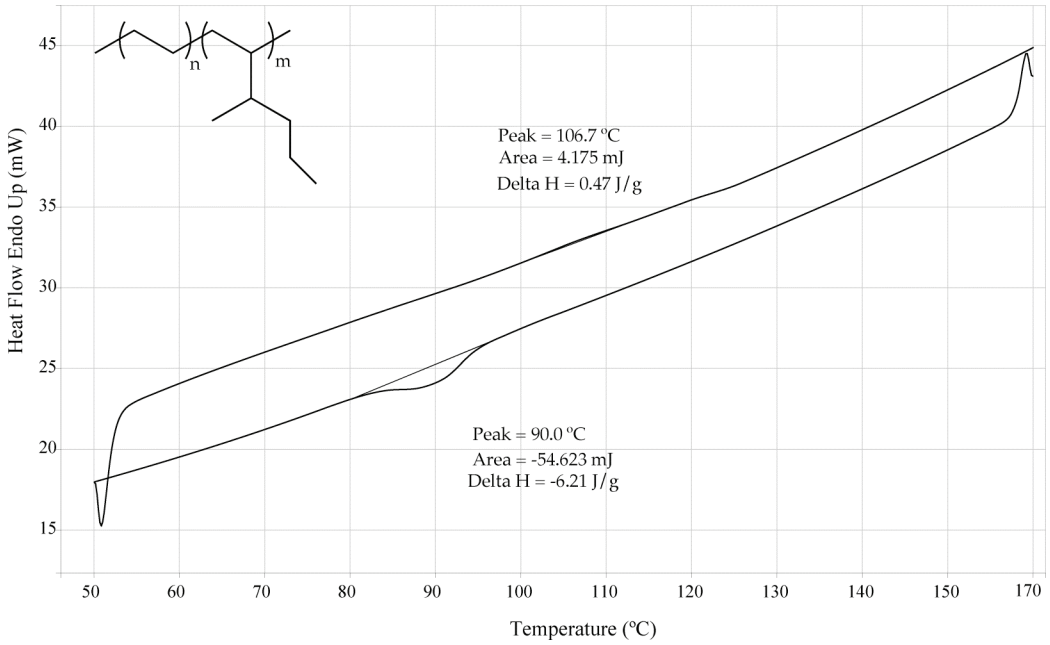

Figure B.8 $^{13}C\{^{1}H\}$ NMR (125 MHz, *o*-dichlorobenzene-d_4, 100 ºC) spectrum for poly(3,5,5-trimethyl-1-hexene-*co*-ethylene).

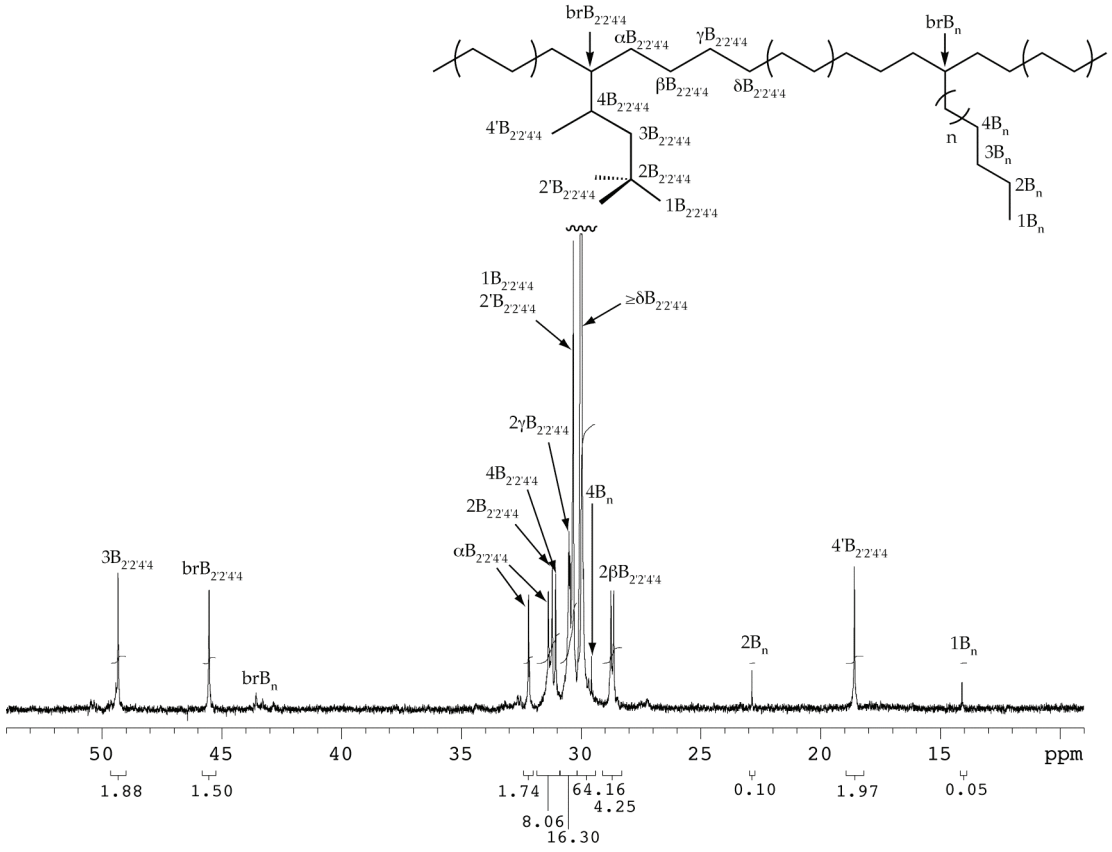

Figure B.9 DSC thermograph of poly(3,5,5-trimethyl-1-hexene-*co*-ethylene).

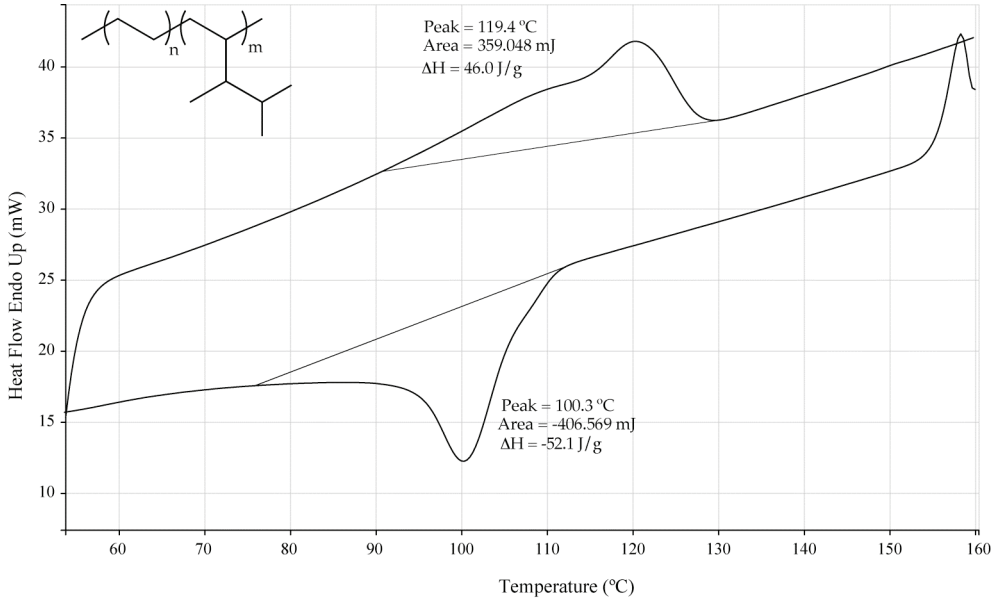

Figure B.10 $^{13}C\{^{1}H\}$ NMR (125 MHz, *o*-dichlorobenzene-d_4, 100 ºC) spectrum for poly(3,4-dimethyl-1-pentene-*co*-ethylene).

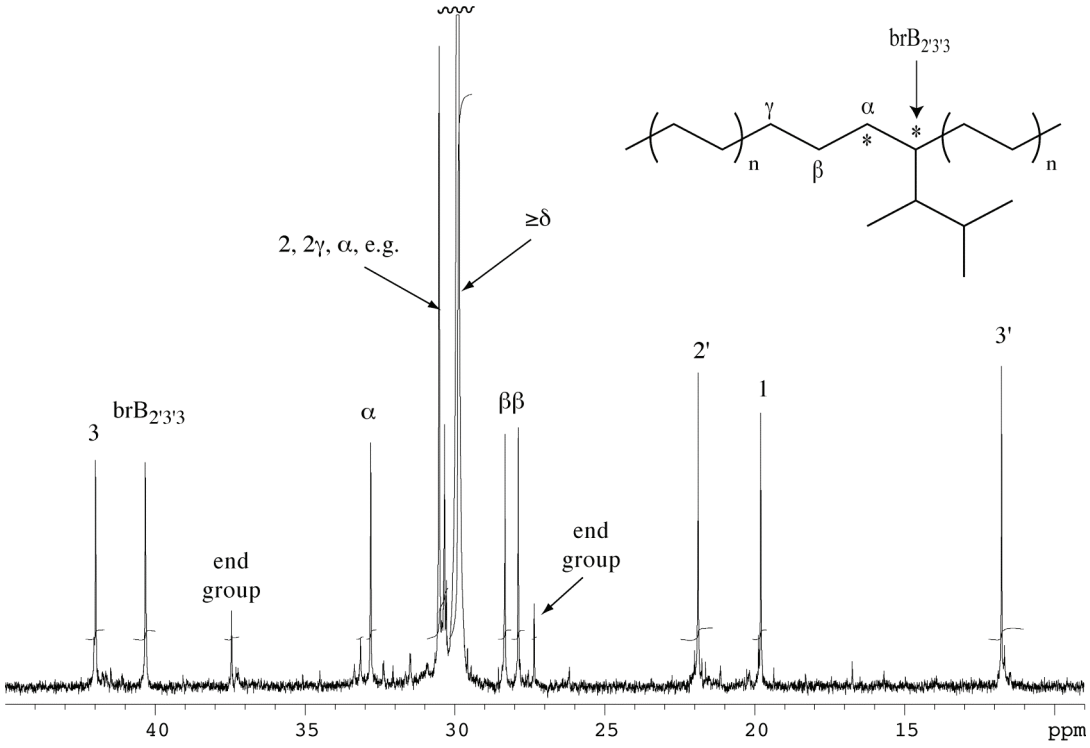

Figure B.11 DSC thermograph for poly(3,4-dimethyl-1-pentene-*co*-ethylene).

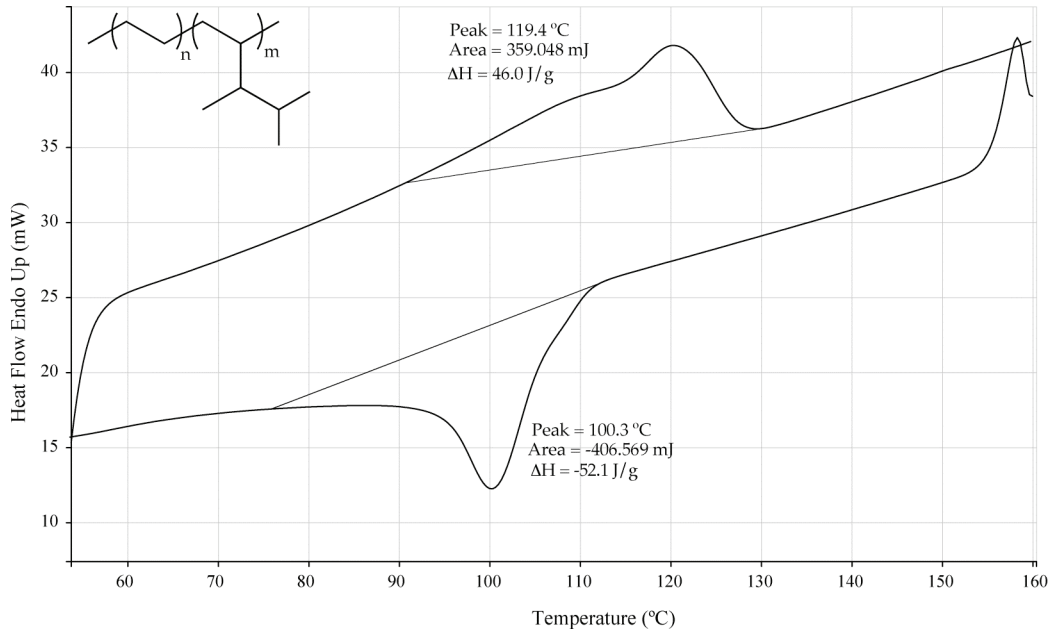

Figure B.12 $^{13}C\{^{1}H\}$ NMR (125 MHz, *o*-dichlorobenzene-d_4, 100 ºC) spectrum poly(3,4,4-trimethyl-1-pentene-*co*-ethylene).

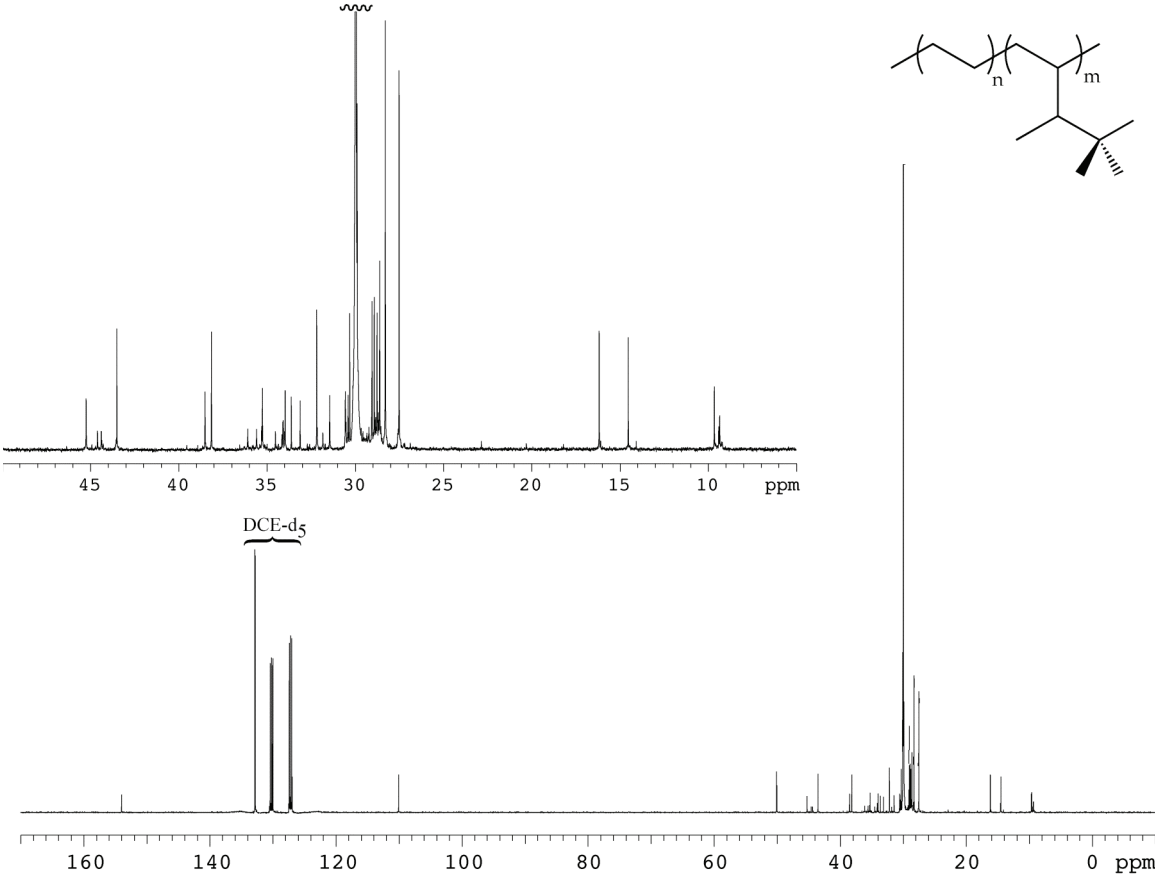

Figure B.13 DSC thermograph of poly(3,4,4-trimethyl-1-pentente-*co*-ethylene).

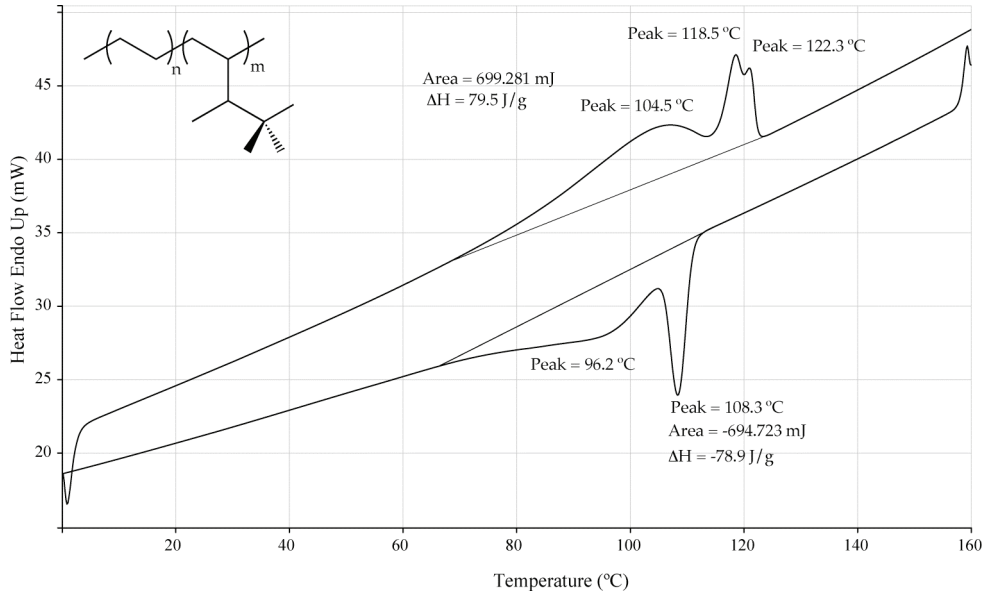

Table B.1 Experimental and theoretical ^{13}C NMR chemical shifts for poly(3-methyl-1-pentene-*co*-ethylene).

carbon	$B_{3'3}$[a]	1,3-$B_{3'3}$[b]	1,5-$B_{3'3}$[c]	poly(1,3-$B_{3'3}$)	observed	assignment	Δ[d]
1	11.36	11.36	11.36	11.36	12.41	$1B_{3'3}$	1.05
					12.86	1,3-$1B_{3'3}$[g]	1.50
3'	16.64	16.64	16.64	16.64	15.66	$3'B_{3'3}$	0.98
2	27.16	27.16	27.16	27.16	27.24	$2B_{3'3}$	0.08
β[f]	27.77	27.77	27.77	N/A	28.34, 28.54	$\beta B_{3'3}$	0.67
δ	30.00	30.00	30.00	30.00	30.00	$\delta B_{3'3}$	0.00
γ	30.21	30.21	30.21	N/A	30.47, 30.54	$\gamma B_{3'3}$	0.30
α	31.78	32.03	32.03	34.1	30.96, 32.25	$\alpha B_{3'3}$	0.18
					32.76	1,3-$\alpha B_{3'3}$[g]	0.73
					37.56	1,3-$3B_{3'3}$[g]	0.12
3	37.31	37.44	37.31	37.56	37.63	$3B_{3'3}$	0.32
br	41.84	40.02	41.84	38.2	42.88	$brB_{3'3}$	1.04
α'[e]	N/A	33.6	32.03	N/A			
β'	N/A	N/A	25.58	N/A			

[a] isolated branch; [b] consecutive branches; [c] branches separated by one ethylene unit; [d] Δ = |expt.-calc.| experimental diastereotopic carbons are averaged to get Δ; [e] α' and β' indicate carbons on the polymer chain between branching points; [f] α, β, γ, and δ indicate carbons on the polymer chain adjacent to the branching units; [g] may also be assigned to poly(1,3-$B_{3'3}$) or 1,5-$B_{3'3}$ microstructures

Table B.2 Experimental and theoretical ^{13}C NMR chemical shifts for poly(3-methyl-1-hexene-*co*-ethylene).

carbon	$B_{4'4}$[a]	1,3-$B_{4'4}$[b]	1,5-$B_{4'4}$[c]	poly(1,3-$B_{4'4}$)	observed	assignment	Δ[d]
					14.07	$1B_n$	
1	14.35	14.35	14.35	14.35	14.47	$1B_{4'4}$	0.12
4'	17.13	17.13	17.13	17.13	16.01	$4'B_{4'4}$	1.12
2	20.21	20.21	20.21	20.21	21.16	$2B_{4'4}$	0.95
					22.86	$2B_n$	
β[f]	27.77	27.77	27.77	N/A	28.34, 28.51	$\beta B_{4'4}$	0.67
δ	30.00	30.00	30.00	30.00	30.00	$\delta B_{4'4}$	0.00
γ	30.21	30.21	30.21	N/A	30.46, 30.51	$\gamma B_{4'4}$	0.28
α	31.78	32.03	31.78	27.15	30.78, 32.07	$\alpha B_{4'4}$	0.36
4	35.24	35.365	35.24	35.49	35.01	$4B_{4'4}$	0.23
3	36.91	36.91	36.91	36.91	36.90	$3B_{4'4}$	0.01
br	41.965	40.145	41.965	38.325	42.96	$brB_{4'4}$	1.00
α'[e]	N/A	33.6	32.03	N/A			
β'	N/A	N/A	25.58	N/A			

[a] isolated branch; [b] consecutive branches; [c] branches separated by one ethylene unit; [d] Δ = |expt.-calc.| experimental diastereotopic carbons are averaged to get Δ; [e] α' and β' indicate carbons on the polymer chain between branching points; [f] α, β, γ, and δ indicate carbons on the polymer chain adjacent to the branching units

Table B.3 Experimental and theoretical ^{13}C NMR chemical shifts for poly(3,5,5-trimethyl-1-hexene-*co*-ethylene).

carbon	$B_{2'2'4'4}$ [a]	1,3-$B_{2'2'4'4}$ [b]	1,5-$B_{2'2'4'4}$ [c]	poly(1,3-$B_{2'2'4'4}$)	observed	assignment	Δ [d]
					14.09	$1B_n$	
4'	18.11	18.11	18.11	18.11	18.59	$4'B_{2'2'4'4}$	0.48
					22.86	$2B_n$	
β [f]	27.77	27.77	27.52	N/A	28.64, 28.75	$\beta B_{2'2'4'4}$	0.93
					29.51	$4B_n$	
δ	30.00	30.00	30.00	30.00	30.00	$\delta B_{2'2'4'4}$	0.00
γ	30.21	30.21	30.21	N/A	30.46, 30.50	$\gamma B_{2'2'4'4}$	0.27
1	30.27	30.27	30.27	30.27	30.32	$1B_{2'2'4'4}$, $2'B_{2'2'4'4}$	0.05
2'	30.27	30.27	30.27	30.27			
4	31.1	31.23	31.1	31.35	31.06	$4B_{2'2'4'4}$	0.04
2	31.39	31.39	31.39	31.39	31.20	$2B_{2'2'4'4}$	0.19
α	31.78	32.03	31.78	34.1	31.37, 32.19	$\alpha B_{2'2'4'4}$	0.00
					43.5	brB_n	
br	42.22	40.4	42.22	38.58	45.53	$brB_{2'2'4'4}$	3.32
3	48.59	48.59	48.59	48.59	49.33	$3B_{2'2'4'4}$	0.74
α' [e]	N/A	33.6	32.03	N/A			
β'	N/A	N/A	25.58	N/A			

[a] isolated branch; [b] consecutive branches; [c] branches separated by one ethylene unit; [d] Δ = |expt.-calc.| experimental diastereotopic carbons are averaged to get Δ; [e] α' and β' indicate carbons on the polymer chain between branching points; [f] α, β, γ, and δ indicate carbons on the polymer chain adjacent to the branching units

Table B.4 Experimental and theoretical ^{13}C NMR chemical shifts for poly(3,4-dimethyl-1-pentene-*co*-ethylene).

carbon	$B_{2'3'3}$ [a]	1,3-$B_{2'3'3}$ [b]	1,5-$B_{2'3'3}$ [c]	poly(1,3-$B_{2'3'3}$)	observed	assignment	Δ [d]
3'	13.65	13.65	13.65	13.65	11.86	$3'B_{2'3'3}$	1.76
1, 2'	19.63	19.63	19.63	19.63	19.89, 21.98	$1B_{2'3'3}$, $2'B_{2'3'3}$	1.31
β' [e]	N/A	N/A	25.58	N/A	27.45		
β [f]	27.77	27.77	27.70	N/A	27.98, 28.43	$\beta B_{2'3'3}$	0.44
δ	30.00	30.00	30.00	30.00	30.00	$\delta B_{2'3'3}$	0.00
γ	30.21	30.21	30.21	N/A	30.63	$\gamma B_{2'3'3}$	0.08
2	30.71	30.71	30.71	30.71	30.63	$2B_{2'3'3}$	0.42
α	32.03	32.28	32.03	N/A	30.44, 32.91	$\alpha B_{2'3'3}$	0.36
α'	N/A	34.10	32.03	34.60	37.55		
br	39.77	37.95	39.77	36.13	40.43	$brB_{2'3'3}$	0.66
3	41.85	41.98	41.85	42.10	42.09	$3B_{2'3'3}$	0.24

[a] isolated branch; [b] consecutive branches; [c] branches separated by one ethylene unit; [d] Δ = |expt.-calc.| experimental diastereotopic carbons are averaged to get Δ; [e] α' and β' indicate carbons on the polymer chain between branching points; [f] α, β, γ, and δ indicate carbons on the polymer chain adjacent to the branching units

Table B.5 Experimental and theoretical ^{13}C NMR chemical shifts for poly(3,4,4-trimethyl-1-pentene-*co*-ethylene).

carbon	$B_{2'2'3'3}$ [a]	1,3-$B_{2'2'3'3}$ [b]	1,5-$B_{2'2'3'3}$ [c]	poly(1,3-$B_{2'2'3'3}$)	observed	assignment
3'	10.66	10.66	10.66	10.66	See	cannot assign
1	27.28	27.28	27.28	27.28	experimental	
2'	27.28	27.28	27.28	27.28	section	
β[d]	27.77	27.77	27.77	N/A		
γ	30.21	30.21	30.21	N/A		
α	32.28	32.53	32.28	N/A		
2	33.09	33.09	33.09	33.09		
br	37.7	35.88	37.7	34.06		
3	45.41	45.535	45.41	45.66		
α'[e]	N/A	34.6	32.53	35.1		
β'	N/A	N/A	25.58	N/A		
3'	10.66	10.66	10.66	10.66		

[a] isolated branch; [b] consecutive branches; [c] branches separated by one ethylene unit; [d] α, β, γ, and δ indicate carbons on the polymer chain adjacent to the branching units; [e] α' and β' indicate carbons on the polymer chain between branching points

APPENDIX C

CHARACTERIZATION DATA FOR PROPYLENE/CHIRAL α-OLEFIN COPOLYMERS

The following pages contain: gel permeation chromatographs (GPC), differential scanning calorimetry (DSC) thermographs, and proton decoupled carbon-13 nuclear magnetic resonance ($^{13}C\{^{1}H\}$ NMR), data for propylene/chiral α-olefin copolymers described in Chapter One. For detailed experimental procedures see the experimental section of Chapter One.

Figure C.1 GPC traces and corresponding molecular weight data for propylene/chiral α-olefin copolymers

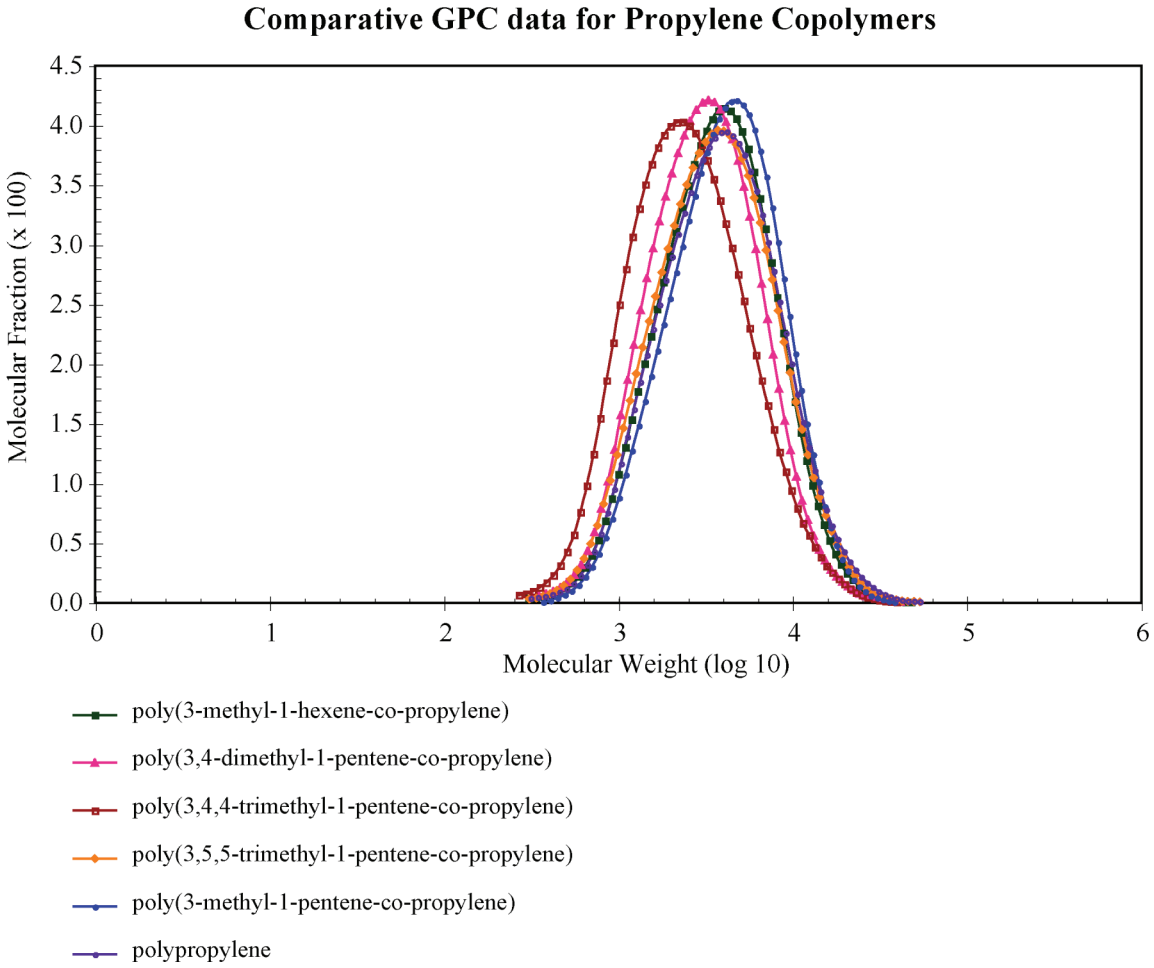

polymer	M_n	M_w	M_p	PDI = M_w/M_n
polypropylene	2,878	5,219	4,059	1.81
poly(3-methyl-1-pentene-*co*-propylene	3,155	5,291	4,600	1.68
poly(3-methyl-1-hexene-*co*-propylene)	2,812	4,873	4,038	1.73
poly(3,5,5-trimethyl-1-hexene-*co*-propylene)	2,673	4,891	3,813	1.83
poly(3,4-dimethyl-1-pentene-*co*-propylene)	2,455	4,121	3,290	1.68
poly(3,4,4-trimethyl-1-pentene-*co*-propylene)	1,912	3,484	2,262	1.82

Figure C.2 $^{13}C\{^{1}H\}$ NMR (125 MHz, 1,1,2,2-tetrachloroethane-d_2, 100 ºC) spectrum for polypropylene.

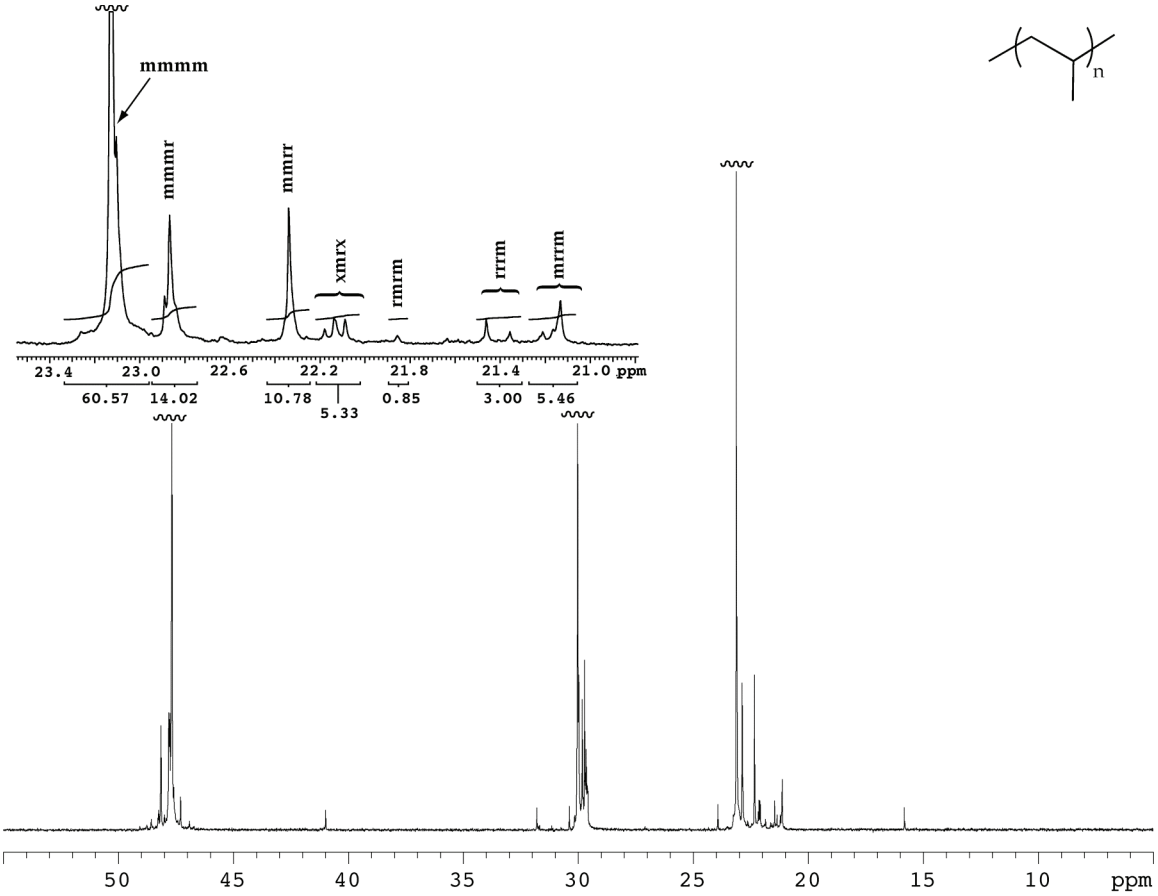

Figure C.3 DSC thermograph for polypropylene

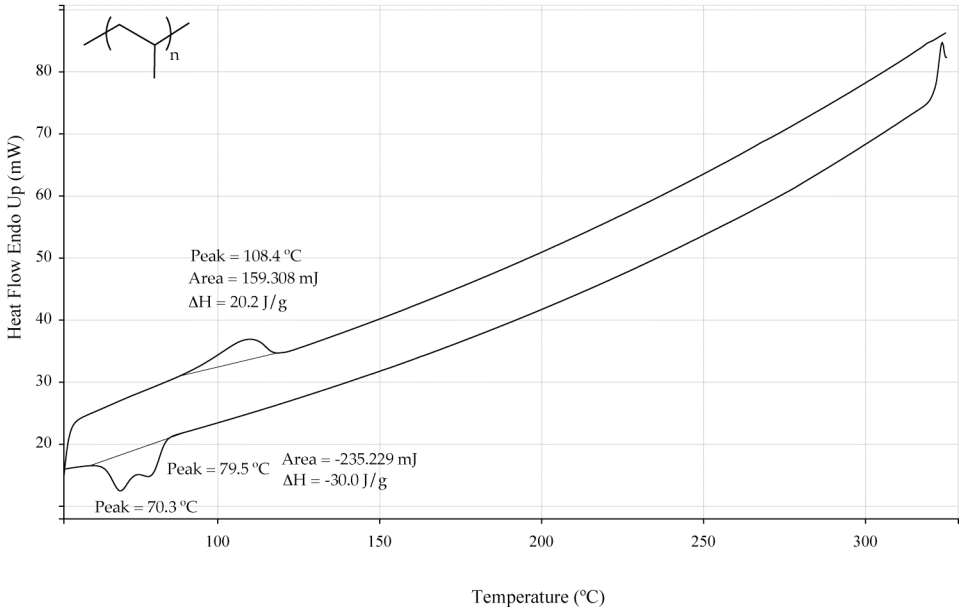

Figure C.4 $^{13}C\{^{1}H\}$ NMR (125 MHz, 1,1,2,2-tetrachloroethane-d_2, 100 ºC) spectrum for poly(3-methyl-1-pentene-*co*-propylene).

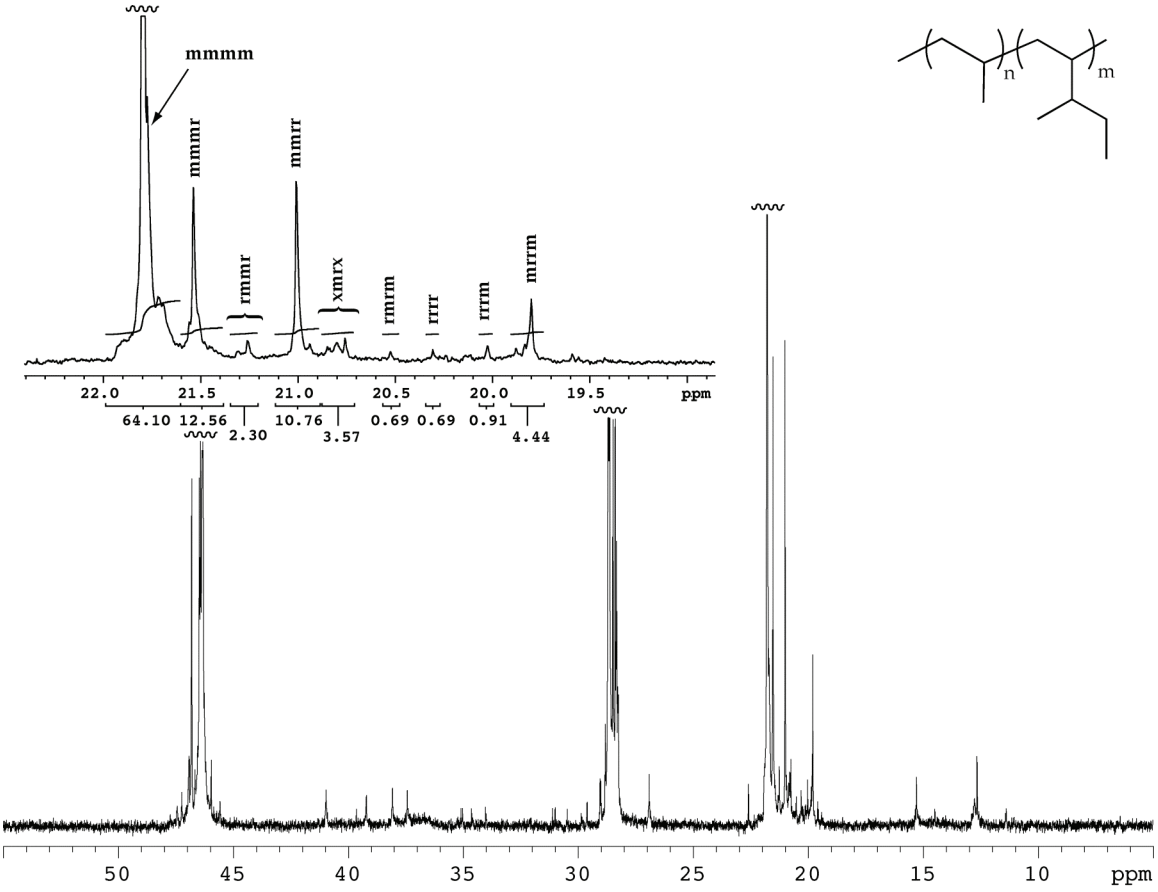

Figure C.5 DSC thermograph for poly(3-methyl-1-pentene-*co*-propylene).

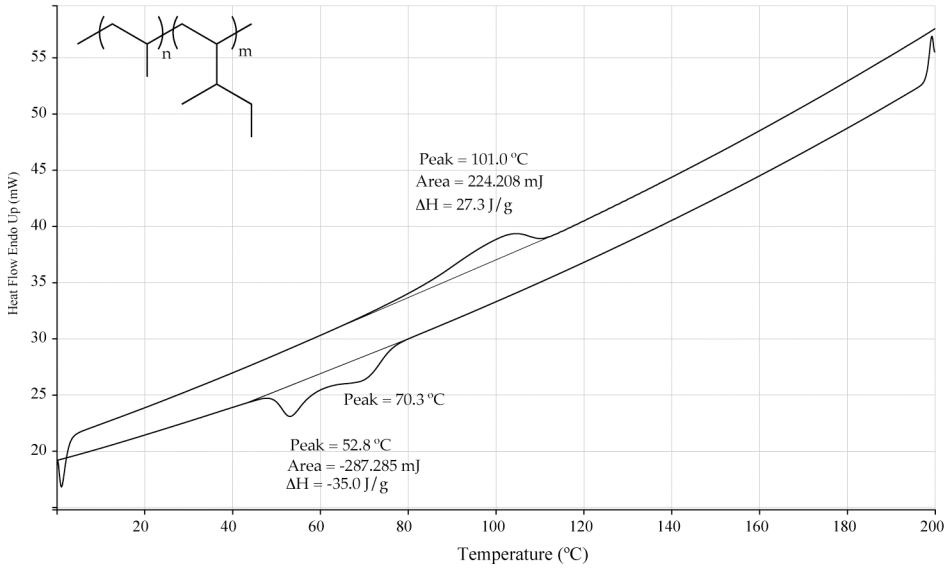

Figure C.6 $^{13}C\{^{1}H\}$ NMR (125 MHz, 1,1,2,2-tetrachloroethane-d_2, 100 ºC) spectrum for poly(3-methyl-1-hexene-*co*-propylene).

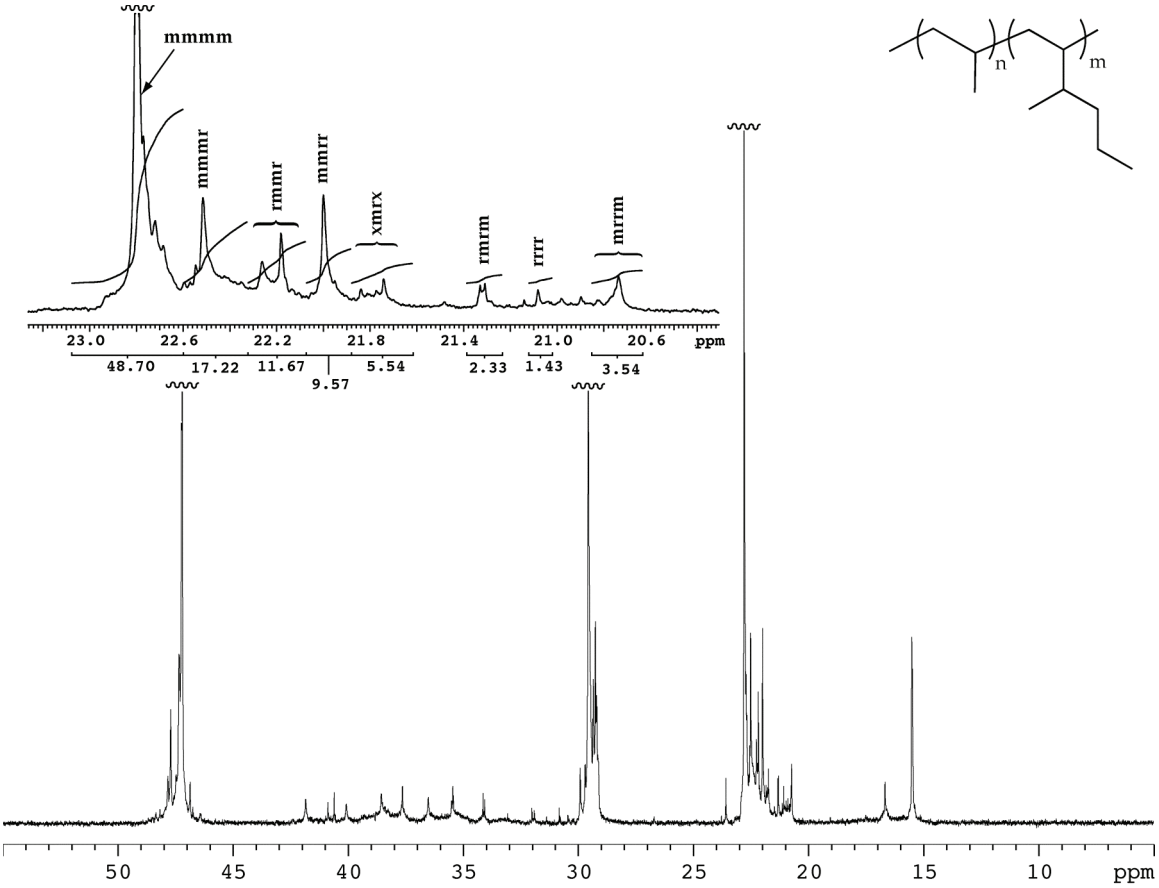

Figure C.7 DSC thermograph for poly(3-methyl-1-hexene-*co*-propylene).

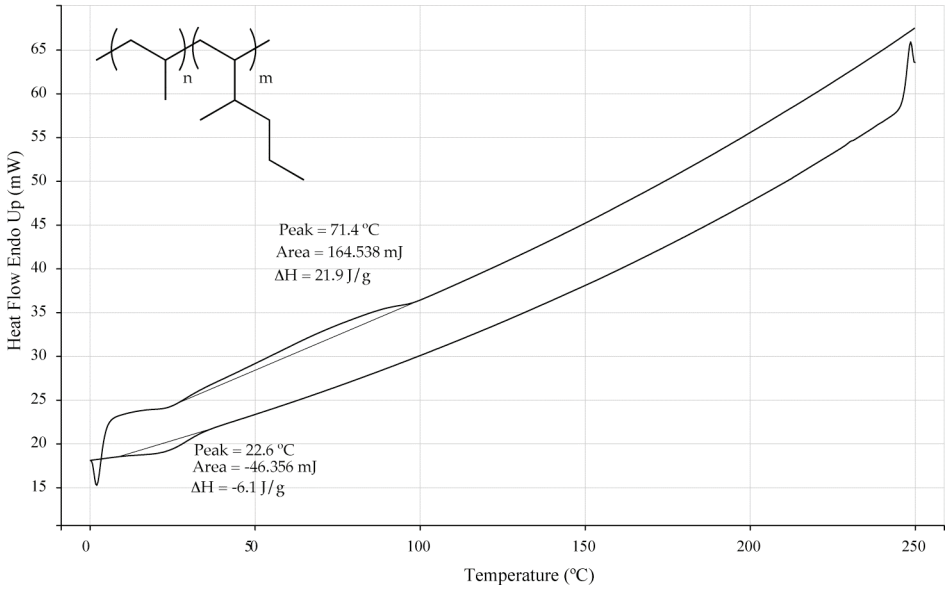

Figure C.8 $^{13}C\{^{1}H\}$ NMR (125 MHz, 1,1,2,2-tetrachloroethane-d_2, 100 ºC) spectrum for poly(3,5,5-trimethyl-1-hexene-*co*-propylene).

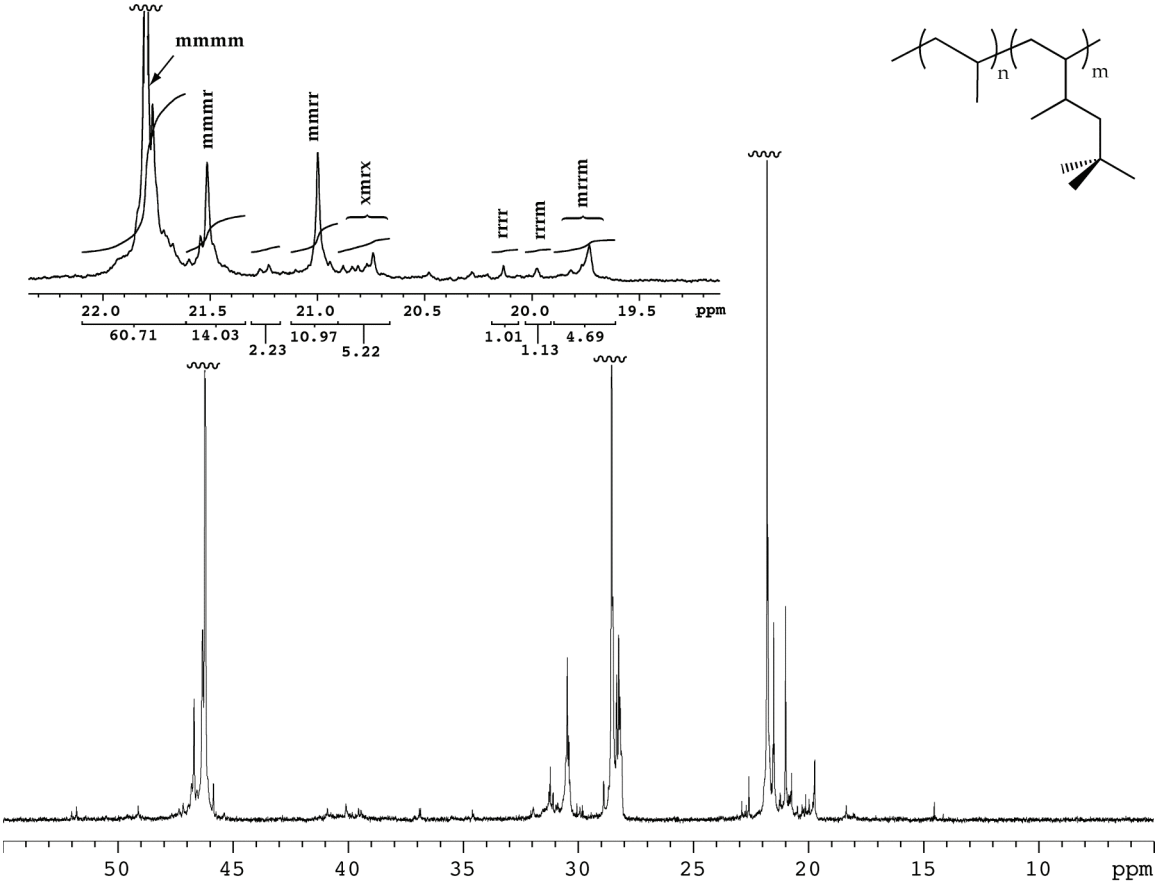

Figure C.9 DSC thermograph of poly(3,5,5-trimethyl-1-hexene-*co*-propylene).

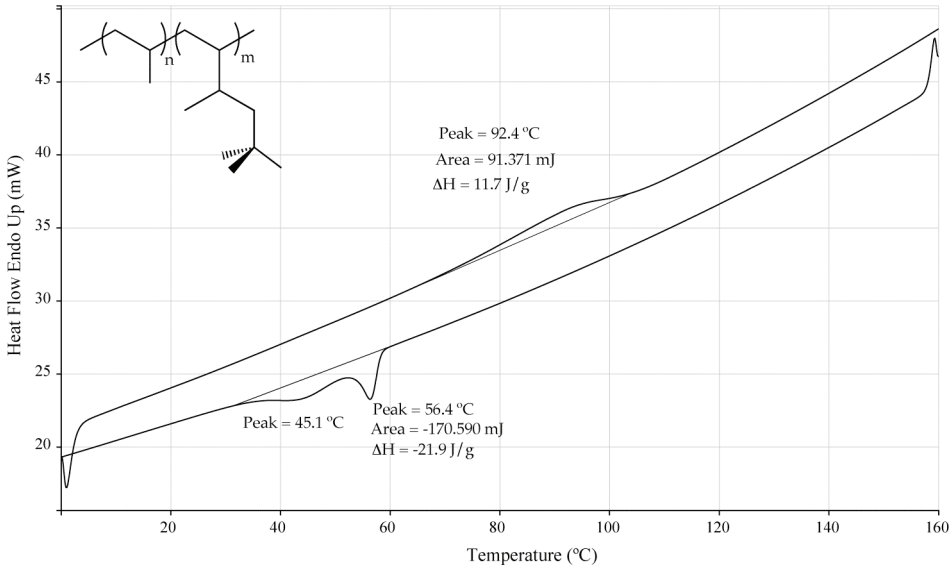

Figure C.10 $^{13}C\{^{1}H\}$ NMR (125 MHz, 1,1,2,2-tetrachloroethane-d_2, 100 ºC) spectrum for poly(3,4-dimethyl-1-pentene-*co*-propylene).

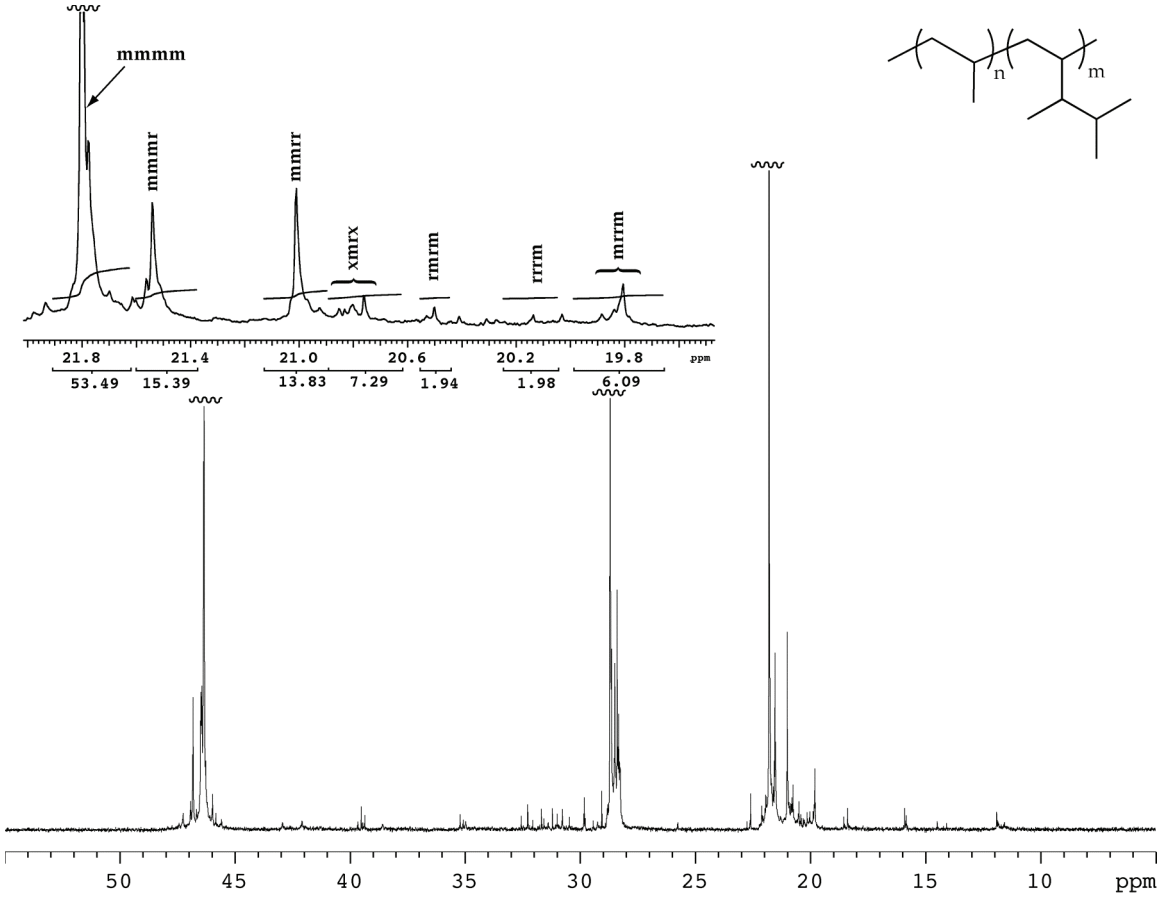

Figure C.11 DSC thermograph for poly(3,4-dimethyl-1-pentene-*co*-propylene).

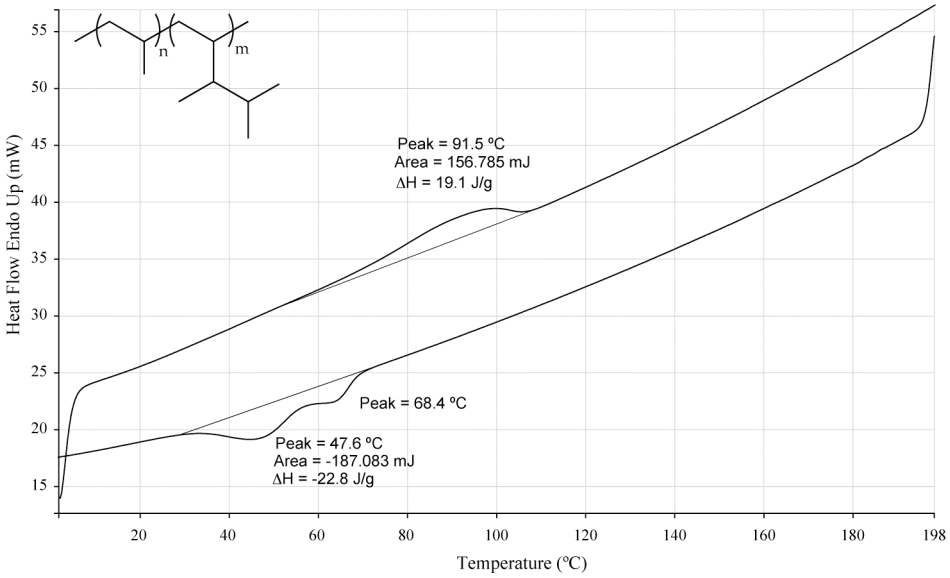

Figure C.12 $^{13}C\{^{1}H\}$ NMR (125 MHz, 1,1,2,2-tetrachloroethane-d_2, 100 ºC) spectrum poly(3,4,4-trimethyl-1-pentene-*co*-propylene).

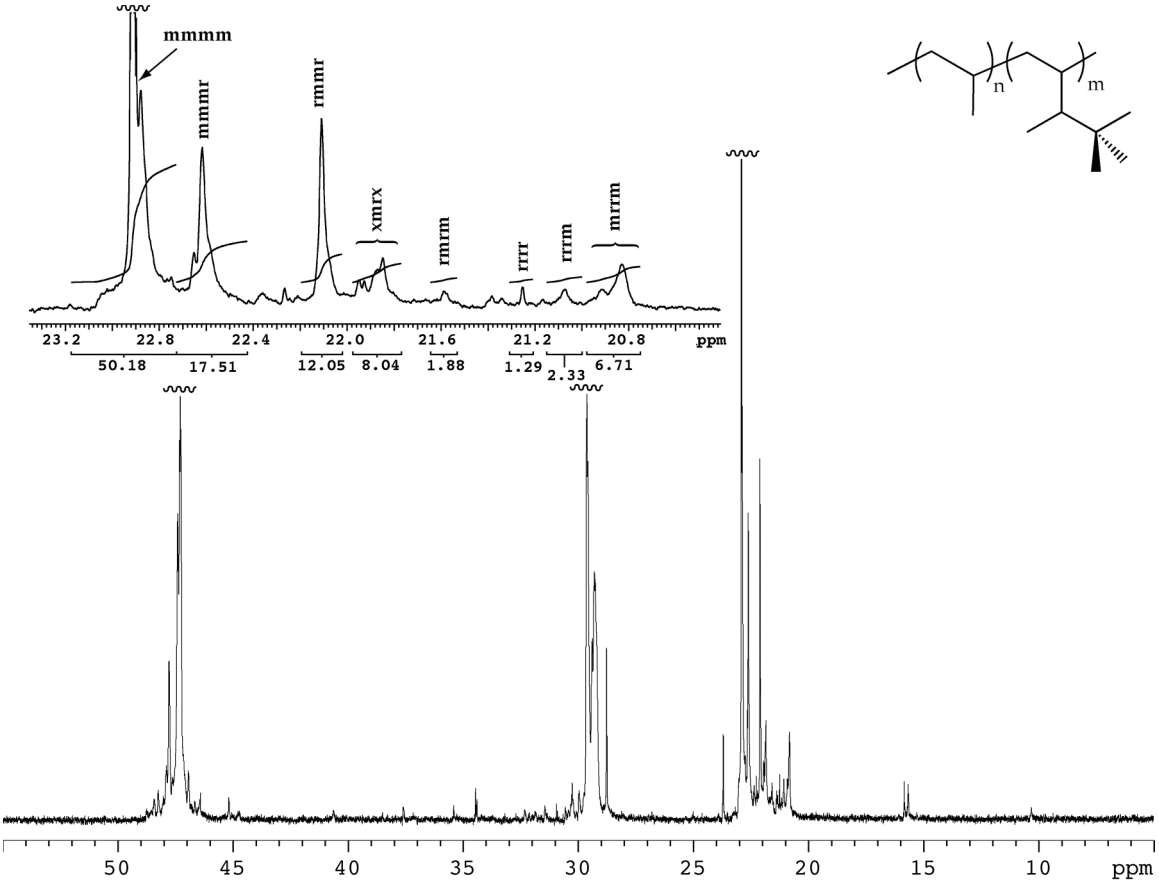

Figure C.13 DSC thermograph of poly(3,4,4-trimethyl-1-pentente-*co*-propylene).

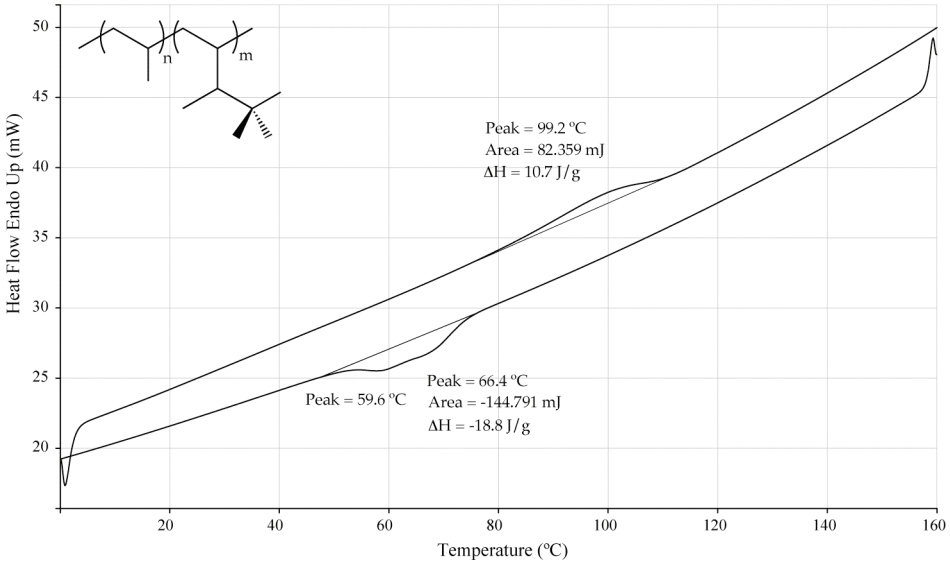

APPENDIX D

DATA FOR THE DETERMINATION OF REACTIVITY RATIOS FOR α-OLEFIN/CHIRAL MONOMER COPOLYMERS

Reactivity ratios for the prochiral α-olefin/chiral monomer copolymerizations discussed in Chapter 1 was determined using the method of Fineman and Ross. A good description of this method is in Odian's, *Principles of Polymerization*. The method is a linear least-squares regression analysis that relates the copolymer composition to the relative rates of homo- and copolymerization for each monomer following relationship (D.1):

$$G = r_1 F - r_2 \tag{D.1}$$

where r_1 and r_2 are the reactivity ratios for monomer 1 and 2, respectively. G and F are related to the initial concentration of each olefin ($[M_n]$) and the change in this concentration ($d[M_n]$) at low conversion by (D.2) and (D.3):

$$G = \frac{\left(\frac{[M_1]}{[M_2]}\right)\left(\left(\frac{d[M_1]}{d[M_2]}\right) - 1\right)}{\left(\frac{d[M_1]}{d[M_2]}\right)} \tag{D.2}$$

$$F = \frac{[M_1]^2 * d[M_2]}{[M_2]^2 * d[M_1]} \tag{D.3}$$

Practically, reactivity ratios can be determined with a technique that can monitor olefin conversion dat low overall conversion. Using this data, G and F can be determined from equations (D.2) and (D.3) and plotting G vs. F will give a line with a slope that is the reactivity ratio of one monomer and the intercept giving the reactivity ratio of the other monomer.

The method of Fineman and Ross is congruent with the GC aliquot method that we use to follow our reactions, so determining reactivity ratios with this method was possible. Figures D.1 and D.2 are plots of G *vs.* F for 1-pentene/3-methyl-1-pentene and 3-methyl-1-butene/3-methyl-1-pentene copolymerizations, respectively. For a discussion of the reactivity ratios obtained from these plots see Chapter 1.

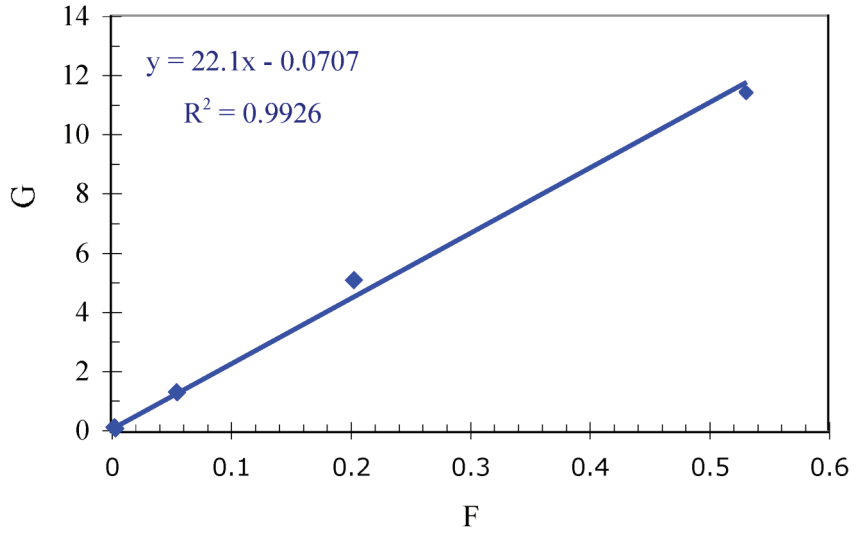

Figure D.1 Fineman and Ross plot for 1-pentene/3-methyl-1-pentene copolymerizations.

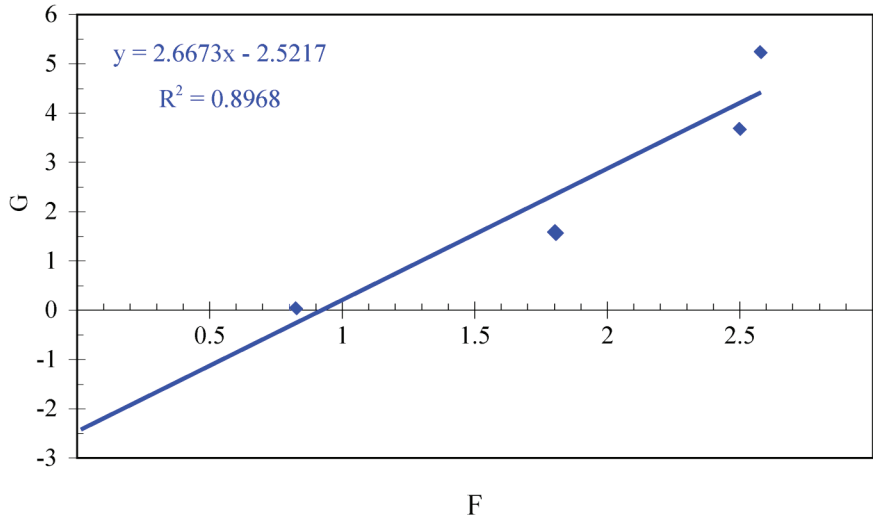

Figure D.2 Fineman and Ross plot for 3-methyl-1-butene/3-methyl-1-pentene copolymerizations.

APPENDIX E

SUMMARY OF GAS CHROMATOGRAPHIC METHODS

As this project has progressed a great deal of empirical information has been gained and passed by word of mouth. In particular, the gas chromatograph (GC) methods used to follow the polymerization of racemic α-olefins as well as for the determination of their enantiomeric excess have been tediously determined, but no permanent record of this information exists. Below is a summary of the GC methods and some empirical observations that my predecessors and I have made during the course of our work. Many experiments have been conducted to optimize these conditions, and several months of work have been ruined by some unfortunate discoveries pertaining to either the GC runs used to follow the reactions or the GC runs obtained for enantioassays. Hopefully, the summary will help future coworkers from making similar mistakes to those that we have encountered.

For most of the olefins studied, conversion of the racemic a-olefin polymerizations were followed by GC's using a Agilent 19091S-433 "HP-5" column (5% Phenyl Methyl Siloxane 30.0 m x 250 μm x 0.25 μm) with the following instrument parameters and temperature program (called "Method 3" on the Bercaw Group GC):

Flow = 2.0 mL/m Inlet T = 200 ºC Split Ratio = 150:1 Detector T = 250 ºC

Temperature Program:

1) Isothermal step at the initial temperature of 35 ºC for 1 minute

2) Temperature ramp at 10 ºC/min to 150 ºC

3) Isothermal step at 150 ºC for 5 minutes

Total run time = 17 minutes 50 seconds

Table E.1 is a table of common compounds and their retention times using this method

compound	retention time (m)
acetone	1.15
hexanes	1.17
benzene	1.46
toluene	3.38
isopropanol	1.48
3-methyl-1-pentene	1.56
butanol	2.53
3-methyl-1-hexene	2.04
3,5,5-trimethyl-1-pentene	3.38
3,4-dimethyl-1-pentene	2.07
3,4,4-trimethyl-1-pentene	2.66
tetradecane	12.74
chlorobenzene	4.57
1,2-dichlorbenzene	7.59

Table E.1 Retention times for common compounds using the standard GC method for monitoring conversion during polymerizations.

A few observations have been made for the chromatographs used to follow conversion of the reaction. Generally, aliquots (<0.1 mL) from polymerization reactions are removed from the reaction vessel and diluted in an alcoholic solvent. This is done to quench any MAO in the reaction. It is important to emphasize that the choice of alcohol is critical. As seen in Table E.1, isopropanol is a good solvent for the GC samples for most olefins. The one exception is 3-methyl-1-pentene, as the large solvent peak from isopropanol can sometime overlap with this monomer. For 3-methyl-1-pentene polymerizations, therefore, butanol was generally used as the GC solvent. Butanol is generally not a good GC solvent because the solvent peak tends to be broad and overlaps with many of the olefin peaks. Ethanol was usually not used because of the benzene contaminent used to denature ethanol in reagent grade ethanol. *Methanol should never be*

used as a GC solvent to get conversion! This is not because methanol is harmful to the column, but rather because it is not miscible with tetradecane, the ubiquitous internal standard used in these reactions.

The HP-5 column works well for most olefins, but it is problematic for 3,5,5-trimethyl-1-hexene because the retention time for this olefin coincides with retention times for toluene. It is important to keep this fact in mind for all 3,5,5-trimethyl-1-pentene polymerizations. These reactions should be carried out using benzene as the solvent for the catalyst or (preferably) using a different GC column. We have found that the DC-5 column (Agilent 127-1013E, 10.0 m x 100 μm x 0.4 μm) achieves clean separation of toluene and 3,5,5-trimethyl-1-hexene peaks when operating under the below instrumental conditions and temperature program (called "Method 3b" on the Bercaw Group GC):

Flow = 0.2 ml/m Inlet T = 250 ºC Split Ratio = 500:1 Detector T = 320 ºC

Temperature Program:

1) Isothermal step at initial temperature = 35 for 1 minute
2) Temperature ramp at 10 ºC/min to 150 ºC.
3) Isothermal step at 150 ºC for 10 minutes

The retention times for isopropanol, toluene, 3,5,5-trimethyl-1-hexene, and tetradecane using this method are: 1.563, 4.650, 4.772, 15.973 minutes respectively.

Enantiomeric excess for the reactions were determined on a Chiraldex G-TA chiral column. Initially, conversion was determined on this column, but this shortened the lifetime of the column presumably due to alcoholysis of the column. Care was taken to ensure that water was not introduced onto this column. The GC solvent that was used was either diethyl ether or hexanes. All samples were dried over magnesium sulfate prior to analysis. Each olefin required unique GC conditions and temperature programs.

These methods are presented in Table E.2 along with the retention times for each antipode of the methyl ester of the olefins commonly studied.

flow (ml/m)	initial T (ºC)	isotherm (m)	ramp rate (ºC/m)	Final T (ºC)	isotherm (m)	run time (m)	retiention times (m)	
							R	*S*
1.0	40	10	15	160	5	29.00	10.286	10.89
2.0	50	10	15	160	5	22.33	6.412	6.972
1.0	55	17	15	160	5	29.00	17.97	18.472
1.0	60	20	15	160	5	31.67	11.709	12.29
0.5	40	40	10	160	5	57.00	42.201	43.122

Table E.2 Instrument conditions and temperature programs for enantioassay GC methods. All temperature programs have three parts: 1) isotherm at an initial temperature, 2) temperature ramp to a final temperature, and 3) isotherm at the final temperature. Settings common to all methods are: Inlet T = 200 ºC, Detector T = 250 ºC.

Optical purity was determined from the integrals of the two antipodes multiplied by the sensitivity factor determined from a racemic mixture of the olefin. Identification of the absolute identity of the methyl ester enantiomers was previously described (Baar, C. R.; Levy, C. J.; Min, E. Y.-J.; Henling, L. M.; Day, M. W.; Bercaw, J. E. *J. Am. Chem. Soc.* **2004**, *126*, 8216). As the column aged, the peaks corresponding to each antipode begin to merge. Baseline separation could commonly be obtained by modification of the generic procedure for each olefin, but in such cases new sensitivity factors must be obtained. Care must be taken for determining the e.e. of 3-methyl-1-pentene polymerizations. It is important all of the derivitization solvent (CH_3CN and CCl_4) be removed from 3-methyl-1-butanoic acid before methanolysis to the methyl ester because acetonitrile has the same retention time as the methyl ester of 3-methyl-1-butanoic acid.

APPENDIX F

X-RAY CRYSTALLOGRAPHIC DATA FOR (*S*)-**2**

(CHAPTER 2)

Contents

Note: Crystallographic data have been deposited at the CCDC, 12 Union Road, Cambridge CB2 1EZ, UK and copies can be obtained on request, free of charge, by quoting the publication citation and the deposition number 635262.

Table F.1. Crystal data and structure refinement for (*S*)-2 (CCDC 635262).

Empirical formula	$C_{27}H_{44}Si_2Cl_2Zr$
Formula weight	586.92
Crystallization solvent	Toluene
Crystal habit	Plate
Crystal size	0.25 x 0.22 x 0.07 mm^3
Crystal color	Colorless

Data Collection

Type of diffractometer	Bruker SMART 1000
Wavelength	0.71073 Å MoKα
Data Collection Temperature	100(2) K
θ range for 24444 reflections used in lattice determination	2.27º to 40.09°
Unit cell dimensions	a = 8.7249(3) Å b = 11.4772(4) Å c = 28.8269(11) Å
Volume	2886.65(18) $Å^3$
Z	4
Crystal system	Orthorhombic
Space group	$P2_12_12_1$
Density (calculated)	1.351 Mg/m^3
F(000)	1232
Data collection program	Bruker SMART v5.630
θ range for data collection	1.91º to 40.60°
Completeness to θ = 40.60°	92.3%
Index ranges	$-15 \le h \le 15$, $-19 \le k \le 18$, $-52 \le l \le 50$
Data collection scan type	ω scans at 7 ϕ settings
Data reduction program	Bruker SAINT v6.45A
Reflections collected	67983
Independent reflections	16445 [R_{int}= 0.0944]
Absorption coefficient	0.663 mm^{-1}
Absorption correction	None
Max. and min. transmission	0.9551 and 0.8518

Table F.1 (continued)

Structure solution and Refinement

Structure solution program	Bruker XS v6.12
Primary solution method	Direct methods
Secondary solution method	Difference Fourier map
Hydrogen placement	Geometric positions
Structure refinement program	Bruker XL v6.12
Refinement method	Full matrix least-squares on F^2
Data/restraints/parameters	16445/0/301
Treatment of hydrogen atoms	Riding
Goodness-of-fit on F^2	1.091
Final R indices [I>2σ(I), 12573 reflections]	R1 = 0.0393, *w*R2 = 0.0663
R indices (all data)	R1 = 0.0609, *w*R2 = 0.0698
Type of weighting scheme used	Sigma
Weighting scheme used	$w=1/\sigma^2(Fo^2)$
Max shift/error	0.001
Average shift/error	0.000
Absolute structure determination	Anomalous differences
Absolute structure parameter	-0.031(19)
Largest diff. peak and hole	0.778 and -0.557 e.Å^{-3}

Special Refinement Details

Refinement of F^2 against ALL reflections. The weighted R-factor (*w*R) and goodness of fit (S) are based on F^2, conventional R-factors (R) are based on F, with F set to zero for negative F^2. The threshold expression of $F^2 > 2\sigma(F^2)$ is used only for calculating R-factors (gt) etc. and is not relevant to the choice of reflections for refinement. R-factors based on F^2 are statistically about twice as large as those based on F, and R-factors based on ALL data will be even larger.

All esds (except the esd in the dihedral angle between two l.s. planes) are estimated using the full covariance matrix. The cell esds are taken into account individually in the estimation of esds in distances, angles and torsion angles; correlations between esds in cell parameters are only used when they are defined by crystal symmetry. An approximate (isotropic) treatment of cell esds is used for estimating esds involving l.s. planes.

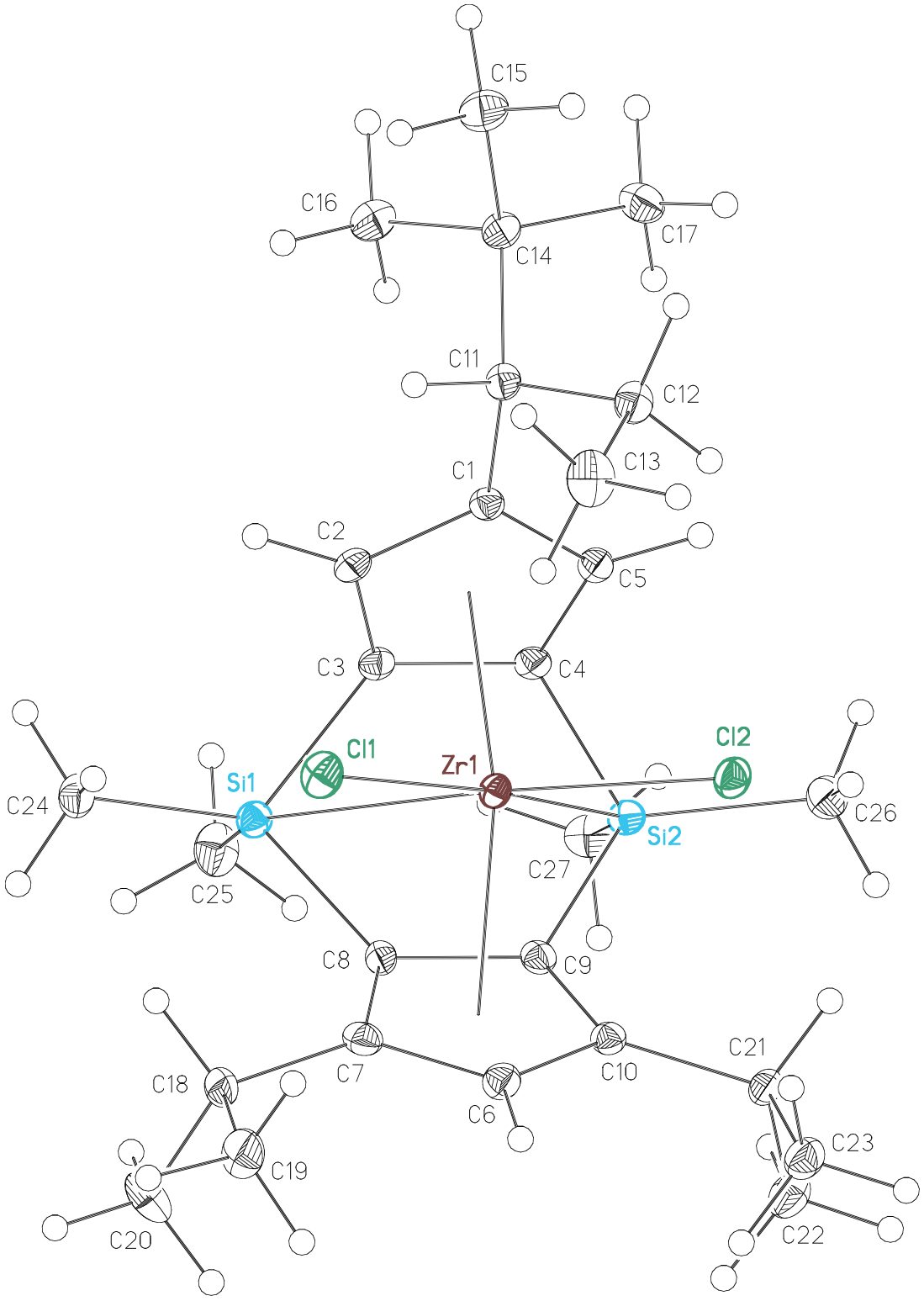

Figure F.1 Minimum overlap view of (*S*)-**2**.

Table F.2 Atomic coordinates (10^4) and equivalent isotropic displacement parameters ($Å^2$ x 10^3) for (*S*)-**2** (CCDC 635262). U(eq) is defined as the trace of the orthogonalized U^{ij} tensor.

	x	y	z	U_{eq}
Zr(1)	387(1)	8003(1)	1238(1)	9(1)
Cl(1)	-347(1)	7967(1)	422(1)	16(1)
Cl(2)	-813(1)	9758(1)	1543(1)	14(1)
Si(1)	2322(1)	5631(1)	1204(1)	11(1)
Si(2)	1918(1)	7286(1)	2211(1)	10(1)
C(1)	2954(2)	9150(2)	1035(1)	10(1)
C(2)	3066(2)	7988(2)	869(1)	11(1)
C(3)	2971(2)	7187(1)	1249(1)	11(1)
C(4)	2781(2)	7892(2)	1666(1)	10(1)
C(5)	2773(2)	9076(2)	1521(1)	11(1)
C(6)	-2068(2)	6747(2)	1482(1)	13(1)
C(7)	-1070(2)	6022(1)	1224(1)	13(1)
C(8)	375(2)	5975(1)	1455(1)	10(1)
C(9)	218(2)	6664(1)	1887(1)	11(1)
C(10)	-1321(2)	7096(2)	1896(1)	11(1)
C(11)	3201(2)	10237(2)	744(1)	11(1)
C(12)	2066(2)	11228(2)	859(1)	14(1)
C(13)	653(2)	11209(2)	544(1)	21(1)
C(14)	4928(2)	10620(2)	761(1)	13(1)
C(15)	5200(2)	11540(2)	384(1)	19(1)
C(16)	5981(2)	9584(2)	665(1)	17(1)
C(17)	5359(2)	11140(1)	1234(1)	17(1)
C(18)	-1567(2)	5334(2)	800(1)	15(1)
C(19)	-3108(2)	5731(2)	611(1)	20(1)
C(20)	-1635(2)	4041(2)	932(1)	24(1)
C(21)	-2112(2)	7701(2)	2297(1)	12(1)
C(22)	-2239(2)	6826(2)	2700(1)	17(1)
C(23)	-3704(2)	8145(2)	2161(1)	16(1)
C(24)	2337(2)	5186(2)	584(1)	16(1)
C(25)	3425(2)	4513(2)	1538(1)	20(1)
C(26)	1462(2)	8509(2)	2615(1)	17(1)
C(27)	3119(2)	6224(2)	2536(1)	16(1)

Table F.3 Selected bond lengths (Å) and angles (°) for (*S*)-**2** (CCDC 635262).

Zr(1)-Cl(2)	2.4356(4)	Cl(2)-Zr(1)-Cl(1)	104.467(15)
Zr(1)-Cl(1)	2.4374(4)		
Zr(1)-Cent(1)	2.222	Cent(1)-Zr(1)-Cent(2)	122.1
Zr(1)-Cent(2)	2.241	Cent(1)-Zr(1)-Cl(1)	107.5
		Cent(2)-Zr(1)-Cl(2)	107.7

Cent(1) is the centroid of C(1), C(2), C(3), C(4), and C(5)
Cent(2) is the centroid of C(6), C(7), C(8), C(9), C(10)

Table F.4 Bond lengths (Å) and angles (°) for (*S*)-**2** (CCDC 635262).

Cent(1)-Zr(1)	2.222	C(4)-Zr(1)-Cl(2)	103.22(4)
Cent(2)-Zr(1)	2.241	C(8)-Zr(1)-Cl(1)	103.54(4)
Zr(1)-C(8)	2.4105(15)	C(9)-Zr(1)-Cl(1)	135.86(4)
Zr(1)-C(9)	2.4262(15)	C(4)-Zr(1)-Cl(1)	135.68(4)
Zr(1)-C(4)	2.4301(14)	Cent(1)-Zr(1)-Cent(2)	122.1
Zr(1)-Cl(2)	2.4356(4)	Cent(1)-Zr(1)-Cl(1)	107.5
Zr(1)-Cl(1)	2.4374(4)	Cent(2)-Zr(1)-Cl(2)	107.7
Zr(1)-C(3)	2.4415(14)	Cl(2)-Zr(1)-Cl(1)	104.467(15)
Zr(1)-C(5)	2.5536(16)	C(8)-Zr(1)-C(3)	68.28(5)
Zr(1)-C(2)	2.5676(15)	C(9)-Zr(1)-C(3)	78.61(5)
Zr(1)-C(7)	2.6051(16)	C(4)-Zr(1)-C(3)	34.84(5)
Zr(1)-C(10)	2.6285(15)	Cl(2)-Zr(1)-C(3)	135.18(4)
Zr(1)-C(1)	2.6629(16)	Cl(1)-Zr(1)-C(3)	104.45(4)
Zr(1)-C(6)	2.6757(16)	C(8)-Zr(1)-C(5)	112.69(5)
Si(1)-C(24)	1.8603(17)	C(9)-Zr(1)-C(5)	96.20(5)
Si(1)-C(25)	1.8702(18)	C(4)-Zr(1)-C(5)	33.02(6)
Si(1)-C(3)	1.8774(16)	Cl(2)-Zr(1)-C(5)	80.54(4)
Si(1)-C(8)	1.8875(17)	Cl(1)-Zr(1)-C(5)	122.09(4)
Si(2)-C(27)	1.8603(18)	C(3)-Zr(1)-C(5)	55.10(5)
Si(2)-C(26)	1.8673(18)	C(8)-Zr(1)-C(2)	96.03(6)
Si(2)-C(4)	1.8762(16)	C(9)-Zr(1)-C(2)	111.72(5)
Si(2)-C(9)	1.8930(17)	C(4)-Zr(1)-C(2)	55.06(5)
C(1)-C(5)	1.414(2)	Cl(2)-Zr(1)-C(2)	123.14(4)
C(1)-C(2)	1.420(2)	Cl(1)-Zr(1)-C(2)	80.80(3)
C(1)-C(11)	1.519(2)	C(3)-Zr(1)-C(2)	33.11(5)
C(2)-C(3)	1.433(2)	C(5)-Zr(1)-C(2)	52.66(5)
C(3)-C(4)	1.459(2)	C(8)-Zr(1)-C(7)	32.79(5)
C(4)-C(5)	1.421(2)	C(9)-Zr(1)-C(7)	55.21(5)
C(6)-C(7)	1.416(2)	C(4)-Zr(1)-C(7)	112.44(6)
C(6)-C(10)	1.419(2)	Cl(2)-Zr(1)-C(7)	121.19(4)
C(7)-C(8)	1.428(2)	Cl(1)-Zr(1)-C(7)	80.92(4)
C(7)-C(18)	1.517(2)	C(3)-Zr(1)-C(7)	96.65(5)
C(8)-C(9)	1.480(2)	C(5)-Zr(1)-C(7)	145.46(5)
C(9)-C(10)	1.432(2)	C(2)-Zr(1)-C(7)	115.58(6)
C(10)-C(21)	1.515(2)	C(8)-Zr(1)-C(10)	55.07(5)
C(11)-C(12)	1.544(2)	C(9)-Zr(1)-C(10)	32.61(5)
C(11)-C(14)	1.571(2)	C(4)-Zr(1)-C(10)	95.71(5)
C(12)-C(13)	1.531(2)	Cl(2)-Zr(1)-C(10)	79.76(4)
C(14)-C(16)	1.528(2)	Cl(1)-Zr(1)-C(10)	122.77(3)
C(14)-C(17)	1.534(2)	C(3)-Zr(1)-C(10)	111.21(5)
C(14)-C(15)	1.535(2)	C(5)-Zr(1)-C(10)	114.95(5)
C(18)-C(19)	1.521(2)	C(2)-Zr(1)-C(10)	144.33(5)
C(18)-C(20)	1.532(3)	C(7)-Zr(1)-C(10)	52.35(5)
C(21)-C(23)	1.531(2)	C(8)-Zr(1)-C(1)	122.54(6)
C(21)-C(22)	1.539(2)	C(9)-Zr(1)-C(1)	122.24(5)
		C(4)-Zr(1)-C(1)	54.14(5)
C(8)-Zr(1)-C(9)	35.63(5)	Cl(2)-Zr(1)-C(1)	91.84(4)
C(8)-Zr(1)-C(4)	79.68(6)	Cl(1)-Zr(1)-C(1)	91.01(4)
C(9)-Zr(1)-C(4)	68.11(5)	C(3)-Zr(1)-C(1)	54.27(5)
C(8)-Zr(1)-Cl(2)	134.63(4)	C(5)-Zr(1)-C(1)	31.35(5)
C(9)-Zr(1)-Cl(2)	102.63(4)	C(2)-Zr(1)-C(1)	31.44(5)

C(7)-Zr(1)-C(1)	146.97(5)	C(1)-C(5)-C(4)	110.36(15)
C(10)-Zr(1)-C(1)	146.21(5)	C(1)-C(5)-Zr(1)	78.59(10)
C(8)-Zr(1)-C(6)	53.71(5)	C(4)-C(5)-Zr(1)	68.71(8)
C(9)-Zr(1)-C(6)	53.65(5)	C(7)-C(6)-C(10)	109.05(14)
C(4)-Zr(1)-C(6)	121.76(5)	C(7)-C(6)-Zr(1)	71.71(9)
Cl(2)-Zr(1)-C(6)	90.36(4)	C(10)-C(6)-Zr(1)	72.65(9)
Cl(1)-Zr(1)-C(6)	91.97(4)	C(6)-C(7)-C(8)	108.61(14)
C(3)-Zr(1)-C(6)	121.93(5)	C(6)-C(7)-C(18)	123.55(14)
C(5)-Zr(1)-C(6)	145.92(5)	C(8)-C(7)-C(18)	127.58(15)
C(2)-Zr(1)-C(6)	146.50(6)	C(6)-C(7)-Zr(1)	77.22(9)
C(7)-Zr(1)-C(6)	31.07(5)	C(8)-C(7)-Zr(1)	66.09(8)
C(10)-Zr(1)-C(6)	31.02(5)	C(18)-C(7)-Zr(1)	127.32(11)
C(1)-Zr(1)-C(6)	175.74(5)	C(7)-C(8)-C(9)	106.95(14)
C(24)-Si(1)-C(25)	107.60(9)	C(7)-C(8)-Si(1)	128.51(11)
C(24)-Si(1)-C(3)	108.97(8)	C(9)-C(8)-Si(1)	121.15(12)
C(25)-Si(1)-C(3)	117.50(8)	C(7)-C(8)-Zr(1)	81.12(9)
C(24)-Si(1)-C(8)	115.62(7)	C(9)-C(8)-Zr(1)	72.76(9)
C(25)-Si(1)-C(8)	114.16(8)	Si(1)-C(8)-Zr(1)	95.63(6)
C(3)-Si(1)-C(8)	92.65(7)	C(10)-C(9)-C(8)	106.75(13)
C(24)-Si(1)-Zr(1)	105.40(6)	C(10)-C(9)-Si(2)	126.49(12)
C(25)-Si(1)-Zr(1)	147.00(6)	C(8)-C(9)-Si(2)	122.93(12)
C(3)-Si(1)-Zr(1)	49.40(4)	C(10)-C(9)-Zr(1)	81.49(9)
C(8)-Si(1)-Zr(1)	48.48(5)	C(8)-C(9)-Zr(1)	71.60(8)
C(27)-Si(2)-C(26)	107.37(8)	Si(2)-C(9)-Zr(1)	95.42(7)
C(27)-Si(2)-C(4)	116.02(8)	C(6)-C(10)-C(9)	108.45(14)
C(26)-Si(2)-C(4)	109.16(8)	C(6)-C(10)-C(21)	124.29(13)
C(27)-Si(2)-C(9)	116.31(8)	C(9)-C(10)-C(21)	126.90(13)
C(26)-Si(2)-C(9)	115.14(8)	C(6)-C(10)-Zr(1)	76.33(9)
C(4)-Si(2)-C(9)	92.35(7)	C(9)-C(10)-Zr(1)	65.91(8)
C(27)-Si(2)-Zr(1)	147.28(6)	C(21)-C(10)-Zr(1)	128.92(11)
C(26)-Si(2)-Zr(1)	105.26(6)	C(1)-C(11)-C(12)	113.31(13)
C(4)-Si(2)-Zr(1)	48.77(4)	C(1)-C(11)-C(14)	110.41(13)
C(9)-Si(2)-Zr(1)	48.70(5)	C(12)-C(11)-C(14)	113.72(14)
C(5)-C(1)-C(2)	106.57(15)	C(13)-C(12)-C(11)	112.31(14)
C(5)-C(1)-C(11)	127.81(16)	C(16)-C(14)-C(17)	108.46(13)
C(2)-C(1)-C(11)	125.15(14)	C(16)-C(14)-C(15)	108.26(14)
C(5)-C(1)-Zr(1)	70.05(9)	C(17)-C(14)-C(15)	108.93(14)
C(2)-C(1)-Zr(1)	70.57(9)	C(16)-C(14)-C(11)	110.67(15)
C(11)-C(1)-Zr(1)	130.28(11)	C(17)-C(14)-C(11)	111.85(13)
C(1)-C(2)-C(3)	109.96(13)	C(15)-C(14)-C(11)	108.59(13)
C(1)-C(2)-Zr(1)	77.99(9)	C(7)-C(18)-C(19)	112.72(15)
C(3)-C(2)-Zr(1)	68.61(8)	C(7)-C(18)-C(20)	108.41(15)
C(2)-C(3)-C(4)	106.28(14)	C(19)-C(18)-C(20)	110.16(15)
C(2)-C(3)-Si(1)	125.09(12)	C(10)-C(21)-C(23)	111.75(13)
C(4)-C(3)-Si(1)	123.41(12)	C(10)-C(21)-C(22)	108.05(14)
C(2)-C(3)-Zr(1)	78.28(9)	C(23)-C(21)-C(22)	110.17(1
C(4)-C(3)-Zr(1)	72.15(8)		
Si(1)-C(3)-Zr(1)	94.88(6)		
C(5)-C(4)-C(3)	106.83(13)		
C(5)-C(4)-Si(2)	126.78(12)		
C(3)-C(4)-Si(2)	121.96(12)		
C(5)-C(4)-Zr(1)	78.27(9)		
C(3)-C(4)-Zr(1)	73.01(8)		
Si(2)-C(4)-Zr(1)	95.74(6)		

Table F.5 Anisotropic displacement parameters ($Å^2 x\ 10^4$) for (*S*)-**2** (CCDC 635262). The anisotropic displacement factor exponent takes the form: $-2\pi^2[\ h^2 a^{*2} U^{11} + ... + 2\ h\ k\ a^*\ b^*\ U^{12}]$.

	U^{11}	U^{22}	U^{33}	U^{23}	U^{13}	U^{12}
Zr(1)	88(1)	102(1)	75(1)	0(1)	-3(1)	7(1)
Cl(1)	171(2)	199(2)	97(1)	5(1)	-23(1)	10(2)
Cl(2)	134(2)	129(2)	148(2)	-8(1)	25(1)	24(1)
Si(1)	109(2)	108(2)	116(2)	1(2)	4(2)	9(1)
Si(2)	102(2)	127(2)	83(2)	12(2)	-11(1)	-9(2)
C(1)	93(6)	108(8)	110(6)	0(5)	1(5)	-3(5)
C(2)	82(6)	140(8)	121(6)	4(6)	12(5)	8(6)
C(3)	74(5)	127(8)	122(6)	-5(6)	1(5)	1(5)
C(4)	72(6)	137(8)	102(6)	-1(6)	-19(4)	-11(6)
C(5)	91(6)	132(8)	103(6)	-6(6)	-12(5)	-4(5)
C(6)	108(6)	156(9)	119(6)	-7(6)	-4(5)	-8(5)
C(7)	138(6)	111(8)	135(6)	15(7)	1(6)	-25(5)
C(8)	143(6)	86(7)	72(5)	8(5)	7(6)	-7(6)
C(9)	132(7)	97(8)	99(6)	11(5)	-1(5)	-14(5)
C(10)	112(6)	109(8)	98(6)	7(6)	2(5)	-11(6)
C(11)	142(7)	106(8)	85(6)	16(5)	3(5)	4(6)
C(12)	173(8)	126(9)	133(7)	12(6)	10(6)	21(6)
C(13)	208(9)	192(10)	218(8)	14(7)	-41(6)	86(7)
C(14)	147(7)	130(8)	99(6)	22(5)	8(5)	-6(5)
C(15)	231(9)	187(9)	165(7)	47(6)	39(7)	-25(7)
C(16)	141(7)	191(10)	178(8)	14(6)	21(6)	7(6)
C(17)	171(7)	162(8)	181(6)	-2(7)	-16(8)	-37(7)
C(18)	135(7)	170(9)	134(7)	-59(6)	1(5)	-27(6)
C(19)	143(8)	294(11)	162(8)	-74(7)	-41(6)	-14(7)
C(20)	276(10)	163(10)	274(10)	-68(8)	-42(8)	-58(8)
C(21)	112(6)	140(8)	105(6)	-12(5)	18(5)	2(5)
C(22)	204(8)	178(10)	140(7)	26(6)	42(6)	28(7)
C(23)	125(7)	184(9)	166(7)	-16(7)	19(5)	14(6)
C(24)	154(7)	186(10)	147(7)	-49(6)	10(6)	-3(7)
C(25)	241(9)	160(10)	190(8)	17(7)	-2(7)	60(7)
C(26)	155(8)	205(10)	154(7)	-32(6)	-12(6)	-23(7)
C(27)	159(8)	202(10)	131(7)	44(6)	-38(6)	-12(7)

APPENDIX G

RESULTS FROM THE UNIDIRECTIONAL SITE EPIMERIZATION MODEL

This appendix contains a summary of the unidirectional site epimerization model used to model polypropylene pentad data discussed in Chapter Two. For a complete derivation of the model and a more extensive discussion see S. A. Miller's Ph D thesis (California Institute of Technology, **2000**). The model considers three parameters that can affect the polymer pentads: enantiofacial selectivity of olefin insertion from the two sites of the catalyst (α and β) and the probability of site epimerization during polymerization (ε). The statistical model calculates the probability of every outcome for a given pentad at an α, β, and, ε. Theoretical fits to the experimental data were obtained iteratively by minimizing the root mean square (RMS) difference between the experimental and theoretical pentads using Excel.

Below is a bar chart for each polypropylene sample analyzed in Chapter 2 that shows the theoretical and experimental pentads along with the RMS value for: (a) a model where all three parameters are varied and (b) a model where only ε is varied using α and β obtained from neat polypropylene data.

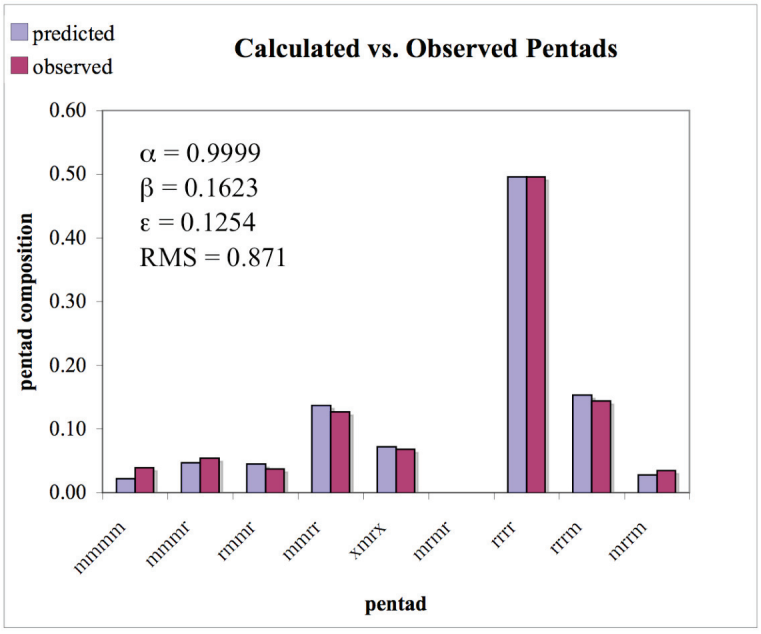

Figure G.1 Unimolecular site epimerization model fits for polypropylene (neat C_3H_6) with catalyst (*S*)-**1** varying all three parameters.

(a) 3-parameter, 8.1 M C_3H_6.

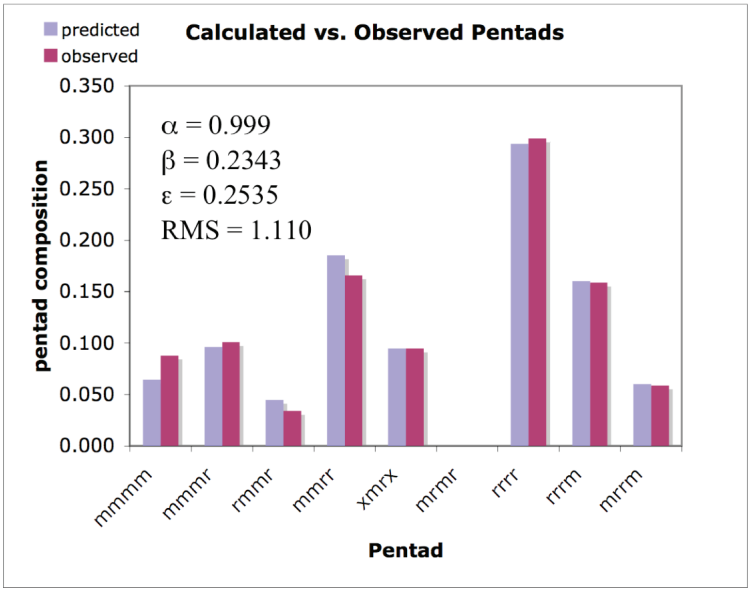

(b) 1-paramater, 8.1 C_3H_6.

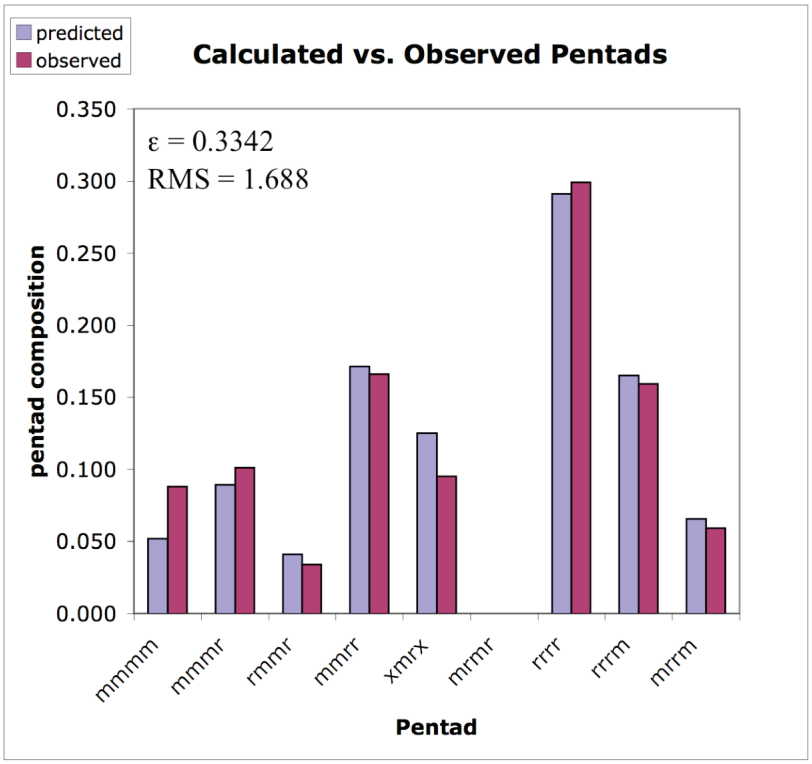

Figure G.2 Unimolecular site epimerization model fits for polypropylene (8.1 M) with catalyst (*S*)-**1** varying (a) all three parameters and (b) only ε.

(a) 3-parameter, 4.6 M C_3H_6.

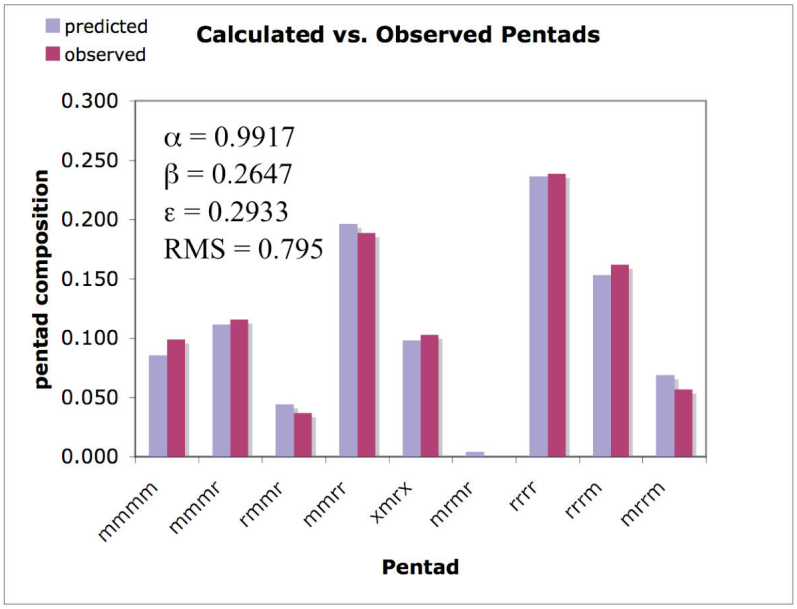

(b) 1-parameter, 4.6 C_3H_6.

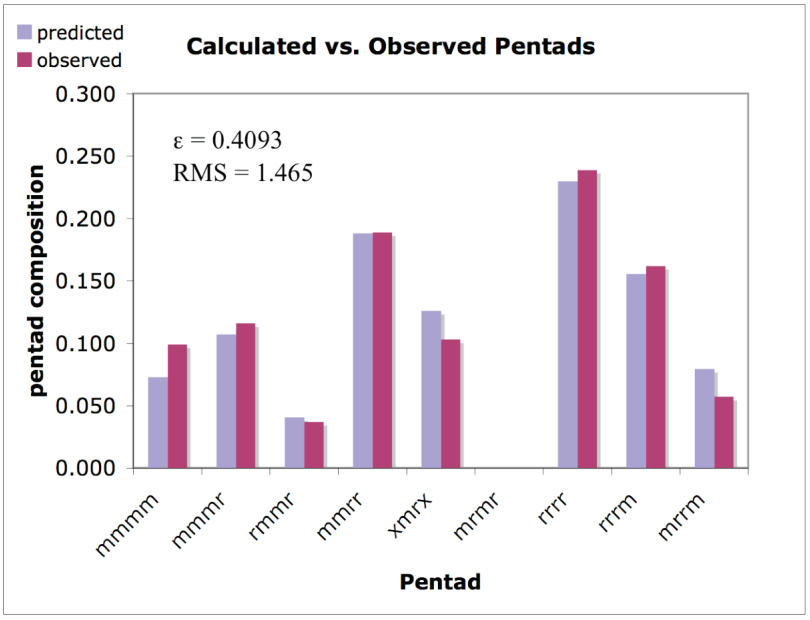

Figure G.3 Unimolecular site epimerization model fits for polypropylene (4.6 M) with catalyst (*S*)-**1** varying (a) all three parameters and (b) only ε.

(a) 3-parameter, 3.4 M C_3H_6.

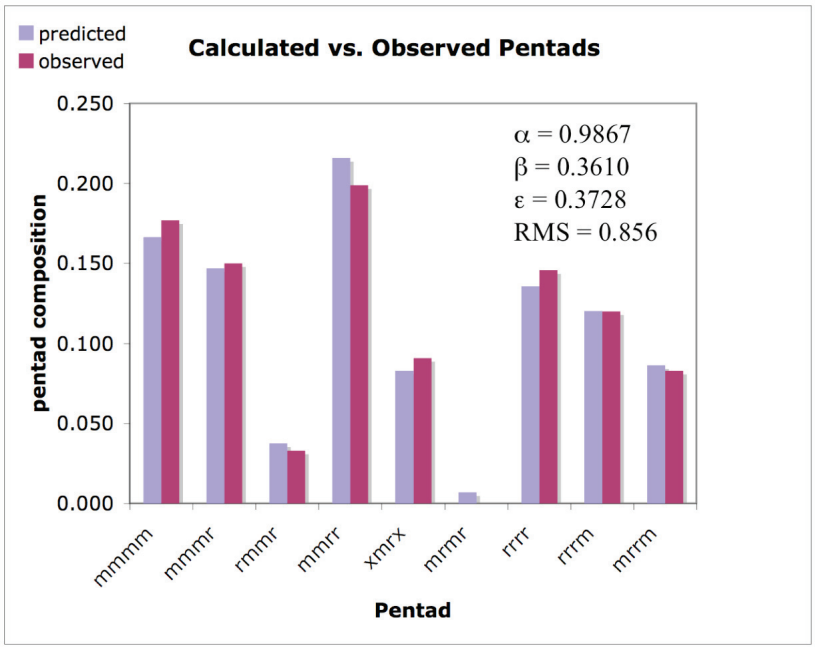

(b) 1-parameter, 3.4 M C_3H_6.

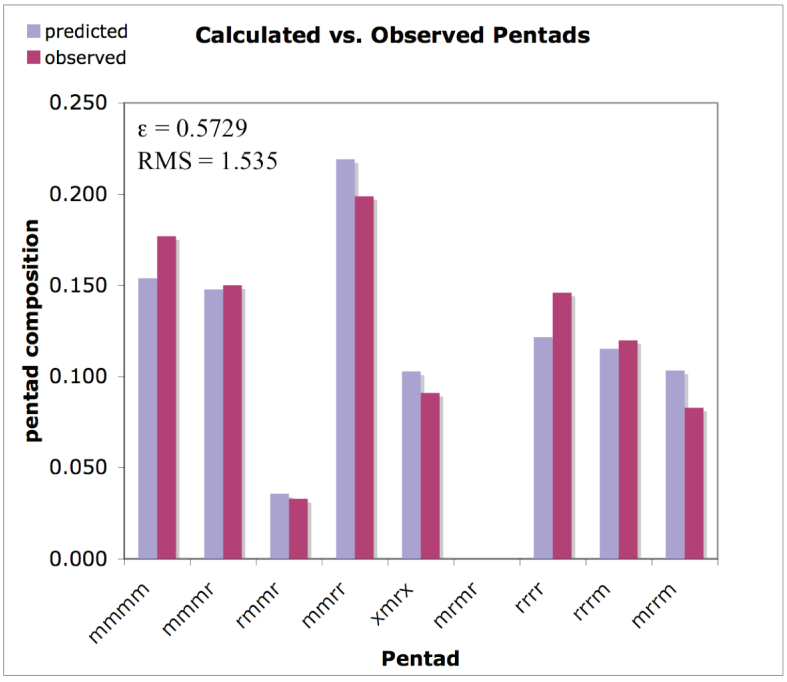

Figure G.4 Unimolecular site epimerization model fits for polypropylene (3.4 M) with catalyst (*S*)-**1** varying (a) all three parameters and (b) only ε.

(a) 3-parameter, 0.8 M C_3H_6.

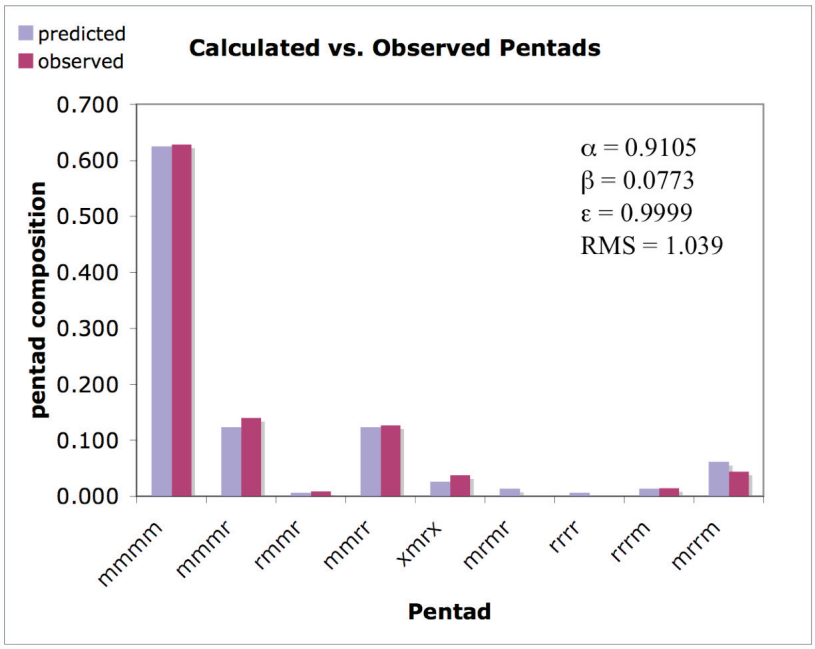

(b) 1-parameter, 0.8 M C_3H_6.

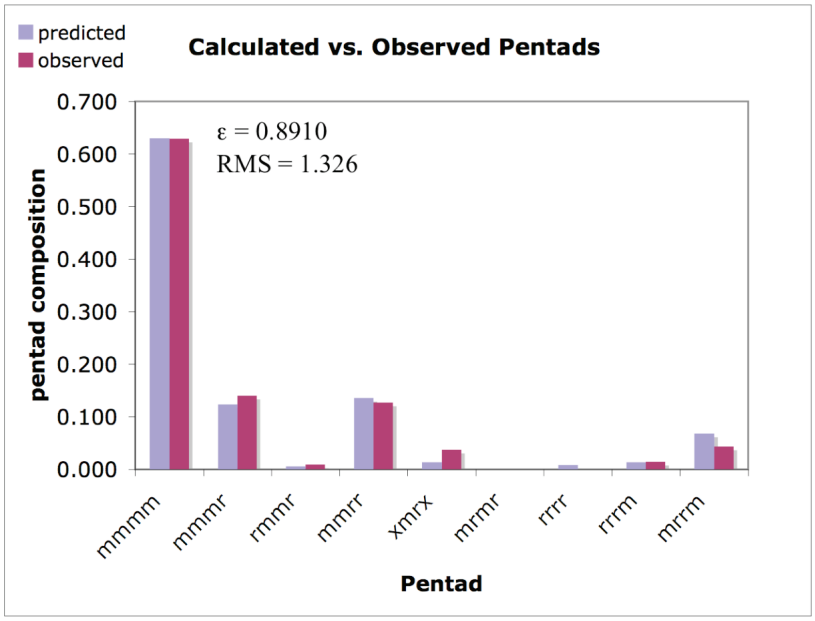

Figure G.5 Unimolecular site epimerization model fits for polypropylene (0.8 M) with catalyst (*S*)-**1** varying (a) all three parameters and (b) only ε.

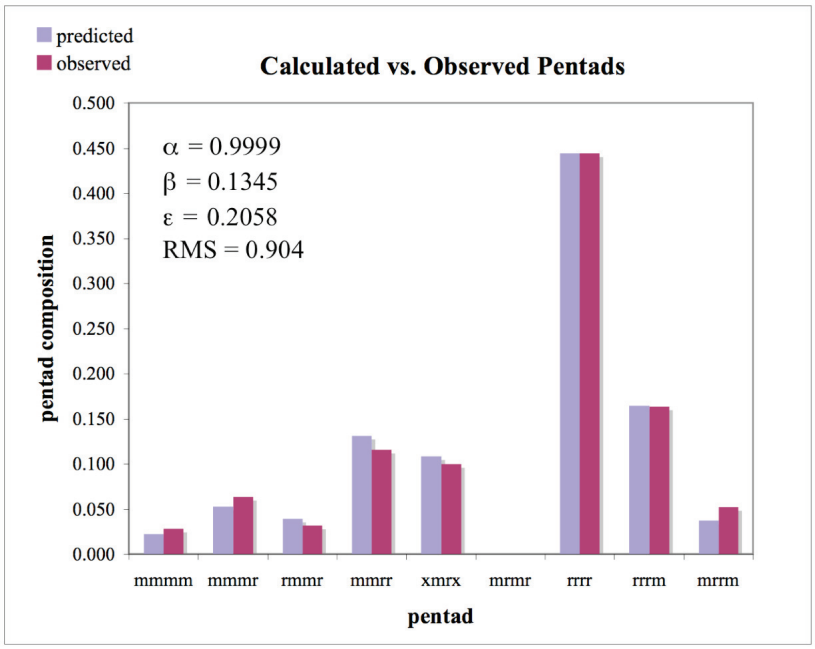

Figure G.6 Unimolecular site epimerization model fits for polypropylene (neat C_3H_6) with catalyst (*S*)-**2** varying all three parameters.

(a) 3-paramater, 8.1 M C_3H_6

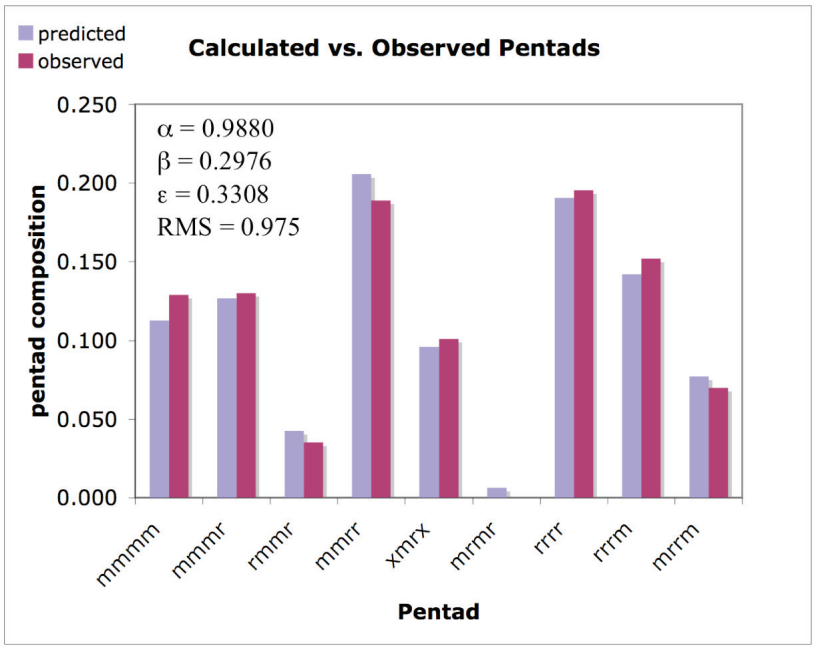

(b) 1-parameter, 8.1 M C_3H_6

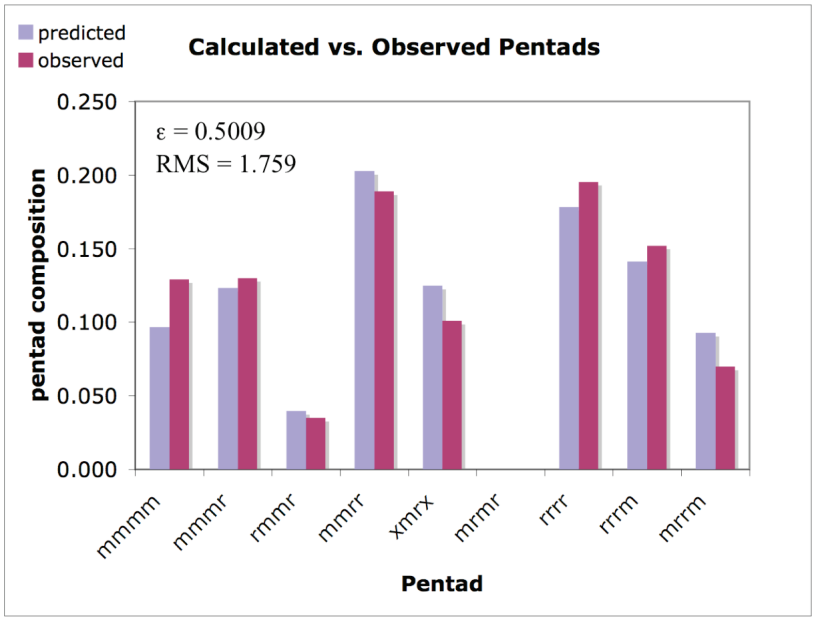

Figure G.7 Unimolecular site epimerization model fits for polypropylene (8.1 M) with catalyst (*S*)-**2** varying (a) all three parameters and (b) only ε.

a) 3-parameter, 4.6 M C_3H_6

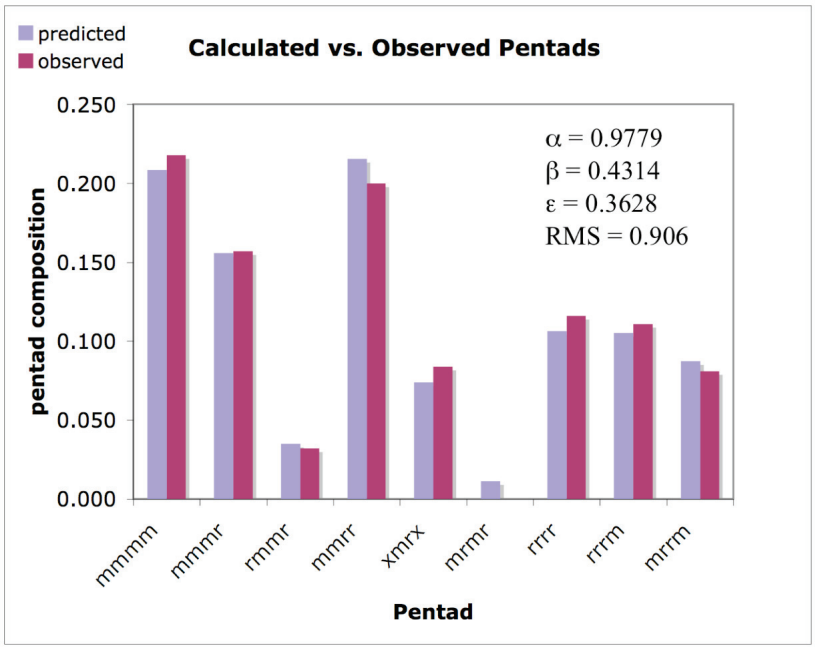

b) 1-parameter, 4.6 M C_3H_6

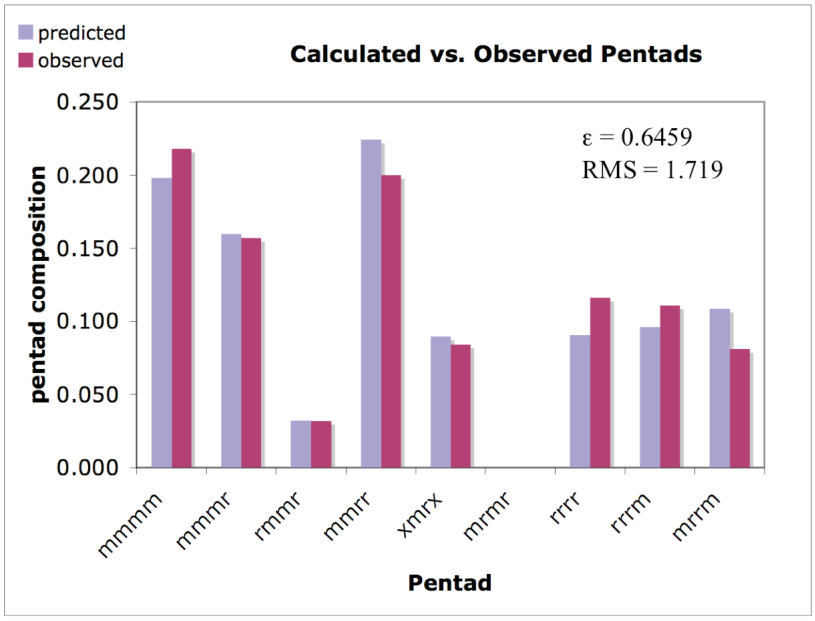

Figure G.8 Unimolecular site epimerization model fits for polypropylene (4.6 M) with catalyst (*S*)-**2** varying (a) all three parameters and (b) only ε.

a) 3-parameter, 3.4 M C_3H_6

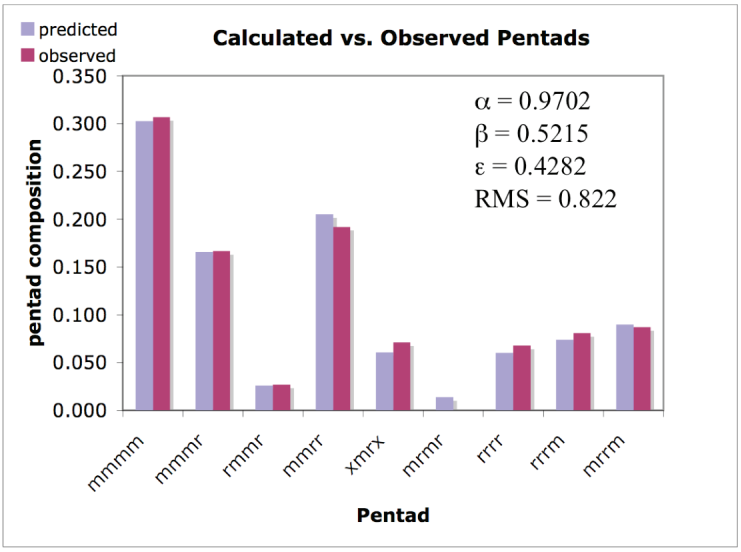

b) 1-paramter, 3.4 M C_3H_6

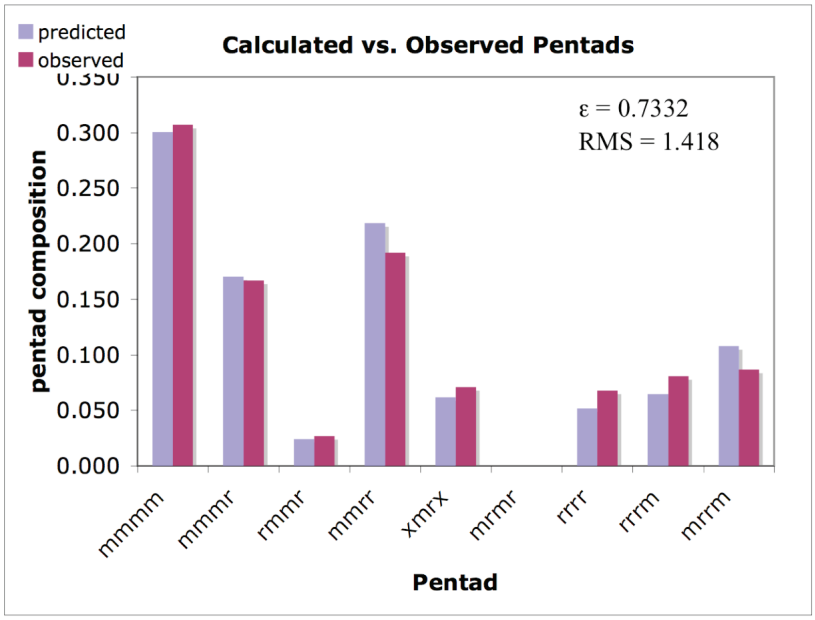

Figure G.9 Unimolecular site epimerization model fits for polypropylene (3.4 M) with catalyst (*S*)-**2** varying (a) all three parameters and (b) only ε.

a) 3-paramter, 0.8 M C_3H_6

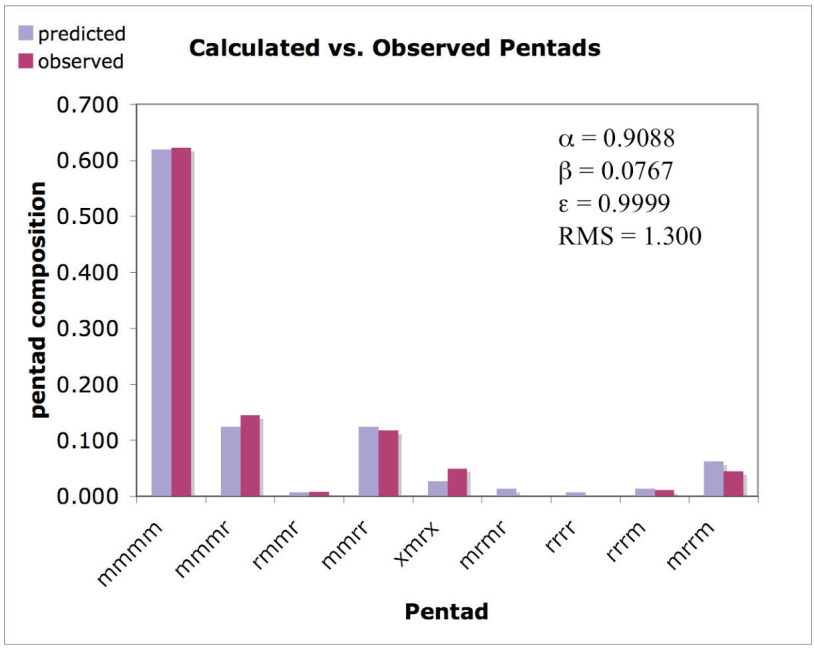

b) 1-parameter, 0.8 M

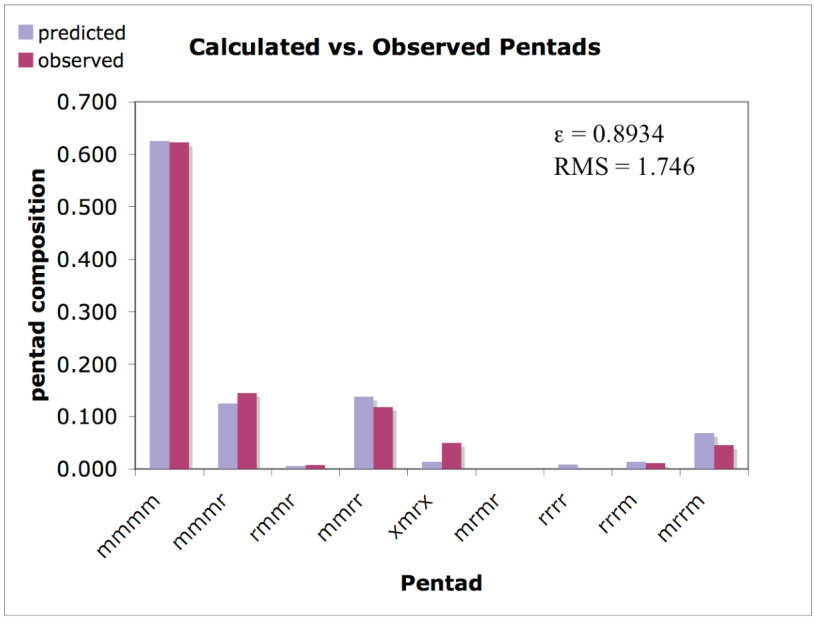

Figure G.10 Unimolecular site epimerization model fits for polypropylene (0.8 M) with catalyst (*S*)-**2** varying (a) all three parameters and (b) only ε.

APPENDIX H

X-RAY CRYSTALLOGRAPHIC DATA FOR (*rac*)-(EBI)Zr(NMe_2)Cl

Contents

Note: Crystallographic data have been deposited at the CCDC, 12 Union Road, Cambridge CB2 1EZ, UK and copies can be obtained on request, free of charge, by quoting the publication citation and the deposition number 602362.

Table H.1 Crystal data and structure refinement for (*rac*)-(EBI)Zr(NMe_2)Cl (CCDC 602362).

Empirical formula	$C_{22}H_{22}NClZr$
Formula weight	427.08
Crystallization Solvent	Diethylether/toluene
Crystal Habit	Needle
Crystal size	0.04 x 0.31 x 0.11 mm^3
Crystal color	Red

Data Collection

Type of diffractometer	Bruker SMART 1000
Wavelength	0.71073 Å MoKα
Data Collection Temperature	100(2) K
θ range for 9675 reflections used in lattice determination	2.28º to 32.00°
Unit cell dimensions	a = 7.5960(5) Å b = 9.5569(7) Å β = 98.315(2)° c = 25.6267(19) Å
Volume	1840.8(2) $Å^3$
Z	4
Crystal system	Monoclinic
Space group	$P2_1/n$
Density (calculated)	1.541 Mg/m^3
F(000)	872
Data collection program	Bruker SMART v5.630
θ range for data collection	1.61º to 32.72°
Completeness to θ = 32.72°	84.2%
Index ranges	$-11 \le h \le 11$, $-12 \le k \le 12$, $-37 \le l \le 34$
Data collection scan type	ω scans at 5 ϕ settings
Data reduction program	Bruker SAINT v6.45A
Reflections collected	27995
Independent reflections	5735 [R_{int}= 0.0752]
Absorption coefficient	0.746 mm^{-1}
Absorption correction	None
Max. and min. transmission	0.9224 and 0.7545

Table H.1 (continued)

Structure solution and refinement

Structure solution program	Bruker XS v6.12
Primary solution method	Direct methods
Secondary solution method	Difference Fourier map
Hydrogen placement	Difference Fourier map
Structure refinement program	Bruker XL v6.12
Refinement method	Full matrix least-squares on F^2
Data/restraints/parameters	5735/0/314
Treatment of hydrogen atoms	Unrestrained
Goodness-of-fit on F^2	1.101
Final R indices [$I>2\sigma(I)$, 3824 reflections]	R1 = 0.0361, *w*R2 = 0.0511
R indices (all data)	R1 = 0.0701, *w*R2 = 0.0545
Type of weighting scheme used	Sigma
Weighting scheme used	$w=1/\sigma^2(Fo^2)$
Max shift/error	0.000
Average shift/error	0.000
Largest diff. peak and hole	0.573 and -0.840 e.Å^{-3}

Special Refinement Details

Refinement of F^2 against ALL reflections. The weighted R-factor (*w*R) and goodness of fit (S) are based on F^2, conventional R-factors (R) are based on F, with F set to zero for negative F^2. The threshold expression of $F^2 > 2\sigma(F^2)$ is used only for calculating R-factors (gt) etc. and is not relevant to the choice of reflections for refinement. R-factors based on F^2 are statistically about twice as large as those based on F, and R-factors based on ALL data will be even larger.

All esds (except the esd in the dihedral angle between two l.s. planes) are estimated using the full covariance matrix. The cell esds are taken into account individually in the estimation of esds in distances, angles and torsion angles; correlations between esds in cell parameters are only used when they are defined by crystal symmetry. An approximate (isotropic) treatment of cell esds is used for estimating esds involving l.s. planes.

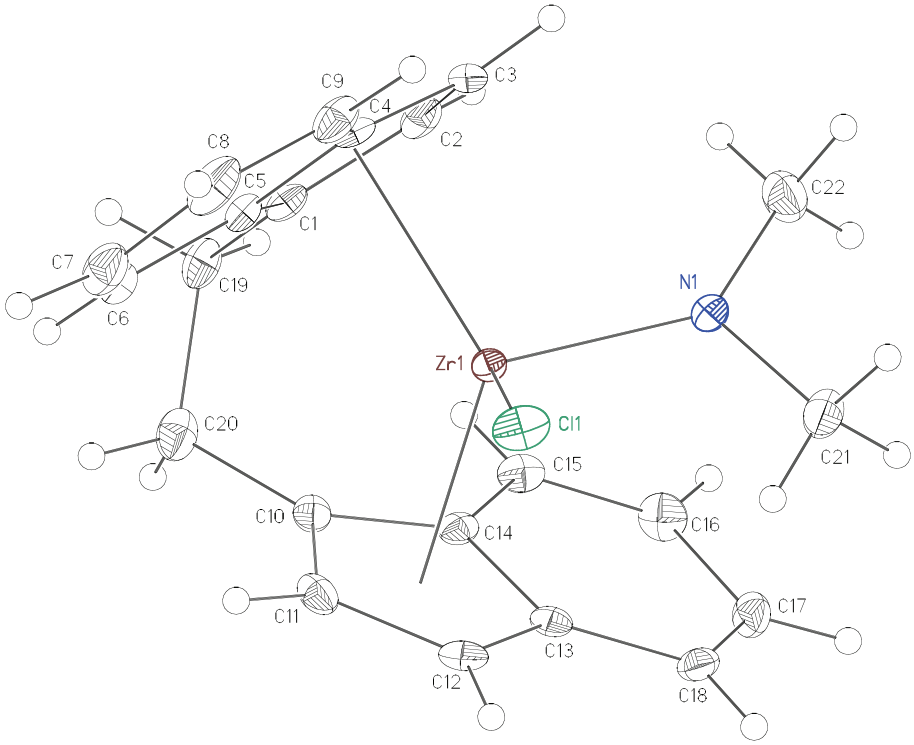

Figure H.1 Minimum overlap view of (*rac*)-(EBI)Zr(NMe_2)Cl.

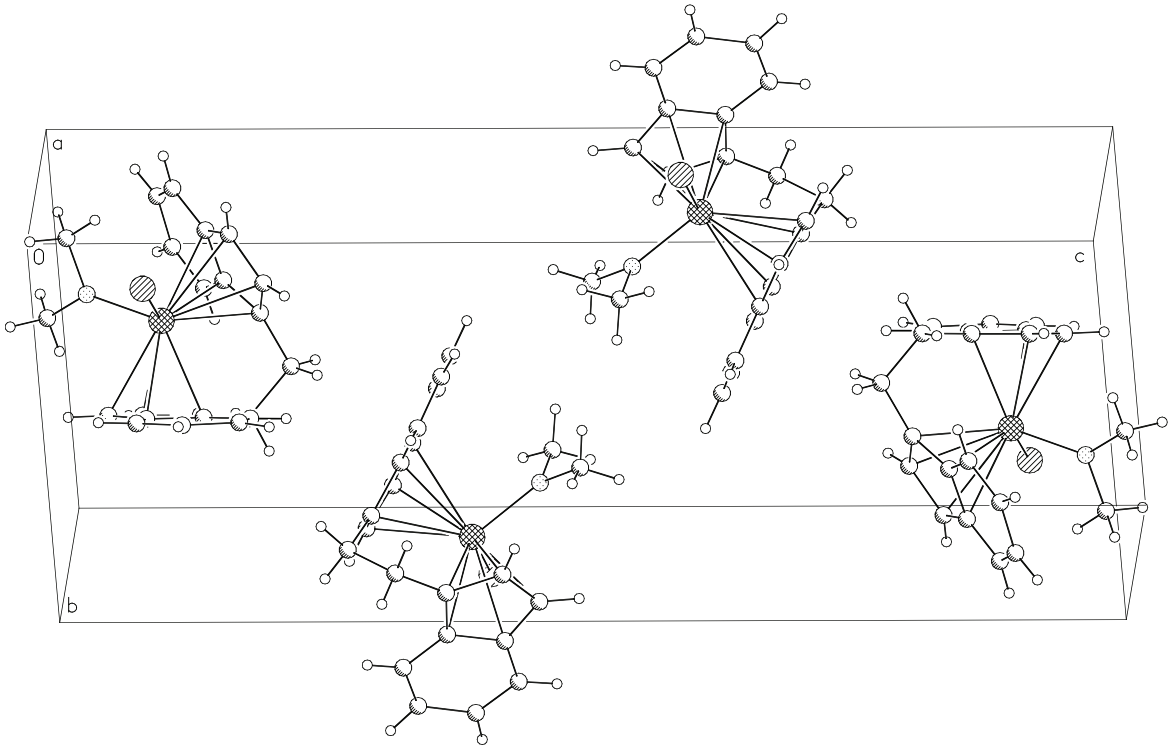

Figure H. 2 Unit cell contents for (*rac*)-(EBI)Zr(NMe_2)Cl

Table H.2 Atomic coordinates (10^4) and equivalent isotropic displacement parameters ($Å^2 x\ 10^3$) for (*rac*)-(EBI)Zr(NMe_2)Cl (CCDC 602362). U(eq) is defined as the trace of the orthogonalized U^{ij} tensor.

	x	y	z	U_{eq}
Zr(1)	3702(1)	3159(1)	1099(1)	9(1)
Cl(1)	6733(1)	3228(1)	864(1)	18(1)
N(1)	2510(2)	2092(2)	452(1)	12(1)
C(1)	2007(2)	5145(2)	1436(1)	12(1)
C(2)	1215(3)	4904(2)	913(1)	14(1)
C(3)	2405(3)	5265(2)	559(1)	13(1)
C(4)	3962(3)	5826(2)	869(1)	12(1)
C(5)	3732(3)	5724(2)	1414(1)	12(1)
C(6)	5128(3)	6175(2)	1812(1)	16(1)
C(7)	6632(3)	6731(2)	1664(1)	20(1)
C(8)	6824(3)	6860(2)	1121(1)	22(1)
C(9)	5548(3)	6422(2)	730(1)	17(1)
C(10)	3101(3)	2773(2)	2044(1)	12(1)
C(11)	4946(3)	2549(2)	2049(1)	14(1)
C(12)	5222(3)	1333(2)	1759(1)	14(1)
C(13)	3536(3)	717(2)	1589(1)	11(1)
C(14)	2209(2)	1641(2)	1751(1)	11(1)
C(15)	368(3)	1292(2)	1615(1)	14(1)
C(16)	-75(3)	66(2)	1363(1)	17(1)
C(17)	1249(3)	-874(2)	1225(1)	16(1)
C(18)	3010(3)	-552(2)	1329(1)	14(1)
C(19)	1128(3)	4894(2)	1921(1)	16(1)
C(20)	2249(3)	3928(2)	2316(1)	18(1)
C(21)	3528(3)	918(2)	280(1)	18(1)
C(22)	815(3)	2208(3)	109(1)	21(1)

Table H.3 Selected bond lengths (Å) and angles (°) for (*rac*)-(EBI)Zr(NMe_2)Cl (CCDC 602362).

Zr(1)-N(1)	2.0435(16)	N(1)-Zr(1)-Cl(1)	97.78(5)
Zr(1)-Cl(1)	2.4623(5)	Cent(1)-Zr(1)-Cent(2)	123.9
Zr(1)-Cent(1)	2.255	Cent(1)-Zr(1)-N(1)	107.6
Zr(1)-Cent(2)	2.289	Cent(1)-Zr(1)-Cl(1)	106.8
		Cent(2)-Zr(1)-N(1)	110.3
		Cent(2)-Zr(1)-Cl(1)	107.3

Cent(1) is the centroid of C(1), C(2), C(3), C(4), and C(5)
Cent(2) is the centroid of C(10), C(11), C(12), C(13), and C(14)

Table H.4 Bond lengths (Å) and angles (°) for (*ra c*)-(EBI)Zr(NMe_2)Cl (CCDC 602362).

Zr(1)-N(1)	2.0435(16)	C(18)-H(18)	0.89(2)
Zr(1)-Cl(1)	2.4623(5)	C(19)-C(20)	1.533(3)
Zr(1)-C(2)	2.5132(19)	C(19)-H(19A)	0.916(18)
Zr(1)-C(1)	2.5158(19)	C(19)-H(19B)	0.946(19)
Zr(1)-C(11)	2.548(2)	C(20)-H(20A)	0.986(19)
Zr(1)-C(10)	2.5573(19)	C(20)-H(20B)	0.93(2)
Zr(1)-C(3)	2.557(2)	C(21)-H(21A)	0.97(2)
Zr(1)-C(5)	2.5793(19)	C(21)-H(21B)	0.97(2)
Zr(1)-C(12)	2.585(2)	C(21)-H(21C)	1.00(2)
Zr(1)-C(14)	2.5954(18)	C(22)-H(22A)	0.98(3)
Zr(1)-C(4)	2.6298(19)	C(22)-H(22B)	0.88(3)
Zr(1)-C(13)	2.6618(19)	C(22)-H(22C)	0.91(3)
N(1)-C(22)	1.454(3)		
N(1)-C(21)	1.465(3)	N(1)-Zr(1)-Cl(1)	97.78(5)
C(1)-C(2)	1.406(3)	N(1)-Zr(1)-C(2)	86.86(7)
C(1)-C(5)	1.432(3)	Cl(1)-Zr(1)-C(2)	129.80(5)
C(1)-C(19)	1.513(3)	N(1)-Zr(1)-C(1)	117.82(6)
C(2)-C(3)	1.414(3)	Cl(1)-Zr(1)-C(1)	127.38(5)
C(2)-H(2)	0.912(19)	C(2)-Zr(1)-C(1)	32.46(6)
C(3)-C(4)	1.430(3)	N(1)-Zr(1)-C(11)	136.09(7)
C(3)-H(3)	0.94(2)	Cl(1)-Zr(1)-C(11)	90.49(5)
C(4)-C(9)	1.424(3)	C(2)-Zr(1)-C(11)	119.81(7)
C(4)-C(5)	1.435(3)	C(1)-Zr(1)-C(11)	88.96(7)
C(5)-C(6)	1.428(3)	N(1)-Zr(1)-C(10)	125.31(6)
C(6)-C(7)	1.363(3)	Cl(1)-Zr(1)-C(10)	122.45(5)
C(6)-H(6)	0.89(2)	C(2)-Zr(1)-C(10)	92.41(6)
C(7)-C(8)	1.425(3)	C(1)-Zr(1)-C(10)	67.19(6)
C(7)-H(7)	0.94(2)	C(11)-Zr(1)-C(10)	32.22(6)
C(8)-C(9)	1.356(3)	N(1)-Zr(1)-C(3)	82.13(7)
C(8)-H(8)	0.95(2)	Cl(1)-Zr(1)-C(3)	98.50(5)
C(9)-H(9)	0.94(2)	C(2)-Zr(1)-C(3)	32.38(6)
C(10)-C(11)	1.417(3)	C(1)-Zr(1)-C(3)	54.28(7)
C(10)-C(14)	1.431(3)	C(11)-Zr(1)-C(3)	139.25(7)
C(10)-C(20)	1.500(3)	C(10)-Zr(1)-C(3)	121.24(6)
C(11)-C(12)	1.410(3)	N(1)-Zr(1)-C(5)	135.33(6)
C(11)-H(11)	0.93(2)	Cl(1)-Zr(1)-C(5)	94.87(5)
C(12)-C(13)	1.420(3)	C(2)-Zr(1)-C(5)	53.21(7)
C(12)-H(12)	0.945(19)	C(1)-Zr(1)-C(5)	32.61(6)
C(13)-C(18)	1.414(3)	C(11)-Zr(1)-C(5)	86.17(7)
C(13)-C(14)	1.446(3)	C(10)-Zr(1)-C(5)	80.51(6)
C(14)-C(15)	1.431(3)	C(3)-Zr(1)-C(5)	53.63(7)
C(15)-C(16)	1.356(3)	N(1)-Zr(1)-C(12)	107.32(7)
C(15)-H(15)	0.90(2)	Cl(1)-Zr(1)-C(12)	80.40(5)
C(16)-C(17)	1.431(3)	C(2)-Zr(1)-C(12)	145.49(7)
C(16)-H(16)	0.943(18)	C(1)-Zr(1)-C(12)	119.10(7)
C(17)-C(18)	1.361(3)	C(11)-Zr(1)-C(12)	31.88(7)
C(17)-H(17)	0.93(2)	C(10)-Zr(1)-C(12)	53.55(7)

C(3)-Zr(1)-C(12)	170.55(7)	C(9)-C(4)-C(5)	119.84(19)
C(5)-Zr(1)-C(12)	116.98(7)	C(3)-C(4)-C(5)	107.94(17)
N(1)-Zr(1)-C(14)	93.44(6)	C(9)-C(4)-Zr(1)	122.49(13)
Cl(1)-Zr(1)-C(14)	133.09(4)	C(3)-C(4)-Zr(1)	71.23(11)
C(2)-Zr(1)-C(14)	96.07(6)	C(5)-C(4)-Zr(1)	72.08(11)
C(1)-Zr(1)-C(14)	84.66(6)	C(6)-C(5)-C(1)	132.63(19)
C(11)-Zr(1)-C(14)	52.62(6)	C(6)-C(5)-C(4)	119.53(18)
C(10)-Zr(1)-C(14)	32.23(6)	C(1)-C(5)-C(4)	107.83(17)
C(3)-Zr(1)-C(14)	128.19(6)	C(6)-C(5)-Zr(1)	118.85(13)
C(5)-Zr(1)-C(14)	108.32(6)	C(1)-C(5)-Zr(1)	71.26(11)
C(12)-Zr(1)-C(14)	52.83(6)	C(4)-C(5)-Zr(1)	75.96(12)
N(1)-Zr(1)-C(4)	109.94(6)	C(7)-C(6)-C(5)	118.9(2)
Cl(1)-Zr(1)-C(4)	79.44(4)	C(7)-C(6)-H(6)	119.9(14)
C(2)-Zr(1)-C(4)	52.65(6)	C(5)-C(6)-H(6)	121.1(14)
C(1)-Zr(1)-C(4)	53.46(6)	C(6)-C(7)-C(8)	121.0(2)
C(11)-Zr(1)-C(4)	113.98(7)	C(6)-C(7)-H(7)	120.0(12)
C(10)-Zr(1)-C(4)	112.42(6)	C(8)-C(7)-H(7)	118.7(12)
C(3)-Zr(1)-C(4)	31.97(6)	C(9)-C(8)-C(7)	122.1(2)
C(5)-Zr(1)-C(4)	31.97(6)	C(9)-C(8)-H(8)	122.4(14)
C(12)-Zr(1)-C(4)	139.51(7)	C(7)-C(8)-H(8)	115.4(14)
C(14)-Zr(1)-C(4)	137.72(6)	C(8)-C(9)-C(4)	118.6(2)
N(1)-Zr(1)-C(13)	84.22(6)	C(8)-C(9)-H(9)	123.2(12)
Cl(1)-Zr(1)-C(13)	104.38(4)	C(4)-C(9)-H(9)	118.1(12)
C(2)-Zr(1)-C(13)	125.80(6)	C(11)-C(10)-C(14)	106.39(17)
C(1)-Zr(1)-C(13)	115.94(6)	C(11)-C(10)-C(20)	126.91(19)
C(11)-Zr(1)-C(13)	52.05(6)	C(14)-C(10)-C(20)	126.63(18)
C(10)-Zr(1)-C(13)	53.07(6)	C(11)-C(10)-Zr(1)	73.54(11)
C(3)-Zr(1)-C(13)	154.71(6)	C(14)-C(10)-Zr(1)	75.35(11)
C(5)-Zr(1)-C(13)	133.18(7)	C(20)-C(10)-Zr(1)	118.79(13)
C(12)-Zr(1)-C(13)	31.36(6)	C(12)-C(11)-C(10)	110.03(18)
C(14)-Zr(1)-C(13)	31.89(6)	C(12)-C(11)-Zr(1)	75.48(12)
C(4)-Zr(1)-C(13)	164.93(6)	C(10)-C(11)-Zr(1)	74.23(11)
C(22)-N(1)-C(21)	109.67(18)	C(12)-C(11)-H(11)	126.6(12)
C(22)-N(1)-Zr(1)	134.54(14)	C(10)-C(11)-H(11)	123.3(12)
C(21)-N(1)-Zr(1)	115.79(13)	Zr(1)-C(11)-H(11)	115.4(12)
C(2)-C(1)-C(5)	107.03(17)	C(11)-C(12)-C(13)	107.92(18)
C(2)-C(1)-C(19)	125.34(18)	C(11)-C(12)-Zr(1)	72.64(12)
C(5)-C(1)-C(19)	127.56(19)	C(13)-C(12)-Zr(1)	77.32(12)
C(2)-C(1)-Zr(1)	73.67(11)	C(11)-C(12)-H(12)	124.2(12)
C(5)-C(1)-Zr(1)	76.14(11)	C(13)-C(12)-H(12)	127.6(12)
C(19)-C(1)-Zr(1)	118.16(13)	Zr(1)-C(12)-H(12)	120.6(12)
C(1)-C(2)-C(3)	110.33(18)	C(18)-C(13)-C(12)	132.97(19)
C(1)-C(2)-Zr(1)	73.87(11)	C(18)-C(13)-C(14)	119.91(18)
C(3)-C(2)-Zr(1)	75.53(11)	C(12)-C(13)-C(14)	107.07(18)
C(1)-C(2)-H(2)	125.6(13)	C(18)-C(13)-Zr(1)	124.02(14)
C(3)-C(2)-H(2)	124.0(13)	C(12)-C(13)-Zr(1)	71.33(11)
Zr(1)-C(2)-H(2)	117.8(13)	C(14)-C(13)-Zr(1)	71.52(10)
C(2)-C(3)-C(4)	106.75(19)	C(15)-C(14)-C(10)	132.55(18)
C(2)-C(3)-Zr(1)	72.09(12)	C(15)-C(14)-C(13)	118.99(18)
C(4)-C(3)-Zr(1)	76.80(11)	C(10)-C(14)-C(13)	108.45(16)
C(2)-C(3)-H(3)	128.3(13)	C(15)-C(14)-Zr(1)	118.42(13)
C(4)-C(3)-H(3)	124.6(13)	C(10)-C(14)-Zr(1)	72.42(10)
Zr(1)-C(3)-H(3)	121.7(13)	C(13)-C(14)-Zr(1)	76.59(10)
C(9)-C(4)-C(3)	132.2(2)	C(16)-C(15)-C(14)	119.0(2)

C(16)-C(15)-H(15)	121.7(13)
C(14)-C(15)-H(15)	119.3(13)
C(15)-C(16)-C(17)	121.7(2)
C(15)-C(16)-H(16)	120.7(11)
C(17)-C(16)-H(16)	117.5(11)
C(18)-C(17)-C(16)	121.1(2)
C(18)-C(17)-H(17)	120.3(13)
C(16)-C(17)-H(17)	118.6(13)
C(17)-C(18)-C(13)	119.2(2)
C(17)-C(18)-H(18)	119.9(14)
C(13)-C(18)-H(18)	120.8(14)
C(1)-C(19)-C(20)	111.62(17)
C(1)-C(19)-H(19A)	108.7(12)
C(20)-C(19)-H(19A)	109.6(12)
C(1)-C(19)-H(19B)	108.8(11)
C(20)-C(19)-H(19B)	110.9(11)
H(19A)-C(19)-H(19B)	107.1(16)
C(10)-C(20)-C(19)	111.87(18)
C(10)-C(20)-H(20A)	110.3(11)
C(19)-C(20)-H(20A)	110.2(11)
C(10)-C(20)-H(20B)	109.5(12)
C(19)-C(20)-H(20B)	110.9(12)
H(20A)-C(20)-H(20B)	103.8(17)
N(1)-C(21)-H(21A)	110.1(11)
N(1)-C(21)-H(21B)	115.3(11)
H(21A)-C(21)-H(21B)	102.3(16)
N(1)-C(21)-H(21C)	110.1(12)
H(21A)-C(21)-H(21C)	110.1(16)
H(21B)-C(21)-H(21C)	108.6(16)
N(1)-C(22)-H(22A)	112.1(16)
N(1)-C(22)-H(22B)	111.7(17)
H(22A)-C(22)-H(22B)	106(2)
N(1)-C(22)-H(22C)	114.0(16)
H(22A)-C(22)-H(22C)	105(2)
H(22B)-C(22)-H(22C)	108(2

Table H.5. Anisotropic displacement parameters ($Å^2 x10^4$) for (*rac*)-(EBI)Zr(NMe_2)Cl (CCDC 602362). The anisotropic displacement factor exponent takes the form: $-2\pi^2 [h^2 a^{*2} U^{11} + ... + 2 h k a^* b^* U^{12}]$.

	U^{11}	U^{22}	U^{33}	U^{23}	U^{13}	U^{12}
Zr(1)	77(1)	93(1)	100(1)	2(1)	16(1)	5(1)
Cl(1)	105(2)	183(3)	251(3)	42(3)	67(2)	14(2)
N(1)	125(8)	109(10)	125(9)	-7(7)	20(7)	18(7)
C(1)	93(9)	85(11)	178(11)	-3(9)	49(8)	23(8)
C(2)	99(10)	112(11)	201(12)	-26(9)	30(9)	33(9)
C(3)	165(11)	105(11)	115(11)	17(9)	-12(9)	45(9)
C(4)	125(10)	68(11)	163(12)	23(8)	27(8)	32(8)
C(5)	131(10)	79(11)	148(12)	-14(9)	33(9)	12(8)
C(6)	199(11)	105(11)	168(13)	-23(9)	16(9)	16(9)
C(7)	160(10)	144(12)	289(13)	-56(11)	4(9)	-12(10)
C(8)	173(10)	122(11)	371(14)	-35(12)	112(10)	-52(11)
C(9)	233(12)	98(11)	201(13)	10(9)	116(10)	-3(9)
C(10)	159(10)	104(11)	95(10)	20(8)	33(8)	-22(8)
C(11)	165(11)	145(11)	110(11)	21(9)	-18(9)	-55(9)
C(12)	128(10)	133(11)	146(12)	65(9)	6(9)	15(9)
C(13)	135(10)	112(11)	93(11)	49(8)	19(8)	-2(8)
C(14)	135(9)	98(11)	104(10)	32(8)	43(8)	10(8)
C(15)	126(10)	145(11)	150(12)	37(9)	51(9)	11(9)
C(16)	108(10)	197(12)	204(12)	1(10)	15(9)	-25(9)
C(17)	197(11)	120(12)	150(12)	-16(9)	17(9)	-39(9)
C(18)	175(11)	98(11)	134(12)	24(9)	33(9)	31(9)
C(19)	169(11)	139(12)	183(12)	-44(10)	78(9)	3(10)
C(20)	242(12)	149(12)	160(12)	-19(10)	89(10)	-37(10)
C(21)	240(13)	135(12)	166(13)	-20(10)	66(10)	-14(10)
C(22)	193(12)	239(15)	179(13)	-33(10)	-19(10)	-2(11)

Table H.6 Hydrogen coordinates (10^4) and isotropic displacement parameters ($Å^2 x10^3$) for (*rac*)-(EBI)Zr(NMe_2)Cl (CCDC 602362).

	x	y	z	U_{iso}
H(2)	90(30)	4570(20)	812(8)	18(6)
H(3)	2200(30)	5250(20)	187(9)	22(6)
H(6)	5000(30)	6140(20)	2151(9)	19(6)
H(7)	7510(30)	7120(20)	1917(8)	15(6)
H(8)	7920(30)	7230(20)	1053(9)	40(7)
H(9)	5680(30)	6440(20)	369(9)	17(6)
H(11)	5820(30)	3150(20)	2212(8)	16(5)
H(12)	6350(30)	970(20)	1722(8)	16(6)
H(15)	-460(30)	1870(20)	1712(8)	21(6)
H(16)	-1280(20)	-167(19)	1252(7)	9(5)
H(17)	880(30)	-1700(20)	1051(8)	22(6)
H(18)	3820(30)	-1160(20)	1246(8)	20(6)
H(19A)	30(20)	4499(19)	1819(7)	4(5)
H(20A)	1510(30)	3535(19)	2567(8)	12(5)
H(21A)	3800(20)	1090(20)	-74(8)	11(5)
H(22A)	960(30)	2480(30)	-249(12)	62(9)
H(19B)	930(20)	5770(20)	2078(7)	6(5)
H(20B)	3120(30)	4430(20)	2529(8)	10(5)
H(21B)	2900(30)	30(20)	237(8)	15(6)
H(22B)	240(30)	1400(30)	78(10)	47(9)
H(21C)	4650(30)	780(20)	531(8)	15(6)
H(22C)	70(30)	2860(30)	217(10)	50(8)

APPENDIX I

X-RAY CRYSTALLOGRAPHIC DATA FOR (*rac*)-**18**

(CHAPTER 3)

Contents

Note: Crystallographic data have been deposited at the CCDC, 12 Union Road, Cambridge CB2 1EZ, UK and copies can be obtained on request, free of charge, by quoting the publication citation and the deposition number 246589.

Table I.1 Crystal data and structure refinement for (*ra c*)-**18** (CCDC 246589).

Empirical formula	$C_{61}H_{50}N_2Zr$
Formula weight	902.25
Crystallization Solvent	Toluene/petroleum ether
Crystal Habit	Fragment
Crystal size	0.36 x 0.16 x 0.05 mm^3
Crystal color	Orange

Data Collection

Type of diffractometer	Bruker SMART 1000
Wavelength	0.71073 Å MoKα
Data Collection Temperature	100(2) K
θ range for 10520 reflections used in lattice determination	2.25º to 30.86°
Unit cell dimensions	a = 9.0168(6) Å α= 96.911(2)° b = 11.8062(6) Å β= 97.5720(10)° c = 22.5649(14) Å γ = 111.8280(10)°
Volume	2172.7(2) $Å^3$
Z	2
Crystal system	Triclinic
Space group	P-1
Density (calculated)	1.379 Mg/m^3
F(000)	940
Data collection program	Bruker SMART v5.054
θ range for data collection	1.85º to 32.94°
Completeness to θ = 32.94°	83.2%
Index ranges	$-13 \le h \le 13, -17 \le k \le 17, -34 \le l \le 34$
Data collection scan type	ω scans at 5 ϕ settings
Data reduction program	Bruker SAINT v6.45
Reflections collected	36571
Independent reflections	13576 [R_{int}= 0.0761]
Absorption coefficient	0.298 mm^{-1}
Absorption correction	None
Max. and min. transmission	0.9852 and 0.9002

Table I.1 (continued)

Structure solution and Refinement

Structure solution program	SHELXS-97 (Sheldrick, 1990)
Primary solution method	Patterson method
Secondary solution method	Difference Fourier map
Hydrogen placement	Geometric positions
Structure refinement program	SHELXL-97 (Sheldrick, 1997)
Refinement method	Full matrix least-squares on F^2
Data/restraints/parameters	13576/0/580
Treatment of hydrogen atoms	Riding
Goodness-of-fit on F^2	1.227
Final R indices [$I>2\sigma(I)$, 8720 reflections]	R1 = 0.0537, *w*R2 = 0.0899
R indices (all data)	R1 = 0.0913, *w*R2 = 0.0949
Type of weighting scheme used	Sigma
Weighting scheme used	$w=1/\sigma^2(Fo^2)$
Max shift/error	0.001
Average shift/error	0.000
Largest diff. peak and hole	1.490 and -1.009 e.Å^{-3}

Special Refinement Details

Refinement of F^2 against ALL reflections. The weighted R-factor (*w*R) and goodness of fit (S) are based on F^2, conventional R-factors (R) are based on F, with F set to zero for negative F^2. The threshold expression of $F^2 > 2\sigma(F^2)$ is used only for calculating R-factors(gt) etc. and is not relevant to the choice of reflections for refinement. R-factors based on F^2 are statistically about twice as large as those based on F, and R-factors based on ALL data will be even larger.

All esds (except the esd in the dihedral angle between two l.s. planes) are estimated using the full covariance matrix. The cell esds are taken into account individually in the estimation of esds in distances, angles and torsion angles; correlations between esds in cell parameters are only used when they are defined by crystal symmetry. An approximate (isotropic) treatment of cell esds is used for estimating esds involving l.s. planes.

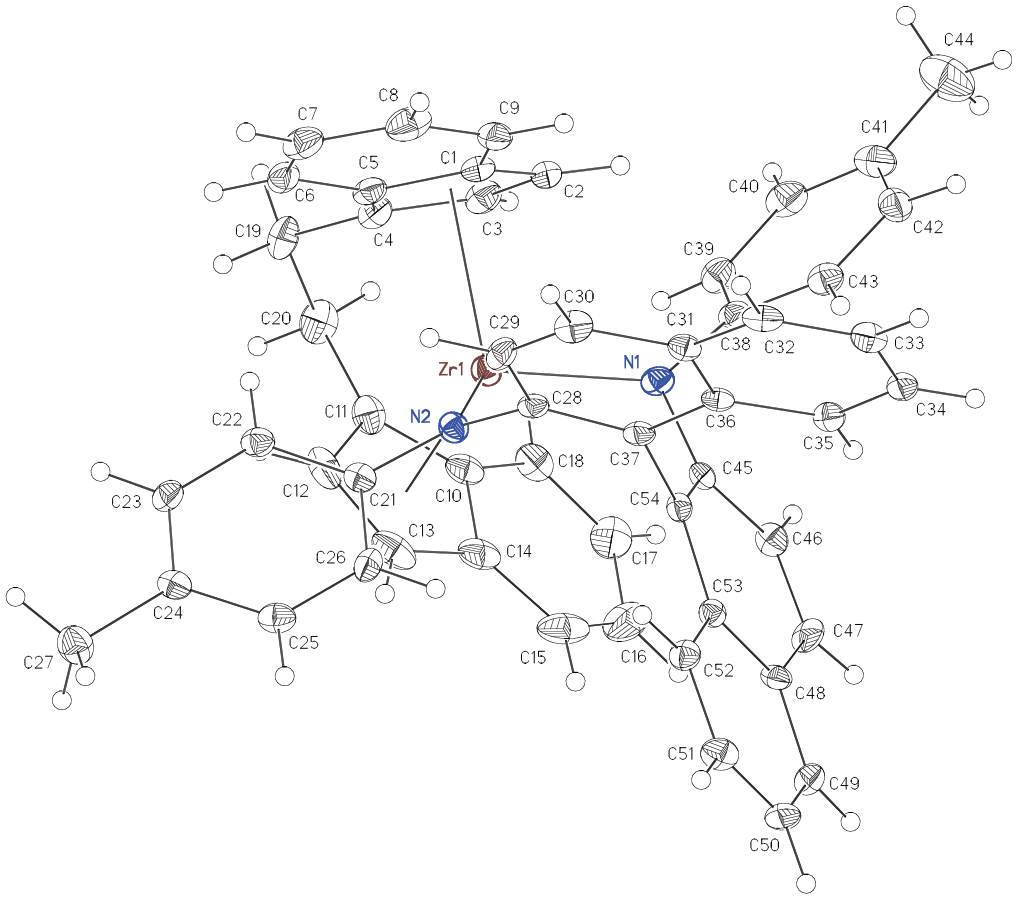

Figure I.1 Minimum overlap view of (*rac*)-**18**.

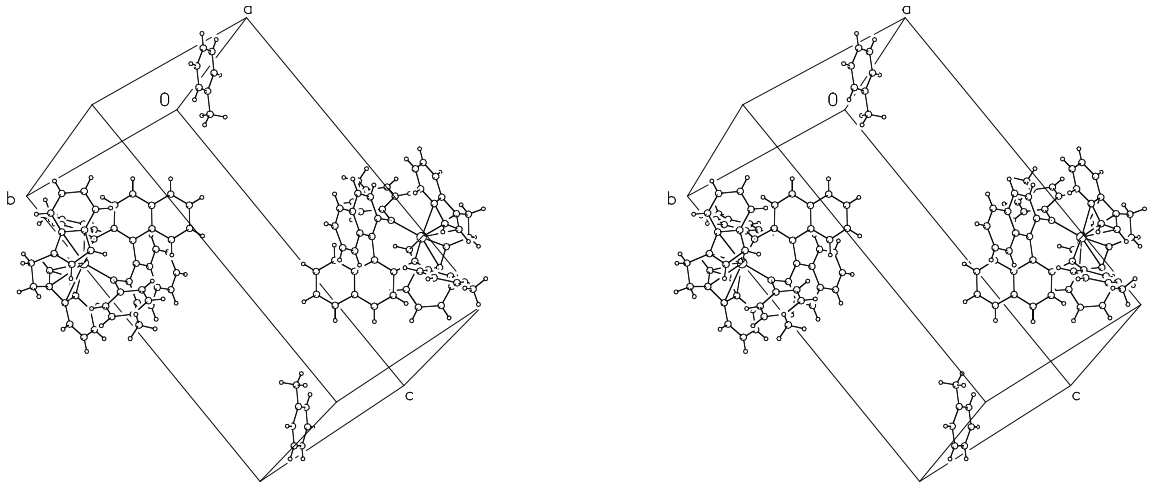

Figure I.2 Crystal packing of (*rac*)-**18**.

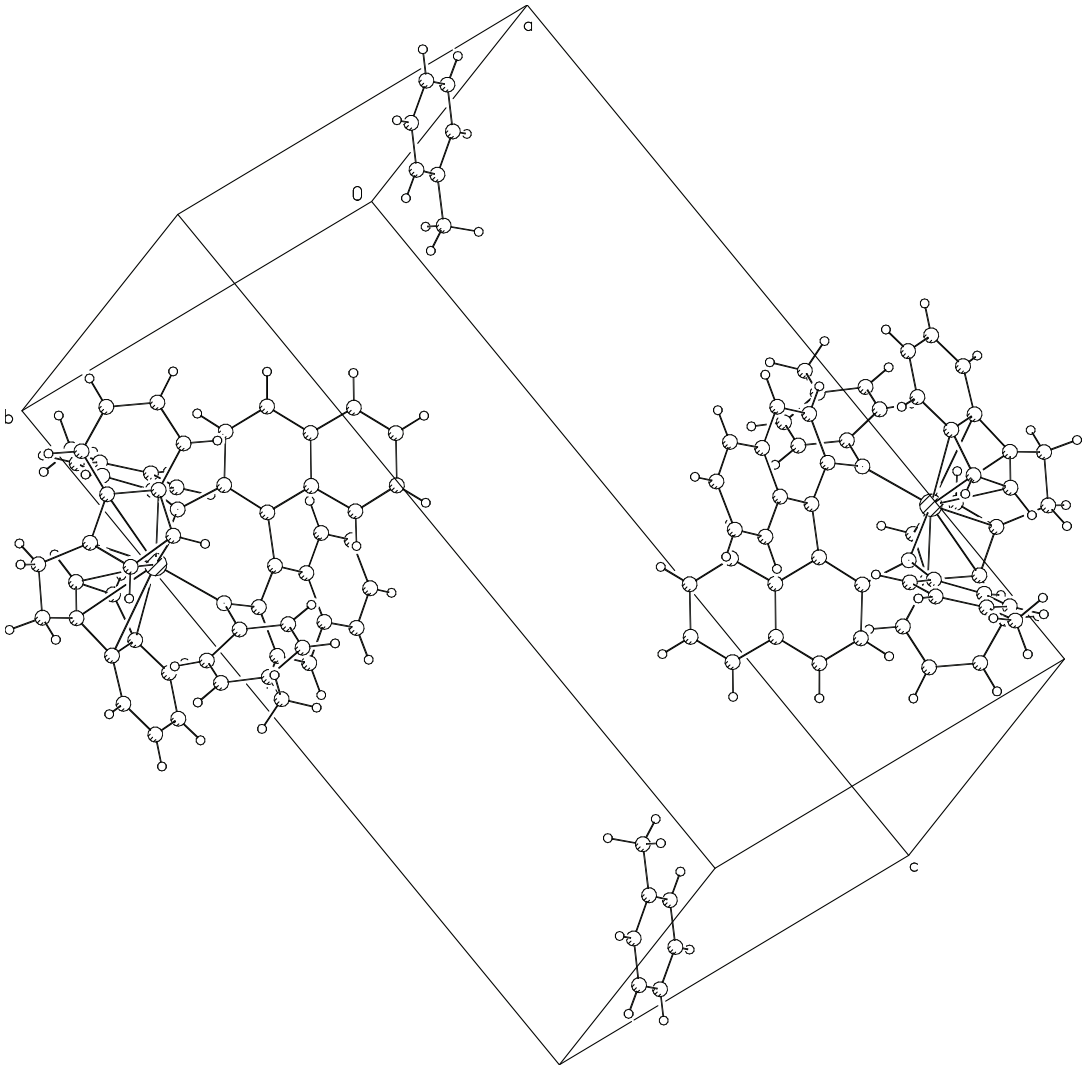

Figure I.3 Unit cell contents of (*rac*)-**18**.

Table I.2 Atomic coordinates (10^4) and equivalent isotropic displacement parameters ($Å^2x10^3$) for (*rac*)-**18** (CCDC 246589). U(eq) is defined as the trace of the orthogonalized U^{ij} tensor.

	x	y	z	U_{eq}
Zr(1)	8343(1)	-870(1)	7429(1)	15(1)
N(1)	9247(2)	973(2)	7954(1)	15(1)
N(2)	7573(2)	-636(2)	6530(1)	15(1)
C(1)	11200(3)	-715(2)	7081(1)	18(1)
C(2)	11420(3)	-289(2)	7709(1)	19(1)
C(3)	10590(3)	-1306(2)	7976(1)	19(1)
C(4)	9749(3)	-2375(2)	7513(1)	19(1)
C(5)	10170(3)	-2031(2)	6956(1)	16(1)
C(6)	9923(3)	-2720(2)	6366(1)	18(1)
C(7)	10662(3)	-2145(2)	5934(1)	22(1)
C(8)	11634(3)	-863(2)	6057(1)	26(1)
C(9)	11907(3)	-149(2)	6614(1)	21(1)
C(10)	6579(3)	-1765(2)	8260(1)	18(1)
C(11)	6774(3)	-2738(2)	7887(1)	20(1)
C(12)	5889(3)	-2877(2)	7298(1)	23(1)
C(13)	5227(3)	-1972(2)	7284(1)	24(1)
C(14)	5603(3)	-1303(2)	7884(1)	22(1)
C(15)	5071(3)	-411(2)	8153(1)	28(1)
C(16)	5430(3)	-52(2)	8772(1)	30(1)
C(17)	6398(3)	-511(2)	9143(1)	26(1)
C(18)	6983(3)	-1332(2)	8901(1)	22(1)
C(19)	8727(3)	-3645(2)	7618(1)	23(1)
C(20)	7670(3)	-3525(2)	8080(1)	25(1)
C(21)	6357(3)	-1491(2)	6037(1)	15(1)
C(22)	6175(3)	-2719(2)	5901(1)	16(1)
C(23)	4922(3)	-3561(2)	5453(1)	17(1)
C(24)	3825(3)	-3218(2)	5104(1)	15(1)
C(25)	4044(3)	-1974(2)	5221(1)	18(1)
C(26)	5290(3)	-1125(2)	5680(1)	17(1)
C(27)	2420(3)	-4175(2)	4648(1)	23(1)
C(28)	8474(3)	517(2)	6373(1)	13(1)
C(29)	9137(3)	506(2)	5829(1)	17(1)
C(30)	10068(3)	1572(2)	5658(1)	18(1)
C(31)	10449(3)	2742(2)	6028(1)	14(1)
C(32)	11445(3)	3872(2)	5875(1)	16(1)
C(33)	11819(3)	4985(2)	6237(1)	17(1)
C(34)	11213(3)	5019(2)	6780(1)	16(1)
C(35)	10232(3)	3950(2)	6937(1)	15(1)
C(36)	9800(3)	2773(2)	6570(1)	13(1)
C(37)	8730(3)	1636(2)	6725(1)	13(1)
C(38)	10578(3)	1605(2)	8446(1)	15(1)
C(39)	10872(3)	1042(2)	8933(1)	19(1)

C(40)	12295(3)	1613(2)	9368(1)	23(1)
C(41)	13445(3)	2776(2)	9358(1)	23(1)
C(42)	13105(3)	3372(2)	8897(1)	21(1)
C(43)	11710(3)	2797(2)	8447(1)	18(1)
C(44)	14978(3)	3365(3)	9831(1)	41(1)
C(45)	8273(3)	1654(2)	7814(1)	14(1)
C(46)	7733(3)	2199(2)	8299(1)	16(1)
C(47)	6676(3)	2745(2)	8189(1)	19(1)
C(48)	6044(3)	2779(2)	7585(1)	14(1)
C(49)	4885(3)	3302(2)	7455(1)	18(1)
C(50)	4340(3)	3377(2)	6880(1)	19(1)
C(51)	4909(3)	2914(2)	6396(1)	19(1)
C(52)	6018(3)	2387(2)	6502(1)	15(1)
C(53)	6629(3)	2309(2)	7097(1)	13(1)
C(54)	7840(3)	1790(2)	7224(1)	13(1)
C(61)	2658(3)	6539(3)	8534(1)	32(1)
C(62)	1550(3)	6548(2)	8978(1)	25(1)
C(63)	302(3)	5466(2)	9024(1)	28(1)
C(64)	-732(4)	5472(3)	9428(1)	33(1)
C(65)	-534(3)	6551(3)	9788(1)	33(1)
C(66)	717(3)	7650(3)	9750(1)	33(1)
C(67)	1752(3)	7648(2)	9348(1)	28(1)

Table I.3 Selected bond lengths (Å) and angles (°) for (*ra c*)-**18** (CCDC 246589).

Zr(1)-Cent1	2.322	Cent1-Zr(1)-Cent2	122.4
Zr(1)-Cent2	2.312	Cent1-Zr(1)-N(1)	104.4
Zr(1)-N(2)	2.1393(18)	Cent1-Zr(1)-N(2)	108.9
Zr(1)-N(1)	2.1460(19)	Cent2-Zr(1)-N(1)	110.3
		Cent2-Zr(1)-N(2)	105.9

Cent(1) is the centroid of C(1), C(2), C(3), C(4), and C(5)
Cent(2) is the centroid of C(10), C(11), C(12), C(13), and C(14)

Table I.4 Bond lengths (Å) and angles (°) for (*ra c*)-**18** (CCDC 246589).

Zr(1)-Cent1	2.322	C(30)-C(31)	1.420(3)
Zr(1)-Cent2	2.312	C(31)-C(32)	1.418(3)
Zr(1)-N(2)	2.1393(18)	C(31)-C(36)	1.426(3)
Zr(1)-N(1)	2.1460(19)	C(32)-C(33)	1.359(3)
Zr(1)-C(3)	2.483(2)	C(33)-C(34)	1.408(3)
Zr(1)-C(12)	2.522(2)	C(34)-C(35)	1.364(3)
Zr(1)-C(4)	2.549(2)	C(35)-C(36)	1.415(3)
Zr(1)-C(11)	2.560(2)	C(36)-C(37)	1.446(3)
Zr(1)-C(2)	2.567(2)	C(37)-C(54)	1.498(3)
Zr(1)-C(13)	2.575(2)	C(38)-C(39)	1.395(3)
Zr(1)-C(10)	2.679(2)	C(38)-C(43)	1.398(3)
Zr(1)-C(14)	2.698(2)	C(39)-C(40)	1.390(3)
Zr(1)-C(1)	2.739(2)	C(40)-C(41)	1.384(4)
Zr(1)-C(5)	2.743(2)	C(41)-C(42)	1.387(3)
N(1)-C(38)	1.420(3)	C(41)-C(44)	1.501(4)
N(1)-C(45)	1.424(3)	C(42)-C(43)	1.391(3)
N(2)-C(28)	1.418(3)	C(45)-C(54)	1.384(3)
N(2)-C(21)	1.429(3)	C(45)-C(46)	1.431(3)
C(1)-C(2)	1.407(3)	C(46)-C(47)	1.349(3)
C(1)-C(9)	1.412(3)	C(47)-C(48)	1.419(3)
C(1)-C(5)	1.452(3)	C(48)-C(49)	1.415(3)
C(2)-C(3)	1.410(3)	C(48)-C(53)	1.422(3)
C(3)-C(4)	1.422(3)	C(49)-C(50)	1.351(3)
C(4)-C(5)	1.423(3)	C(50)-C(51)	1.402(3)
C(4)-C(19)	1.506(3)	C(51)-C(52)	1.371(3)
C(5)-C(6)	1.417(3)	C(52)-C(53)	1.409(3)
C(6)-C(7)	1.362(3)	C(53)-C(54)	1.451(3)
C(7)-C(8)	1.409(3)	C(61)-C(62)	1.507(3)
C(8)-C(9)	1.365(3)	C(62)-C(63)	1.379(3)
C(10)-C(11)	1.420(3)	C(62)-C(67)	1.393(3)
C(10)-C(18)	1.426(3)	C(63)-C(64)	1.390(3)
C(10)-C(14)	1.436(3)	C(64)-C(65)	1.363(4)
C(11)-C(12)	1.414(3)	C(65)-C(66)	1.388(4)
C(11)-C(20)	1.506(3)	C(66)-C(67)	1.386(3)
C(12)-C(13)	1.406(3)		
C(13)-C(14)	1.412(3)	Cent1-Zr(1)-Cent2	122.4
C(14)-C(15)	1.415(3)	Cent1-Zr(1)-N(1)	104.4
C(15)-C(16)	1.366(4)	Cent1-Zr(1)-N(2)	108.9
C(16)-C(17)	1.424(3)	Cent2-Zr(1)-N(1)	110.3
C(17)-C(18)	1.357(3)	Cent2-Zr(1)-N(2)	105.9
C(19)-C(20)	1.530(3)	N(2)-Zr(1)-N(1)	103.49(7)
C(21)-C(22)	1.388(3)	N(2)-Zr(1)-C(3)	137.35(7)
C(21)-C(26)	1.397(3)	N(1)-Zr(1)-C(3)	92.01(7)
C(22)-C(23)	1.382(3)	N(2)-Zr(1)-C(12)	90.97(8)
C(23)-C(24)	1.390(3)	N(1)-Zr(1)-C(12)	137.80(8)
C(24)-C(25)	1.393(3)	C(3)-Zr(1)-C(12)	103.79(8)
C(24)-C(27)	1.501(3)	N(2)-Zr(1)-C(4)	116.48(7)
C(25)-C(26)	1.395(3)	N(1)-Zr(1)-C(4)	124.62(7)
C(28)-C(37)	1.378(3)	C(3)-Zr(1)-C(4)	32.79(7)
C(28)-C(29)	1.434(3)	C(12)-Zr(1)-C(4)	80.12(8)
C(29)-C(30)	1.362(3)	N(2)-Zr(1)-C(11)	123.27(8)

N(1)-Zr(1)-C(11)	120.18(7)	C(1)-Zr(1)-C(5)	30.71(7)
C(3)-Zr(1)-C(11)	78.36(8)	C(38)-N(1)-C(45)	113.88(18)
C(12)-Zr(1)-C(11)	32.31(7)	C(38)-N(1)-Zr(1)	131.48(14)
C(4)-Zr(1)-C(11)	66.86(8)	C(45)-N(1)-Zr(1)	114.46(14)
N(2)-Zr(1)-C(2)	113.42(7)	C(28)-N(2)-C(21)	113.34(17)
N(1)-Zr(1)-C(2)	76.49(7)	C(28)-N(2)-Zr(1)	115.98(14)
C(3)-Zr(1)-C(2)	32.38(7)	C(21)-N(2)-Zr(1)	130.50(14)
C(12)-Zr(1)-C(2)	133.37(8)	C(2)-C(1)-C(9)	132.4(2)
C(4)-Zr(1)-C(2)	53.69(8)	C(2)-C(1)-C(5)	107.6(2)
C(11)-Zr(1)-C(2)	110.73(8)	C(9)-C(1)-C(5)	119.6(2)
N(2)-Zr(1)-C(13)	78.29(8)	C(2)-C(1)-Zr(1)	67.94(13)
N(1)-Zr(1)-C(13)	112.30(8)	C(9)-C(1)-Zr(1)	128.68(15)
C(3)-Zr(1)-C(13)	131.85(8)	C(5)-C(1)-Zr(1)	74.79(12)
C(12)-Zr(1)-C(13)	32.01(8)	C(1)-C(2)-C(3)	108.2(2)
C(4)-Zr(1)-C(13)	112.10(8)	C(1)-C(2)-Zr(1)	81.53(14)
C(11)-Zr(1)-C(13)	53.53(8)	C(3)-C(2)-Zr(1)	70.54(13)
C(2)-Zr(1)-C(13)	164.09(7)	C(2)-C(3)-C(4)	109.3(2)
N(2)-Zr(1)-C(10)	129.85(7)	C(2)-C(3)-Zr(1)	77.08(13)
N(1)-Zr(1)-C(10)	90.62(7)	C(4)-C(3)-Zr(1)	76.17(13)
C(3)-Zr(1)-C(10)	88.63(8)	C(3)-C(4)-C(5)	107.0(2)
C(12)-Zr(1)-C(10)	51.75(8)	C(3)-C(4)-C(19)	125.2(2)
C(4)-Zr(1)-C(10)	91.53(7)	C(5)-C(4)-C(19)	127.6(2)
C(11)-Zr(1)-C(10)	31.34(7)	C(3)-C(4)-Zr(1)	71.04(12)
C(2)-Zr(1)-C(10)	116.66(7)	C(5)-C(4)-Zr(1)	82.07(13)
C(13)-Zr(1)-C(10)	52.09(8)	C(19)-C(4)-Zr(1)	116.41(15)
N(2)-Zr(1)-C(14)	101.11(7)	C(6)-C(5)-C(4)	133.1(2)
N(1)-Zr(1)-C(14)	86.81(7)	C(6)-C(5)-C(1)	118.8(2)
C(3)-Zr(1)-C(14)	119.47(8)	C(4)-C(5)-C(1)	107.7(2)
C(12)-Zr(1)-C(14)	51.28(8)	C(6)-C(5)-Zr(1)	129.75(15)
C(4)-Zr(1)-C(14)	118.66(7)	C(4)-C(5)-Zr(1)	67.00(12)
C(11)-Zr(1)-C(14)	51.96(7)	C(1)-C(5)-Zr(1)	74.50(12)
C(2)-Zr(1)-C(14)	144.18(8)	C(7)-C(6)-C(5)	119.8(2)
C(13)-Zr(1)-C(14)	30.96(8)	C(6)-C(7)-C(8)	121.0(2)
C(10)-Zr(1)-C(14)	30.98(7)	C(9)-C(8)-C(7)	121.9(2)
N(2)-Zr(1)-C(1)	86.87(7)	C(8)-C(9)-C(1)	119.0(2)
N(1)-Zr(1)-C(1)	96.93(7)	C(11)-C(10)-C(18)	132.2(2)
C(3)-Zr(1)-C(1)	51.55(7)	C(11)-C(10)-C(14)	107.7(2)
C(12)-Zr(1)-C(1)	123.63(8)	C(18)-C(10)-C(14)	119.5(2)
C(4)-Zr(1)-C(1)	51.94(7)	C(11)-C(10)-Zr(1)	69.68(13)
C(11)-Zr(1)-C(1)	118.79(7)	C(18)-C(10)-Zr(1)	127.41(16)
C(2)-Zr(1)-C(1)	30.53(7)	C(14)-C(10)-Zr(1)	75.25(13)
C(13)-Zr(1)-C(1)	149.51(8)	C(12)-C(11)-C(10)	106.7(2)
C(10)-Zr(1)-C(1)	139.53(7)	C(12)-C(11)-C(20)	125.9(2)
C(14)-Zr(1)-C(1)	170.20(7)	C(10)-C(11)-C(20)	127.3(2)
N(2)-Zr(1)-C(5)	88.43(7)	C(12)-C(11)-Zr(1)	72.39(13)
N(1)-Zr(1)-C(5)	126.33(7)	C(10)-C(11)-Zr(1)	78.98(13)
C(3)-Zr(1)-C(5)	51.61(7)	C(20)-C(11)-Zr(1)	116.70(16)
C(12)-Zr(1)-C(5)	92.95(8)	C(13)-C(12)-C(11)	110.1(2)
C(4)-Zr(1)-C(5)	30.93(7)	C(13)-C(12)-Zr(1)	76.08(14)
C(11)-Zr(1)-C(5)	92.58(7)	C(11)-C(12)-Zr(1)	75.30(14)
C(2)-Zr(1)-C(5)	51.37(7)	C(12)-C(13)-C(14)	106.9(2)
C(13)-Zr(1)-C(5)	121.36(8)	C(12)-C(13)-Zr(1)	71.91(14)
C(10)-Zr(1)-C(5)	121.08(7)	C(14)-C(13)-Zr(1)	79.33(14)
C(14)-Zr(1)-C(5)	142.60(7)	C(13)-C(14)-C(15)	131.7(2)

C(13)-C(14)-C(10)	108.3(2)	C(49)-C(48)-C(47)	121.8(2)
C(15)-C(14)-C(10)	119.7(2)	C(49)-C(48)-C(53)	119.1(2)
C(13)-C(14)-Zr(1)	69.71(13)	C(47)-C(48)-C(53)	119.0(2)
C(15)-C(14)-Zr(1)	127.32(17)	C(50)-C(49)-C(48)	121.5(2)
C(10)-C(14)-Zr(1)	73.78(13)	C(49)-C(50)-C(51)	119.8(2)
C(16)-C(15)-C(14)	119.1(2)	C(52)-C(51)-C(50)	120.4(2)
C(15)-C(16)-C(17)	121.0(2)	C(51)-C(52)-C(53)	121.3(2)
C(18)-C(17)-C(16)	121.7(2)	C(52)-C(53)-C(48)	117.9(2)
C(17)-C(18)-C(10)	118.8(2)	C(52)-C(53)-C(54)	122.4(2)
C(4)-C(19)-C(20)	109.51(19)	C(48)-C(53)-C(54)	119.7(2)
C(11)-C(20)-C(19)	109.50(19)	C(45)-C(54)-C(53)	118.5(2)
C(22)-C(21)-C(26)	117.5(2)	C(45)-C(54)-C(37)	124.0(2)
C(22)-C(21)-N(2)	121.4(2)	C(53)-C(54)-C(37)	116.69(19)
C(26)-C(21)-N(2)	121.1(2)	C(63)-C(62)-C(67)	118.4(2)
C(23)-C(22)-C(21)	121.0(2)	C(63)-C(62)-C(61)	120.7(2)
C(22)-C(23)-C(24)	122.2(2)	C(67)-C(62)-C(61)	120.9(2)
C(23)-C(24)-C(25)	117.1(2)	C(62)-C(63)-C(64)	120.9(3)
C(23)-C(24)-C(27)	120.4(2)	C(65)-C(64)-C(63)	120.6(3)
C(25)-C(24)-C(27)	122.3(2)	C(64)-C(65)-C(66)	119.5(3)
C(24)-C(25)-C(26)	120.9(2)	C(67)-C(66)-C(65)	120.1(3)
C(25)-C(26)-C(21)	121.2(2)	C(66)-C(67)-C(62)	
C(37)-C(28)-N(2)	122.14(19)		
C(37)-C(28)-C(29)	119.5(2)		
N(2)-C(28)-C(29)	118.34(19)		
C(30)-C(29)-C(28)	122.0(2)		
C(29)-C(30)-C(31)	120.2(2)		
C(32)-C(31)-C(30)	122.1(2)		
C(32)-C(31)-C(36)	119.3(2)		
C(30)-C(31)-C(36)	118.6(2)		
C(33)-C(32)-C(31)	121.5(2)		
C(32)-C(33)-C(34)	119.4(2)		
C(35)-C(34)-C(33)	120.5(2)		
C(34)-C(35)-C(36)	122.0(2)		
C(35)-C(36)-C(31)	117.3(2)		
C(35)-C(36)-C(37)	122.4(2)		
C(31)-C(36)-C(37)	120.3(2)		
C(28)-C(37)-C(36)	119.0(2)		
C(28)-C(37)-C(54)	124.9(2)		
C(36)-C(37)-C(54)	115.76(19)		
C(39)-C(38)-C(43)	116.9(2)		
C(39)-C(38)-N(1)	121.8(2)		
C(43)-C(38)-N(1)	121.2(2)		
C(40)-C(39)-C(38)	120.7(2)		
C(41)-C(40)-C(39)	122.3(2)		
C(40)-C(41)-C(42)	117.0(2)		
C(40)-C(41)-C(44)	121.1(2)		
C(42)-C(41)-C(44)	121.9(2)		
C(41)-C(42)-C(43)	121.3(2)		
C(42)-C(43)-C(38)	121.5(2)		
C(54)-C(45)-N(1)	121.31(19)		
C(54)-C(45)-C(46)	119.9(2)		
N(1)-C(45)-C(46)	118.81(19)		
C(47)-C(46)-C(45)	121.5(2)		
C(46)-C(47)-C(48)	120.6(2)		

Table I.5. Anisotropic displacement parameters ($Å^2x10^4$) for (*ra c*)-**18** (CC246589). The anisotropic displacement factor exponent takes the form: $-2\pi^2 [h^2 a^{*2} U^{11} + ... + 2 h k a^* b^* U^{12}]$.

	U^{11}	U^{22}	U^{33}	U^{23}	U^{13}	U^{12}
Zr(1)	144(1)	149(1)	137(1)	25(1)	8(1)	53(1)
N(1)	159(11)	186(10)	124(10)	33(8)	8(8)	95(9)
N(2)	144(10)	149(10)	133(10)	17(8)	24(8)	48(8)
C(1)	143(13)	191(13)	225(13)	30(11)	18(10)	102(11)
C(2)	146(13)	169(13)	259(14)	-7(11)	-5(11)	86(11)
C(3)	229(14)	220(13)	176(13)	42(11)	34(11)	137(11)
C(4)	208(14)	200(13)	178(13)	28(11)	39(11)	113(11)
C(5)	165(13)	194(13)	162(12)	30(10)	22(10)	114(11)
C(6)	195(13)	190(13)	175(13)	-3(10)	-21(10)	116(11)
C(7)	241(15)	304(15)	182(13)	20(11)	49(11)	172(12)
C(8)	258(15)	299(15)	324(16)	133(13)	147(13)	166(13)
C(9)	128(13)	185(13)	320(15)	48(11)	67(11)	63(11)
C(10)	128(13)	213(13)	204(13)	91(11)	55(10)	40(11)
C(11)	215(14)	171(13)	198(13)	52(10)	55(11)	36(11)
C(12)	202(14)	203(13)	195(13)	14(11)	30(11)	-16(11)
C(13)	155(13)	273(14)	235(14)	137(12)	26(11)	-3(11)
C(14)	131(13)	250(14)	279(15)	126(12)	87(11)	45(11)
C(15)	186(14)	354(16)	410(18)	234(14)	143(13)	137(13)
C(16)	305(16)	277(15)	402(18)	146(13)	214(14)	149(13)
C(17)	276(16)	264(15)	260(15)	81(12)	139(12)	77(13)
C(18)	204(14)	211(14)	221(14)	72(11)	12(11)	56(11)
C(19)	328(16)	154(13)	229(14)	36(11)	57(12)	114(12)
C(20)	327(16)	208(14)	234(14)	96(11)	85(12)	109(12)
C(21)	139(12)	180(12)	131(12)	32(10)	30(10)	57(10)
C(22)	156(13)	197(13)	146(12)	27(10)	22(10)	86(11)
C(23)	186(13)	172(13)	180(13)	7(10)	59(10)	92(11)
C(24)	135(12)	226(13)	93(11)	9(10)	41(9)	65(10)
C(25)	168(13)	242(14)	149(12)	49(10)	34(10)	100(11)
C(26)	205(13)	130(12)	192(13)	20(10)	47(10)	79(10)
C(27)	224(14)	227(14)	209(14)	24(11)	0(11)	69(11)
C(28)	118(12)	169(12)	120(11)	27(9)	4(9)	81(10)
C(29)	208(13)	180(13)	129(12)	3(10)	31(10)	108(11)
C(30)	207(13)	271(14)	89(11)	42(10)	43(10)	125(11)
C(31)	126(12)	175(12)	136(12)	58(10)	10(9)	68(10)
C(32)	134(13)	266(14)	128(12)	101(10)	47(10)	103(11)
C(33)	147(13)	170(12)	213(13)	113(10)	47(10)	56(10)
C(34)	141(13)	154(12)	198(13)	36(10)	4(10)	70(10)
C(35)	150(12)	185(12)	113(12)	19(10)	14(9)	75(10)
C(36)	105(12)	172(12)	121(11)	53(9)	8(9)	70(10)
C(37)	113(12)	180(12)	118(12)	31(10)	8(9)	77(10)
C(38)	153(13)	191(13)	123(12)	-7(10)	18(10)	104(11)
C(39)	237(14)	204(13)	166(13)	32(11)	41(11)	113(11)

C(40)	279(15)	304(15)	160(13)	49(11)	8(11)	185(13)
C(41)	182(14)	362(16)	150(13)	-12(11)	18(11)	124(12)
C(42)	165(13)	219(13)	201(13)	-5(11)	62(11)	46(11)
C(43)	195(13)	220(13)	153(12)	36(10)	54(10)	104(11)
C(44)	290(17)	560(20)	291(17)	51(15)	-39(13)	109(16)
C(45)	100(12)	110(11)	175(12)	19(9)	31(10)	16(9)
C(46)	177(13)	192(13)	109(12)	22(10)	22(10)	63(11)
C(47)	229(14)	213(13)	141(12)	-21(10)	63(10)	120(11)
C(48)	92(12)	174(12)	139(12)	18(10)	26(9)	45(10)
C(49)	182(13)	165(12)	206(13)	-1(10)	56(10)	82(11)
C(50)	150(13)	200(13)	245(14)	46(11)	-2(11)	105(11)
C(51)	179(13)	210(13)	198(13)	90(11)	21(10)	87(11)
C(52)	157(13)	162(12)	150(12)	31(10)	50(10)	63(10)
C(53)	125(12)	115(11)	136(12)	30(9)	26(9)	39(10)
C(54)	129(12)	106(11)	129(12)	16(9)	29(9)	32(10)
C(61)	313(17)	374(17)	298(16)	76(13)	108(13)	130(14)
C(62)	220(15)	307(15)	203(14)	63(12)	7(11)	102(12)
C(63)	305(16)	267(15)	301(16)	72(12)	80(13)	135(13)
C(64)	364(18)	338(17)	348(17)	155(14)	143(14)	142(14)
C(65)	341(18)	463(19)	280(16)	128(14)	145(13)	219(15)
C(66)	391(18)	383(18)	249(15)	-22(13)	30(13)	218(15)
C(67)	276(16)	261(15)	260(15)	42(12)	6(12)	78(13)